OVERTRAWLABILITY AND MECHANICAL DAMAGE OF PIPE-IN-PIPE

Zheng Jiexin

(B. Eng., M. Eng.)

A THESIS SUBMITTED

FOR THE DEGREE OF DOCTOR OF PHILOSOPHY
DEPARTMENT OF CIVIL AND ENVIRONMENTAL ENGINEERING
NATIONAL UNIVERSITY OF SINGAPORE

2014

DECLARATION

I hereby declare that this thesis is my original work and it has been written by me in its entirety.

I have duly acknowledged all the sources of information which have been used in the thesis.

This thesis has also not been submitted for any degree in any university previously.

Zheng Jiexin

18 March 2014

Acknowledgment

First of all, I would like to express my deepest appreciation to my supervisor Professor Andrew Palmer, who is an admirable pioneer in the subsea pipeline area. Without him, my PhD study in NUS would not have been possible. I am grateful for his support, his patience, his motivation, his enthusiasm, and immense knowledge; all of them play an important part in the success of this PhD program. He encourages me, supports my choices, offers me opportunities and builds up my confidence. Without his guidance throughout these four years, my PhD study would not have been so worthwhile and fruitful. The way he treats research, as well as other aspects will definitely leave a long term impact on my future.

I would also like to convey my heartfelt thanks to Prof. Stelios Kyriakides at University of Texas at Austin for his guidance and help in simulating the external pressure using hydrostatic fluid elements as well as his inspirational ideas. He is a great professor, for whom I have utmost respect.

I also would like to thank Prof. Qian Xudong for taking time to discuss finite element models and the results with me, and his suggestions of ways to improve them. I would like to thank my colleague Sun Shu, the research assistant for this project, for her help in measuring the deformed profile of the pipes after the experiments and helping me with the pull-over model tests. The preparation of the pull-over model tests was not easy. She helped me in correspondence with contractors, purchasing of pipes and sensors, preparing

drawings, and offering her valuable ideas in the design. After she has finished her master and began work in her current company, the contractors Martin Loh, Tay Poh Chuan and Khoo Ah Muan continued to help me with the laborious works. Poh Chuan is very helpful: carrying pipe and trawl gear, handling of the boat and so on. He joked that he should be a co-author of the thesis. I never expected I could do 100 tests, but we did it. I also want to thank Wang Yu, Kazi Md. Abu Sohel for their generous sharing. Moreover, I want to thank Ee Weng for his generous help with the impact tests.

I would also like to thank the laboratory staffs, Mr. Ang Beng Oon, Mr. Koh Yian Kheng, Mr. Ishak Bin A Rahman, Mr. Lim Huay Bak, Mr. Yip Richard, Mr. Choo Peng Kin, Mr. Kamsan Bin Rasman, Mr. Ow Weng Moon, Mr. Shaja Khan, Mr. Krishna Sanmugam, Mr. Semawi Bin Sadi and Mr. Koh Seng Chee. Without their assistance, the laboratory would not have been functional and my extensive experiments would not have been finished.

I am indebted to SUBSEA 7 for the financial and technical supports for this research. Particular thanks to Paul Brunning, who continually renders me help on this project for three years and the other project managers Wacek Lipski, Gan Cheng Ti, and Gerry Lim.

Special thanks to Simon Falser, Hendrik Tjiawi, Matilda Loh, Xie Peng and Too Jun Lin. The Oppenheim meeting with them every week gave me motivation and pressure to finish my plan and achieve more. I also want to thank my friends, my lunch partners and my colleagues on the 8th floor of Block E1, in the structural lab and in the hydraulic lab. Without their company, the life in school and the lunches in the canteen would be much less joyful.

Last but not least, I would like to give thanks to my family and my husband Yap Kim Thow for their unwavering support and understanding. Their unconditional love gives me warmth and the strength to carry on.

Financial supports in the form of the NUS Research Scholarship and the President Graduate Fellowship for my Ph.D. candidature are gratefully acknowledged.

Contents

Acknowledgment..i

Contents v

Summary...ix

List of tables...xi

List of figures.. xiii

List of Symbols xxiii

Abbreviations xxiii

Symbols.. xxiii

1 Introduction 1

1.1 Background..1

1.2 Motivation 2

1.3 Objective and Scope 3

1.3.1 Objective of Research 3

1.3.2 Scope of Research 5

1.4 Layout of Current Thesis 5

2 Literature Review on Overtrawlability of Subsea Pipelines 7

2.1 Trawl Gear..7

2.2 Impact Response...11

2.3 Dent Behaviour...30

2.3.1 Stress concentration 31

2.3.2 Burst pressure..33

2.3.3 Fatigue...34

2.3.4 Summary of dent behaviour..35

2.4 Pull-over Response...36

2.5 Pull-over Induced Lateral Buckling 45

2.6 Hooking 46

2.7 Existing Guidelines...47

2.7.1 Guidelines for Trenching Design of Submarine Pipelines (Trevor Jee Associates, 1999) 47
2.7.2 DNV-RP-F111: Interference between Trawl Gear and Pipelines (2010) 51
2.7.3 NORSOK Standard U-001(2002) 57
2.8 Pipe-in-Pipe system and Overtrawlability 58

3 Quasi-static Indentation Test Program 61
3.1 Test Specimen Preparation 61
3.2 Indenter Design 65
3.3 Quasi-static Indentation Test Set-ups 68
3.4 Instrumentations 71
3.5 Quasi-static Indentation Test 74
3.6 Test Results of Quasi-static Indentation Test 75
3.6.1 Single Wall Pipe Indentation Test Results 75
3.6.2 Pipe-in-pipe Indentation Test Results 77
3.7 Discussion of Test Results 79
3.8 Model Test Data Scale Up 85
3.9 Summary 86

4 Impact Test Program 89
4.1 Impact Test Design 89
4.2 Test Results of Impact Experiments 96
4.3 Discussion 104
4.3.1 Model Test Scaling Laws of Impact 104
4.3.2 Impact Energy 107
4.4 Summary 108

5 Finite Element Modelling and Further Analysis 111
5.1 Single Wall Pipe Quasi-static Indentation Model 111
5.2 Pipe-in-Pipe Quasi-static Indentation Model 122
5.3 Summary of the Finite Element Model of Quasi-static Indentation ..132
5.4 Impact FE Models 132
5.5 Quasi-static Indentation & Dynamic Impact 143
5.5.1 Quasi-static Response & Impact Response 144
5.5.2 Strain Rate Effect 145
5.6 Prototype Comparisons 150
5.6.1 Impact Energy 150

5.6.2 PIP12 & PIP14 151
5.7 Parametric Analysis and Empirical Relationship 156
5.8 New Model of Indentation Force and Displacement 162
5.9 Theories for Pipe-in-Pipes 173
5.10 Summary 178

6 Interaction between External Pressure and Indentation 181
6.1 FE Modelling Methodology and Validation 182
6.1.1 FE Model of External Pressure 182
6.1.2 FE model of Denting with Existence of External Pressure 189
6.2 Effect of External Pressure 193
6.2.1 Pipe-in-Pipe FE model of Denting with Existence of External Pressure 195
6.3 Combination of Internal Pressure, External Pressure and Indentation 198
6.4 Conclusion 203

7 Pull-over Test Program 207
7.1 Motivation and Purpose 208
7.2 Experiment Design 209
7.2.1 Model Pipeline Design 209
7.2.2 Trawl Gear Design 213
7.2.3 Warp-line Design 215
7.2.4 Driving Force System Design 217
7.2.5 Pull-over Test Set-up in the Wave Basin 218
7.2.6 Experiment Data Collection and Analysis 222
7.2.7 Test Program Design 224
7.3 Test Results and Analysis 225
7.4 Different Crossing Angles 229
7.4.1 90 Degree Crossing vs. Smaller Degree Crossing 231
7.4.2 Sliding at Low Crossing Angle 232
7.5 Summary 235

8 Analysis of Pull-over Model Test 237
8.1 Overtrawlability of Pipe-in-Pipe 237
8.1.1 Comparison between Single Wall Pipe and Pipe-in-Pipe 237
8.1.2 Prototype Scale Up 239
8.2 Parametric Study 243

8.2.1 Boundary Condition Effect 243
8.2.2 Pipeline Geometry Effect 244
8.2.3 Water Depth Effect 251
8.2.4 Kinetic Energy Effect 252
8.3 Discussion of Froude Scaling Law 254
8.4 Velocity Effect 257
8.5 Parameter $V(MK)^{0.5}$ 261
8.6 Proposed Model 264
8.6.1 Components of Warp-line Force 264
8.6.2 A Possible Scaling Law 265
8.7 Summary 270

9 Conclusion and Future Work 273
9.1 Conclusion 273
9.2 Future Work 275

References 279

A. Appendix A Specimen Details 287

B. Appendix B Indenter Design 289

C. Appendix C Coupon Test Results 290
C.1 Coupons 290
C.2 Tensile Test Results 292
C.3 FE Modelling Material Property Input 294

D. Appendix D Test Specimen Details 298

E. Appendix E Dimensions of Different Trawl Gears 301

F. Appendix F Pull-over Test Results 304

G. Appendix G Papers 326

Summary

Pipe-in-pipe and bundled pipeline systems are widely used in the offshore industry, because they make it possible to achieve a high level of thermal insulation and because they lead themselves to rapid and economical installation. Traditionally, mechanical design of these systems with regards to fishing gear interaction and dropped objects have used the same approach as for single pipe systems. However, this approach is likely to result in a conservative design as the outer pipe is not required to resist internal pressure and can accommodate a greater level of indentation than a single, pressure containing pipe. Eliminating conservatism in this aspect of design has the potential to eliminate the need for trenching in areas of high fishing activity and can therefore have considerable economic benefits.

The current research studies the pipe-in-pipe's response during trawl gear crossing. When trawl gear crosses the pipeline, it impacts the pipeline, and then pulls-over the pipeline. The impact response and the pull-over response are both investigated. As the outer pipe is not required to resist internal pressure and can accommodate a greater level of indentation than a single, pressure containing pipe, the possibility of relaxing the criteria of the outer pipe is studied on aspects of the external pressure effect.

An extensive experimental program is set up to study the pipe-in-pipe's impact response and pull-over response under trawl gear crossing. The experimental program includes the quasi-static indentation test program, the impact test program and the pull-over model test program. A large amount of first-hand test data is collected. Through the experiments, the behaviour of the pipe-in-pipe is investigated.

FE models, including models for quasi-static indentation test condition, impact test condition and the pipeline under external pressure and the indentation condition for both the single wall pipe and the pipe-in-pipe, are developed and verified against the experimental data. FE models and the modelling methodology can also be used for other applications. Based on the experimental results and FE results, two semi-empirical models for predicting the maximum indentation force and the force-deformation curve are developed.

100 pull-over tests are conducted with various parameters. The results show the pull-over response is not linearly proportional to the trawl gear moving velocity. This finding disagrees with the equation the DNV gave. A new theory is proposed that the pull-over force is formed by more than one component, and every component has a different relationship with the velocity. Moreover, scaling law used now distorts some of the components.

The current research presents methods to analyse the overtrawlability of pipe-in-pipes, including the impact response and pull-over response. These methods fill the gap for analysing the pipe-in-pipe under trawl gear crossing. The results of the current research show that different methods and criteria can be applied in the analysis of pipe-in-pipe systems, and it is possible to lay the pipe-in-pipe on the seabed without a trench. Moreover, the current research also improves the methods of impact response and pull-over response analysis of single wall pipes, which eliminate conservative estimation.

List of tables

Table 2-1 Data for largest trawl gear in the use in the North Sea and the Norwegian Sea in 2005 (DNV, 2010) 10

Table 2-2 Recommended methods in the pipeline defect assessment manual for assessing the burst strength and fatigue life of mechanical damage defects (dent and gouge) subject to internal pressure loading (Cosham and Hopkins, 2001) 36

Table 2-3 Total VHL model and field study of bottom trawl loading on submarine pipelines (Moshagen and Kjeldsen, 1980) 38

Table 2-4 Acceptable dent sizes relative to outer diameter (DNV, 2010) 57

Table 3-1 Ideal scaled pipe 62

Table 3-2 Test pipes 62

Table 3-3 Single wall pipe specimens 63

Table 3-4 Pipe-in-pine specimens 65

Table 3-5 Tests summary of quasi-static indentation test 74

Table 4-1 Impact tests 89

Table 4-2 Results from the Laser Light Data 102

Table 4-3 Maximum Deformation 104

Table 4-4 Variables 104

Table 4-5 Relationships between the model and prototype with Jones' approach 106

Table 4-6 Relationships between the model and prototype with Calladine's approach 107

Table 4-7 Model and prototype energy 107

Table 5-1 Contact definitions in quasi-static indentation FE models 114

Table 5-2 Deviations between experimental data and FE results of single wall pipes 122

Table 5-3 Deviations between experimental data and FE results of pipe-in-pipes 131

Table 5-4 Contact definitions of impact FE models 133

Table 5-5 Dynamic coupon tensile test 136

Table 5-6 Dimensions of PIP12, PIP14 and SP16 154

Table 5-7 Failure Criteria (DNV, 2010) 154

Table 5-8 Acceptable indenter displacement for PIP12, PIP14 and SP16 ...154
Table 5-9 Details of 24 cases 160
Table 6-1 Geometric and material parameters of dented tubes 187
Table 6-2 Collapse pressure of dented pipe by hydrostatic fluid element....188
Table 7-1 Details of specimens 210
Table 7-2 Details of pull-over specimen 210
Table 7-3 Details of the springs 216
Table 7-4 Different pulley set and corresponding pull speed 218
Table 7-5 Sensors and corresponding measurements 222
Table 7-6 Summary of Parameters 225
Table 8-1 Scaling Factors based on Froude’s law 240
Table 8-2 Prototype Force by Froude scaling 241
Table A-1 Single wall pipe specimens 287
Table A-2 Two different type of pipe-in-pipe specimens 287
Table A-3 Pipe-in-pine specimens 287
Table C-1 Coupons for tensile test 290
Table C-2 Tensile test results summary 294
Table D-1 Specimen details 298
Table F-1 Test program 304
Table F-2 Summary of test results of 90 degree crossing 306
Table F-3 Summary of test results of 60, 45, 30 degree crossing 308
Table F-4 Summary of pull-over force time history 309

List of figures

Figure 2-1 Fishing methods (SEAFISH, 2005) 7

Figure 2-2 Twin rig (SEAFISH, 2005) 8

Figure 2-3 Otterboards (SEAFISH et al., 1995) 8

Figure 2-4 Beam Trawl (SEAFISH, 2005) 9

Figure 2-5 (a) Unreformed tube geometry and loading arrangements; (b) DeRuntz and Hodge collapse mode (1963); (c) Reid and Reddy (1978) 12

Figure 2-6 Morris indentation test rig (1971) 12

Figure 2-7 Soreide and Amdahl's indentation test rig (1982) 13

Figure 2-8 Thomas et al. indentation test rig (1976) 15

Figure 2-9 Deformed shape of the cross-section (1983) 16

Figure 2-10 Deformed cross-section (De Oliveira et al., 1982) 18

Figure 2-11 Approximate cross-section (De Oliveira et al., 1982) 18

Figure 2-12 Plastic moment of different cross-sections (De Oliveira et al., 1982) 18

Figure 2-13 Geometry of the plastically deforming cross-section (Wierzbicki and Suh, 1988) 20

Figure 2-14 Present computational model of the shell consisting of a system of rings and generators (Wierzbicki and Suh, 1988) 20

Figure 2-15 Quasi-static test rig (Jones et al., 1992) 22

Figure 2-16 Dynamic test rig (Jones et al., 1992) 22

Figure 2-17 Original and deformed cross-section of a pipeline in the plane of impact (Jones and Shen, 1992) 23

Figure 2-18 Brooker's indentation test rig (2005) 23

Figure 2-19 Brooker's dent tools (2005) 24

Figure 2-20 Palmer et al.'s test set-up (2006) 25

Figure 2-21 Alexander's quasi-static test rig (2007) 26

Figure 2-22 Alexander's small scale dynamic test (2007) 26

Figure 2-23 Alexander's full scale dynamic test (2007) 26

Figure 2-24 Sketch for dynamic test with inner pressure (Jones and Birch, 1996) 28

Figure 2-25 Ng and Shen's impact test rig (2006) 29

Figure 2-26 Model test (Gjørsvik et al., 1975) 37
Figure 2-27 Horenberg and Guijt's model test (1987)....................................39
Figure 2-28 Verley et al.'s pipe support (1992)....................................40
Figure 2-29 Schematic of detailed simulation model 49
Figure 2-30 Reduction factor of impact energy....................................53
Figure 2-31 Structure of pipe-in-pipe 58
Figure 2-32 Configuration of bundle (Song et al., 2009) 58
Figure 3-1 Six meter pipes, four different sizes....................................62
Figure 3-2 Pipe cutting....................................63
Figure 3-3 Rubber spacer....................................64
Figure 3-4 Nylon spacer....................................65
Figure 3-5 Beam Shoe(DNV, 2010) 66
Figure 3-6 Different otter board design 66
Figure 3-7 Recommendation of indenters referring to DNV-RP-F111(DNV, 2010) 67
Figure 3-8 Indenter presented in Guidelines for Trenching Design of Submarine Pipelines(Trevor Jee Associates, 1999) 67
Figure 3-9 Set-up I....................................69
Figure 3-10 Set-up I....................................69
Figure 3-11 Set-up II....................................70
Figure 3-12 Set-up II....................................70
Figure 3-13 Set-up II on another rig with simple support boundary condition....................................71
Figure 3-14 (a) Rosette strain gauge (b) single strain gauge 71
Figure 3-15 Layout of the transducers of boundary condition 1 set-up....................................72
Figure 3-16 Layout of the transducers of boundary condition 2 set-up (a) front view (b) 3D view....................................73
Figure 3-17 Pipe end turned up (a) Original position (b) Turn up....................................75
Figure 3-18 Test results of SPS4_BCrigid....................................76
Figure 3-19 Test results of SPS1 to SPS4....................................77
Figure 3-20 Strain gauge reading of outer pipe and inner pipe 78
Figure 3-21 Squeezed rubber spacer....................................78
Figure 3-22 Test results of pipe-in-pipe indentation tests 79
Figure 3-23 Comparison between the SPS4-BCrigid test result and theories of pure denting....................................82

Figure 3-24 SPS4 deformed shape....83
Figure 3-25 SPS4 denting and bending relationship....83
Figure 3-26 De Oliveira theory compare with the test result of SPS4....84
Figure 3-27 Prototype indentation force and indentation energy....86
Figure 4-1 Impact test set-up....92
Figure 4-2 Steel block and the indenter....92
Figure 4-3 Pipe supporting system....93
Figure 4-4 Strain gauge layout of single wall pipe or the outer pipe....94
Figure 4-5 Potentiometers....94
Figure 4-6 Potentiometer attached to the pipe....95
Figure 4-7 A view from high speed camera....95
Figure 4-8 I-SPS2 Impact Force Time History....98
Figure 4-9 I-SPS2 Displacement Time History....98
Figure 4-10 I-SPS2 Force Deflection Relationship....99
Figure 4-11 I-PPSA2-nylon Impact Force Time History....99
Figure 4-12 I-PPSA2-nylon displacement time history....100
Figure 4-13 I-PPSA2-nylon force deflection relationship....100
Figure 4-14 I-PPSB2-nylon impact force time history....101
Figure 4-15 I-PPSB2-nylon displacement time history....101
Figure 4-16 I-PPSB2-nylon Force deflection relationship....102
Figure 4-17 Laser lights and pipe position....102
Figure 4-18 I-SPS2 high speed camera image of the beginning and the end103
Figure 4-19 I-PPSA2-nylon high speed camera image of the beginning and the end....103
Figure 4-20 I-PPSB2-nylon high speed camera image of the beginning and the end....103
Figure 4-21 Indentation Energy versus indenter displacement and bottom deflection....108
Figure 5-1 Deformed shape of PPSB2-nylon with shell element....112
Figure 5-2 Deformed shape of PPSB2-nylon with shell element, thickness rendered....112
Figure 5-3 Single wall pipe quasi-static indentation FE model under set-up I....116
Figure 5-4 Single wall pipe quasi-static indentation FE model under set-up II....117

Figure 5-5 Comparison among different elements of SPS4 118

Figure 5-6 Comparison of SPS4-BCrigid between FE and experiment results 118

Figure 5-7 SPS4_BCrigid failure shape comparison 119

Figure 5-8 Comparison of SPS4 between FE and experiment results 119

Figure 5-9 SPS4 failure shape comparison 119

Figure 5-10 Comparison of SPS1 between FE and experiment results 120

Figure 5-11 Comparison of SPS2 between FE and experiment results 121

Figure 5-12 Comparison of SPS3 between FE and experiment results 122

Figure 5-13 Pipe-in-pipe quasi-static indentation FE model under set-up II 123

Figure 5-14 Uniaxial compression test of rubber 125

Figure 5-15 Comparison between test result and FE results of PPSA2-rubber 126

Figure 5-16 Comparison between test result and FE results of PPSB2-rubber 127

Figure 5-17 Nylon compression and tension test 127

Figure 5-18 Comparison between test results and FE results of PPSA1-nylon 128

Figure 5-19 Comparison between test results and FE results of PPSA2-nylon 129

Figure 5-20 Comparison between test results and FE results of PPSA3-nylon 130

Figure 5-21 Comparison between test result and FE result of PPSB2-nylon 131

Figure 5-22 Impact FE model of single wall pipe 132

Figure 5-23 Impact FE model of pipe-in-pipe 133

Figure 5-24 Test specimen on the test machine 135

Figure 5-25 Strain rate sensitivities according to different models 136

Figure 5-26 Impact force time history of I-SPS2 139

Figure 5-27 Displacement Time History I-SPS2 139

Figure 5-28 Final shape of I-SPS2 140

Figure 5-29 Impact force time history of I-PPSA2 140

Figure 5-30 Displacement time history of I-PPSA2 141

Figure 5-31 Final shapes of I-PPSA2 141

Figure 5-32 Impact force time history of I-PPSB2 142

Figure 5-33 Displacement time history of I-PPSB2 142

Figure 5-34 Final shapes of I-PPSB2..143
Figure 5-35 Boundary condition of quasi-static indentation test..................144
Figure 5-36 Boundary condition of impact test 144
Figure 5-37 Comparison of the quasi-static response and impact response .145
Figure 5-38 Comparison of Strains on the top and bottom for SPS2 146
Figure 5-39 Comparison of strains on the middle cross section for SPS2....147
Figure 5-40 Strain measurements of I-SPS2..147
Figure 5-41 Bottom strain - deflection comparison between impact and quasi-static...148
Figure 5-42 Strain time history from the I-SPS2 FE result 149
Figure 5-43 Maximum Principal Strain of SPS2 149
Figure 5-44 Indentation Energy of SPS2 and SPS2-BC impact...................150
Figure 5-45 Prototype of PPSA2-nylon and PIP12 152
Figure 5-46 Prototype of PPSB2-nylon and PIP14 152
Figure 5-47 Comparison among PIP12, PIP14 and SP16............................155
Figure 5-48 Energy versus indenter displacement or dent depth (displacement up to 240 mm)..155
Figure 5-49 Energy versus indenter displacement or dent depth (displacement up to 100 mm)..156
Figure 5-50 Beam under a concentrated load 157
Figure 5-51 Maximum force of 24 cases and linear fitting curve................162
Figure 5-52 Comparison betweenSPS4-denting FE result and theories of pure denting...164
Figure 5-53 Different theories of plastic moment of deformed cross-section 165
Figure 5-54 Denting and bending alone compare with the FE result of SPS4..165
Figure 5-55 Relationship *b-d* of SPS1 169
Figure 5-56 Relationship *b-d* of SPS2 169
Figure 5-57 Relationship *b-d* of SPS3 170
Figure 5-58 Relationship *b-d* of SPS4 170
Figure 5-59 Indentation force *F* - indenter displacement *u* of SPS1 172
Figure 5-60 Indentation force *F* - indenter displacement *u* of SPS2 172
Figure 5-61 Indentation force *F* - indenter displacement *u* of SPS3 173
Figure 5-62 Indentation force *F* - indenter displacement *u* of SPS4 173

Figure 5-63 Comparison of semi-empirical models of pipe-in-pipes and test data....177

Figure 6-1 Cross-section of the structure and cavity....184

Figure 6-2 FE model of the pipe collapse under pure external pressure....186

Figure 6-3 Result of FE model and Kyriakides' BETPICO result (material X52, ovality 0.2%)(Kyriakides and Corona, 2007a)....186

Figure 6-4 Comparison with Park's result (Figure 13. Comparison of measured and calculated collapse pressures of tubes as a function of dent ovality for various indentor diameters (D/t = 24.2)) (Park and Kyriakides, 1996)....188

Figure 6-5 FE model of denting pipe with simply supported boundary condition and the existence of external pressure....190

Figure 6-6 FE model of denting pipe with rigid boundary condition and the existence of external pressure....190

Figure 6-7 Comparison between FE results and experiment result of SPS4 (EP 4 MPa)....191

Figure 6-8 Deformation Comparison of SPS4 with or without external pressure (EP 4 MPa)....192

Figure 6-9 Comparison between FE results and experiment result of SPS4-BCrigid (EP 4 MPa)....192

Figure 6-10 Deformation Comparison of SPS4-BCrigid with or without external pressure (EP 4 MPa)....192

Figure 6-11 Parametric study of SPS4 under different external pressure....193

Figure 6-12 Parametric study of SPS4-BCrigid under different external pressure....194

Figure 6-13 Collapse points under different boundary conditions and external pressure....194

Figure 6-14 FE model of PPSB2-NYLON with hydrostatic fluid elements 195

Figure 6-15 Comparison between FE results and experiment result of PPSB2-nylon....196

Figure 6-16 PPSB2-nylon under different external pressure....197

Figure 6-17 Comparison between PPSB2-nylon and SPS4 under different external pressure....198

Figure 6-18 Process of reducing internal pressure simulation Final shape: collapsed pipe....200

Figure 6-19 FE model of PPSB2-NYLON with hydrostatic fluid elements 201

Figure 6-20 External pressure and the internal pressure at different steps as well as the deformation of the pipe....202

Figure 6-21 Comparison between PPSB2-nylon with or without internal pressure (IP) 203

Figure 7-1 Free body diagram of the system (G. Horenberg and Guijt, 1987) 209

Figure 7-2 Spacers installed on the inner pipe...211

Figure 7-3 Sand property 212

Figure 7-4 Boundary Condition of the Pipe...212

Figure 7-5 Fixed ends boundary condition (a) Left End (b) Right End........212

Figure 7-6 Fixed ends boundary condition with a shorter pipe section........213

Figure 7-7 Largest dimensions of trawl gear shoes 214

Figure 7-8 Trawl gear borrowed from SEAFISH Authority 214

Figure 7-9 Weight of F beam trawl..215

Figure 7-10 Solid beam trawl (S)...215

Figure 7-11 Load Cells in between the warp line 216

Figure 7-12 Scaled Warp-line 217

Figure 7-13 (a) Winch (b) Speed sensor installed on the Winch.................218

Figure 7-14 Experiment Design...220

Figure 7-15 Set-up for different angles..221

Figure 7-16 Wire potentiometer connection (a) Sketch (b) Set-up...............223

Figure 7-17 3-Axial Accelerometer on the beam trawl 224

Figure 7-18 Pull-over force time history of PIPAB-FDF1-1-90 226

Figure 7-19 Displacement time history of PIPAB-FDF1-1-90....................227

Figure 7-20 Tension time history of PIPAB-FDF1-1-90.............................227

Figure 7-21 Liner relationship of maximum tension & maximum displacement...228

Figure 7-22 Acceleration time history of PIPAB-FDF1-1-90 229

Figure 7-23 Pull-over force time history of SPSD-FSF1-1-60....................230

Figure 7-24 Pull-over force time history of SPSD-FSF1-1-60....................230

Figure 7-25 Crossing at different angles under FSS2 condition..................231

Figure 7-26 Crossing at different angles under FSF1 condition..................232

Figure 7-27 PIPAB-FSF1-1-30 sliding along the pipe (a) the right shoe impacts the pipe (b) the right shoe slides along the pipe (c) the trawl beam slides on the pipe (d) the left trawl shoe cross the pipe (Black solid line: pipe, Yellow dash line: trawl beam)....................233

Figure 7-28 SPSD-FSS1-1-30 (a) Right shoe impacts (b) Right shoe slides (c) Trawl beam slide (d)Left shoe blocked by the connector (Black solid line: pipe, Yellow dash line: trawl beam)................................234

Figure 7-29 SPSD-FSS2-1-30 (a) Right shoe impacts (b) Right shoe slides (c) Trawl beam slide (d)Left shoe crosses the pipe (Black solid line: pipe, Yellow dash line: trawl beam) 234

Figure 7-30 SPSD-FSS3-1-30 left shoe crosses the pipe (Black solid line: pipe, Yellow dash line: trawl beam) 235

Figure 8-1 Comparison among SPSD, PIPAB and PIPABS at FDS2 condition..238

Figure 8-2 Comparison among SPSD, PIPAB and PIPABS at FDF1 condition..239

Figure 8-3 Prototype Force by Froude scaling 241

Figure 8-4 Replot data of Moshagen and Kjeldsen's...................................243

Figure 8-5 Pipe-in-pipes with different Boundary conditions 244

Figure 8-6 Single wall pipes with SSS2 conditions.....................................246

Figure 8-7 Single wall pipes with FDS2 conditions 246

Figure 8-8 Single wall pipes with FDF1 conditions 247

Figure 8-9 Pipe-in-pipe with SSS2 conditions...247

Figure 8-10 Pipe-in-pipe with FDS2 conditions..248

Figure 8-11 Pipe-in-pipes with FDF1 conditions 248

Figure 8-12 Single wall pipe & pipe-in-pipe with SSS2 conditions............249

Figure 8-13 Single wall pipe & pipe-in-pipe with FDS2 conditions............249

Figure 8-14 Single wall pipe & pipe-in-pipe with FDF1 conditions............249

Figure 8-15 Pipe-in-pipe with different spacing..250

Figure 8-16 Pipe-in-pipes with different length...250

Figure 8-17 Pipe-in-pipes with different water depth (S trawl gear)............251

Figure 8-18 Pipe-in-pipes with different water depth (F trawl gear)............252

Figure 8-19 Pipe-in-pipes with different kinetic energy..............................253

Figure 8-20 Pipe-in-pipes with same kinetic energy 253

Figure 8-21 F trawl gear moving at different velocities 254

Figure 8-22 Pull-over force time history of PIPAC-FDF3-1-90 255

Figure 8-23 Forces on a moving trawl gear 256

Figure 8-24 Baseline forces of different cases...258

Figure 8-25 S trawl gear moving at different velocities 259

Figure 8-26 Maximum pull-over force versus velocity 260

Figure 8-27 Maximum delta force versus velocity......................................260

Figure 8-28 Warp force for Perfect door as a function of velocity^2 (JEE Ltd, 2003)...261

Figure 8-29 Maximum pull-over force versus $V(MK)^{0.5}$...............................262

Figure 8-30 Maximum pull-over force versus $V(MK)^{0.5}$ of S and F trawl gear...263

Figure 8-31 Delta force versus $V(MK)^{0.5}$ of S and F trawl gear....................263

Figure 8-32 Model test of PIPAB scaled by Froude scaling law..................269

Figure 8-33 Model test of PIPAB scaled by Froude scaling law..................270

Figure C-1 Specimen Size 290

Figure C-2 SPS1 tensile test result...292

Figure C-3 SPS2 tensile test result...293

Figure C-4 SPS3 tensile test result...293

Figure C-5 SPS4 tensile test result...294

Figure C-6 SPS1 stress-strain curve in plastic range...................................296

Figure C-7 SPS2 stress-strain curve in plastic range...................................296

Figure C-8 SPS3 stress strain-curve in plastic range...................................297

Figure C-9 SPS4 stress strain-curve in plastic range...................................297

Figure E-1 Dimensions of SEAFISH trawl gear..301

Figure E-2 Small scale trawl shoe design..302

Figure E-3 Small scale beam dimension..303

List of Symbols

Abbreviations

DNV	Det Norske Veritas
FE	Finite Element
NUS	National University of Singapore
PIP	Pipe-in-Pipe

Symbols

B	Half of the trawl board height
C_b	Factor of effective mass, 0.5 for beam trawl and 1 for clump weight
C_h	Span height correction factor
C_F	Empirical coefficient of pull-over force based on laboratory and full-scale data
D	Diameter of the pipe
E	Energy
ΔE	Kinetic energy change
E_d	Indentation energy

E_i	Impact energy absorbed by the pipe
E_{ia}	Impact energy of added mass
E_{is}	Impact energy of steel mass
F_0	Full plastic bending force
F_b	Bending force
$F_{b(tb)}$	Impact force due to trawl board bending action
F_d	Indentation force
F_p	Pull-over force
H_{sp}	Span height
I	Second moment of pipe’s cross section area
I_g	Steel mass of the gear
k	Stiffness of the warp-line
$k_{b(tb)}$	Lateral bending stiffness of the board
L	Half the pipe length
M	Trawl gear steel mass
M_a	Trawl gear added mass
M_c	Plastic moment capacity of the pipe’s cross-section (deformed)
M_{0c}	Full plastic moment of the pipe’s cross-section $M_{0c} = \sigma_0 t D^2$

M_{0t}	Full plastic Moment $M_{0t} = \sigma_0 t^2/4$
$m_{e(tow)}$	Mass of the steel of the trawl gear plus the added mass
N	Tension force in the pipe
N_0	Plastic tension capacity of cross-section
P	External pressure
P_c	Collapse pressure
Q	Coefficient in Cowper-Symonds model
q	Coefficient in Cowper-Symonds model
R	Pipe radius
R_{fa}	Reduction factor depending on the pipe diameter and the soil type
R_{fs}	Reduction factor depending on the outer pipe diameter
S	Span length
t	Pipe wall thickness
T	Pull-over time
T_f	Factor, 2 for trawl boards and 1.5 for beam trawls
V	Tow velocity
β	Scale factor $\beta = l/L$
δ	Dent depth at one side
δ_p	Displacement of the pipe in the pull-over response

ε_b	Bending strain
ε_{bc}	Critical bending strain
η	Pipeline usage factor
κ	$\kappa = 150$, empirical factor in Ellinas and Walker's formula
σ_{d0}	Longitudinal compressive stress
σ_0	Yield stress.
$\sigma_0{}'$	Dynamic yield stress
u	Velocity after pull-over
υ	Velocity after pull-over
ψ	Velocity after pull-over
ω	Central deflection at the point of impact

1 Introduction

1.1 Background

In the very beginning, pipelines in the North Sea were all trenched. Trenching is a very expensive way to protect the pipe. Sometimes the pipe needs to be trenched because the pipeline is not stable on the seabed, and sometimes the pipe needs to be trenched to provide protection against fishing activities.

The first line that was not trenched was the Shell FLAGS line in 1979. Shell conducted extensive research to demonstrate that this pipeline can resist the trawl gear interaction and trawl force. Based on research carried out between 1974 and 1980, the industry developed a consensus that the pipelines less than 16 inches in diameter should be buried.

With the growing trend towards deep water development and the economical requirement, engineers considered the possibility to lay smaller diameter pipe on the seabed. In 1999, a Joint Industry Project sponsored by many oil companies investigated this possibility and developed the "*Guidelines for Trenching Design of Submarine Pipelines (Trevor Jee Associates, 1999)*". This trenching guideline was set up by Trevor Jee Associates, and provided methods, models and criteria of trawl gear interaction with pipeline. In the trenching guideline, the trenching decision is based on a quantitative risk assessment to determine the probability of damage and the subsequent lifetime costs of the pipeline, which means that even below 16 inches diameter, the pipe might be able to lay on the seabed if the risk of damage is low and the subsequent lifetime costs are less than the trenched pipeline option.

In 1990s, there was an extensive model test program carried out by Verley (1992), and this formed another source of a guideline, the DET NORSKE VERITAS (DNV) recommended practice DNV-RP-F111.(Longva et al., 2013) Based on the test results, Verley (1994) suggested that the pipe smaller than 16 inch (406.4 mm) might sometimes be laid on the seabed, but that the pipe larger than 16 inch (406.4 mm) might sometimes be unsafe to lay on the seabed. More analysis is needed. Therefore, the DNV-RP-F111 is to provide the guidance on design methods of the pipeline subjected to the trawl load. Criteria are given to ensure the pipe's integrity under trawl gear crossing. They are applicable to a pipeline with a diameter larger than 10 inch.

Recently, some researchers' work indicated that the method of DNV-RP-F111 is too conservative, and more work is being done to improve the methods and criteria.

1.2 Motivation

The existing methods are mainly applicable to single wall pipes. Nowadays, an increasing number of pipe-in-pipe systems are used for transportation of oil, because of their significantly better thermal insulation than the single pipe system. The pipe-in-pipe system can provide *U*-values less than 0.5 *W*/m by using highly efficient insulation materials such as low-density polyurethane, rock wool or aerogel, and also because the insulation system is protected from external pressure and water ingress. This development raises questions about the trenching decision for pipe-in-pipe, as the previous research and guidelines are aimed at single wall pipe. The outer pipe of pipe-in-pipe is not required to resist internal pressure and can accommodate a greater level of indentation than a single, pressure-containing pipe. Therefore, to apply the same methods and criteria of single wall pipes to pipe-in-pipe systems might result in a conservative result and lead to unnecessary trenching. The trenching decision for the pipe-in-pipe system with outer diameter more than 16 inch (406.4 mm) is more straight-forward; however, for the pipe-in-pipe system with outer diameter less than 16 inch, the trenching decision should be based on reliable analysis results.

In order to gain a better understanding of the overtrawlability of pipe-in-pipe which relates to the trenching decision directly, and also because there is little guidance available for the overtrawlability of pipe-in-pipe, a research programme were initiated by SUBSEA 7, one of the leading contracting companies in the Oil and Gas Industry and carried out as a Ph.D. research program in National University of Singapore.

1.3 Objective and Scope

1.3.1 Objective of Research

In order to understand the overtrawlability of pipe-in-pipe and to arrive at a reasonable trenching decision, the mechanical behaviour and pipe-in-pipe's force-deformation characteristics under trawl gear crossing should be investigated. When trawl gear crosses a pipeline on the seabed, the responses are two phases. Firstly, the trawl gear impacts the pipeline, and this phase only lasts some hundredths of a second, and mainly gives the pipe a local deformation. The second phase is pull-over. It lasts longer than the impact phase, and induces a more global response of the pipeline (DNV, 2010). Both the impact phase and the pull-over phase have to be studied.

Therefore, the over-arching objective of the present research is to develop methods to assess the overtrawlability of pipe-in-pipes in order to make reasonable trenching decision for pipe-in-pipes. It can be achieved by following sub-objectives:

- To review and improve the methods of overtrawlability analysis of single wall pipes.
- To investigate the mechanical behaviour of impact response of pipe-in-pipes.
- To establish Finite Element (FE) models to simulate the impact response of pipe-in-pipes.
- To generalize the load-deformation characteristics of the pipe-in-pipe under trawl gear impact.
- To investigate the pipe-in-pipe’s impact response under external pressure, as well as to investigate the failure mode under different load combinations.
- To study the mechanical behaviour of pull-over response of pipe-in-pipe to identify the important parameters.
- To improve the model test methodology for future pull-over tests.

1.3.2 Scope of Research

This research is applicable to pipe-in-pipe systems, with rigid outer pipes and inner pipes. Both the inner pipe and the outer pipe are bare pipes, without concrete coating or any other coatings. The diameters of the outer pipes are not more than 16 inches, and the diameter/thickness ratios of the outer pipes are about 25. The diameter/thickness ratio of the inner pipe is about 15. The inner pipes are centralized by the spacers, and therefore the spacer material and spacing distance are considered. The insulation material in between the outer pipe and the inner pipe is not considered here because it is very soft material. Only the impact response and the pull-over response are considered in this PhD programme.

The results of this research will help pipeline engineers to develop rational trenching decisions for pipe-in-pipe systems. All these results are based on research on a pipe-in-pipe structure; however, some of the results are applicable to bundles, an alternative pipe-in-pipe system, as well as to other geometrically similar systems.

1.4 Layout of Current Thesis

There are altogether nine chapters. Chapter 2 is the literature review. Chapter 3 and Chapter 4 describe the quasi-static indentation test program and impact test program. Chapter 5 develops and validates their FE models respectively, and based on that demonstrates that quasi-static analysis can be used to determine the impact response. Moreover, based on the experimental and FE results, the load-deformation characteristics of the pipe-in-pipe under trawl gear impact is studied and semi-empirical models are developed. Chapter 6 analyzes the impact response under external pressure, as well as the situations that the internal pressure, external pressure and dents are all involved. Chapter 7 describes the pull-over tests, including the objective of the test, the design and the test results. Chapter 8 discusses the pull-over model tests results, conducts the parametric study, and investigates the scaling law. Chapter 9 concludes the whole thesis, and suggests future work.

2 Literature Review on Overtrawlability of Subsea Pipelines

2.1 Trawl Gear

There are many fishing methods in the water column as Figure 2-1 shows. Different trawling methods are used to capture different fish species. Among them, bottom trawling creates possible hazards for subsea pipelines.

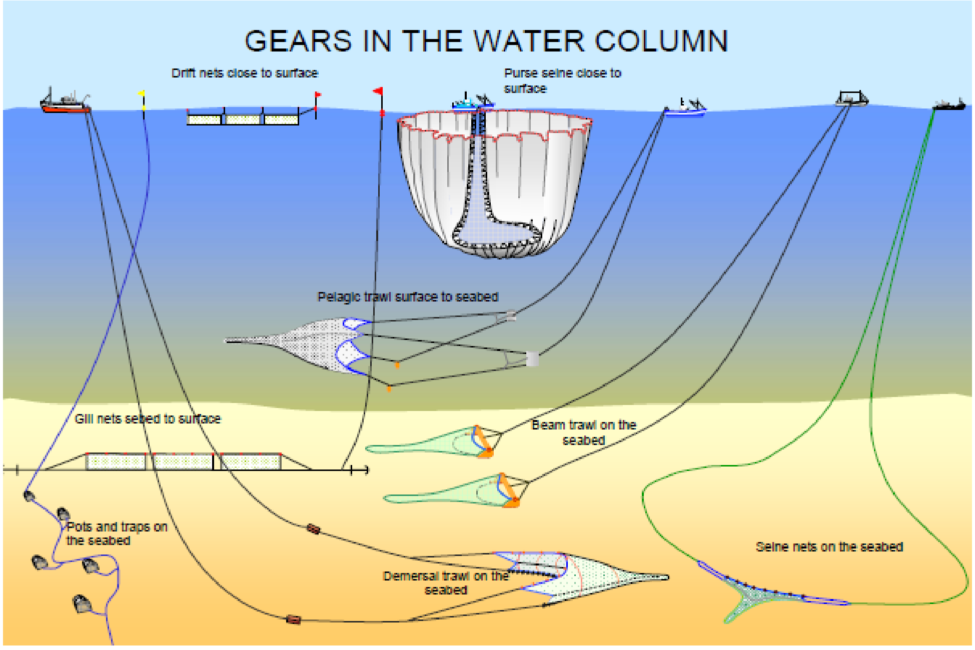
GEARS IN THE WATER COLUMN
Drift nets close to surface
Purse seine close to surface
Pelagic trawl surface to seabed
Gill nets seabed to surface
Beam trawl on the seabed
Pots and traps on the seabed
Demersal trawl on the seabed
Seine nets on the seabed

Figure 2-1 Fishing methods (SEAFISH, 2005)

There are mainly three types of bottom trawling method: demersal trawl on the seabed using otterboard (different name of “trawl door” “trawl board”), beam trawl and twin trawling with clump-weight. One kind of Twin trawl systems is illustrated as Figure 2-2. There are two otterboards at the sides and one clump weight in the middle. There are mainly six otterboard types: Flat otterboard, Vee otterboard, Camber otterboard, Oval otterboard, Slot otterboard and Multi-foil/slot otterboard (SEAFISH et al., 1995) as Figure 2-3 shows. Otterboard designs are continously being improved upon.

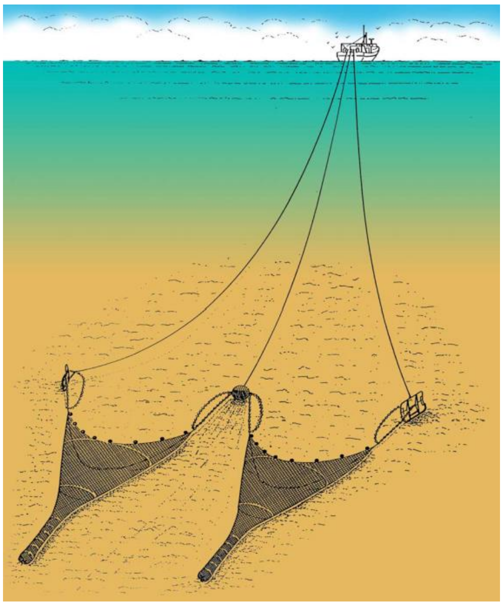

Figure 2-2 Twin rig (SEAFISH, 2005)

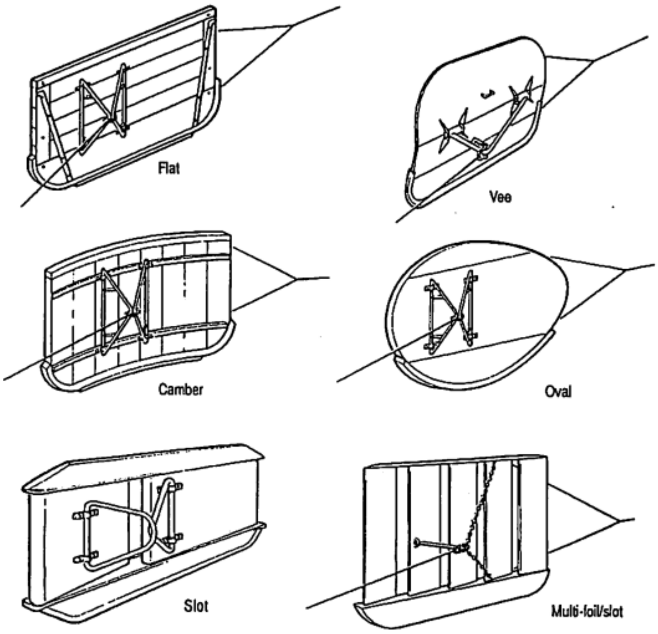

Figure 2-3 Otterboards (SEAFISH et al., 1995)

The beam trawl is one of the earliest forms of towed fishing gear. The net is held open by the steel frame; therefore, it does not depend on the towing speed as the otterboard does. The beam trawl moves on the seabed with a velocity around 3 m/s (5.8 knots). A typical beam trawl is shown in Figure 2-4, which has a heavy steel beam in the middle connecting two steel beam shoes at the end. The vessel is connected to the beam trawl by the warp line and towing chains.

The most popular type in the North Sea and the Norwegian Sea is the otterboard. The number of clump weight trawls is decreasing because of the fuel consumption issue. The beam trawl is not as popular as the otterboard, but it might induce a more critical damage force to the pipeline.

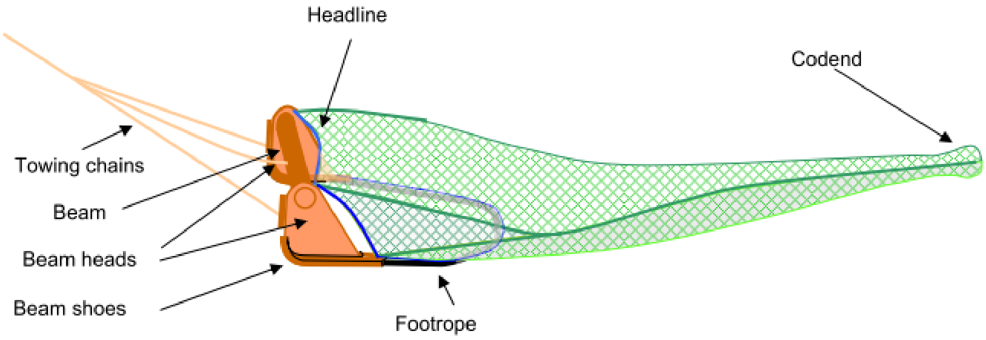

Figure 2-4 Beam Trawl (SEAFISH, 2005)

The type of trawl gear directly influences the damage loading as well as the response. Therefore, basic data including the trawling gear category, trawl gear equipment type, shape, size, mass, trawl speeds and the frequency of crossing over the pipeline are important to determine the damage energy (DNV, 2010).

DNV has listed the largest trawl gear data of the North Sea and Norwegian Sea in 2005 as Table 2-1shows. According to that, the clump weight is the heaviest, up to 9000 kg, and the beam trawl moves the fastest, up to 3.4 m/s. The *Guidelines for trenching design of submarine pipelines (Trevor Jee*

Associates, 1999) also gives the typical fishing gear parameters in the appendix A. These data are more detailed, but might be older than the DNV data. With developments in the fishing industry, these data are always changing and different from place to place. Nowadays, the weight of the trawl board in the North Sea, Norwegian Sea and the Barents Sea has increased to possibly more than 6000 in 2013, and the velocity has increased up to 4 m/s (Emesum, 2013).

Table 2-1 Data for largest trawl gear in the use in the North Sea and the Norwegian Sea in 2005 (DNV, 2010)

	Consumption	**Industrial**	**Beam**	**Clump Weight**
Mass (kg)	4500	5000	5500	9000
Dimension *l*x*h* (m)	4.5x3.5	4.9x3.8	17 2)	1)
Trawl velocity (m/s)	2.8	1.8	3.4	2.8

1) Typical dimension of the largest clump weights of 9 tonnes are l=4 m wide (i.e. length of roller) by 0.76 meter diameter cross section. For smaller size roller type clump weights (i.e.3500 to 6000 kg), the width l is typically 3.2 m, whereas the roller diameter is unchanged.

2) Beam trawl length (i.e. distance between outside of each shoe)

When the trawl gear crosses a pipeline, the response is normally considered in two phases. The first phase is impact, which may cause a dent in the pipe wall. The second phase is pull-over which leads to the bending of the pipe at the contact point. Sometimes, though not often, trawl gear might be hooked by a pipeline, which is dangerous because the intense loading will give the pipeline a large lateral deflection and also put the fisherman in danger (Trevor Jee Associates, 1999).

Although there is little research about the overtrawlability of pipe-in-pipe, the overtrawlability of single wall pipe has been investigated and many conclusions are published. The following sections summarize the state-of-the-art of the overtrawlability of single wall pipes.

2.2 Impact Response

Impact is the first phase of trawl gear interaction. The impact loads are the transfer of kinematic energy from the trawl gear, which constitutes effective masses with effective velocity. Before impact, the system only contains kinetic energy. During the impact, part or all the kinetic energy transforms into strain energy, vibration energy, and thermal energy. After the impact, part of the strain and vibration energy might convert back to kinetic energy. (Emesum, 2013)

The impact energy induces pipe deformations. As the edges of the trawl gear are relatively sharp and because of the way the trawl gear moves, the trawl gear impact problem may be idealized as a knife edge indenter impacting a pipeline transversely. There are various researches carried out to study the relationship of force and deformation of this kind.

A ring under the compression load has been studied by DeRuntz and Hodge (1963) and Reid and Reddy (1978). The model is shown in Figure 2-5. Deruntz and Hodge(1963) analysed the load-deflection relationship based on the rigid-perfectly plastic theory while Reid and Reddy considered the strain hardening effect. Figure 2-5 shows the system of forces and moments on a quadrant of the tube. Based on the analysis, the equation of the force and deflection relationship is shown in equation (2.1).

$$F_d = \frac{4M_{0t}}{R(1-(\delta/R)^2)^{1/2}} \tag{2.1}$$

where F_d is the indentation force, R is the radius, δ is the dent depth at one side and $M_{0t} = \sigma_0 t^2/4$, σ_0 is the yield stress.

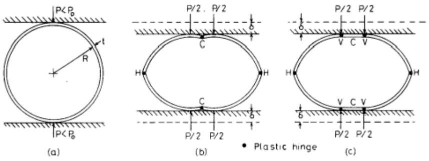

Figure 2-5 (a) Unreformed tube geometry and loading arrangements; (b) DeRuntz and Hodge collapse mode (1963); (c) Reid and Reddy (1978)

Morris (1971) used the indentation test rig in Figure 2-6 for small scale pipe indentation tests under quasi-static condition. The pipe was subjected to two equal and opposite loads, different from most indentation tests. The experiments were with or without edge constraints. The specimen was an aluminium alloy tube of 6.788 inch (172.4 mm) nominal diameter and 0.064 inch (1.63 mm) wall thickness. The specimen length was 2 ft. In the test, displacement and indentation loads were recorded. The result showed that the end conditions greatly affect the elastic-plastic behaviour.

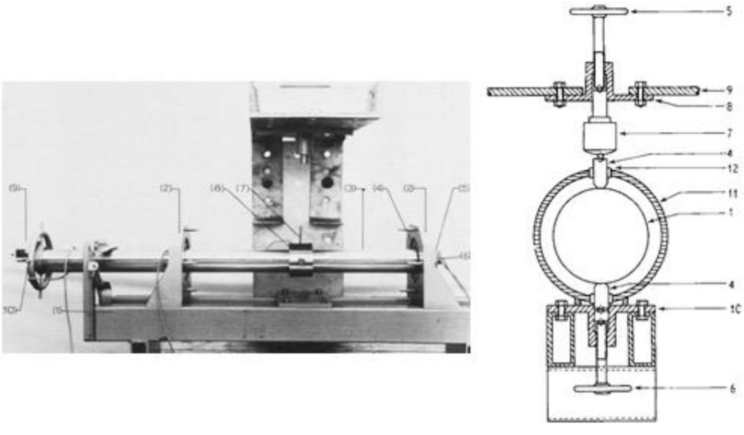

Figure 2-6 Morris indentation test rig (1971)

Soreide and Amdahl (1982) conducted indentation tests both quasi-statically and dynamically. The test rig is shown in Figure 2-7. Both ends were fully clamped. The load was applied by a hydraulic actuator. A rectangular indenter was connected to the actuator, and the bottom width was 50 mm. In the quasi-static phase, the hydraulic actuator applied the displacement at a rate of 0.15 mm/s. In the dynamic phase, the rate was changed to 54 mm/s. Although the hydraulic actuator gave a higher rate, it is not considered as an impact test.

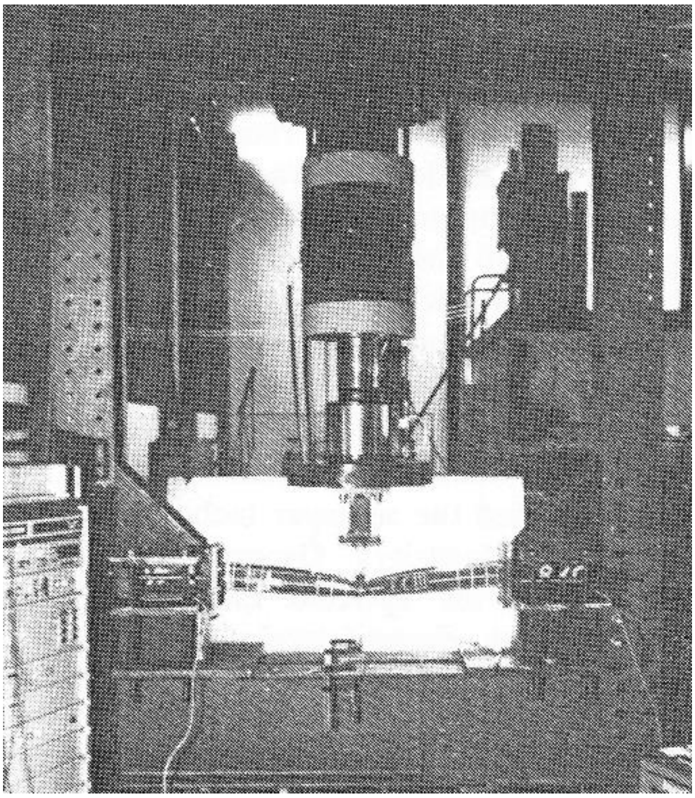

Figure 2-7 Soreide and Amdahl’s indentation test rig (1982)

They derived a static rigid-plastic method to analyse a fully-clamped beam under three-point bending. However, they did not consider the effect of changing of the cross-sectional shape, therefore, the relationship is similar to the beam bending theory.

$$\frac{F_d}{F_0} = \sqrt{1 - \left(\frac{\omega}{D}\right)^2} + \frac{\omega}{D} arc\, sin \frac{\omega}{D}; \quad \frac{\omega}{D} \leq 1$$

$$\frac{F_d}{F_0} = \frac{\pi}{2}\frac{\omega}{D}; \qquad \frac{\omega}{D} > 1$$

(2.2)

where D is the pipe diameter, ω is the central deflection at the point of impact and $F_0 = {}^{4M_{0c}}/_{L} = {}^{4\sigma_0 D^2 t}/_{L}$, L is half the pipe length.

During the denting interaction, the cross-section change is not only because of ovalization but mainly because of denting. Some other researchers considered the cross-section geometry change is due to indentation in the bending deformation.

Thomas et al. (1976) conducted a series of quasi-static indentation tests with the test rig shown in Figure 2-8. The specimens were small-scale aluminium alloy and steel tubes, and simply supported over various span lengths. The experiment aimed to study the effect of various parameters: diameters D, wall thickness t, D/t and span length S. The D/t ratio was from 27 to 190, and the span was 3 inch to 11 inch. The denting tool was a knife edge indenter, which dented the pipe transversely. However, the specimen length was too short, and therefore a large deformation occurred at both ends. According to the experiment, there were three modes of the deformation: a pure crumpling phase occurred first, followed by a bending and crumpling phase and finally a structural collapse phase. If the D/t ratio was bigger, the second phase started later. If the span was larger, the deformation in the first phase was reduced.

However, the three modes only applied to the pipes with similar D/t ratio as in the experiments.

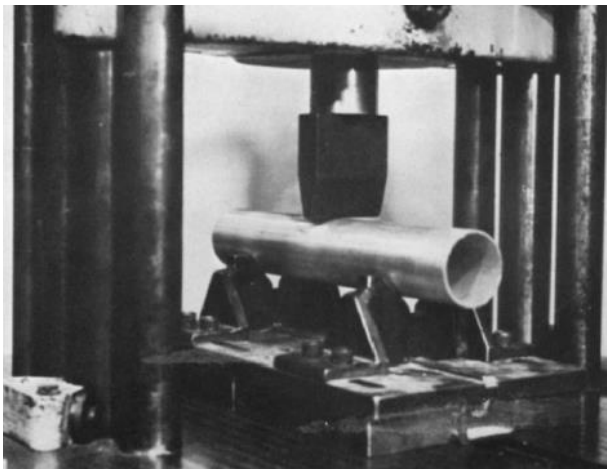

Figure 2-8 Thomas et al. indentation test rig (1976)

Based on the experiments carried out by Thomas et al. (1976), a model of dent force and dent depth relationship was developed by Ellinas and Walker (1983). The formula is a semi-empirical equation. As shown in (2.3), κ is an empirical factor that was chosen using the experiment results reported in references (Thomas et al., 1976).

$$F_d = \kappa M_{0t}(\frac{\delta}{D})^{1/2} \tag{2.3}$$

where $\kappa = 150$.

Integrating the dent force, the indentation energy has the relationship with the dent depth as following equation shows

$$\delta = \sqrt[3]{\frac{D \cdot {E_i}^2}{(25 \cdot \sigma_0 \cdot t^2)^2}} \tag{2.4}$$

where E_i is the impact energy absorbed by the pipe.

Ellinas and Walker (1983) studied overall bending damage. They indicated that the end support condition influences the response considerably. To maintain a conservative approach, they assumed that the ends were fully restrained. They treated the denting and bending separately, which means they assumed the denting phase ceases immediately before the global deformation occurs. As a result, the bending response included the consideration of the cross-section changing because of the denting. They assumed the deformed shape of the cross-section as Figure 2-9 shows. Therefore, the plastic moment capacity of the tube's cross-section changes to the equation (2.5).

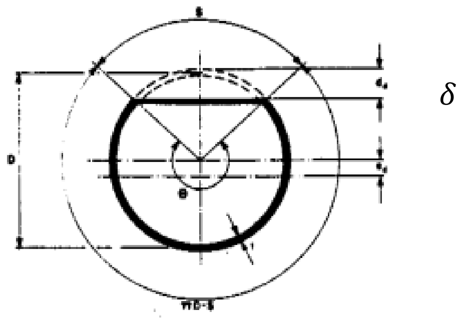

Figure 2-9 Deformed shape of the cross-section (1983)

$$M_c = \sigma_0 D^2 t \cdot (cos\chi - \chi) \tag{2.5}$$

where $\chi = \left(\frac{\delta}{D}\right)^{1/2}\left[1 - \frac{\sigma_{d0}}{\sigma_0}\right]$ and $\sigma_{d0} = \sigma_0 \left(\frac{D}{t}\right)\left[\sqrt{\frac{16}{9}\left(\frac{\delta}{D}\right)^2 + \left(\frac{t}{D}\right)^2} - \frac{4}{3}\left(\frac{\delta}{D}\right)\right]$

which is the longitudinal compressive stress that applies in the damaged part of the tube's cross-section.

Therefore, the relationship between the load related to the bending is given in equation (2.6). If there is no dent depth, the equation reverts to represent the beam with the original cross-section shape.

$$F_b = \frac{4\sigma_0 D^2 t}{L}\left[1 + \frac{\sigma_0 D^2 t \cdot (cos\beta - \beta)}{\sigma_0 D^2 t}\right] \tag{2.6}$$

where F_b is the bending force.

De Oliveira et al. (1982) studied this issue and came out with a simple closed form solution. They simplified this problem by transforming the 3-D problem into two 2-D problems. They assumed that the external thin shell can only take extensions, and in addition a series of rings takes the crushing load. Moreover, they also used a square section to represent the circular section, based on the comparison that the plastic moments for both the square section and the circular section were about the same. The relationship between the indentation force and the dent depth was given as equation (2.7).

$$F_d = 4Dt\sigma_0\sqrt{\pi\frac{t\delta}{D^2}\left[1 - \frac{1}{2}(n-1)^2\right]} \tag{2.7}$$

where D is the diameter, t is the thickness, n equals to 1 for fully clamped boundary condition and equals to 0 for simply supported and free to slide condition. This work forms the theory base for the equation 3.5 in DNV-RP-F111. (Mellem et al., 1996)

De Oliveira et al. (1982) also treated the denting phase and the bending phase separately. They considered the reduced plastic bending moment because of the deformed cross-section. The deformed cross-section of the circular tube is shown in Figure 2-10. They used a square cross-section shown in Figure 2-11 to represent the deformed cross-section of a tube based on the comparison that the plastic bending is similar between them as Figure 2-12 shows. Moreover, they simplified it further by introducing a linear best fit curve. The plastic moment took the form given in equation (2.8).

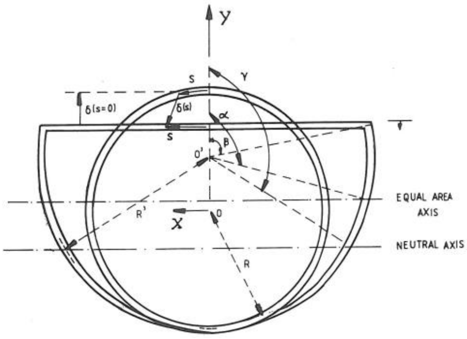

Figure 2-10 Deformed cross-section (De Oliveira et al., 1982)

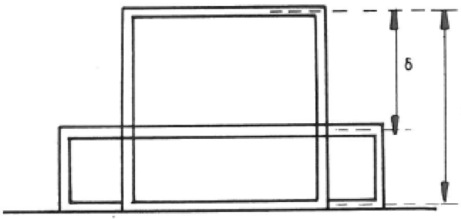

Figure 2-11 Approximate cross-section (De Oliveira et al., 1982)

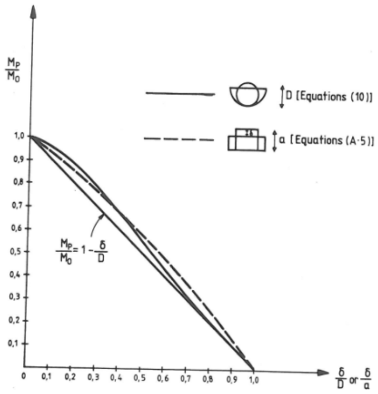

Figure 2-12 Plastic moment of different cross-sections (De Oliveira et al., 1982)

$$\frac{M_c}{M_{0c}} = 1 - \frac{\delta}{D} \tag{2.8}$$

Considering the cross-section is not changing everywhere, at the hinge, the plastic moment is $C_c M_{0c}$ and at others the plastic moment is $C_s M_{0c}$, and $C_s M_0 > C_c M_0$. For fully clamped ends, the relationship of bending force and deflection is shown as equation (2.9). For simply supported tube, the relationship changes to the form in equation (2.10).

$$\frac{F_b}{4M_0/L} = \frac{1}{2}\left[\left(2 - \frac{\delta^*}{D}\right) cos\left[\frac{\pi N}{2N_0}\right] + \frac{\pi N}{N_0}\frac{\omega}{D}\right]$$

(2.9)

$$\frac{F_b}{2M_0/L} = (1 - \frac{\delta^*}{D})$$

(2.10)

where δ^* is the dent depth when global deformation begins, when the local deformation ceases, N is the tension force in the pipe, and N_0 is the plastic force capacity of cross-section.

Wierzbicki and Suh (1988) developed the theory by dropping the approximate representation of the cross-section. The original and deformed cross-sections are shown in Figure 2-13. They were again idealized this problem into two 2-D problems, as shown in Figure 2-14. The tube was treated as a bundle of unconnected generators and rings. The generators and the rings were loosely connected in order to make the lateral deformations compatible. The shear effect was ignored. The rings were only allowed to take the circumferential bending, and not allowed to extend. The generators were actually rigid-plastic beams, which can be bent and stretched. But the stretch effect was ignored as it was so small.

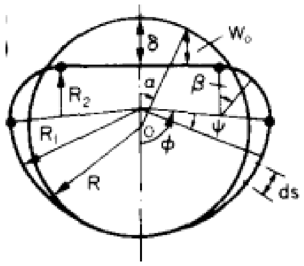

Figure 2-13 Geometry of the plastically deforming cross-section (Wierzbicki and Suh, 1988)

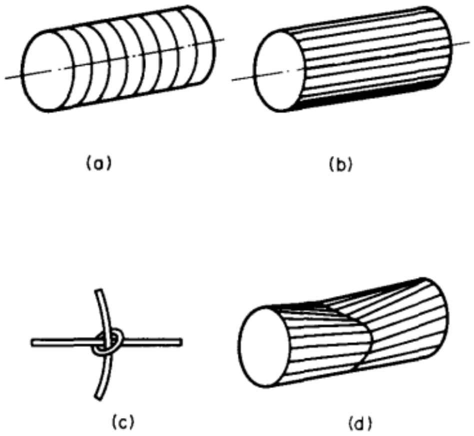

Figure 2-14 Present computational model of the shell consisting of a system of rings and generators (Wierzbicki and Suh, 1988)

The relationship of indentation force and deflection is described by equation (2.11).

$$\frac{F_d}{M_{0t}} = 16\sqrt{\frac{\pi}{3}}\sqrt{\frac{D}{t}\frac{\delta}{R}}\sqrt{1-\frac{1}{4}\left(1-\frac{N}{N_0}\right)^3} \tag{2.11}$$

where N is the tension force in the pipe, and N_0 is the plastic force capacity of cross-section. $N=N_0$ when the tube is fully clamped, and $N=0$ when the tube is simply supported.

When the pipe is totally free for the rotational and axial motion, the indentation force and displacement relationship change to equation (2.12).

$$\frac{F_d}{M_{0t}} = 16\sqrt{\frac{\pi}{16}\frac{\delta}{R}\frac{D}{t}}$$

(2.12)

This model was based on a rigid-plastic assumption, and neglected shear effects. Both Palmer et al. (2006) and Alexander (2007) have demonstrated that the equation can provide a reasonable accurate solution. Wierzbicki and Suh (1988) only considered the local deformation and did not consider the global deformation.

To treat the denting and bending phase separately as Ellinas et al. and De Oliveira et al. did is oversimplified. Reid and Goudie (1989) pointed out that according to their experiment results that the global deformation was from the beginning of the load process. They also claimed that the relationship of local deformation and global deformation relates to the plastic collapse mechanism and the elastic bending stiffness of the entire tube. They also commented on using the rigid-plastic material property. By using this, the dent length was overestimated, and the dent depth when the global deformation occurs was significantly underestimated.

Based on the test results, Reid and Goudie (1989) developed a semi-empirical relationship to consider the denting and bending together. They assumed the indenter displacement is the sum of the dent depth and the bottom central deflection. The ratio of the indenter displacement and dent depth has to be decided by at least one experiment. The stiffness of the local denting and the stiffness of the global bending like two different springs in series and their stiffness are changing along with the deformation.

Jones et al. (1992) at the University of Liverpool conducted a series of indentation tests on pipelines including quasi-static tests and dynamic impact. The quasi-static test rig is shown in Figure 2-15 and the dynamic test rig is shown in Figure 2-16. The indenter for all the tests was a 15 degree wedge-shape indenter. The specimen was fully clamped at both ends, and the span was ten times the diameter. However, according to Jones' descriptions and the test results, the specimen was not fully clamped in large displacement conditions as the end constraints were not strong enough.

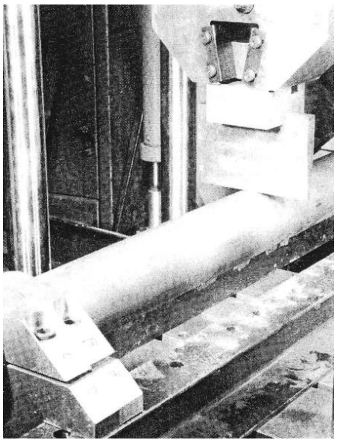

Figure 2-15 Quasi-static test rig (Jones et al., 1992)

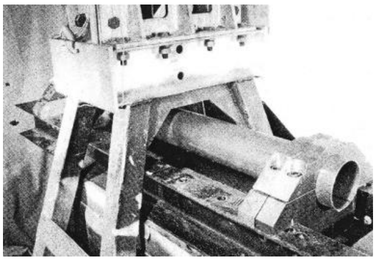

Figure 2-16 Dynamic test rig (Jones et al., 1992)

Jones and Shen (1992) presented a theoretical study of the lateral impact of fully clamped pipelines. Differently from Wierzbicki and Suh, the cross-section that they chose is shown in Figure 2-17. Consequently the fully plastic bending moment capacity of the dented cross-section is different from previous ones. Series equations had been developed, and to solve the equations needs the numerical procedure. Their method loses the simplicity of having a simple closed form equation.

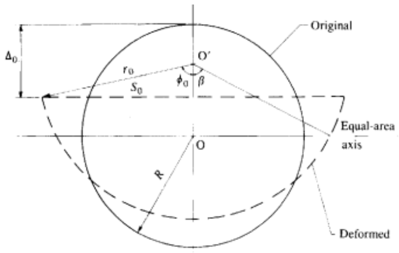
Original
Δ_0
O'
r_0
S_0
ϕ_0
β
Equal-area axis
O
R
Deformed

Figure 2-17 Original and deformed cross-section of a pipeline in the plane of impact (Jones and Shen, 1992)

Brooker (2005) conducted a series of pipeline puncture tests. The test rig is shown in Figure 2-18, which is a universal testing machine. Five denting tools were designed for these tests as Figure 2-19 shows. The boundary condition was different from previous indentation test. The pipe rested on a sand surface, and was restrained by belts at both ends.

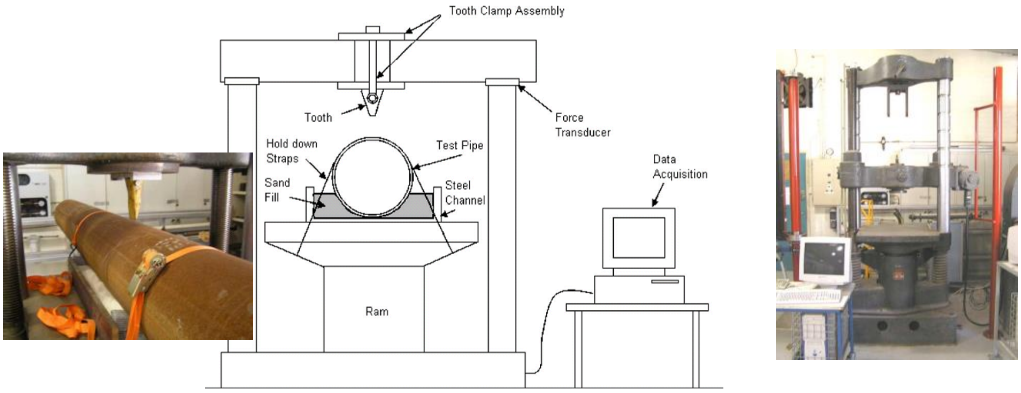
Tooth Clamp Assembly
Tooth
Force Transducer
Hold down Straps
Test Pipe
Data Acquisition
Sand Fill
Steel Channel
Ram

Figure 2-18 Brooker’s indentation test rig (2005)

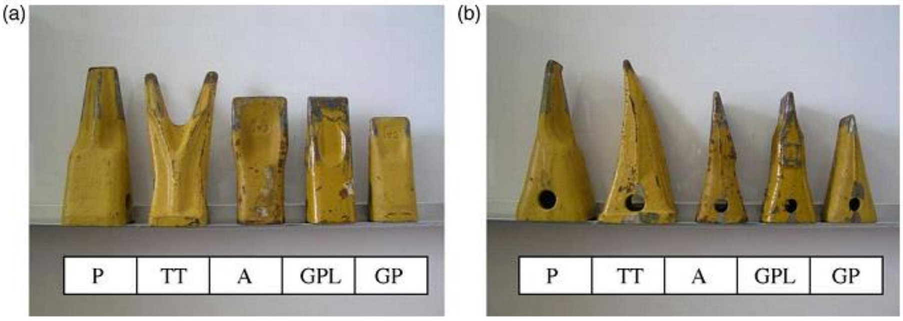

Figure 2-19 Brooker’s dent tools (2005)

He conducted a numerical study on the lateral indentation of continuously supported tubes. ABAQUS/Standard has been used in this numerical study. Only 1/4 pipe was modelled in this FE modelling because of the symmetry characteristics. The element type was a shell element. The denting tool had a knife edge and was modelled as a rigid surface, with frictionless contact. The pipe rested on a rigid surface floor, with frictionless contact. The material was rigid, perfectly plastic, and the analysis has nonlinear material and geometry. Several analytical models were compared with the FE results, and a parametric study was conducted. The parametric study included the wall thickness, tube length, diameter and yield stress. The results showed that the diameter did not much influence the result; and the result significantly depended on the tube length, a result that had not been previously recognized.

Palmer et al. (2006) conducted the dynamic impact test shown in Figure 2-20. This test aimed to evaluate the pipe’s safety if another pipeline dropped on it. Therefore, the dent tool of this experiment was a pipe section. The boundary condition was sand support as Figure 2-20 shows. The test results showed that the deformation and bending strains of the pipes were low, but the concrete coating was crushed. Wierzbicki and Suh’s model was used to predict the impact performance.

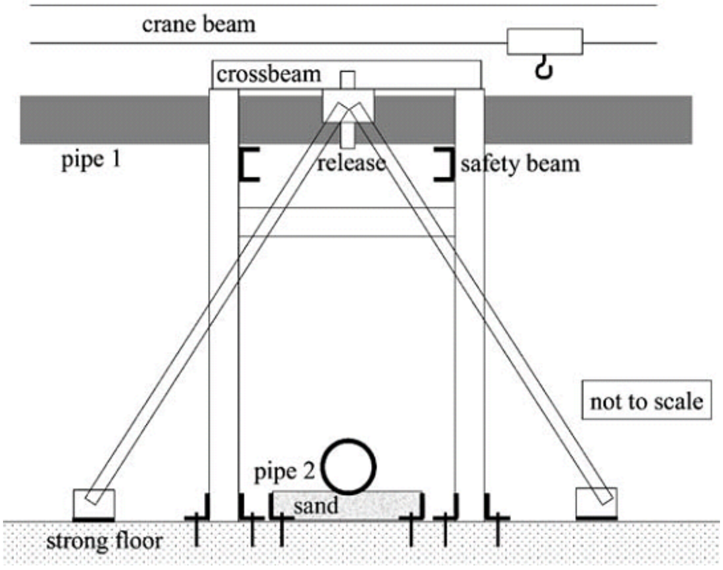

Figure 2-20 Palmer et al.’s test set-up (2006)

Alexander (2007) conducted indentation tests both in quasi-static conditions and in dynamic conditions. Figure 2-21 shows the quasi-static test set up, Figure 2-22 shows the small scale dynamic test, and Figure 2-23 shows the full scale dynamic test. In his quasi-static test, he used a flat dent tool to dent the pipe. The small scale test sample was a 12 inch (323.85 mm) diameter pipe, and the pipe was placed on steel or sand in the lab. A full test with 12 inch (323.85 mm) flowline was conducted outdoors. There were several dropped objects, including one that dropped a 10900 kg weight from 9.1 m. A FE model of 12 inch (323.85 mm) diameter and 1.375 inch thickness pipe was built. This model was constructed with solid elements in ABAQUS, and accounting for material nonlinearity. The soil effect boundary condition was modelled by spring elements. The FE results were compared with his experiment data, and were found closely to match the test results.

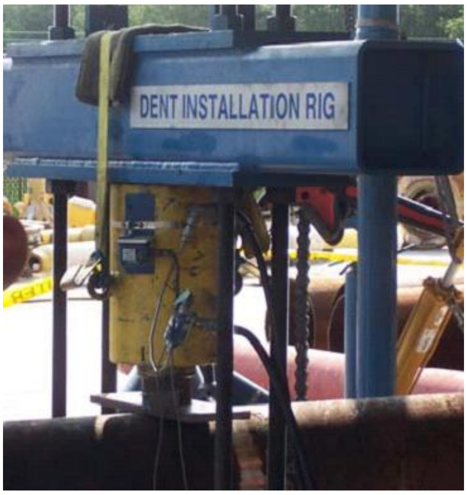

Figure 2-21 Alexander's quasi-static test rig (2007)

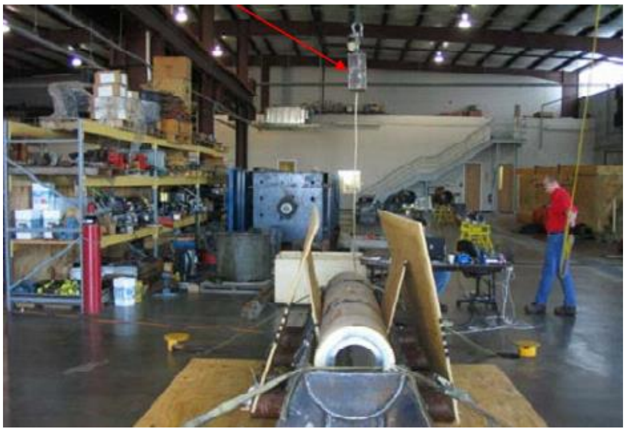

Figure 2-22 Alexander's small scale dynamic test (2007)

Figure 2-23 Alexander's full scale dynamic test (2007)

All the previous models and tests are with no internal pressure. The following are some models which considered the internal pressure effect. Hopkins et al. (1992) described a series of dent/puncture tests on buried 914 mm diameter pressured pipe. In twenty-four of the tests, a hydraulic ram gave the buried, pressurized pipe quasi-static loading, and the other sixteen tests used an excavating machine to impact the pipes. The pressures were 7, 30 and 70 bars. The pipe's steel grades were X52 and X70; the thicknesses were 9.5 and 12.5 mm. During the tests, the dent depth and spring back were measured. The test data illustrated that the wall thickness was the most important parameter for puncture force, and the material grade was least important parameter for puncture force and dent depth. Internal pressure had little influence on puncture force but influenced the dent depth. The dynamic force to puncture and dent response was lower than the corresponding level in static tests.

Additional tests were carried out by European Pipeline Research Group on 219 and 406 mm diameter pressurized pipe. Based on a total of 89 quasi-static tests and 46 dynamic tests, a semi-empirical relationship has been built. However, as a semi-empirical model, these equations are better for smaller diameter pipe (168mm) and excavator weight range from 13 tonne to 32 tonne (Corder and Chatain, 1995).

Jones and Birch (1996) conducted impact tests for pressurized pipes. A sketch of the test set-up is shown in Figure 2-24. Altogether 54 impact tests were conducted. The pipes were fully clamped. The span length was 600 mm, ten times the pipe diameter. The wall thickness was 1.7 mm. The impact velocity was up to 13.6 m/s. At lower velocity, there was a dent, and at a higher velocity, either near the indenter or at the end, there was a loss of integrity.

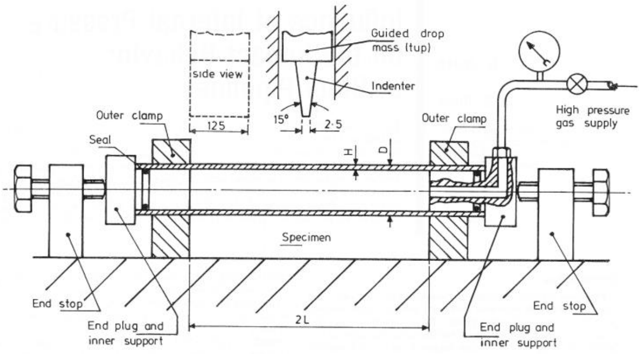
Guided drop mass (tup)
side view
Indenter
125
15°
2·5
Outer clamp
Seal
Outer clamp
High pressure gas supply
H
D
Specimen
End stop
End plug and inner support
2L
End stop
End plug and inner support

Figure 2-24 Sketch for dynamic test with inner pressure (Jones and Birch, 1996)

Ng and Shen (2006) conducted a dynamic impact test on small scale pipes with internal pressure. The test rig is shown in Figure 2-25. The specimens in these tests were cold-drawn seamless mild steel pipe with an outer diameter 57 mm, wall thickness 1.6 mm and span length 570 mm. Boundary conditions were sand support, kaolin support and fully clamped with no foundation support. The indenter in this test was rigid wedge-shape, cylindrical impact surface of radius 2.65 mm at the front and mass 80 kg. The internal pressure was produced by nitrogen, to keep the pressure stable during the impact process. Altogether 52 tests were conducted. According to the test results, the circumferential stress influenced the result significantly because of the internal pressure and the foundation.

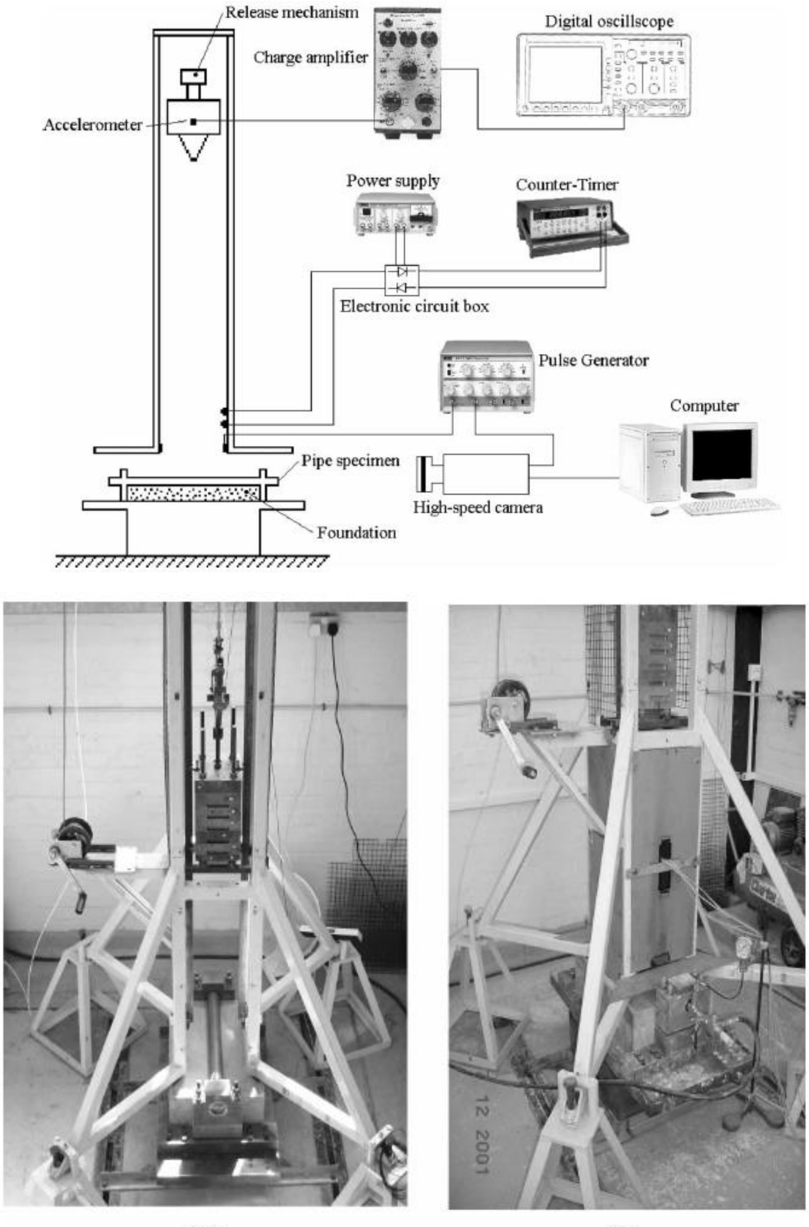
Release mechanism
Charge amplifier
Digital oscillscope
Accelerometer
Power supply
Counter-Timer
Electronic circuit box
Pulse Generator
Computer
Pipe specimen
High-speed camera
Foundation
12 2001

(a) (b)

Figure 2-25 Ng and Shen’s impact test rig (2006)

An analytical model for local indentation on pressured pipe has been developed by Liu and Francis (2004). In this case, the indenter impacted the pipe longitudinally rather than transversely. That kind of dent does not represent the trawl gear impact situation. The results showed the internal pressure increased the resistance against indentation.

Karamanos and Andreadakis (2006) used the finite element method to analyse a pressurized pipeline under lateral quasi-static loading. The pipe was modelled with shell finite elements, element type S4R in ABAQUS, a four-node reduced-integration shell element. This analysis is a geometric and material nonlinear analysis, and the numerical results were compared with available pipe denting data from tests conducted by TNO Institute for Building Materials and Construction. Based on the good agreement with test data, an extensive parameter study has been conducted, including changing the D/t, changing the inner pressure level from zero to 0.8, changing boundary conditions, and changing different dent tool dimension and direction. Based on the numerical results, a simplified analytical model based on Wierzbicki and Suh's model was developed to consider the internal pressure effect.

2.3 Dent Behaviour

Sometimes the damage is so severe that a pipeline is no longer fit for service and has to be replaced, but more often the damage is comparatively minor. It then becomes important to be able to evaluate the damage accurately, because the cost of unnecessary repair or replacement is very high indeed. An investigation of dent behaviour will help to assess the damage and make a correct decision.

A smooth dent without a defect and with no wall thickness reduction is defined as a plain dent. Dents with defects could be classified into dents with gouges, dents on welds and dents with other type of defects. A dent with defects is the most severe type of damage. Another severe dent type is a kinked dent which causes an abrupt change in the curvature of the pipe wall (Cosham and Hopkins, 2004).

Dent behaviour is analysed from three points of view: stress concentration under inner pressure, burst pressure, and fatigue life under cyclic loading.

2.3.1 Stress concentration

Ong et al. (1989) used Sanders’ non-linear shell theory to analyse long dents , short and local dents on a pressurized cylinder. The classification into long dent, short dent and local dent was based on the dimension of the dent geometry. If the length of dent was greater than twice the width, it was a long dent; if the length was less than twice the width, it was a short dent. A Local dent was produced by a straight knife edge perpendicular to the pipe axis (Lancaster and Palmer, 1994). For the long dent, the stress pattern varied very little along the axial direction of the dent. For the short and local dents, the stress distribution varied along the length of the cylinder. The results showed that the peak stress at the root of the dent was greatly influenced by the depth, size and profile of the dent. The peak stress obtained in the case of the long dent is higher than in a short dent. A sharp dent induced a higher bending stress than a shallow dent does. Ong (1991) later applied this method to analyze four different dent geometries. However, he concluded that this method was not suitable for short and local dents, because the stresses induced in a local dent were much smaller than those in a long dent. Therefore, the experimental and finite element method was used to investigate local dent on a pressurized pipe (Ong et al., 1992). In the test, strain gauges were used to measure the elastic strain distributions in the dent region. According to the local dent test data, the maximum strain was the hoop strain located at the flank, along the dent axis, whereas for a long dent it was located at the central deepest part of the dent.

Lancaster investigated the strain concentration issue by model tests (Lancaster and Palmer, 1996b). In Lancaster’s model tests, strain gauges and the photoelasticity method were both used to measure the strain in the dent area (Lancaster and Palmer, 1992). The results showed two regions of high strain on the axial extremities of the dent rim (Lancaster and Palmer, 1993). For a dent with d/D =13%, the maximum elastic and plastic hoop strain concentration factors were 10 and 22 (Lancaster and Palmer, 1993). They also compared his work with Ong et al. (1992)’s work. The high stress regions were the same in two experiments, but because of different geometry and material property, no further conclusion could be reached. The maximum strain concentration factor in Lancaster’s test was 1.85 times higher than in Ong’s test, and Lancaster concluded that was because of the different material stress-strain curves and geometric ratios (Lancaster and Palmer, 1996a). In Lancaster’s work, flip-out and rerounding effects were noticed (Lancaster and Palmer, 1996b). The works of both Ong and Lancaster have been investigated by finite element method by Korml (1993).

A high stress concentration may lead to rupture or to the potential fatigue failure. The high stress area may suffer from other problems.

2.3.2 Burst pressure

Full scale tests were conducted by two organizations, Battelle and British Gas. Battelle Columbus Laboratories' test data have been published in the NG 18 report. British Gas' test data have been reported by Corder and Chatain (1995). The European Pipeline Research Group (EPRG) reviewed these test data, which contained 74 tests and provided a wide range of results. However, for investigating the plain dent behaviour, some test data from dents on weld or other factors need to be excluded. Moreover, as the dents were introduced on unpressured pipe, the effect of springback should be considered, and it was investigated by EPRG.

British Gas test data (Hopkins et al., 1988) showed that plain smooth dents of depth from 8% pipe diameter to possibly 24% (Jones and Hopkins, 1983) did not significantly reduce the burst pressure. However, a dent on a weld can cause a low burst pressure due to the presence of cracks.

If dents with defects, for example, a dent with gouge, the failure was very complex, and had ductile tearing within an unstable structure. British Gas developed a fracture model for a dent introduced on unpressurised pipe (Hopkins et al., 1988). EPRG developed a model which can be used for any pipe geometry.

2.3.3 Fatigue

Normally, pipelines will be under cyclic loading, and then presence of a dent will influence the fatigue life of the pipeline. If the defect is within the dent, the fatigue life will be more difficult to predict.

EPRG (Corder and Chatain, 1995) have developed a model for analysis of fatigue of plain dents. This model considers the stress concentration because of the dent and compares it with the DIN code which gave the ultimate tensile strength of the material.

If a dent contains a gouge, experiments showed that the dented rings containing gouge with sub-surface cracking would fail at a constant pressure within 85% of the straight-off failure pressure. The cracking below a gouge and dent would significantly influence the failure and fatigue life (Hopkins et al., 1983). They concluded: ‘The neighbouring defects interaction will further reduce the failure pressure, but there has been a lack of investigation (Hopkins and Corbin, 1988).

Many fatigue tests have been conducted, and they demonstrated that a dent with a gouge had a lower fatigue life than a plain dent without a gouge or the same gouge without a dent (Cosham and Hopkins, 2004). Hagiwara and Oguchi (1999) has conducted fatigue tests on pipes, which were first dented and then a gouge was machined . The crack growth significantly reduced the fatigue life. The depth of gouge in a dent dominated both ductile and fatigue crack growth, which means the depth of gouge influences the fatigue life significantly.

Recently, Rinehart and Keating (2002) at Texas A&M University concluded that long unrestrained pipeline dents will have shorter fatigue lives compared to other dent types, based on a full scale test experiment.

Although much work has been done in this field, the method is still empirically based. It is still necessary to refer to the test data or sometimes to do new tests.

2.3.4 Summary of dent behaviour

A Joint Industry Project named PDAM, sponsored by fifteen international oil and gas companies, developed a pipeline defect assessment manual and was completed in 2003 (Cosham and Hopkins, 2004). This project was based on an extensive critical review of pipeline “fit-for-purpose” methods and published test data. The motivation of this project was that many of the existing methods were semi-empirical, and therefore limited by the extent of the relevant test data, which means the methods may become invalid or unreliable if they were applied outside of these empirical limits(Cosham and Hopkins, 2002). “It is unreasonable to expect that 30 years old methods will be applicable to newer steels, thicker wall, and higher strain. PDAM based on critical, comprehensive and authoritative review of available pipeline defect assessment methods, did not present new methods, but presents the current state of art in fitness-for-purpose assessment (Cosham and Hopkins, 2001). ” PDAM summarized the state of art in 2004 for dent behaviour as Table 2-2 shows.

Table 2-2 Recommended methods in the pipeline defect assessment manual for assessing the burst strength and fatigue life of mechanical damage defects (dent and gouge) subject to internal pressure loading (Cosham and Hopkins, 2001)

	Internal pressure (static) longitudinally oriented	**Internal pressure (fatigue)**
Gouges	NG-18 equations	BS 7910 or API 579
Plain dent	Dent depth less than 7 or 10 percent of pipe diameter (empirical limit)	EPGR
Kinked dent	No method	No method
Smooth dents on welds	No method	No method
Smooth dents and gouges	Dent-gouge fracture model	No method
Smooth dents and other types of defect	Dent-gouge fracture model	No method

According to the table, it is clear that the kinked dents are not covered by any method for burst and fatigue analysis, and that except for plain dents; other types of dents have not been covered by developed methods for fatigue assessment. Therefore, a lot of recent and current researches are focused on fatigue analysis.

2.4 Pull-over Response

Pull-over induces a more global response, and lasts longer than the impact phase, about 1 second to 10 seconds (Fyrileiv et al., 2006). During this phase, the pipeline will be subjected to high horizontal and vertical forces.

Since the 70s many model tests investigated the interaction between pipelines and trawl gear. In Gjorsvik et al.’s model test (Gjørsvik et al., 1975) , a wave basin with 54 m long, 5 m wide and 1.45 m deep at the River and Harbour Laboratory in Trondheim was used. The prototypes had diameters of 900 and 400 mm, and the scale factor was 1:4, therefore, the model pipelines had diameters 225 and 100 mm. As the wave basin’s width was 5 m, the length of the model pipelines was less than 5 m. Two towing speeds were chosen corresponding to 3.5 and 5 knots under prototype, but no specific numbers were given. No scaling laws were mentioned, however, it indicated that the force scale is 1:64. For the boundary condition, a 0.2 meter thick sand layer was used under the pipeline. A frame on each end gave the pipeline a rigid support, and the other frame was used to investigate the elastic properties in the horizontal direction. Dynamometers were used to record the towing force, interaction force and reaction forces at both ends. Altogether, 164 tests were conducted. The test set-up is shown in Figure 2-26.

Gjorsvik et al. (1975) conducted a field test with a small trawler in 20 m shallow water, and described it as a “half scale model”. The test pipeline they used was 300 m long and 16 inch (406.4 mm) in diameter with coating. Moshagen and Kjeldsen (1980) summarised some of the model tests and field tests as table 2-2 shows.

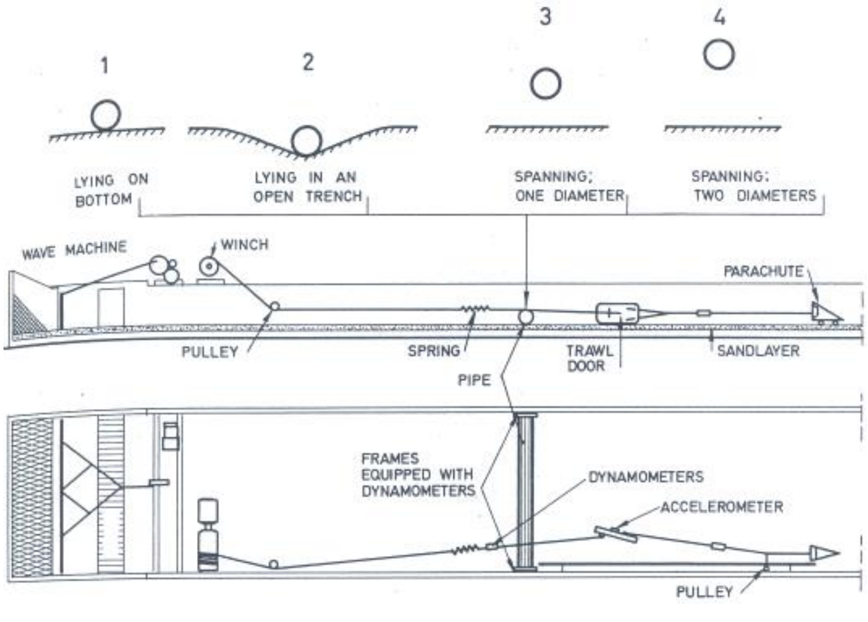
1
2
3
4
LYING ON BOTTOM
LYING IN AN OPEN TRENCH
SPANNING; ONE DIAMETER
SPANNING: TWO DIAMETERS
WAVE MACHINE
WINCH
PARACHUTE
PULLEY
SPRING
PIPE
TRAWL DOOR
SANDLAYER
FRAMES EQUIPPED WITH DYNAMOMETERS
DYNAMOMETERS
ACCELEROMETER
PULLEY

Figure 2-26 Model test (Gjørsvik et al., 1975)

Horenberg and Guijt (1987) conducted model tests which were supported by Shell Research B.V. and Netherland Oil and Gas Exploration and Production Association (NOGEPA). Their wave basin was 10 m long, 9 m wide and 1 m deep, as Figure 2-27 shows. Prototype pipelines were 16 inch, 23 inch and 35 inch. With a scale factor 5, the model test pipe sections were 80, 116 and 180 mm, and the length was 4.5 m. The towing speed was 1.4 m/s throughout the whole test series. Froude scaling was selected. Reynolds' number could not be scaled since the hydrodynamic drag on the beam trawl is small. The test set-up is shown in Figure 2-27. A layer of fine grain sand and crushed stone was used to represent the sea bed. The boundary conditions at both ends were simple support on both vertical and horizontal directions. Force transducers were used to measure the towing force, sweep line forces and pipeline reaction forces. The speedometer measured the towing speed.

Table 2-3 Total VHL model and field study of bottom trawl loading on submarine pipelines (Moshagen and Kjeldsen, 1980)

Project	*Main, Phase II*	*Main, Phase III*	*Main, Extension I*	*Main, Extension II*	*Shell*	*Main, Extension III*	*Norpipe*
Type of test	Model,1:4	Field	Field	Model, 1:4	Model, 1:5	Field	Field
Pipe Diameter (inch)	16,36	16	16	16,48	36	36	36
Pipe Coating	No	Polyethylene and concrete	Polyethylene and concrete	No	No	Concrete	Concrete
Trawl gear type and weight	V-500 1500	V-500 975	CB-1720	CB-1720	CB-4000	CB-1840	CB-1840
	O-1200		O-2320 1150	MB-1720		MB-2010	V-570 1080 1490
	R-1100		P-1176			V-1490	O-2320
			R-1472 850			O-2320	R-1050
						R-860	
						1472	

Project	*Main, Phase II*	*Main, Phase III*	*Main, Extension I*	*Main, Extension II*	*Shell*	*Main, Extension III*	*Norpipe*
Type of force studied	Warp contact pull over	Pull over Impact	Pull over Impact	Pull over Impact	Warp contact pull over Impact	Pull over Impact	Pull over Impact

CB - conventional beam trawl MB - modified beam trawl V - V-shaped trawl door

O - oval-shaped trawl door P - polyvalent trawl door R - rectangular trawl door

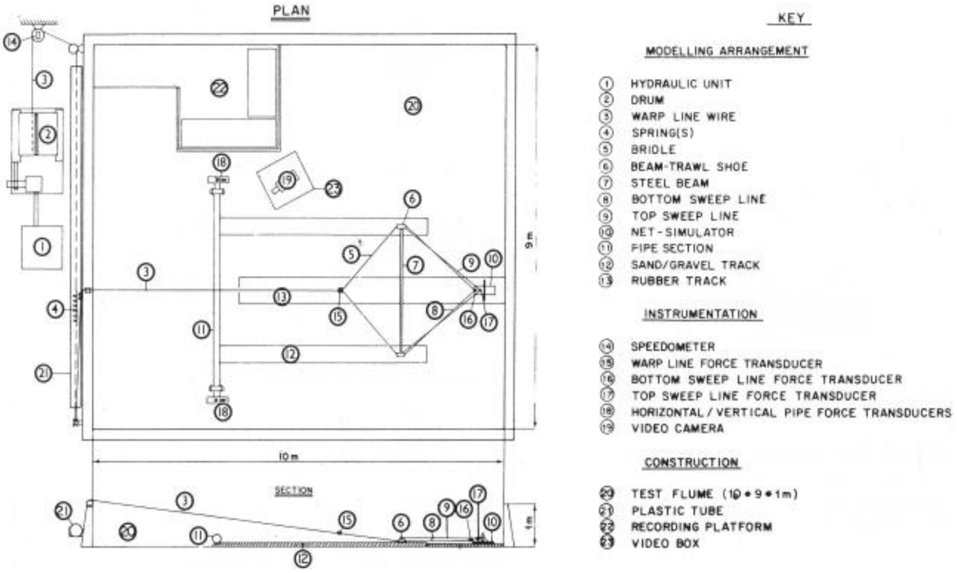
PLAN
SECTION
10 m
9 m
1 m
KEY
MODELLING ARRANGEMENT
① HYDRAULIC UNIT
② DRUM
③ WARP LINE WIRE
④ SPRING(S)
⑤ BRIDLE
⑥ BEAM-TRAWL SHOE
⑦ STEEL BEAM
⑧ BOTTOM SWEEP LINE
⑨ TOP SWEEP LINE
⑩ NET-SIMULATOR
⑪ PIPE SECTION
⑫ SAND/GRAVEL TRACK
⑬ RUBBER TRACK
INSTRUMENTATION
⑭ SPEEDOMETER
⑮ WARP LINE FORCE TRANSDUCER
⑯ BOTTOM SWEEP LINE FORCE TRANSDUCER
⑰ TOP SWEEP LINE FORCE TRANSDUCER
⑱ HORIZONTAL / VERTICAL PIPE FORCE TRANSDUCERS
⑲ VIDEO CAMERA
CONSTRUCTION
⑳ TEST FLUME (10 * 9 * 1m)
㉑ PLASTIC TUBE
㉒ RECORDING PLATFORM
㉓ VIDEO BOX

Figure 2-27 Horenberg and Guijt’s model test (1987)

Guijt and Horenberg (1987b) used an existing pipeline in the Dutch sector of the Southern North Sea to conduct field tests. The water depth was between 30 m and 35 m, and the pipeline overall length was 9.35 km. The pipeline was 18 inch (457.2 mm) with 12.7 mm thickness. These tests concluded that the free span induced larger pull-over force, the perpendicular crossing brought larger pull-over force and hooking rarely happens. Nygaard conducted model tests of trawl boards and beam trawl crossing subsea structures and found the mechanical behaviour relates to gear geometry, weight and the initial conditions.(Longva et al., 2013)

Verley et al. (1992) conducted an extensive model test program. He concluded that most of the previous experiments did not take account of the flexibility of the pipeline, and noted that only the forces on the warp were measured, and that does not necessarily represent the force applied to the pipe. In his experiment, the pipe support system can flexibly support the rigid pipe section on springs and dampers as Figure 2-28 shows. The effects of span height, span and warp flexibility were investigated. He concluded that the maximum warp force and the maximum pipe force were proportional to $Vk^{1/2}$. The total time of the interaction depends on the tow velocity, the water depth, span height and the warp and pipeline flexibilities.

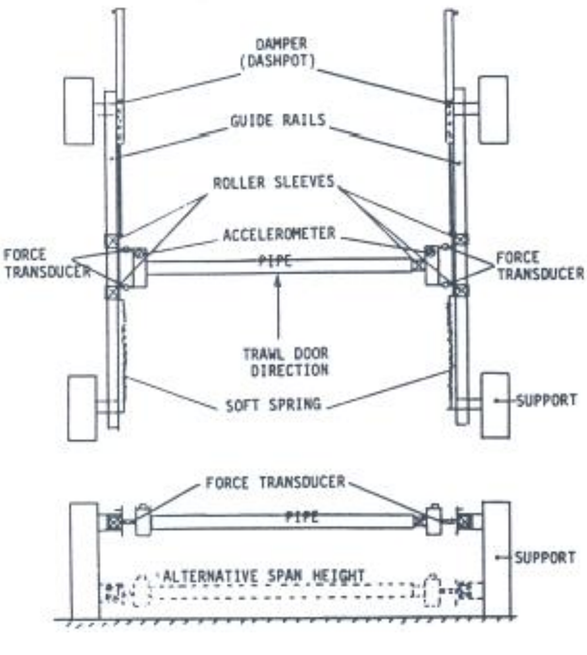
DAMPER (DASHPOT)
GUIDE RAILS
ROLLER SLEEVES
ACCELEROMETER
FORCE TRANSDUCER
PIPE
FORCE TRANSDUCER
TRAWL DOOR DIRECTION
SOFT SPRING
SUPPORT
FORCE TRANSDUCER
PIPE
SUPPORT
ALTERNATIVE SPAN HEIGHT

Figure 2-28 Verley et al.'s pipe support (1992)

Verley (1994) conducted parametric studies. Six dimensionless groups were found and they were sufficient to describe the pull-over problem. The stress can be found based on the pull-over force according to the dimensionless groups. Based on the analysis, the author concluded that the pipe larger than

16 inch (406.4 mm) might be not safe lying on the seabed if there was a large compressive force, and also that a pipe smaller than 16 inch (406.4 mm) might be strong enough to withstand the pull-over force.

Fyrileiv et al. (1997), Fyrileiv et al. (2006) and Askheim and Fyrileiv (2006) made further progresses of the recommended design methods and which were included in the DNV-RP-F111. Fyrileiv et al. (2006) showed that the clump weight gives higher pull-over force than traditional trawl boards; therefore it might govern the trawl design of pipelines. Fyrileiv and Spiten (2004) also made suggestions on platform safety zones and pointed out that even if the fishing vessel is outside the safety zone, the trawl gear might cross it on the seabed. Therefore, protections against trawl gear must be assessed on a case-by-case basis, even if the pipeline is in the safety zone.

The use of numerical methods to simulate the pull-over process was started by Bergan and Mollestad (1982). They used the finite element method and simulated the pipe with beam elements. A small strain-large displacement formulation was used. The large displacement effects played a dominating role for the overall behaviour of the pipe. The result showed there was only minor plasticity in the pipe.

Guijt and Horenberg (1987a) and Horenberg and Guijt (1987) also used numerical methods to predict the pull-over load time history. The equation of motion and a number of equilibrium equations were derived, and these non-linear equations were solved by time-stepping method. Moreover, a finite difference 2-dimensional model was also developed to solve this problem.

Igland and Soreide (2008) developed a finite element model in ANSYS to analyse a problem where a heavy clump weight was dragged by a warp line along the seabed and pulled over a pipeline. The output of this trawl gear interaction analyses was the pull-over force magnitude, duration, and the impact response on the pipeline. Pull-over loads and duration compared with the loads amplitude and duration gave in DNV-RP-F111 (2010), and results showed that the actual stiffness of pipeline and the pipe-soil interaction would reduce trawl loads; the method on DNV-RP-F111 was therefore conservative.

Teigen et al. (2009) used a numerical method with the computer code WAMIT to compute the coefficients of drag force, lift force and added mass force. The authors also concluded that the sea bed proximity is important and needed more considerations otherwise it might lead to non-conservative results. When the trawl door approached the pipeline, the added mass increased significantly.

A group of researchers in Norwegian University of Science and Technology (NTNU) used the software SIMLA to simulate the trawl gear pipeline interaction. Moller focused on pull-over loads from polyvalent trawl boards with different span heights and trawling velocities. Comparisons were made with DNV-RP-F111, and found the forces were similar only when the free span was high. The velocity change from 2 m/s to 3 m/s had a smaller effect in the simulation than in DNV-RP-F111. (Johnsen, 2013)

Vegard Longva (2010) focused on trawl board pipeline interaction. He developed a new hydrodynamic load model and used the software SIMLA for the simulations. The seabed proximity and forward-speed effects of the trawl board were considered in the finite element model to calculate the pull-over force. (Longva et al., 2011) He looked into the oblique trawl board crossing and concluded that a perpendicular crossing did not predict the largest pull-over load. The comparison with DNV-RP-F111 showed that the DNV-RP-F111 over-predicts the pull-over loading.

This model was enhanced by Longva and Sævik (2012) and Longva and Sævik (2013) on the contact elements. The comparison with experimental results showed good consistency. Longva et al. (2013) made further progress. The finite element model was validated against various experiment results. Parametric study was conducted. The authors concluded if the pipe diameter to trawl board height ratios less than 0.3, it is acceptable to ignore the pipeline. It also found the non-perpendicular crossings at high span heights induced the maximum pull-over load. Newly designed trawl boards have complex geometry, and large weight and surface area. The FE model calculates the response more accurately than the simplified methods; however, even the finite element model needs experimental results to validate it in the first place.

Maalo et al. (2010) worked on the experimental model test and the simulation of clump weight pipeline interaction of a fixed pipe section at low span heights. The main finding is that the increasing in pipeline flexibility resulted in a decrease in pull-over force. The pull-over loads were lower in the simulations than in DNV-RP-F111. (Johnsen, 2013)

Ingrid Berg Johnsen (2013) has investigated the clump-weight trawl gear interaction with submarine pipelines with FE simulations. She mentioned that the pull-over load of clump weight calculation methods in DNV-RP-F111 was based on an experimental model test executed at MARINTEK in 2004. In that test program, 139 tests were made, and all were model tests with scaling according to Froude’s law. The scale factor is 1:10. Three pipelines with diameters 350 mm, 530 mm and 840 mm were modelled. Six different span height were used, and three different pipe end conditions. The modelled pipeline length was 25 m. Four different velocities were utilized, 1.45 m/s, 1.75 m/s, 1.95 m/s and 2.18 to 2.45 m/s for different clump weight types. The sensitivity study showed that the free span height and pipe diameter influenced the pull-over force a lot. The pull-over force and pull-over time increased with decreasing trawling speed. The lower free span induced lower pull-over force. The difference between the simulation and the model test data might come from the absence of the friction effect in the simulation. Comparison with the DNV-RP-F111 showed the design load has a steeper increase in pull-over force than the simulation force for smaller diameter pipes.

In reality, a pull-over analysis is conducted not only to predict the pull-over response, but it also important in defect assessment. It is sometimes difficult to obtain information about the dents, but it is possible to obtain data on lateral displacement. This displacement data will help a engineer to investigate the damage of the pipeline in a pull-over finite element analysis model. (Alexander, 2007).

Espiner et al. (2008) described a project for assessing pipeline damage. This pipeline was a natural gas pipeline, from CATS (the Central Area Transmission System) riser platform to the North East coast of England. In 2007 summer, this 36-inch pipe was damaged by an anchor. The pull-over finite element model was used to identify the loads applied to the pipeline and the stress in the pipeline when the pipeline was impacted and afterwards. Because of various unknown parameters, the analysis compared the finite element results with the pipe position and shape data measured by the survey.

2.5 Pull-over Induced Lateral Buckling

Lateral buckling (Sriskandarajah, 2001) might be induced by the pull-over force. The loading generated by a pull-over event is possibly high enough to generate lateral buckling. The effect can be determined by a dynamic pull-over analysis and lateral buckling analysis combined together.

Herlianto (2011) studied the pull-over force that induced global buckling on high temperature/high pressure subsea pipeline. The pull-over load was calculated according to DNV-RP-F111, and the subsequent pipeline response to that was calculated using a finite element model in software ANSYS. The post buckling condition was further studied after the trawl loads. The results showed the trawl gear did induce the lateral buckling. Herlianto et al. (2012) showed an example on 22 inch high pressure/high temperature pipeline, and the results showed the pipe was at risk from trawl gear crossing. One problem of this work is that the pull-over force time history was obtained based on the DNV-RP-F111, which has been pointed out to be conservative by many researchers.

Amdal et al. (2011) suggested that the current criteria for the pull-over response can be relaxed, by considering the structural reliability analysis to assess quantitatively the annual failure of probability. This method might bring more benefits for small diameter pipelines with low trawling frequencies.

2.6 Hooking

Hooking is the condition that the trawl gear is wedged under the pipeline and stopped. A fisherman will always winch the warp line to free the gear. Therefore, the pipeline will be subjected to a high uplift loading. The gear may not come free until the warp line is broken, which will impose on the pipeline an extreme force.

Hooking is infrequent compared to impact and pull-over. Therefore, hooking response can be neglected if impact frequency in a specific field is low. However, Moshagen and Kjeldsen (1980) suggested that: ‘the hooking possibility for beam trawls and small diameter pipelines should be studied in the future’.

Free spans can increase hooking risk. If the free span height is larger than the critical span height, the pipeline structural integrity under extreme load needs to be considered.

The hooking response can be determined by a static analysis applying the maximum lifting displacement. Maximum warp line tension will limit the maximum lifting force.

2.7 Existing Guidelines

There were some guidelines developed over the past 40 years based on the research. Here is just the repetition of some parts of the guidelines, and no recommendations are given to any of them.

2.7.1 Guidelines for Trenching Design of Submarine Pipelines (Trevor Jee Associates, 1999)

This guideline is applicable for rigid steel subsea pipelines, unbounded flexible pipes and piggy-backed pipelines. There are three level assessments. The first one is a simple “first pass filter”, where the decision can be made straightforwardly. A pipeline, which is concrete weight coated, has an outer diameter is more than 16 inch, and is not operated at high pressure/high temperature, can be considered as overtrawlable. The second level is a deterministic assessment, and it checks if the pipe can withstand the load based on the analysis results. The third one is the risk/cost assessment, that the trenching decision is based on a quantitative risk assessment to determine the probability of damage and the subsequent lifetime costs of the pipeline. This relaxes the criteria in the second pass. The probability of damage is governed by the trawl gear’s parameters in this field including gear type, gear size, the angle of approach of trawl gear and spanning of pipeline. The subsequent lifetime cost may be calculated on a year-by-year basis for trench or non-trench options. An accurate probability of damage assessment ought to be founded on a good understanding of overtrawlability, including the understanding of the trawl loading, the response of pipelines and how the damage will influence the pipeline operation.

2.7.1.1 Impact Phase

The kinetic energy change equals to the impact energy.

$$\Delta E = \frac{1}{2} m_{e(tow)} V^2 - \left[\frac{1}{2} M(u^2 + v^2) + \frac{1}{2} I_g \omega^2\right] \tag{2.13}$$

where

$m_{e(tow)}$	is the mass of the steel in the otter door, beam or clump weight, plus the associated hydrodynamic added mass
V	is the initial velocity
u v and ω	are final velocities
M and I_g	are steel mass of the gear, conservatively neglecting added mass after collision

Beam trawl gear will impact a pipe at two locations. For a single impact, the impact energy is 2/3 times the kinetic energy change.

Not all the energy is absorbed by the pipeline, but some also by the soil, the coating and the global response. Therefore, it may be assumed conservatively that the energy absorbed by the pipeline is equal to 50% of the impact energy, which leads to elastic and plastic local deformation, referred to as denting energy. However, the guideline does not provide any explanation for the recommendation.

The denting model is the Ellinas and Walker's model(1983). However, the equation in the guideline is given as equation (2.14) and which is different with equation (2.4). This might be a typo in the guideline.

$$\delta = \sqrt[3]{D\left(\frac{E}{25\sigma_0 t^2}\right)}$$

(2.14)

The impact response can be examined by the experiments as well. In *Guideline for Trenching Design of Submarine Pipelines,* the test specification for the impact test of coated pipe is shown in section 16. The knife edge indenter has a width of 60 mm. The edges are of 6 mm radius. It is also proposed that the pipeline should lie horizontally and 50% embedded in wet compacted sand.

Finite element models are preferable for predicting the proportion of impact energy for denting. The model is shown in Figure 2-29. The pipeline is modelled by beam elements. The effective non-linear spring stiffness of the pipe wall at the impact location can be calculated by Ellinas-Walker's model.

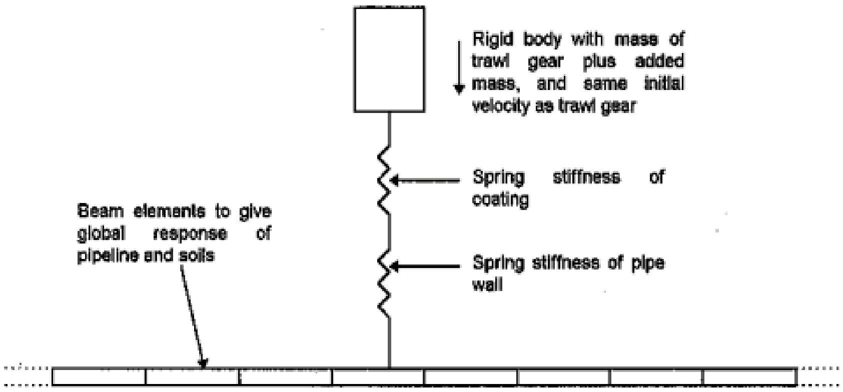
Rigid body with mass of trawl gear plus added mass, and same initial velocity as trawl gear
Spring stiffness of coating
Beam elements to give global response of pipeline and soils
Spring stiffness of pipe wall

Figure 2-29 Schematic of detailed simulation model

2.7.1.2 Pull-over Phase

The force-time history is calculated from a 2-D trawl gear pull-over simulation model. This model considers interaction of the pipeline and trawl gear motions, and this is important for small diameter pipelines. However, Longva et al. (2013) concluded that this method was not able to predict realistic loads for trawl boards.

Another FE model is used to calculate the peak bending strain at the point of impact. The modelled pipe should be long enough to eliminate the end constraints. Lateral buckling should be checked. Multiple crossing at the same point should be considered. The peak bending strain should be examined.

2.7.1.3 Criteria

For D/t less than 18, the dent depth is no more than 4% and for D/t from 18 to 30, the dent depth is no more than 2%. This mainly considers the fatigue life of pipe and the pigging process. In deep water applications, the collapse under external pressure of a dented pipe should be considered.

For the pull-over, the strains in the pipe because of the pull-over and lateral buckling should satisfy equation (2.15).

$$\frac{1.3\varepsilon_b}{\varepsilon_{bc}} + \frac{P}{P_c} + (\frac{N}{N_0})^n \leq 1 \tag{2.15}$$

where ε_b is the bending strain, and ε_{bc} is the critical bending strain, P is the external pressure, P_c is the collapse pressure, N is the local axial compressive force (=0 if tensile), and N_0 is the critical axial compressive force. n is an empirical factor and equals to *1+300*t/D*.

2.7.2 DNV-RP-F111: Interference between Trawl Gear and Pipelines (2010)

2.7.2.1 Impact Phase

DNV (2010) considers the impact energy in a different way. The different trawl gear is considered separately to develop three models to estimate the energy absorbed by the pipelines. The impact energy associated with the steel mass of the trawl board is:

$$E_{is} = R_{fs} \cdot \frac{1}{2} \cdot M \cdot (C_h \cdot V)^2 \tag{2.16}$$

where

M is the trawl board steel mass.

R_{fs} is a reduction factor depending on the outer pipe diameter

C_h is the span height correction factor for the effective velocity

The associated impact energy of the trawl board from added mass is

$$E_{ia} = R_{fa} \cdot \frac{2\left(F_{b(tb)}\right)^3}{75 \cdot \sigma_0^2 \cdot t^3} \tag{2.17}$$

where

$$F_{b(tb)} = C_h \cdot V \cdot \sqrt{M_a \cdot k_{b(tb)}} \tag{2.18}$$

R_{fa} is the reduction factor depending on the pipe diameter and the soil type

$F_{b(tb)}$ is the impact force due to trawl board bending action

σ_0 is the yield stress to be used in design

t is the steel wall thickness

C_h is the span height correction factor

V is the tow velocity

M_a is the trawl board added mass

$k_{b(tb)}$ is the lateral bending stiffness of the board

Therefore, a conservative estimate of the energy absorbed by the pipe is

$$E_i = max\begin{Bmatrix} E_{is} \\ E_{ia} \end{Bmatrix} \tag{2.19}$$

For beam trawls and clump weights, the impact energy absorbed by the pipe and its coating may be calculated as:

$$E_i = R_{fs} \cdot \frac{1}{2} C_b (M + M_a) \cdot V^2 \tag{2.20}$$

where

C_b is the factor of effective mass, set to 0.5 for beam trawl and set to 1 for clump weight

M is the mass of the beam trawl

M_a is the hydrodynamic added mass

The reduction factors for the impact energy are shown in Figure 2-30. They are from 0.1 to 1 according to different sand property and different pipe outer diameters instead of 0.5 as in the *Guidelines for Trenching Design of Submarine Pipelines*.

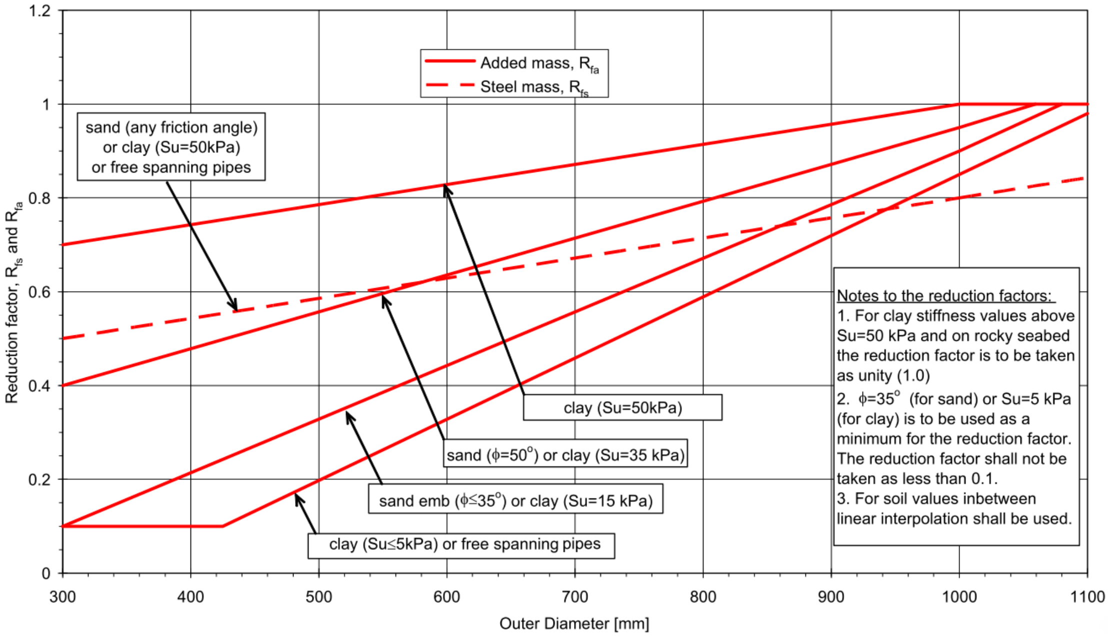

Figure 2-30 Reduction factor of impact energy

DNV-RP-F111(2010) (3.5) suggests that: ‘if no detailed relationship between the impact force and associated indentation of the steel pipe wall is available, the permanent indentation of the pipe shell caused by the impact may be estimated as’:

$$\delta = \left(\frac{F_d}{5\cdot\sigma_0\cdot t^{3/2}}\right)^2 - \left(\frac{F_d\cdot\sqrt{0.005\cdot D}}{5\cdot\sigma_0\cdot t^{3/2}}\right) \qquad (2.21)$$

where

δ	is dent depth
F_d	is the dent force
σ_0	is the yield strength
t	is the pipe wall thickness
D	is the diameter of the pipe

The relationship between impact force and impact energy is

$$F_d = \sqrt[3]{(\frac{75}{2} \cdot E_i \cdot t^3)} \tag{2.22}$$

where

F_d is the dent force

E_i is the impact energy absorbed by the pipe

t is the pipe wall thickness

2.7.2.2 Pull-over Phase

The pull-over loads of trawl boards and beam shoes are mainly came from the dynamic effects, while the pull-over loads of clump weight are governed by quasi-static effects. The maximum pull-over force of trawl boards and beam shoes is given as follows:

$$F_p = C_F V \sqrt{Mk} \tag{2.23}$$

For polyvalent boards $C_F = 8.0(1 - e^{-0.8\bar{H}})$

For V-shaped boards $C_F = 5.7(1 - e^{-1.1\bar{H}})$

$$\bar{H} = \frac{H_{sp} + \frac{D}{2} + 0.2}{B}$$

where

k is the warp line stiffness

V the trawl velocity

M is the steel mass for trawl board or the steel mass of the beam and shoes for beam trawls

C_F is the empirical coefficient of pull-over force based on laboratory and full-scale data. C_F is lower for beam trawls with hoop bars.

H_{sp} is the span height

D is the outer diameter

B is half of the trawl board height.

The total pull-over time T is

$$T = T_f \cdot C_F \cdot \sqrt{M/k} + \delta_p/V \tag{2.14}$$

where

T_f is the factor, 2.0 for trawl boards and1.5 for beam trawls

δ_p is the displacement of the pipe at the point of interaction which is unknown prior to response simulations, therefore, must be assumed before the first simulation.

A comparison of the pull-over force shows that the force from a clump weight is much higher than from trawl boards, especially for seabed pipe or small-diameter pipeline in a span(Askheim and Fyrileiv, 2006). For the pull-over force from a clump weight, a new relationship has been built to consider the quasi-static effects. The maximum horizontal pipeline pull-over force for clump weight is as following:

$$F_p = 3.9 \cdot M \cdot g \cdot \left(1 - e^{-1.8 \cdot h'}\right) \cdot \left(\frac{D}{L_{clump}}\right)^{-0.65}$$

$$h' = \left(H_{sp} + D\right)/L_{clump}$$

(2.15)

where

D is the outer diameter

L_{clump} is the distance from reaction point of centre of gravity of gravity ofthe clump weight

M is the steel mass of a clump weight

g is the gravitational acceleration

The pull-over duration is

$$T = F_p/(k \cdot V) + \delta_p/V$$

(2.16)

where

k is the stiffness of trawl warp

δ_p is the displacement of the pipe at the point of interaction which should be assumed before the first simulation, and correct later.

2.7.2.3 Criteria

DNV-RP-F111 (2010) suggested that the ratio of the permanent dent depth to the outer pipe steel diameter should be below 0.05η, where η is the usage factor. The following table shows the acceptable permanent dent sizes, which are not applicable for notch or sharp indentations because they are not permitted.

Table 2-4 Acceptable dent sizes relative to outer diameter (DNV, 2010)

Frequency class	*Usage*	*Dent depth (% of D)*
High (>100)	0	0
Medium (1-100)	0.3	1.5
Low (<1)	0.7	3.5

Note: Acceptable dent depth also needs to comply with the requirements given in DNV-OS-F101.

For pull-over response, the trawl pull-over load effect should be checked with other loads, and relevant failure modes such as local buckling, global buckling, and accumulated plastic strain should be checked as stated in DNV-OS-F101(2013).

2.7.3 NORSOK Standard U-001(2002)

The NORSOK standard is developed by the Norwegian petroleum industry to ensure the safety for the industry developments and operations. The NORSOK standard U-001(2002) is based on ISO 13628. Section 5.3 gives some regulations on the overtrawlability problem. It states that a model test shall consider the trawl gear type, trawl speed, water depth, friction on seabed and structure, length, stiffness and angle of warp-lines, minimum breaking strength of warp-lines, bobbins and ground ropes.

2.8 Pipe-in-Pipe system and Overtrawlability

Palmer and King (2008) described the pipe-in-pipe system in the book *Subsea Pipelines Engineering*. Pipe-in-pipe (PIP) systems include pipe-in-pipe (Endal and Williams, 1998) and bundles (Song et al., 2009). The inner pipe or the pipe bundles carries the fluid, and the outer pipe or the carrier pipe provides mechanical protection. In between, there is annulus for insulation material, which brings the major advantage for pipe-in-pipe systems that it could achieve high thermal insulation. The structure of the pipe-in-pipe is shown in Figure 2-31, and the structure of bundles is similar that only the inner pipe changes to pipe bundles. One of the bundles cross-sections is given in Figure 2-32.

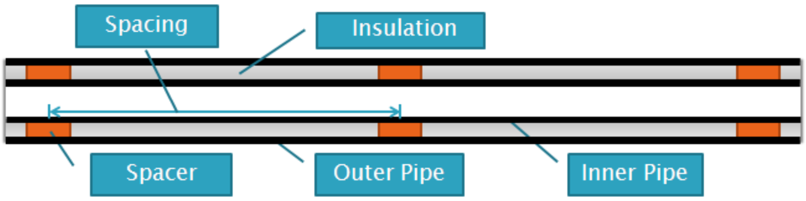

Figure 2-31 Structure of pipe-in-pipe

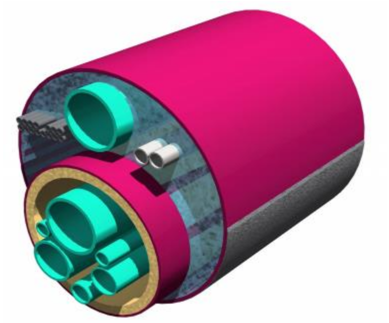

Figure 2-32 Configuration of bundle (Song et al., 2009)

Pipe-in-pipes have distinct advantages for high temperature / high pressure applications. Bundles have the advantage of economical installation(Bai and Bai, 2005). Therefore they are extensively used in the oil industry. Offshore pipeline engineers have also recognized the structural superiorities of the pipe-in-pipe systems (Konuk et al., 2005), so engineers are looking into the possibility of relaxing the criteria of trawl gear interaction with pipe-in-pipe systems.

All the previous tests showed that the large diameter pipelines are generally not affected by the trawl gear impact. However, no test for small diameter pipes was conducted, let alone for a pipe-in-pipe system.

Kristoffersen et al. (2012) shows an example of design under the considerations of buckling and trawling problem for a reeling pipe-in-pipe with outer diameter 15 inch. The main concern for the trawling part was the trawl force might trigger the global buckling. FE models using the software SIMLA were mentioned and the authors think better models could increase the load predictions therefore decrease the design trawl loads. However, the accuracy of the simulations is based on the correction of the pull-over force time history prediction.

Based on the literature review, the goals of this research are as follows:

1. Develop a new model for the dent force and dent depth relationship for pipe-in-pipe systems based on quasi-static and impact tests of pipe-in-pipe systems.

2. Conduct small scale pull-over test for pipe-in-pipe to study the pull-over response of pipe-in-pipe.

3. Investigate the possibility of relaxing the criteria for the outer pipe by FE models.

3 Quasi-static Indentation Test Program

As mentioned in the previous chapter, quasi-static indentation test program and impact test program are used to study the pipe-in-pipe impact response. This chapter describes the quasi-static indentation test.

A quasi-static indentation test is the simplest and most direct way to look into this problem. The specimens are carefully selected to include information such as typical D/t ratio of offshore pipelines, reel-lay restrictions and so on. Two prototypes are decided to study with based on the industry needs. Because of the limitations of the test machine, small-scale pipe specimens are used instead of full-scale pipes. FE models are developed and are validated against the experimental data. The FE method can be a universal method to analyse this issue for other pipes.

3.1 Test Specimen Preparation

The prototype is designed as Table 3-1 shows. OD 323.9 mm and OD 355.6 mm are the two different outer pipes, and OD 219.1 mm is the inner pipe. If all the pipes are scaled with a constant scale factor, an ideal specimen series is shown in Table 3-1. However, these dimensions are not standard sizes, therefore they had to be manufactured specially.

As pipes offered in the Singapore’s market are limited, we have to compromise and not use the ideal sizes. Dependent on what is available in Singapore, the following dimensions are selected, as given in Table 3-2. The scale factors are calculated by ODs. The test pipes' D/t is slightly different compared to the prototypes' D/t. All the pipes were purchased from Super Steel Ltd. The pipes are API pipes grade B, and each length is 6 m as Figure 3-1 shows.

Table 3-1 Ideal scaled pipe

	Original Prototype			*Ideal Model*		
	OD-P (mm)	***t-P (mm)***	***D/t-P***	***D-S (mm)***	***t-S (mm)***	***Scale***
PIP12	323.9	12.70	25.50	80.975	3.18	4.00
	219.1	14.30	15.30	54.775	3.58	4.00
PIP14	355.6	14.30	24.90	88.9	3.58	4.00

Table 3-2 Test pipes

Original Prototype				*Test pipe*				*Prototype of Test Pipe*	
OD-P (mm)	***t-P (mm)***	***D/t-P***	***Scale***	***D-E (mm)***	***t-E (mm)***	***D/t -E***	***Scale***	***OD-tP (mm)***	***t-tP (mm)***
219.1	14.3	15.30	2.46	88.9	5.49	16.19	2.375	211.1	13.04
323.9	12.7	25.50	2.29	141.3	6.55	21.57	2.375	335.6	15.56
219.1	14.3	15.30	2.16	101.6	5.74	17.70	2.135	216.9	12.25
355.6	14.3	24.90	2.11	168.3	7.11	23.67	2.135	359.3	15.18

Figure 3-1 Six meter pipes, four different sizes

Details of the single wall pipe specimens are listed in Table 3-3. For every specimen, the length is 1.5 m, which is about ten times the outside diameter, and cut from the 6 m pipe in the lab as Figure 3-2 shows. A 300 mm section is cut from every 6 m pipe for tensile coupon test. Tensile test results are shown in Appendix C.

Table 3-3 Single wall pipe specimens

	D-E (mm)	*t-E (mm)*	*Length(m)*
SPS1	88.9	5.49	1.5
SPS2	141.3	6.55	1.5
SPS3	101.6	5.74	1.5
SPS4	168.3	7.11	1.5

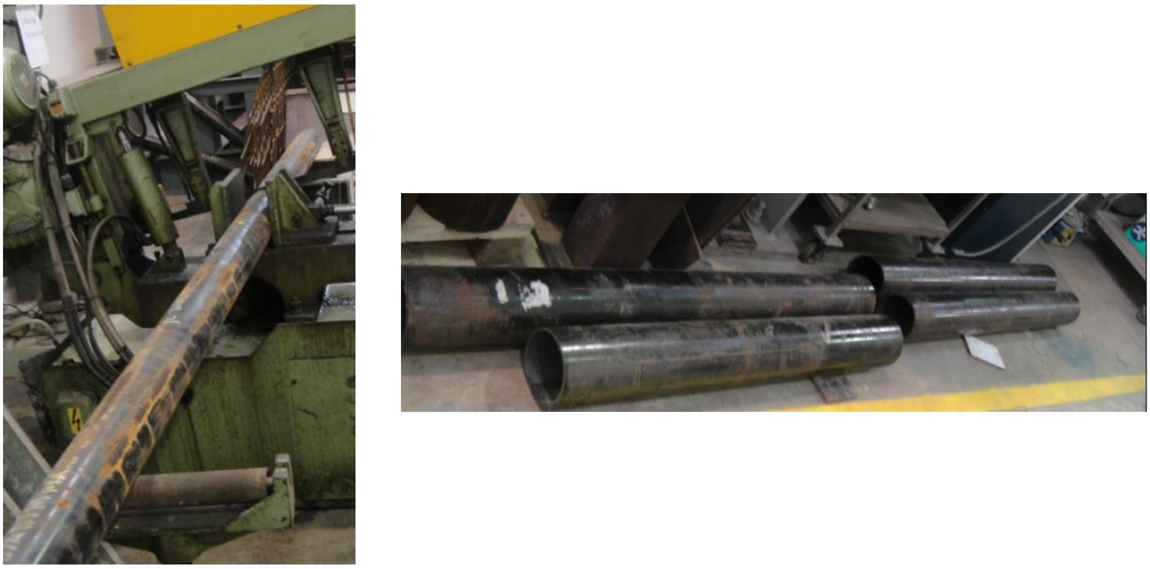

Figure 3-2 Pipe cutting

Two PIP specimens are scaled from the prototypes and assembled with the four single wall pipes. In order to keep the inner pipe's scale factor the same as the outer pipe's scale factor, the model inner pipes are different while there is only one prototype inner pipe. OD 88.9 mm and OD 141.3 mm form a pair, named PPSA, and whose prototypes are OD 219.1 mm and OD 323.9 mm. The scale factors for the inner pipe and the outer pipe are 2.46 and 2.29 respectively. Another pair is OD 101.6 mm and OD 168.3 mm, named PPSB, whose prototypes are OD 219.1 mm and OD 355.6 mm, and the scale factors for the inner pipe and the outer pipe are 2.16 and 2.11 respectively.

The PIP specimen is prepared the same way as used in the offshore industry. Firstly, the pipes were cut to 1.5 m lengths. After preparation of a single wall specimen, the inner pipe had spacers added. There were two types of spacer, one was made of rubber strip, and the other was made of nylon. Nylon material is commonly used as spacer material for pipe-in-pipes in the offshore industry. The spacer material has to be able to support the inner pipe, and at the same time does not reduce the insulation capacity too much. Rubber is softer and easy to prepare, and was used here to study the influence of spacer properties. The rubber strip was wound on the inner pipe to simulate the function of a spacer as Figure 3-3 shows. The nylon spacers were machined into two half rings, connected by bolts, as Figure 3-4 shows. The outer diameters of the spacers are 2 to 3 mm smaller than the inner diameter of the outer pipe. This was for easy installation. Finally, the inner pipe with attached spacers was pulled into the outer pipe. Details of the pipe-in-pipe specimens are listed in Table 3-4.

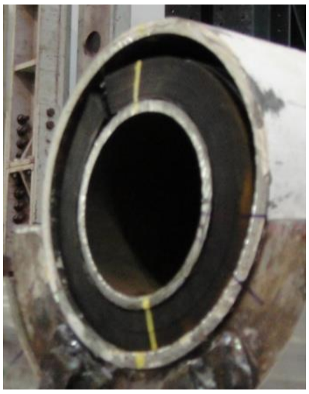

Figure 3-3 Rubber spacer

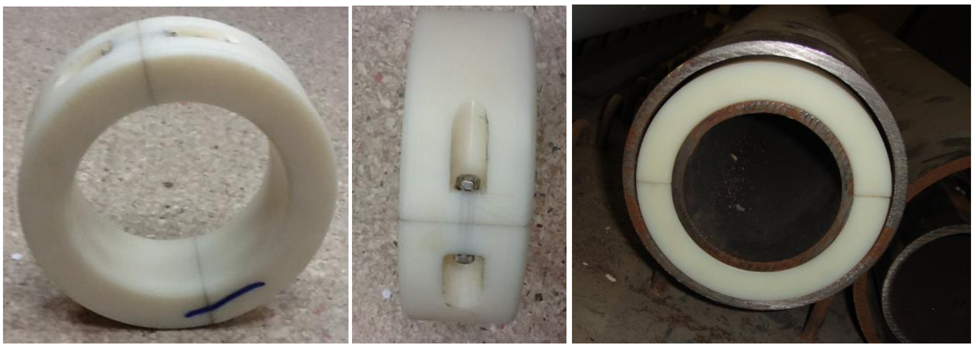

Figure 3-4 Nylon spacer

Table 3-4 Pipe-in-pine specimens

PIP Specimen	**Carrier Pipe**	**Inner Pipe**	**length (m)**	**SPACER**				
				ID (mm)	OD (mm)	Spacing	Width	Material
PPSA1_nylon	141.3	88.9	1.5	88.9	125.1	1 m	50 mm	nylon
PPSA2_rubber	141.3	88.9	1.5	88.9	121	1.5 m	50 mm	rubber
PPSA2 _nylon	141.3	88.9	1.5	88.9	125.1	1.5 m	50 mm	nylon
PPSA3_nylon	141.3	88.9	1.5	88.9	125.1	0.5 m	50 mm	nylon
PPSB2 _nylon	168.3	101.6	1.5	101.6	151.2	1.5 m	50 mm	nylon
PPSB2_rubber	168.3	101.6	1.5	101.6	141.6	1.5 m	50 mm	rubber

3.2 Indenter Design

The indenter used in the experiment should be able to represent the major features of the typical trawl gear. The front of the indenter is the key part as it influences the impact area and shape. There are three typical trawl gear: otter trawl, beam trawl and clump weight (DNV, 2010). The most popular one in North Sea and Norwegian Sea is the otterboard. The population of clump weight is decreasing because of fuel consumption concerns. The clump weight needs much higher horsepower to drive it. The beam trawl is not as popular as the otterboard, however, it will induce a greater damage force to the pipeline. Figure 3-5 shows the beam trawl gear and Figure 3-6 shows the otter trawls in 3-D. According to these data, and the way that the trawl gear interacts with the pipeline, these trawl gear can be idealised as a knife edge indenter that impacts the pipe transversely. Referring to DNV-RP-F111(DNV, 2010), there are two recommended types of indenter. In Figure 3-7, Alt.1 is rounded frontal shape with R equal to 25 mm because both trawl boards and beam trawls have rounded front shapes. Alt.2 has a sharp edge with R equal to 10 mm to simulate a damaged or repaired trawl gear. Figure 3-8 shows the indenter presented in *Guidelines for Trenching Design of Submarine Pipelines* (Trevor Jee Associates, 1999). This indenter is not rounded in front but rounded only at the corner. Indenter width is 60 mm, which is 10 mm wider than DNV type in Figure 3-7.

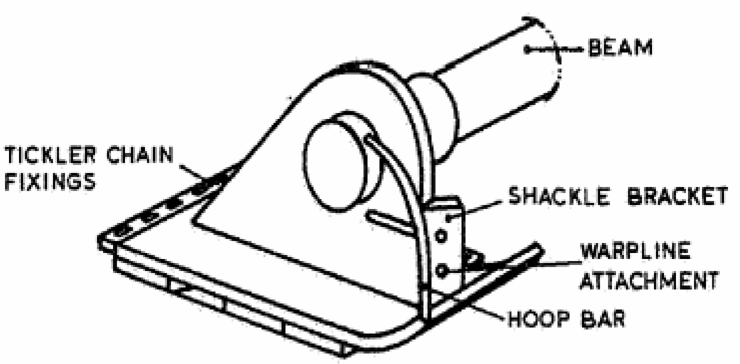
BEAM
TICKLER CHAIN FIXINGS
SHACKLE BRACKET
WARPLINE ATTACHMENT
HOOP BAR

Figure 3-5 Beam Shoe(DNV, 2010)

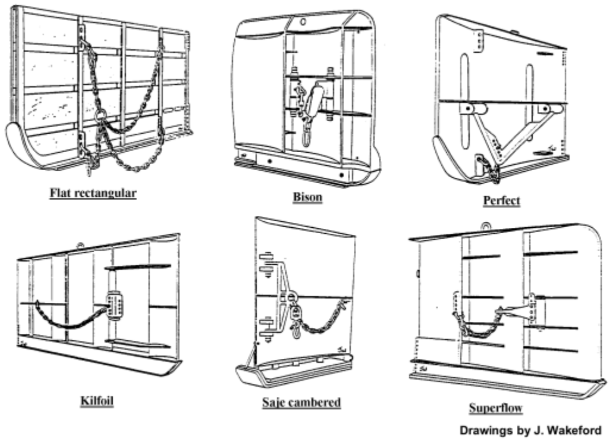
Flat rectangular
Bison
Perfect
Kilfoil
Saje cambered
Superflow
Drawings by J. Wakeford

Figure 3-6 Different otter board design

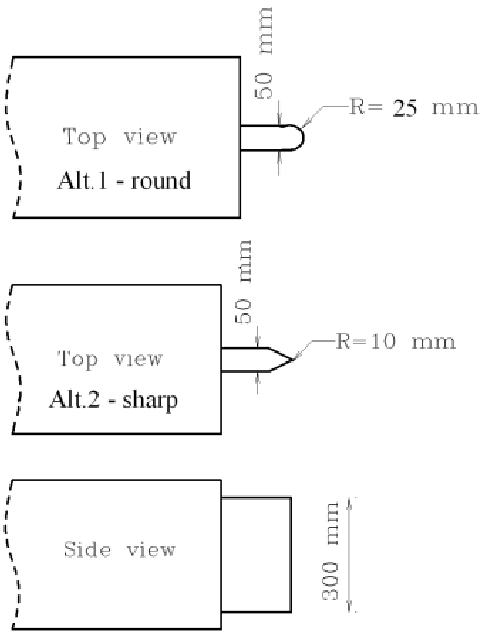
50 mm
R= 25 mm
Top view
Alt.1 - round
50 mm
R=10 mm
Top view
Alt.2 - sharp
Side view
300 mm

Figure 3-7 Recommendation of indenters referring to DNV-RP-F111(DNV, 2010)

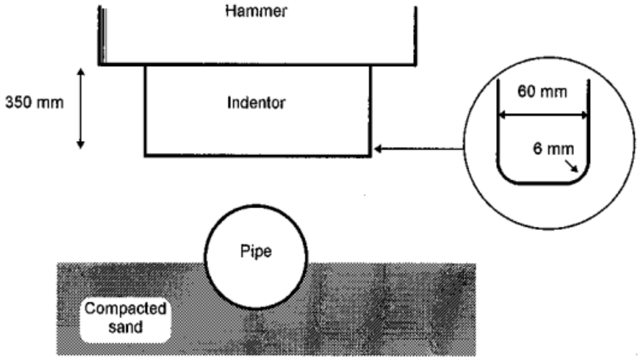
Hammer
350 mm
Indentor
60 mm
6 mm
Pipe
Compacted sand

Figure 3-8 Indenter presented in Guidelines for Trenching Design of Submarine Pipelines(Trevor Jee Associates, 1999)

For our small scale experiment, the indenter has to be scaled in the same way as the pipes. As the scale factor for pipes is about 2.1 to 2.3, based on the DNV-RP-F111(2010) recommendation, R between 11 to 12 mm are suitable for the indentation test. Alternatively R is 13 to 15 mm based on the Guidelines for Trenching Design of Submarine Pipelines. However, if it is too sharp, it may change the failure mechanical behaviour and cannot represent the real situation. Therefore, a front radius r equal to 15 mm is chosen. The design drawing of the indenter is shown in Appendix B, and front radius r is 15 mm and length b is 200 mm.

3.3 Quasi-static Indentation Test Set-ups

Two test rigs are used in quasi-static indentation experiments. The test rig used for the first six tests consists of an vertical actuator that provides the compression force; the displacement control mode is adopted. It can apply a load up to 500 kN, and the stroke of the actuator is from -75 mm to 75 mm. There are two I-beams on the frame, which can be assembled to offer different support conditions. Because this test rig was not available at a later stage, the last six tests used another test rig. That test rig consists of an vertical actuator that provides the compression force up to 10,000 kN; the displacement control mode is adopted. As the capacity of this actuator is much higher than the indentation force in these experiments, and so another load cell with range from 0 to 300 kN is used to measure the indentation force rather than the actuator’s load cell. The stroke of the actuator is from -250 mm to 250 mm. Although the test rig changed, the set-up was not changed. There are two set-ups to offer two different boundary conditions.

Set-up I

Set-up I is illustrated in Figure 3-9. The pipe is sitting on the top of the I-beam, and is fixed with two Omega clamps and several G clamps. A clearer view is shown in Figure 3-10, and Omega clamps are indicated in the figure. Omega clamps are manufactured to fit different size pipes, and named after their shape. This set-up offers the pipeline a rigid boundary condition, which prevents the pipe from developing global deformation. This boundary condition is named as BCrigid.

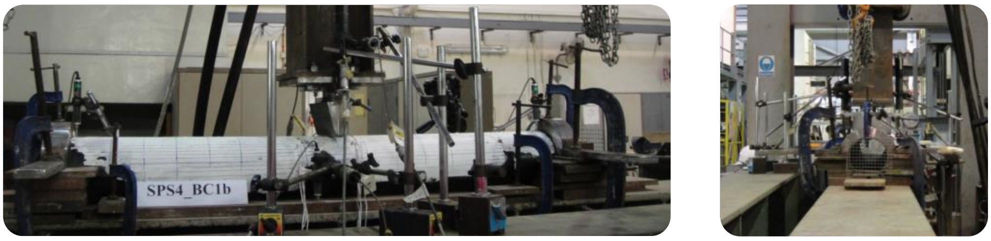

Figure 3-9 Set-up I

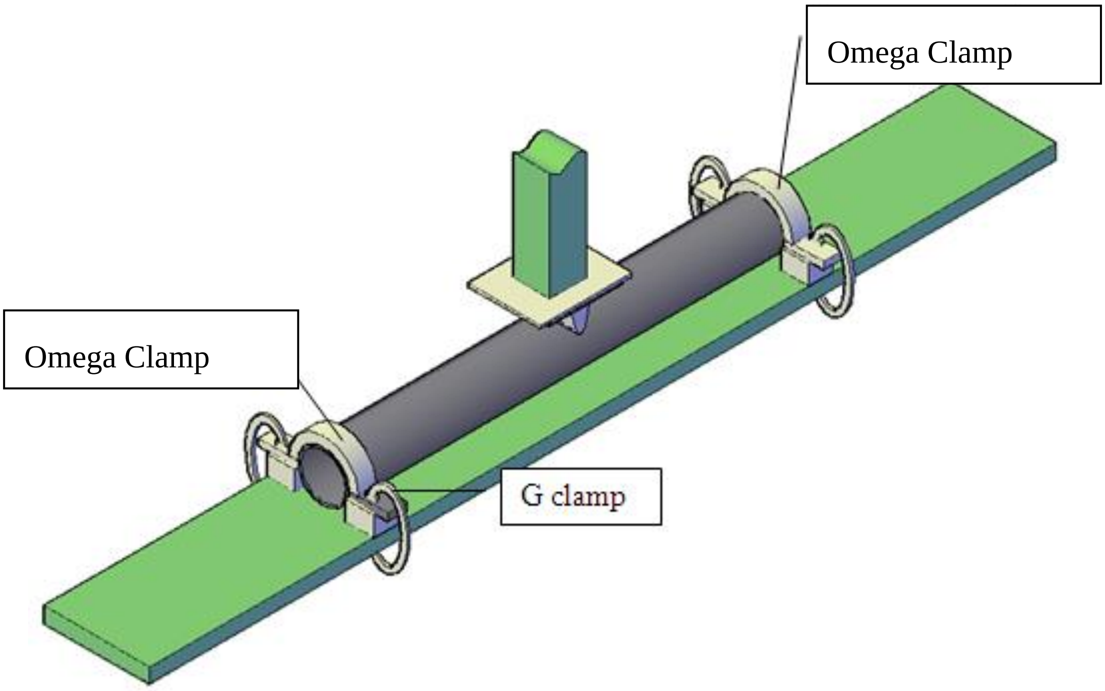

Figure 3-10 Set-up I

Set-up II

Set-up II offers the simple support boundary condition, as Figure 3-11 and Figure 3-12 shows. Both I-beams are used to support the saddle supports, and the specimen is sitting on the saddle supports. The saddle supports are rockers and are free to rotate in one direction. The left side support is fixed on the I-beams, and the right support is supported by rollers, which allow the right side support to move along the pipe axis.

The last six tests were used another test rig to accomplish. There are four I-beams on the frame, and only two of the I-beams are used in the test to give a simple support boundary condition as Figure 3-12 shows. The set-up of the new rig is illustrated in Figure 3-13.

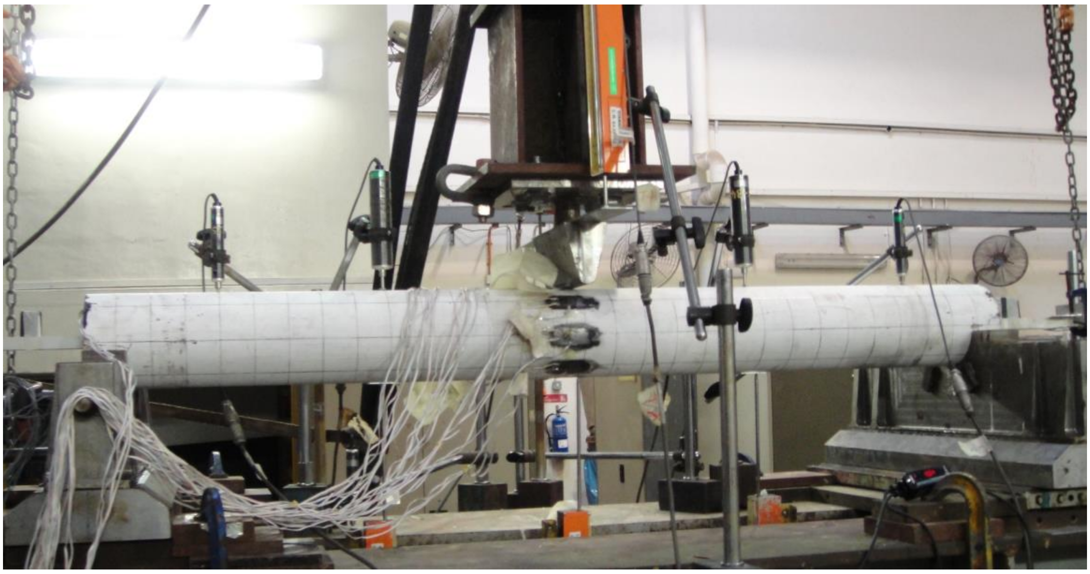

Figure 3-11 Set-up II

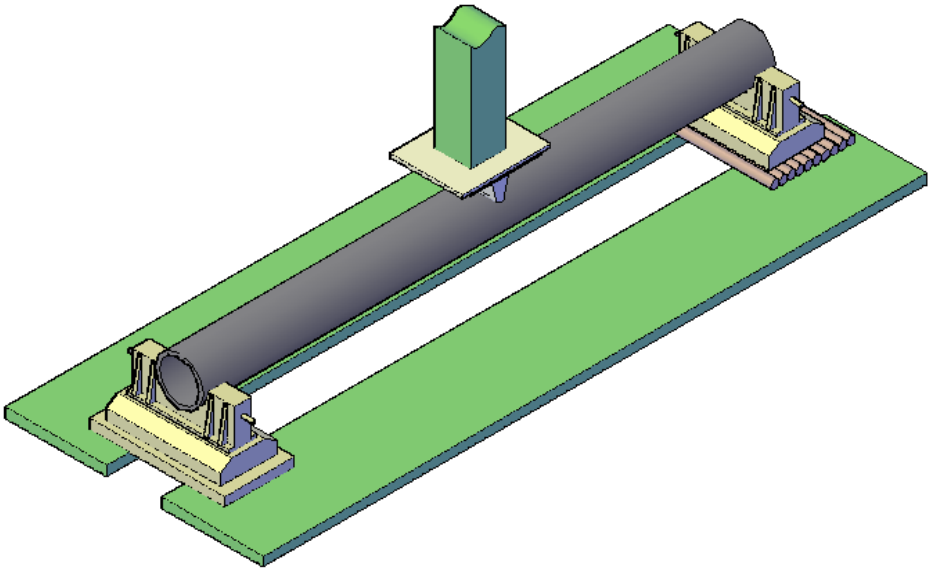

Figure 3-12 Set-up II

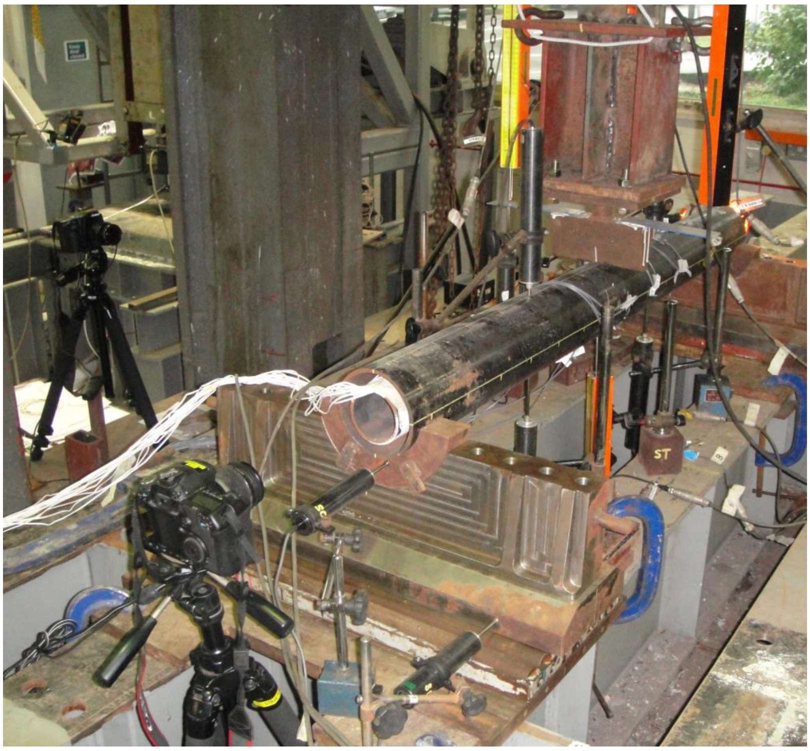

Figure 3-13 Set-up II on another rig with simple support boundary condition

3.4 Instrumentations

All the specimens’ strains are measured by rosette strain gauges and single strain gauges as Figure 3-14 shows. There are two options for gauge length, one 5 mm and the other 2 mm. In the high strain gradient area, strain gauges with the smaller gauge length are used. For SPS1 and SPS3, as the diameters of these two pipes are smaller, strain gauges with gauge length 2 mm are used.

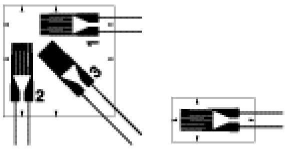

(a) (b)

Figure 3-14 (a) Rosette strain gauge (b) single strain gauge

All these strain gauges are connected by wires in a quarter-bridge configuration to a computer controlled data logger system. The strain gauge output is recorded by the computer with a nominal accuracy of ±1 micro strain.

Transducers are used to measure the displacement of the system. For BCrigid boundary condition, nine transducers are used, as Figure 3-15 shows. Two of them are attached to the indenter on opposite sides, and to measure the indenter's displacement. Another one is attached to the indenter to measure the indenter's horizontal movement. Two of them are placed on the top of the pipe at both ends and they measure the ends movement. Two of them measure the I-beam's deflection, and the rest measure the pipe's radial movements.

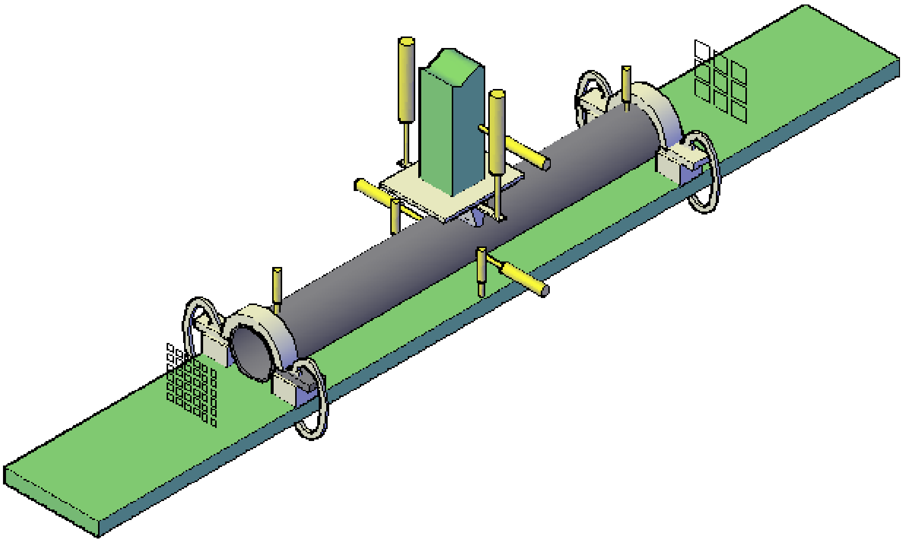

Figure 3-15 Layout of the transducers of boundary condition 1 set-up

The transducers used in the BC simple support experiment are illustrated in Figure 3-16. Two of them are attached to the indenter and measure the indenter's displacement. Two of them measure the deformation at the top, and another three measure the deformation at the bottom. Others monitor the set-up's stability.

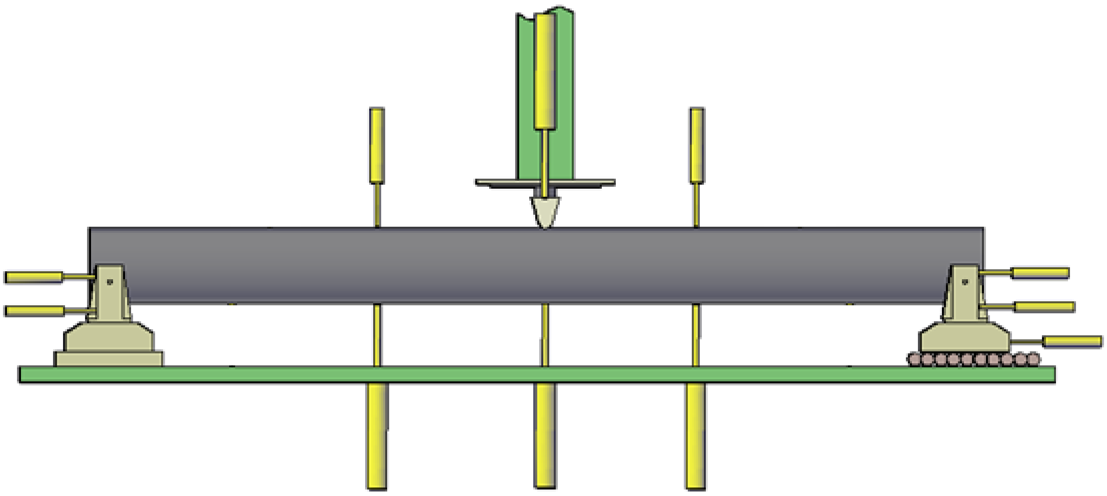

(a)

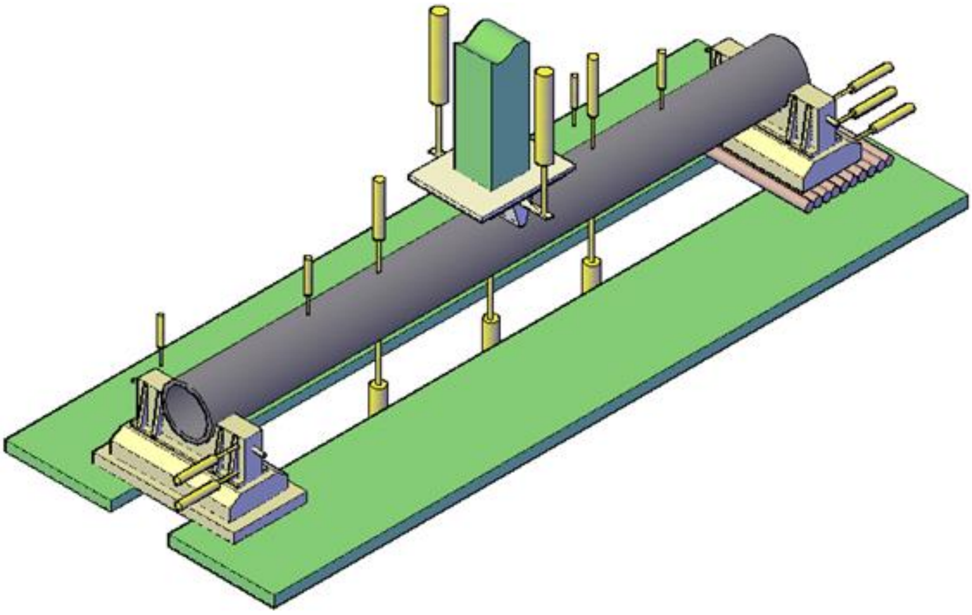

(b)

Figure 3-16 Layout of the transducers of boundary condition 2 set-up (a) front view (b) 3D view

The first step of the procedure is to set up the system. If everything is ready, a formal testing will start. The loading rate is small at the beginning, about 0.1

to 0.2 mm/min. After the curve of indentation force and displacement increase flattens out, the loading rate is slowly increased to 1 or 2 mm/min. The unloading process begins about 120 to 130 mm (with three exceptions). The unloading rate is significantly higher, and unloading data is recorded (with two exceptions). The exceptions will be explained in the next section.

3.5 Quasi-static Indentation Test

This experiment program aims to understand the pipe-in-pipe (PIP) system's response under a concentrated force. This phase concerns only quasi-static loading. Eleven tests are shown in the thesis, and their details are given in Table 3-5. "BCrigid" means that the boundary condition of these tests is clamped ends and rigid bottom support, associated with set-up I. The boundary condition for all other tests is simple support, referring to set-up II. Six of them are single wall pipe tests, and the other six are pipe-in-pipe (PIP) tests.

Table 3-5 Tests summary of quasi-static indentation test

Test Time	*Test Name*	*Test Specimen*	*Set-up*
17/06/2011	SPS4_BCrigid	SPS4	I
23/06/2011	SPS4	SPS4	II
14/07/2011	SPS2	SPS2	
21/07/2011	PPSB2_rubber	PPSB2_rubber	
29/07/2011	PPSA2_rubber	PPSA2_rubber	
27/01/2012	SPS3	SPS3	
30/01/2012	SPS1	SPS1	
31/01/2012	PPSA2_nylon	PPSA2_nylon	
02/02/2012	PPSA1_nylon	PPSA1_nylon	
07/02/2012	PPSB2_nylon	PPSB2_nylon	
09/02/2012	PPSA3_nylon	PPSA3_nylon	

3.6 Test Results of Quasi-static Indentation Test

3.6.1 Single Wall Pipe Indentation Test Results

3.6.1.1 Set-up I

Set-up I offers the rigid boundary condition, which is fixed end with a rigid bottom support. The specimen is supposed to have no global deformation under this boundary condition. However, during the test, it is observed that the pipe bends and the two ends turn up as Figure 3-17 shows. G clamps were not able to resist the bending force, and were damaged. In fact, this boundary condition was no longer fully fix-ended at that moment.

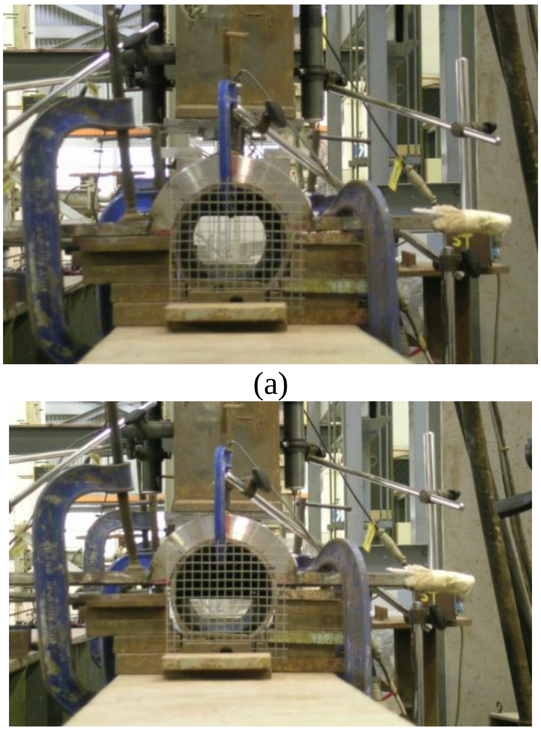
(a)

(b)

Figure 3-17 Pipe end turned up (a) Original position (b) Turn up

Their indentation force-indenter displacement relationships of SPS4_BCrigid are shown in Figure 3-18. The maximum force in the figure is around 235 kN, and at that point, there was no sign of failure.

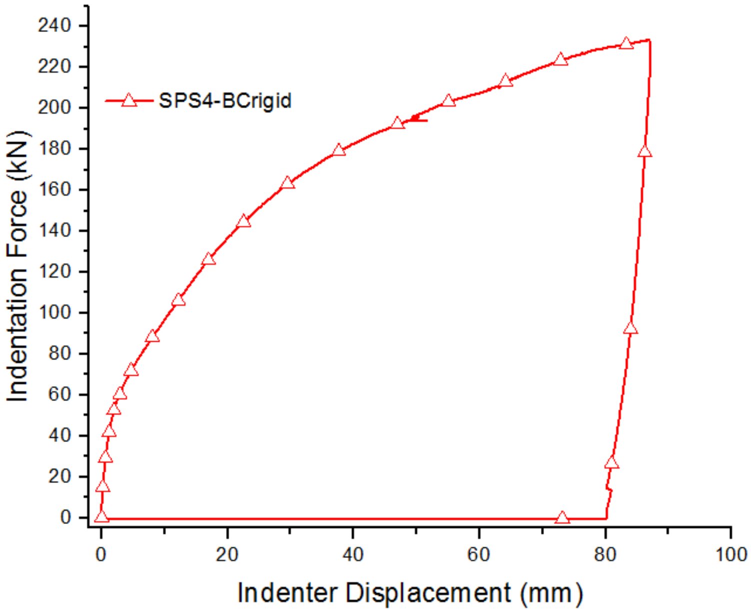

Figure 3-18 Test results of SPS4_BCrigid

3.6.1.2 Set-up II

The pipe is simply supported in Set-up II as Figure 3-12 shows. Specimens associated with set-up II have more global deformation and less local deformation under this boundary condition compares to the previous one. Indentation force-indenter displacement relationships are shown in Figure 3-19.

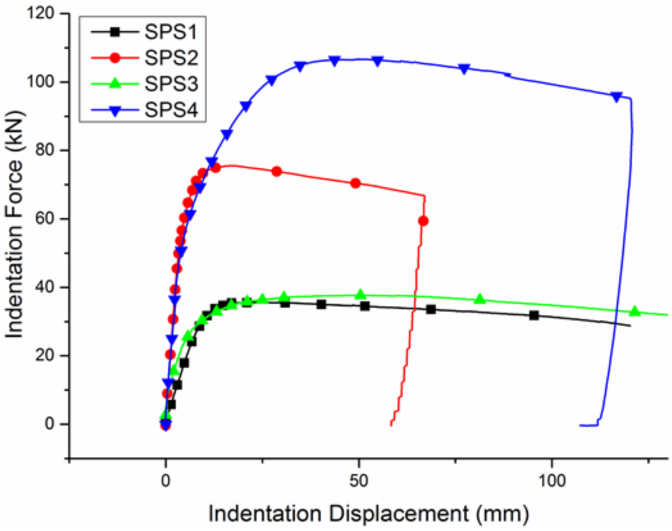

Figure 3-19 Test results of SPS1 to SPS4

According to the comparison, the larger diameter pipe has a higher resistance against indentation loading. The small difference between SPS1 and SPS3 is because of the material difference. Although SPS3 is a slightly larger in diameter, the material of SPS3 is weaker with a lower yield stress than the material of SPS1.

3.6.2 Pipe-in-pipe Indentation Test Results

Pipe-in-pipe quasi-static indentation tests are only conducted using set-up II. During the tests, it is clear that the inner pipe is not deformed before the outer pipe actually touches the inner pipe, unless the indentation is applied directly over the spacer, according to the data from the strain gauges installed on the outer pipe and inner pipe as Figure 3-20 shows. The data show that the outer pipe was deformed at the very beginning, and that the inner pipe’s strain stayed zero for some time. One exception was when the indenter was dented at the position above the spacer. In that case, the inner pipe deformed together with the outer pipe, and it required a higher indentation force.

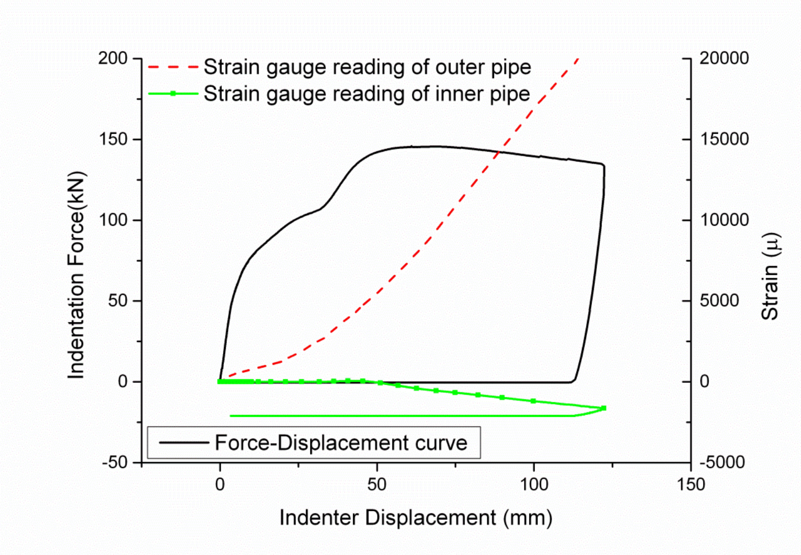

Figure 3-20 Strain gauge reading of outer pipe and inner pipe

There are two different spacers used in the tests. One spacer is made of rubber, which is a hyper-elastic material, and very soft. Another spacer is made of nylon, which is much harder than rubber. For the rubber spacers, the inner pipe did not deform immediately but the rubber spacers did. The rubber spacers were squeezed as Figure 3-21 shows. For the nylon spacers, when the spacing is 1.5 m, the nylon spacers do not deform much. When the spacing is 1 m, nylon spacers deform more. This characteristic should be considered in the design process. A soft spacer protects the inner pipe more but may damage the insulation material and itself.

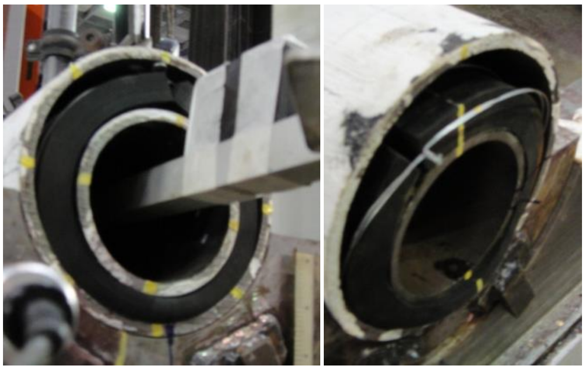

Figure 3-21 Squeezed rubber spacer

Figure 3-22 shows the indentation force – indentation displacement relation of pipe-in-pipe indentation tests. The force data were recorded by the load cell. The displacement shows the indenter’s displacement. Generally speaking, the PPSB group has higher indentation resistance than the PPSA group because of the larger outer pipe. PPSA3 has a higher indentation resistance than PPSA1 and PPSA2 because the impactis directly on the spacer. It requires higher force to deform to the same level; however, in this case, the inner pipe was damaged earlier than in the other cases.

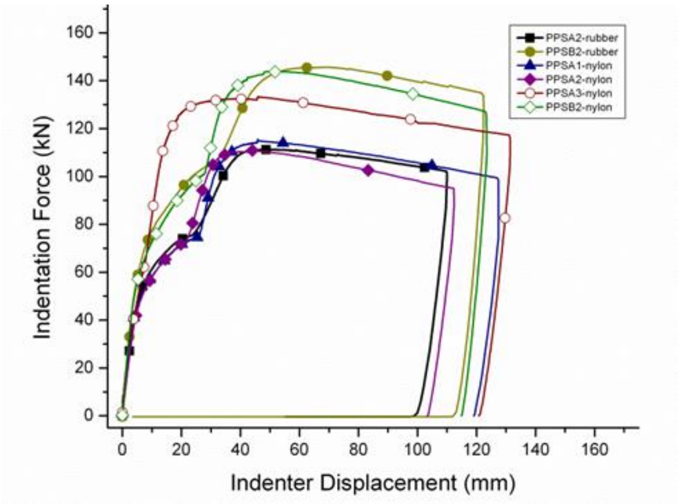

Figure 3-22 Test results of pipe-in-pipe indentation tests

3.7 Discussion of Test Results

The boundary condition that aims to only generate the local deformation is the BCrigid. However, as the G-clamps are not able to hold the pipe on the rigid base, the pipe eventually developed global deformation. The case SPS4-BCrigid is used to compare with various theories mentioned in section 2.2. Some of the theories have limitations in applications, especially the semi-empirical relationships. For example, Soreide and Amdahl (1982) developed a simplified approach and which is valid for thick pipe with *R/H* ratio less than 17.5 or *R/H* less than $4.5 \times 10^9/\sigma_0$. Walker and Kwok (1986) pointed out that many methods are intended for the prediction of the local damage to rather thin tubes over short spans.

For convenience, the equations are reiterated here. Equation EW is the semi-empirical relationship developed by Ellinas and Walker (1983).

Equation EW:
$$F_d = KM_{0t}\left(\frac{\delta}{D}\right)^{1/2} \tag{3.1}$$

Equation DO is the model developed by De Oliveira et al. (1982).

Equation DO:
$$F_d = 4Dt\sigma_0\sqrt{\pi\frac{t\delta}{D^2}\left[1-\frac{1}{2}(n-1)^2\right]} \tag{3.2}$$

Equation WS were developed by Wierzbicki and Suh (1988), and Equation WS1 is for no axial force while Equation WS2 is for axial force equal to fully plastic axial force.

Equation WS1 & WS2:
$$\frac{F_d}{M_{0t}} = 16\sqrt{\frac{\pi}{3}}\sqrt{\frac{D}{t}\frac{\delta}{R}}\sqrt{1-\frac{1}{4}\left(1-\frac{N}{N_0}\right)^3} \tag{3.3}$$

Equation WS3 was developed by Wierzbicki and Suh (1988) for the case of no restriction of rotation.

Equation WS3:
$$\frac{F_d}{M_{0t}} = 16\sqrt{\frac{\pi}{16}\frac{\delta}{R}\frac{D}{t}} \tag{3.4}$$

Equation DNV (DNV, 2010) was based on the model of De Oliveira et al..

Equation DNV: $F_d = 5\sigma_0 t^{2/3}\delta^{1/2}$

(3.5)

The test result of SPS4-BCrigid is compared with the theories in Figure 3-23. Suppose the pipe only has local deformation under boundary condition BCrigid as the global deformation is much smaller in this case, then the indentation force is equal to the denting force, and the indenter displacement is equal to the dent depth. According to the comparison, Equation EW is very conservative compared to the test result in this case as it is limited by the data or the empirical experience. Equations WS1, WS2 and WS3 all agree better with the test result. They are all based on the theory developed by De Oliveira et al. (1982). Wierzbicki and Suh (1988) improved the relationship by restoring the cross-section back to the circular one. Equation WS1 is for no axial force and Equation WS2 is for the axial force equal to the fully plastic axial force. As in the current experiment, there is no axial force generated, Equation WS1 is closer to the test result, while Equation WS2 is more conservative. Moreover, Equation WS3 calculates the response force as only half of Equation WS1, and it is not suitable in the cases here. The difference between the theories and the results is also induced by the material property as in the theories the material is rigid-plastic, and the global deformation as there is some bending developed in the test. More comparable result can be generated by finite element method, because in the finite element model, the material can be treated as rigid-plastic and the boundary condition can be idealised and able to prevent the pipe from having any global deformation.

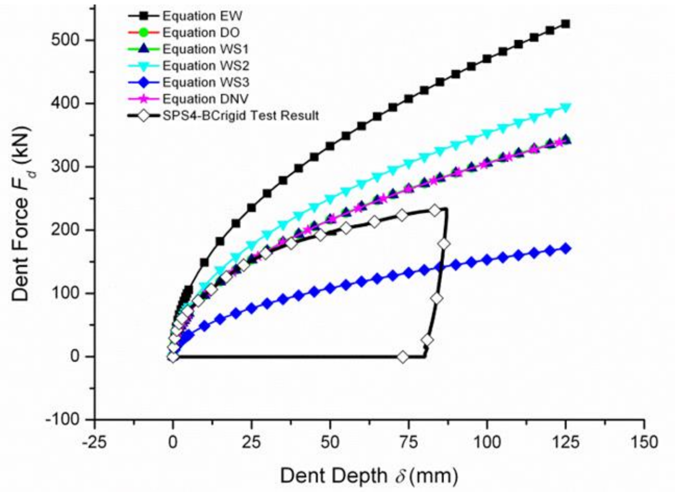

Figure 3-23 Comparison between the SPS4-BCrigid test result and theories of pure denting

The pipe experiences much more global deformation under the simple support boundary condition. Thomas (1976) did experiments with simple support boundary condition and he concluded that there were three phases during the deformation: denting, bending and collapse. However, according to current experimental results, the two deformation processes are began at the beginning and developed together. The bending was not obvious at the beginning of Thomas' experiments, and that might be because the span was short. He also mentioned that if the D/t ratio was bigger, the second phase started later; and if the span was larger, the deformation in the first phase was reduced. This shows the trend that if the span is large enough, the bending deformation will be large enough to be noticed at the beginning.

Take the experiment SPS4 in the current quasi-static indentation test program as an example. For convenience, the deformed shape is repeated here as Figure 3-24 shows. According to that, there is a relationship that $u = d + b$. u is the indenter's displacement, d more relates to the denting deformation (dent depth δ), and b relates more to the bending deformation. u is measured by the displacement transducer attached to the indenter and b is measured by the displacement transducer attached to the middle of the bottom. Based on the relationship $u = d + b$, d can be calculated. d and b are shown in Figure 3-25. According to that, the bending deformation starts at the very beginning, and increases steeply at a later stage.

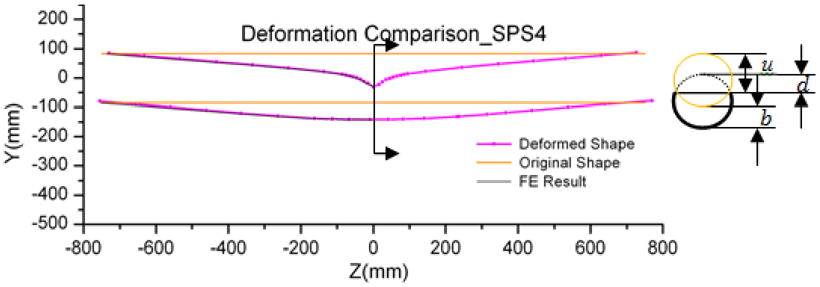

Figure 3-24 SPS4 deformed shape

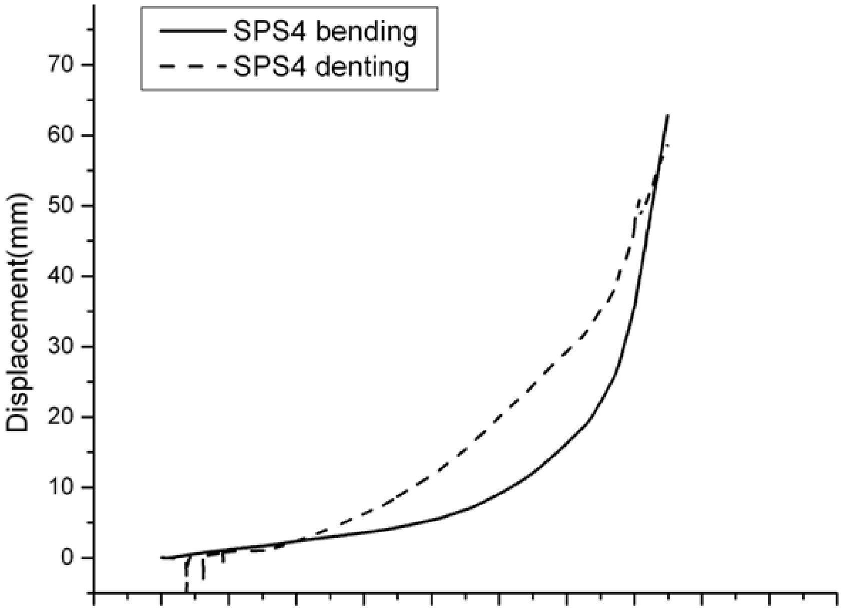

Figure 3-25 SPS4 denting and bending relationship

De Oliveira et al. (1982)treated the denting and bending as two separate phases. The load deflection curve of SPS4 is calculated according to De Oliveira's theory as Figure 3-26shows. The curve marked "De Oliveira F_d" represents the denting process, and the curve marked "De Oliveira F_b"

represents the bending process. Those two curves cross at one point, and before that point, there is only the denting process. After that point, there is only the bending process. The entire curve is indicated by circles. Compare the load deflection curve to the test result of SPS4; the maximum force calculated by De Oliveira’s theory is much higher than the test results. The reason is the denting process is influenced by the bending process from the beginning of the deformation, which has not been accounted. Another misfit is the bending capacity decreases much faster in the theory than in the experiment. This is because u is not the dent depth. Because of the bending deformation, the indenter displacement u is larger than the dent depth. This theory can be improved by considering the interference between the denting effect and the bending effect, and this part of the work is described in Chapter 6.

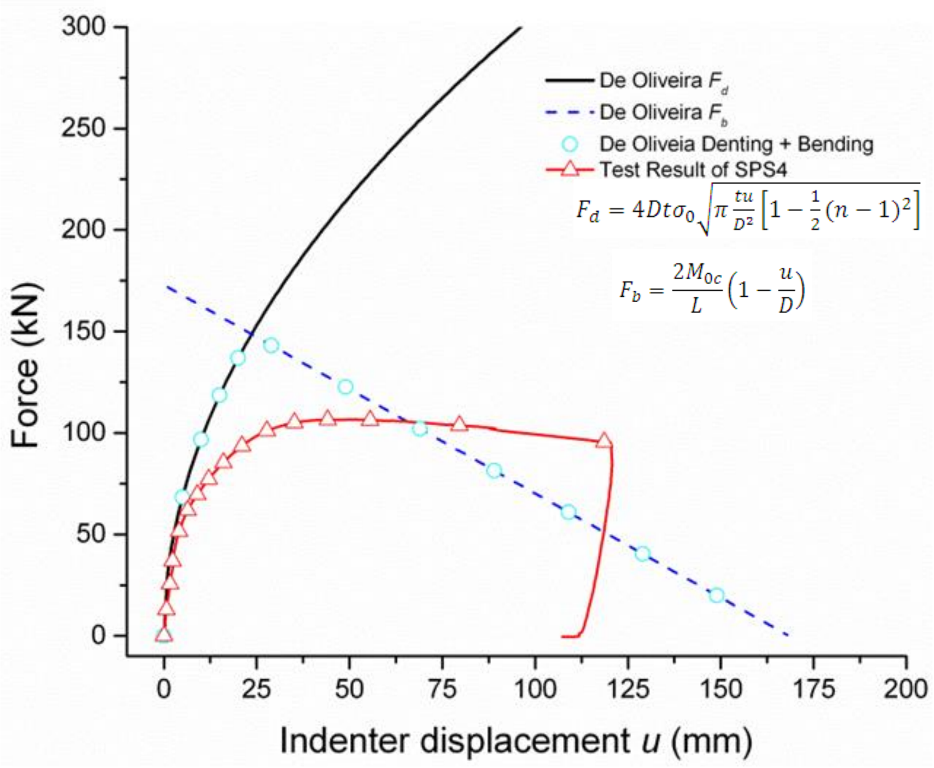

Figure 3-26 De Oliveira theory compare with the test result of SPS4

3.8 Model Test Data Scale Up

To scale up the model test data, according to the scaling law, the force is scaled up by 2.38^2 times (PPSA) or 2.14^2 times (PPSB), and the deformations are scaled by 2.38 or 2.14 times. The indentation force and indenter displacement can be drawn for the prototypes. Here, the case SPS2, PPSA2-nylon and PPSB2-nylon are used as examples to show the scaled up results, as Figure 3-27 shows. The area below the indentation force and indenter displacement curve is the indentation energy, and which is integrated and plotted in the figure. The dimensions of test pipes, prototypes of the test pipes, PIP12 and PIP14 can refer to Table 3-2.

When the indentation force reaches a maximum, the indentation energy is much smaller than the final energy shown in the figure. The energy when the maximum force is reached is about $4.2*10^4$ J. This is about a trawl gear weighted about 9333 kg moving at 3 m/s. Though in reality, the kinetic energy of the trawl gear is not totally transferred to impact energy. Secondly, the boundary condition on the seabed is different. Moreover, with a different length of the pipe, the deformation is different. With a longer section involved, less energy will be absorbed by local deformation.

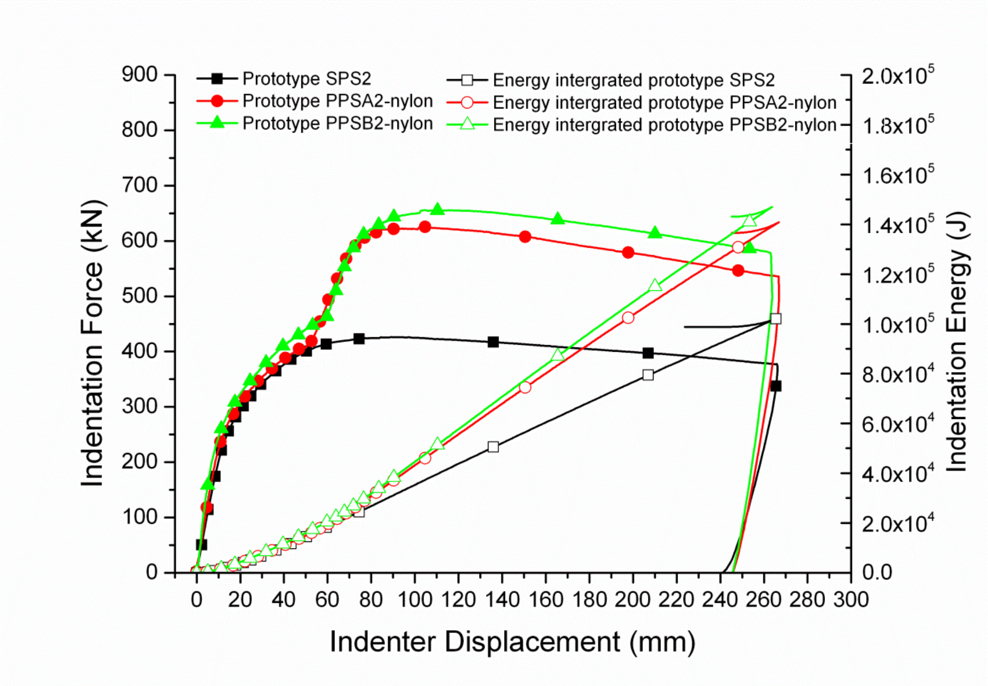

Figure 3-27 Prototype indentation force and indentation energy

3.9 Summary

Quasi-static indentation tests for single wall pipes and pipe-in-pipes were all conducted. The mechanical behaviour of the pipeline under the knife edge indentation was carefully studied. The main findings are:

1. Quasi-static indentation tests show that the deformation of the pipe includes local deformation and global deformation, and that both occur at the beginning. With different combinations of outer diameter, thickness, length and the boundary condition, the proportions of the local deformation and global deformation are different. The pipe will finally buckle, especially when it suffers from a large global deformation.
2. The relationships between indentation force and indentation displacement are compared and investigated. If the location of impact

by the indenter is not above the spacer, the inner pipe will not deform until the outer pipe actually touches the inner pipe. In this way, the outer pipe offers protection to the inner pipe to some extent. When the indenter dents over the spacer, the pipe-in-pipe will act as a single pipe with a higher indentation resistance, but the inner pipe will be deformed from the beginning. This becomes one advantage of pipe-in-pipe that the outer pipe is able to protect the inner pipe to some extent.

4 Impact Test Program

Although quasi-static indentation test is the simplest way to look into trawl gear impact problem, the difference between the quasi-static response and the impact response is unclear, and that makes the quasi-static indentation tests inadequate as the interference between the pipeline and the trawl gear is not a static process. In order to determine whether the impact response is different from the quasi-static response, as well as to quantify how much the difference is, impact tests have been conducted. There are altogether three impact tests, and their details are given in Table 4-1. Impact height gives an impact velocity of about 3 m/s, which is similar to the trawl gear moving velocity.

Table 4-1 Impact tests

Test Time	*Test Name*	*Specimen*	*Set-up*	*Impact Height*
28/03/2012	I_SPS2	SPS2	III	0.5
04/04/2012	I_PPSA2_nylon	PPSA2	III	0.5
05/04/2012	I_PPSB2_nylon	PPSB2	III	0.5

4.1 Impact Test Design

The experiment set-up is shown in Figure 4-1 to Figure 4-3 and called set-up III. The whole system includes an impact tower, steel block and indenter, winch controller, pipe supporting system, laser lights, data logger and high speed cameras. An impact tower 7.5 m high is used to carry out the impact test. The whole frame is firmly bolted on the concrete base to increase the rigidity of the entire system. The indenter is attached to a steel block, and the steel block can slide freely along the guide rails and impact vertically. The steel block and the indenter together can reach to 1400 kg and drop from a 5.5 m height. In this impact test, the drop height of 0.5 m and the total mass of 1350 kg were used. In order to fit the impact machine, the front radius of impact indenter is 30 mm. This indenter is twice of the radius of the indenter used in the quasi-static test. FE analysis is conducted to prove that this change will not influence the result. Three load cells were installed in the indenter to measure the reaction force when the indenter impacts the pipe. The indenter’s direction is perpendicular to the pipe’s longitudinal direction. A mechanical hoisting system (winch) which is controlled by a hydraulic system is used to raise the steel block and indenter to the required height. The pipe is sitting on the saddle supports, which are those used in the quasi-static indentation tests. However, both the supports are not able to move sideways. In order to prevent the pipe from jumping up during the impact, two Omega clamps cover the ends of the pipe as illustrated in Figure 4-3. The plates have slots which allow the saddle supports to rotate but prevent the vertical displacements. The pipe can develop bending deformation together with local deformation with this boundary condition.

Fewer strain gauges are used in the impact tests than in the quasi-static tests because of the limitations of the number of the data logger channels. The strain gauge layout is shown in Figure 4-4. There is a rosette strain gauge on the top, 1D distance from the centre point. Another strain gauge, which is a single element one, is attached to the bottom of the pipe, at the centre point. The inner pipe has only one strain gauge installed and it is a single element strain gauge, on the top of the pipe, 1D distance from the centre point.

Potentiometers are used to measure the displacement. The positions of the potentiometers are illustrated in Figure 4-5. Five potentiometers are used in the impact tests. The distances from the small potentiometers to the centre are one OD, two OD and three OD respectively. In order to set up the potentiometers to measure the bottom deformation and receive better data, tiny plates with screw holes are welded on the bottom of the plate to hold the potentiometers. All the potentiometers are fixed to the concrete floor, and slightly attached to the pipe with welded screw holes.

Both the pipe and the indenter have ruler scales, and they can be recorded by the high speed camera. Figure 4-7 is a picture captured by the high speed camera. These high speed cameras are capable of capturing 1000 frames per second.

Laser lights are used to measure the impact speed and trigger the data acquisition system. There are two laser lights, which are in a vertical line and a fixed distance apart, both placed slightly higher than the top of the pipe. When the indenter blocks the first laser light, the data logger starts to record. Then the timing when the indenter blocks the second laser light can be used to calculate the impact speed.

During the test, firstly the pipe is positioned on the saddle supports and covered by the Omega clamps at both ends. All sensors are connected to the 16-channel oscilloscope to capture the data and be ready. Then the indenter is slowly raised to the desired height, and kept there for a while. All the instrumentations are rechecked again, especially the trigger system. After making sure that everything is ready, the indenter is allowed to fall freely onto the middle of the pipe. At the same time, the high speed cameras record the process. The data acquisition frequency is $5*10^{-6}$ 1/s.

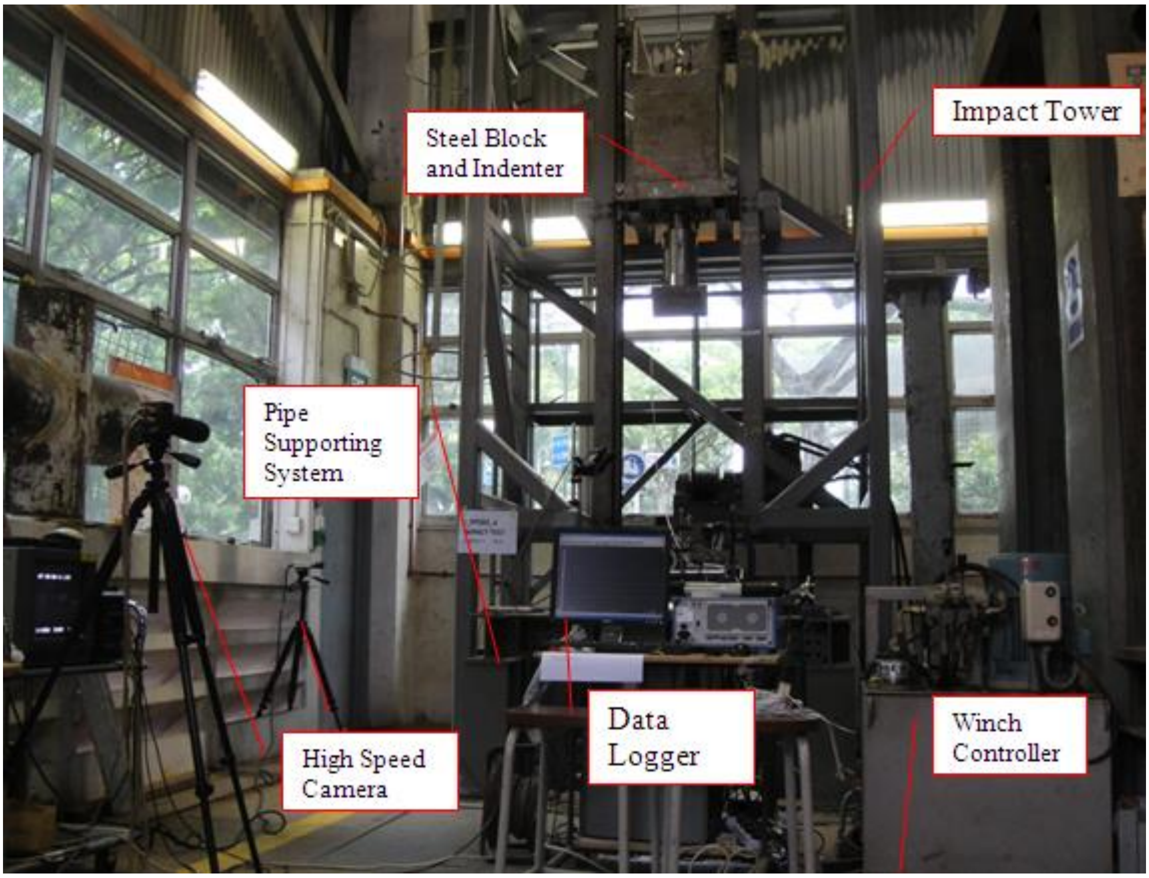
Steel Block and Indenter
Impact Tower
Pipe Supporting System
High Speed Camera
Data Logger
Winch Controller

Figure 4-1 Impact test set-up

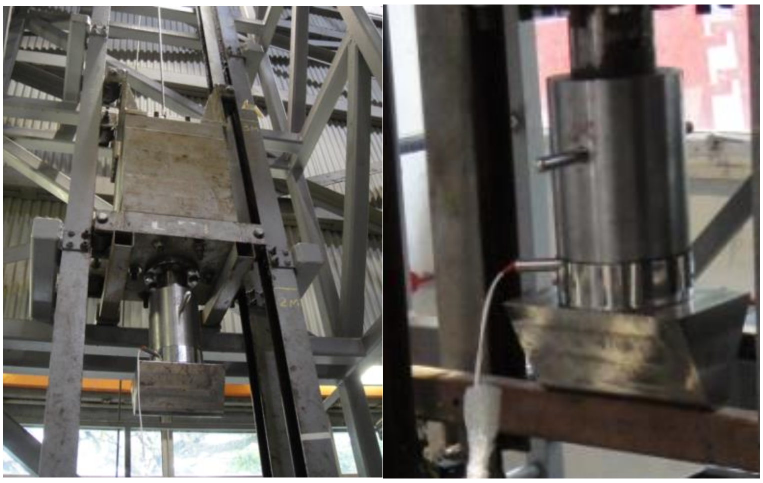

Figure 4-2 Steel block and the indenter

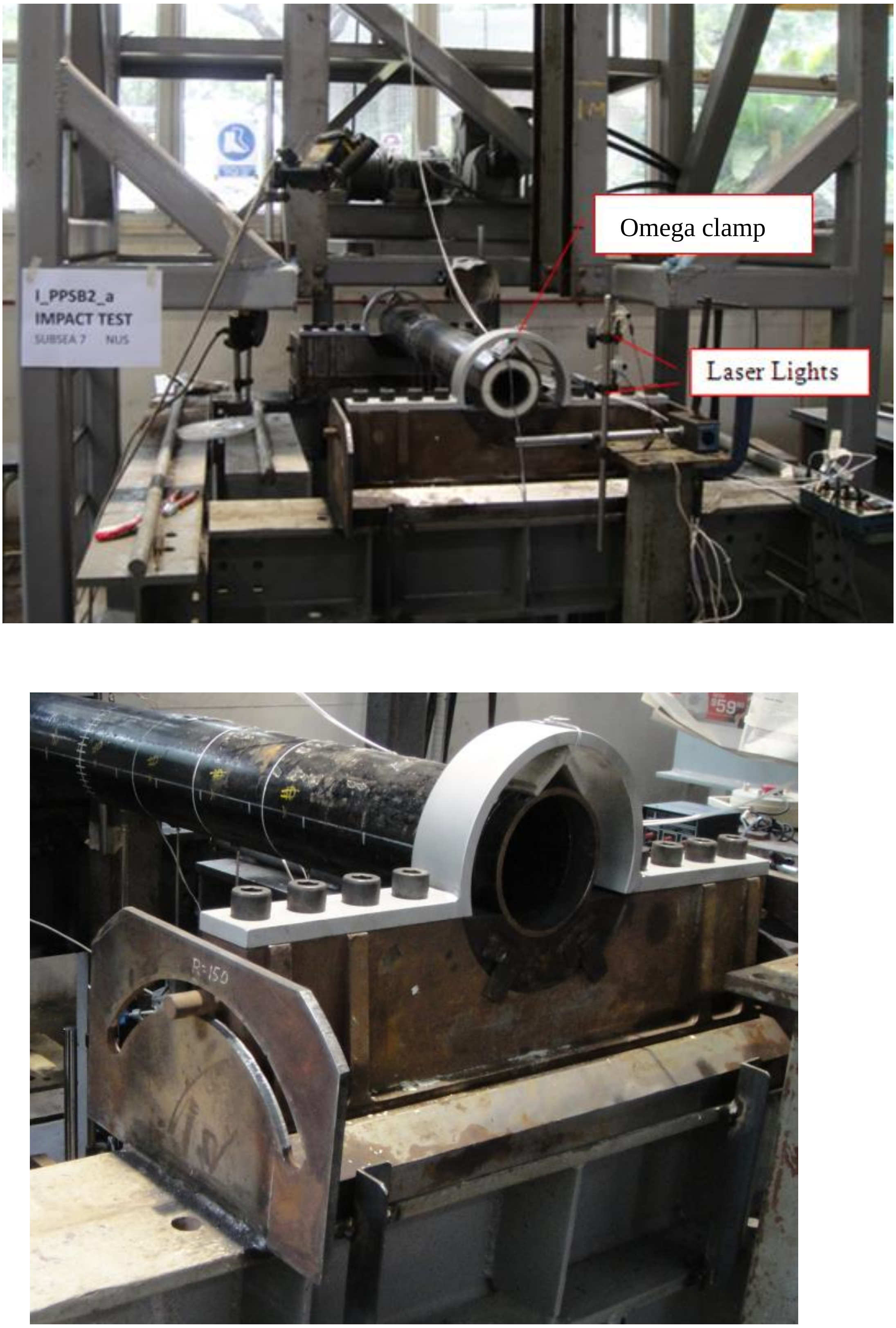
Omega clamp
Laser Lights
I_PPSB2_a
IMPACT TEST
SUBSEA 7 NUS
R=150

Figure 4-3 Pipe supporting system

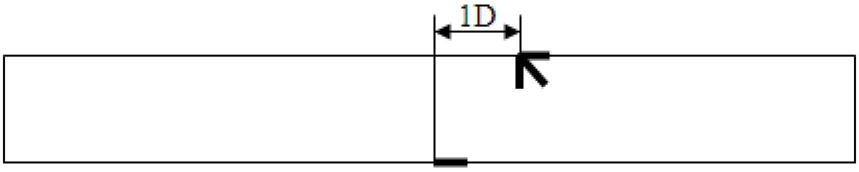

Figure 4-4 Strain gauge layout of single wall pipe or the outer pipe

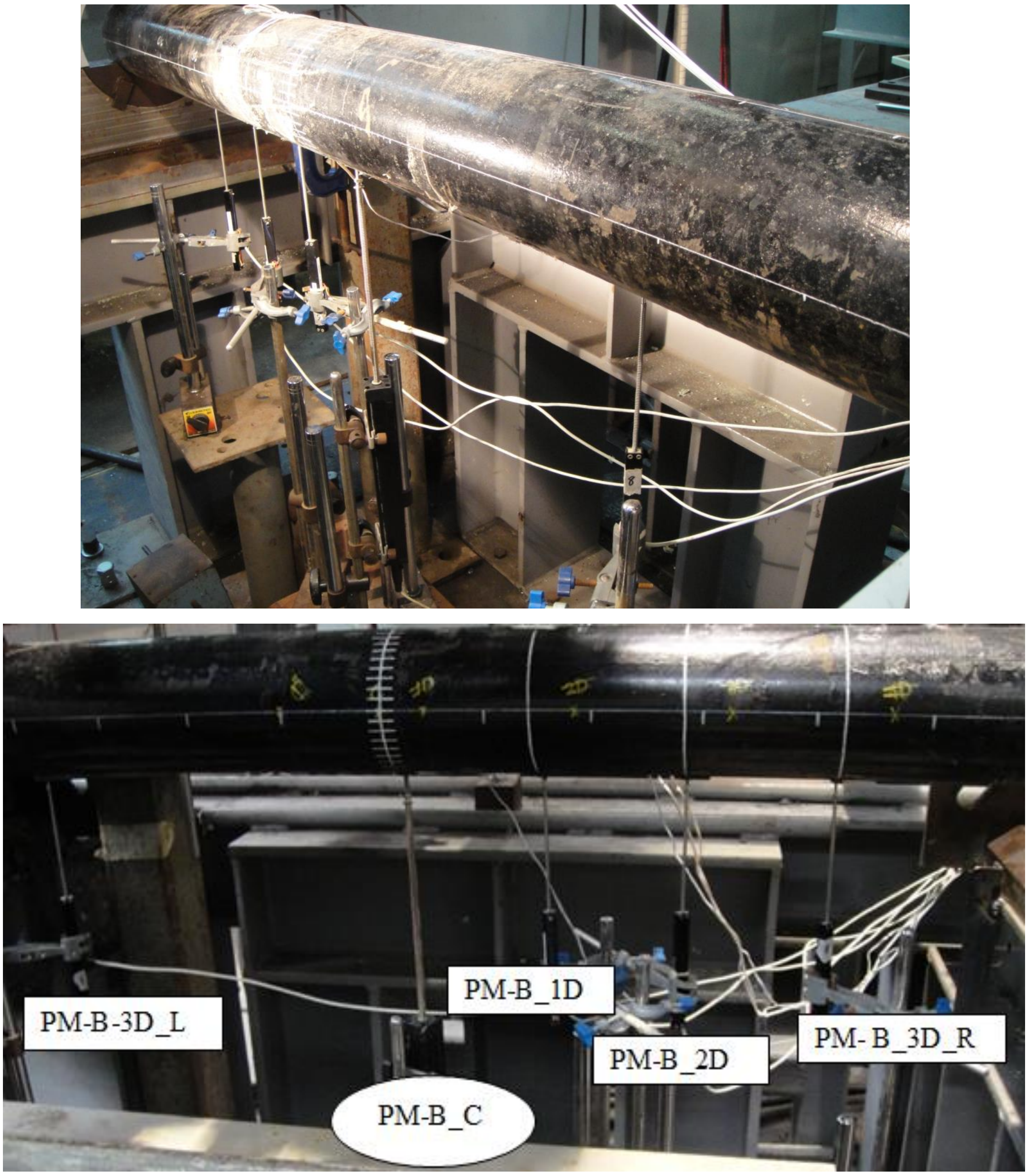
PM-B-3D_L
PM-B_1D
PM-B_2D
PM- B_3D_R
PM-B_C

Figure 4-5 Potentiometers

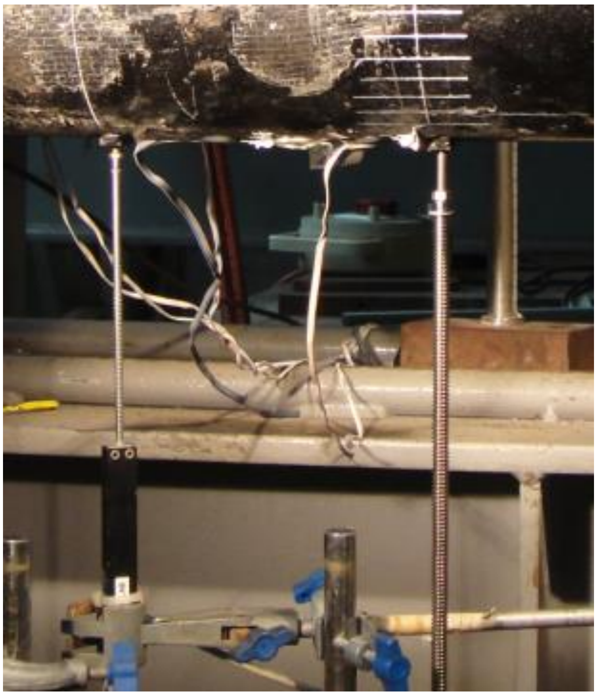

Figure 4-6 Potentiometer attached to the pipe

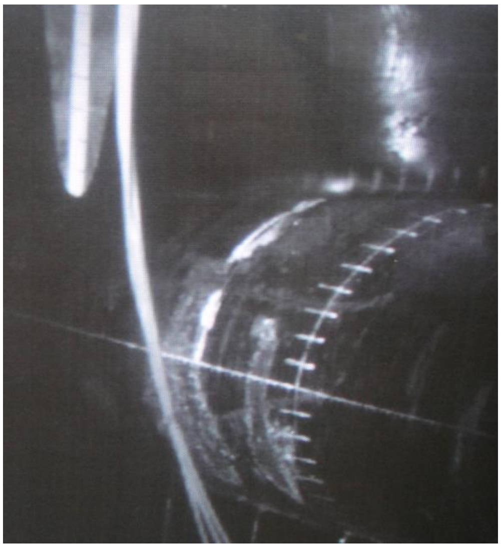

Figure 4-7 A view from high speed camera

4.2 Test Results of Impact Experiments

I-SPS2 is a single wall pipe impact test. Figure 4-8 shows the impact force time history, in which the impact force data is filtered at a frequency of 2000 Hz. The first impact only lasted for less than 0.1 second. The reaction force on the indenter is up to 100 kN. The force is highly influenced by the dynamic response. Figure 4-9 shows the displacement time history. All these data are measured by potentiometers and their positions are given in Figure 4-5. PM-B_3D_R and PM-B_3D_L give similar results, which prove that the measurements are consistent. Figure 4-10 shows the relationship of the indentation reaction force and the bottom maximum deflection, which is distinct from quasi-static indentation force - indenter displacement relationship. (After the first drop, there were several rebound and re-impacts until all the kinetic energy is used up. Only the first one is analysed.)

I-PPSA2 finished earlier than I-SPS2 according to Figure 4-11. As it all happens so quickly, there is no sudden change to be seen from the curve when the inner pipe was impacted. The maximum deflection reaches 40 mm, which is smaller than in the single wall pipe, as shown in Figure 4-12. Figure 4-13 shows the force deflection relationship of I-PPSA2-nylon.

Figure 4-14, Figure 4-15 and Figure 4-16 show the result of I-PPSB2-nylon. The response time is almost as the same as I-PPSA2-nylon, and which is shorter than I-SPS2. According to the test data, PPSB2 requires a much larger impact force to generate the same deflection.

There are two laser lights in the test system to trigger the data logger and measure the impact velocity. The laser lights and the pipe are shown in Figure 4-17. The two red dots are the laser lights and they are higher than the pipe. *d* is the distance, *V* is the velocity and *t* is time. All these distances can be measured, and the time *t1* when the indenter crossed the two laser lights is recorded by the system. All other unknowns can be calculated. Table 4-2 summaries all these details and calculates the kinetic energy based on the calculated velocity. The potential energy is calculated by the steel block and indenter's original height and weight. Obviously there is some energy loss when the indenter drops down but it is not a big amount.

There is no potentiometer to measure the indenter's displacement. According to the high speed camera's images and the markers, the maximum displacement still can be found. Figure 4-18, Figure 4-19 and Figure 4-20 shows the images of the beginning and ending of the first drop. With a ruler in hand, the real scale can be measured and calculated, and one grid on the images is 10 mm. They are summarized in Table 4-3.

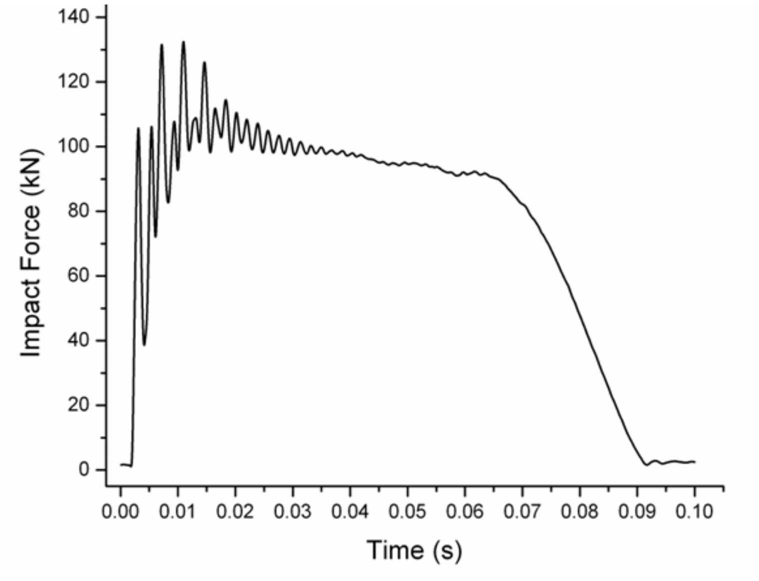

Figure 4-8 I-SPS2 Impact Force Time History

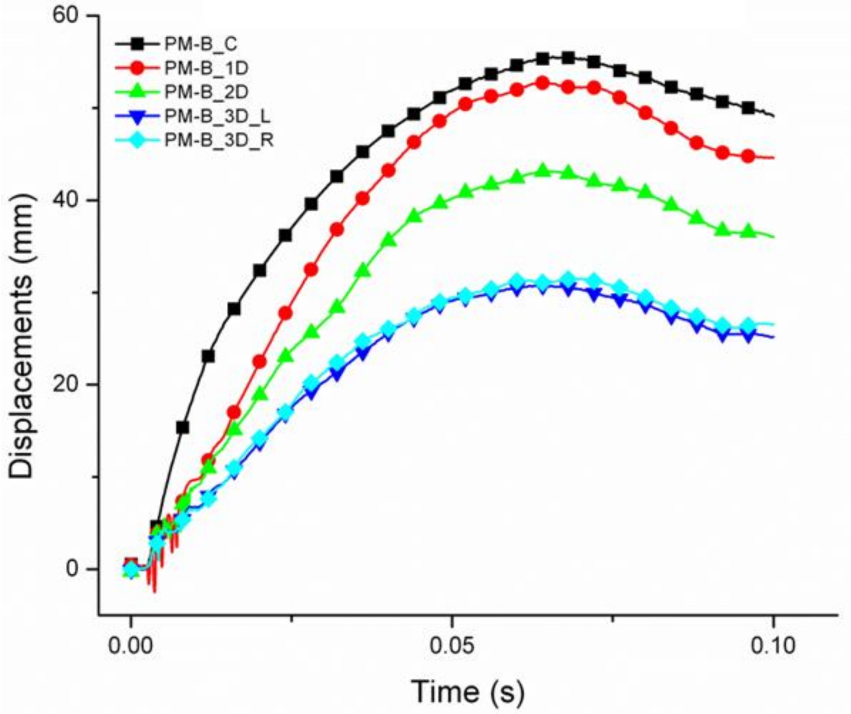

Figure 4-9 I-SPS2 Displacement Time History

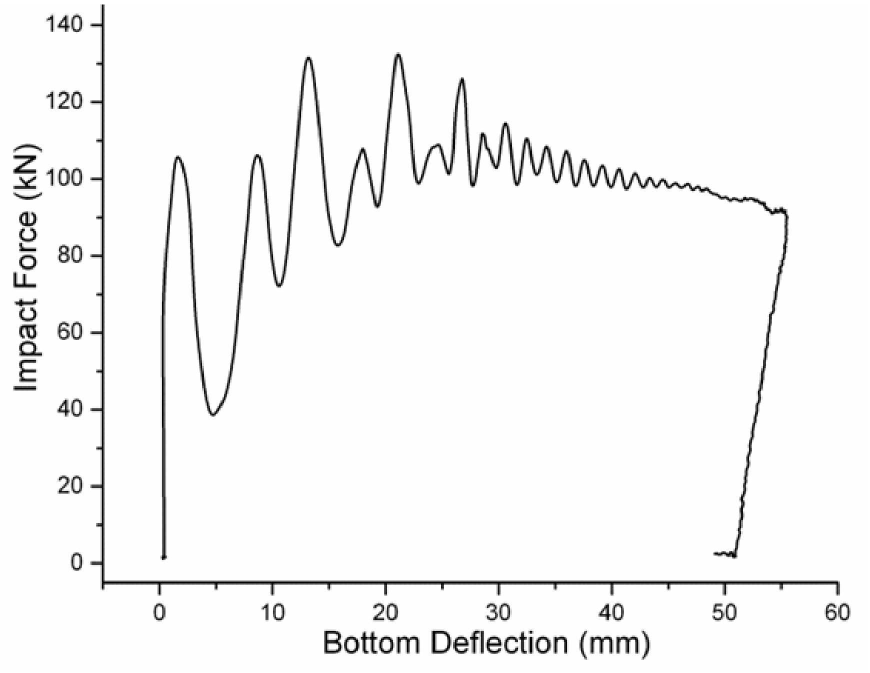

Figure 4-10 I-SPS2 Force Deflection Relationship

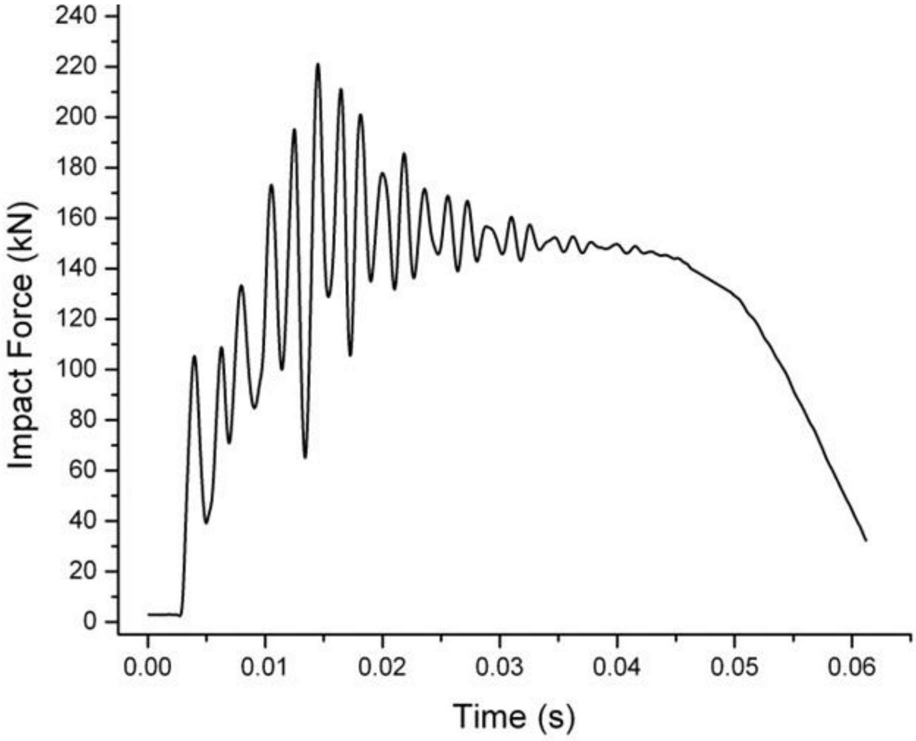

Figure 4-11 I-PPSA2-nylon Impact Force Time History

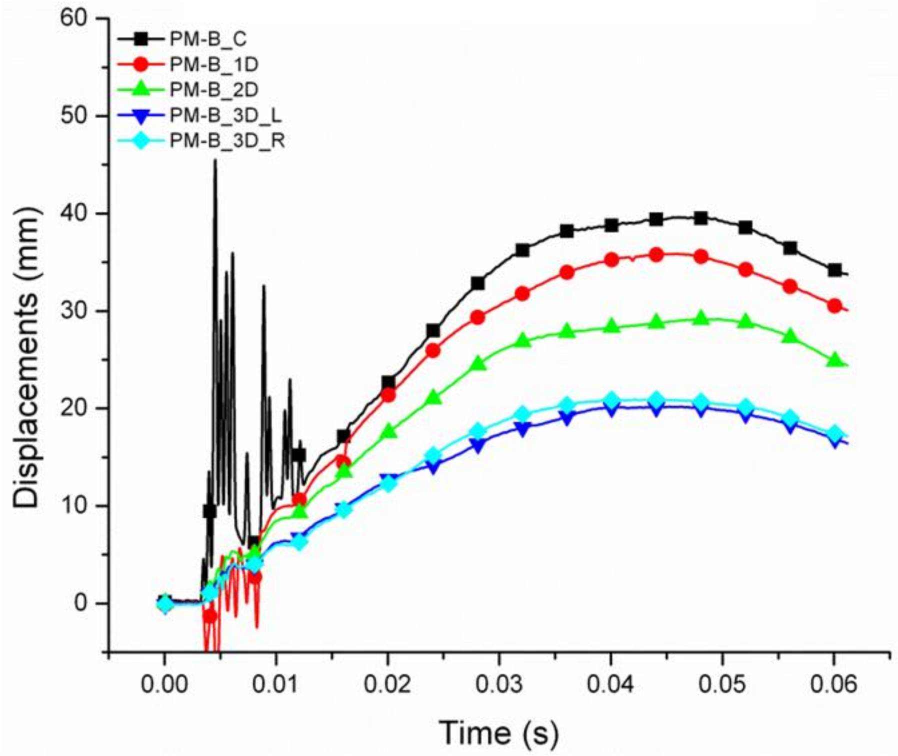

Figure 4-12 I-PPSA2-nylon displacement time history

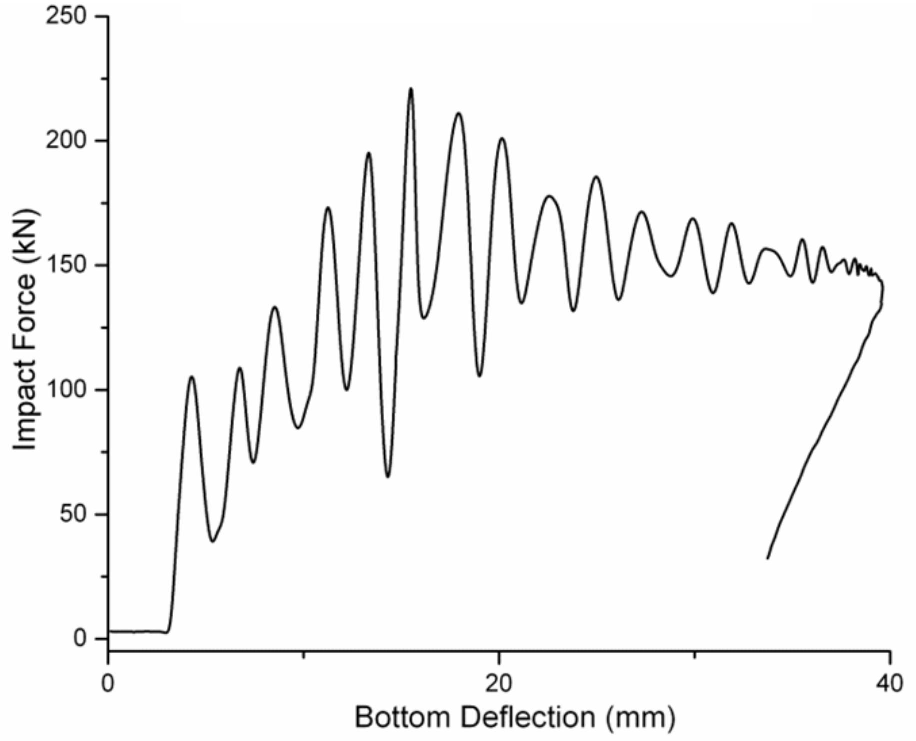

Figure 4-13 I-PPSA2-nylon force deflection relationship

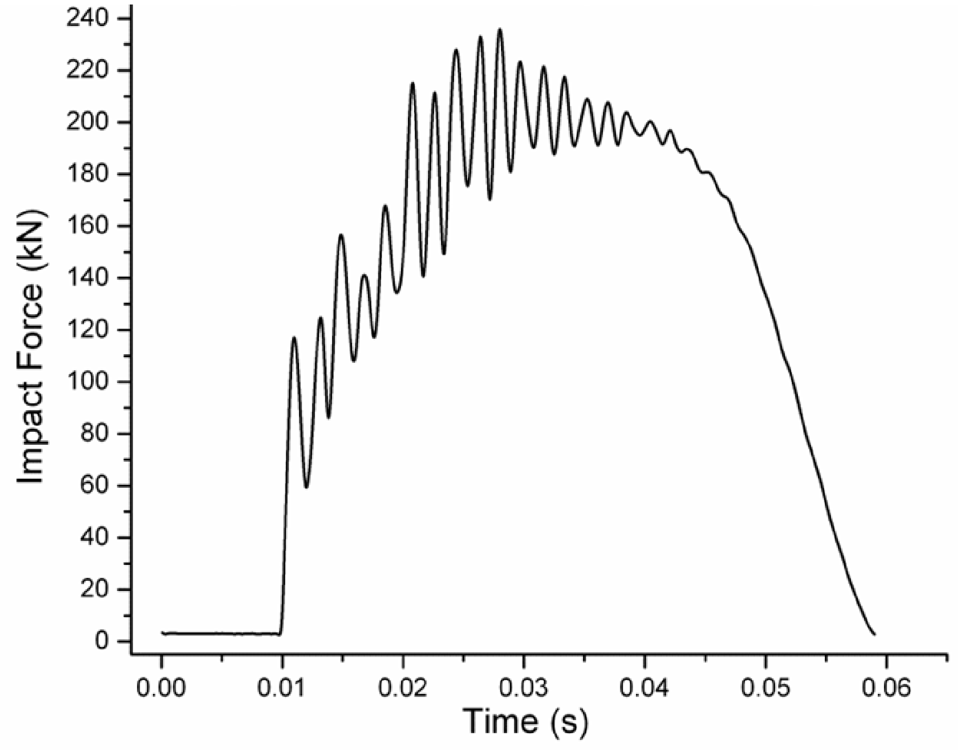

Figure 4-14 I-PPSB2-nylon impact force time history

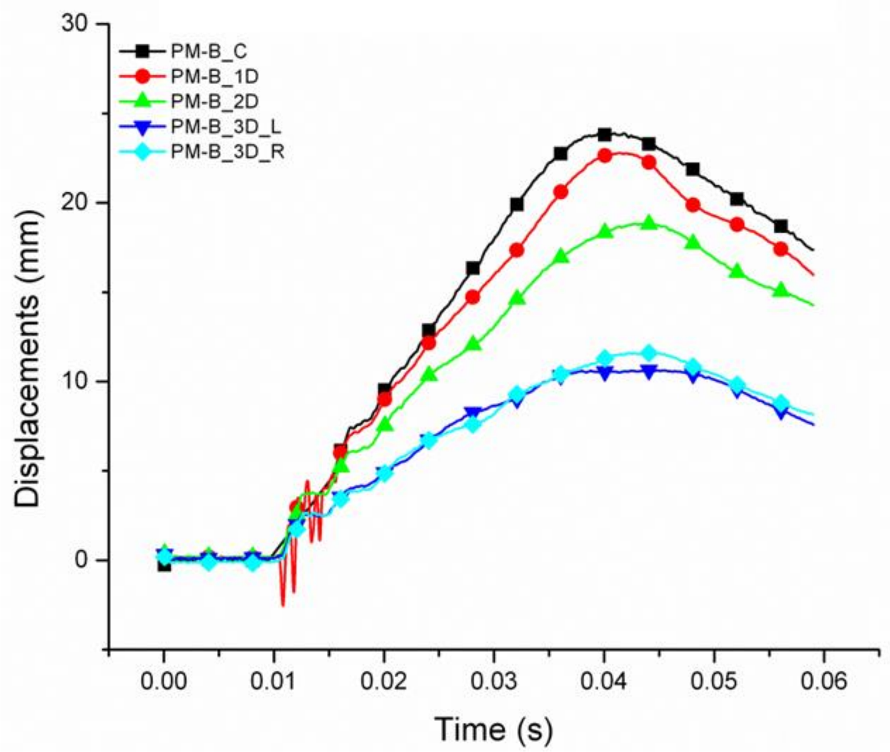

Figure 4-15 I-PPSB2-nylon displacement time history

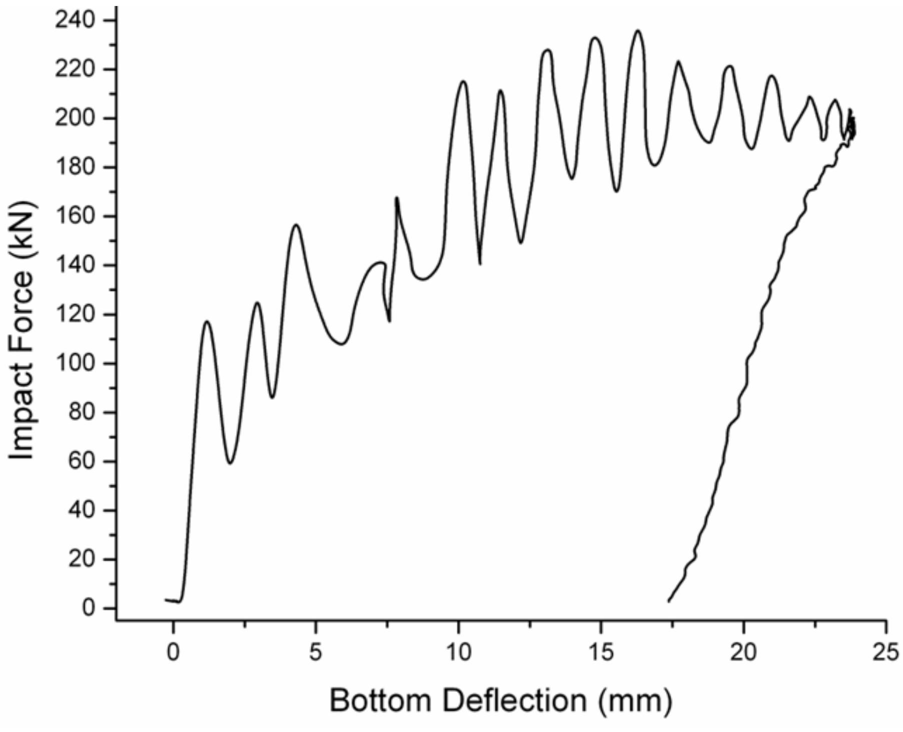

Figure 4-16 I-PPSB2-nylon Force deflection relationship

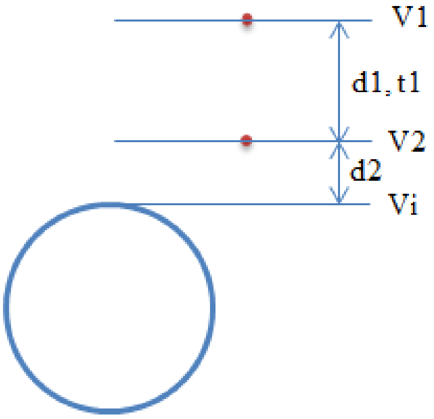

Figure 4-17 Laser lights and pipe position

Table 4-2 Results from the Laser Light Data

	t1 (s)	d1 (m)	V1 (m/s)	V2 (m/s)	d2 (m)	Vi (m/s)	Potential Energy (J)	Kinetic Energy (J)
I-SPS2a	0.039	0.1	2.38	2.76	0.067	2.99	6615	6038.9
I-PPSA2a	0.035	0.1	2.71	3.05	0.011	3.09	6615	6424.4
I-PPSB2a	0.037	0.1	2.58	2.94	0.031	3.04	6615	6244.4

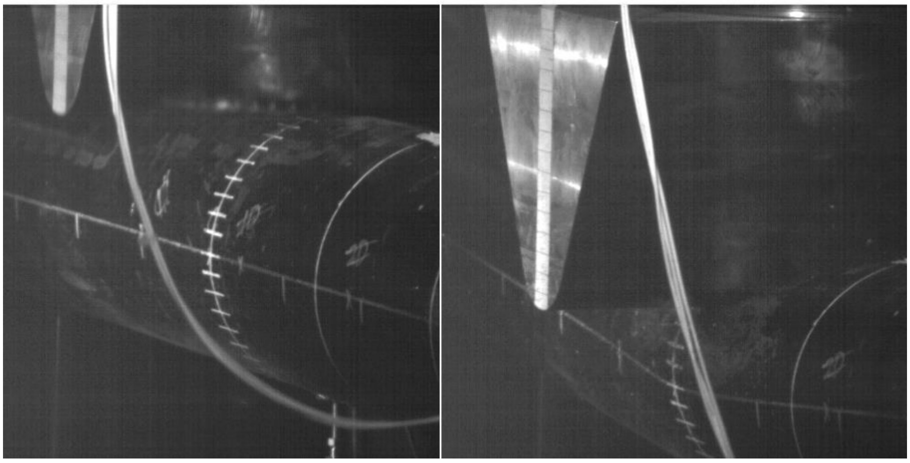

Figure 4-18 I-SPS2 high speed camera image of the beginning and the end

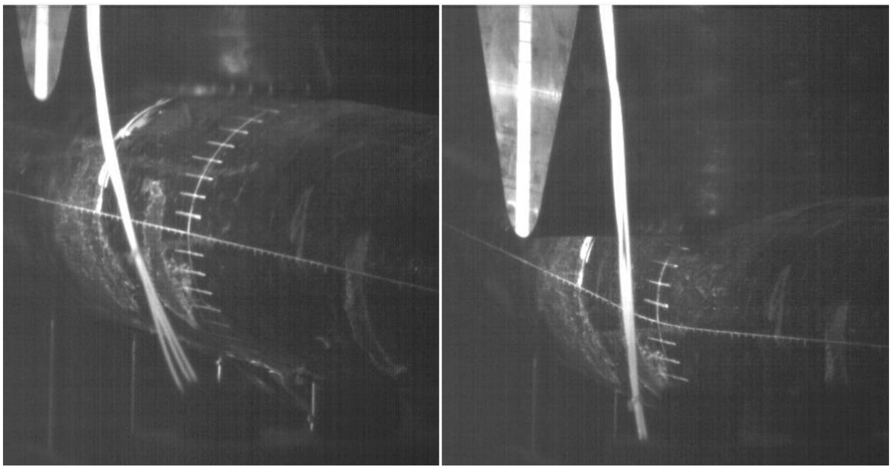

Figure 4-19 I-PPSA2-nylon high speed camera image of the beginning and the end

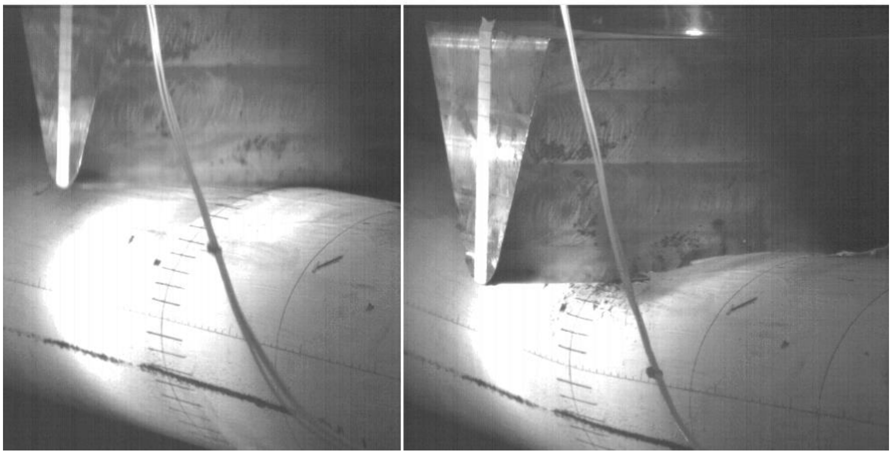

Figure 4-20 I-PPSB2-nylon high speed camera image of the beginning and the end

Table 4-3 Maximum Deformation

	Maximum Indenter Displacement (mm)	**Maximum Bottom Deflection (mm)**
I-SPS2	98.33	55.27
I-PPSA2	69.18	39.58
I-PPSB2	57.69	23.82

4.3 Discussion

4.3.1 Model Test Scaling Laws of Impact

Jones (2012) discussed scaling laws for the impact problem. Table 4-4 shows the variables, and the lower case variables refer to the model while the upper case variables refer to the prototype. The scaling is based on geometrically similar scaling. Therefore, the scale factor is $\beta = \frac{l}{L}$.

Table 4-4 Variables

Structure	Dimension	Prototype Variables	Model Variables
Density	kg/m^3	ρ	ρ
Impact velocity	m/s	V	v
Dimensions	m	L	l
Young's Modules	$kg/m \cdot s^2$	E	E
Material Yield Stress	$kg/m \cdot s^2$	Σ	σ_0
Strain rate	s^{-1}	$\dot{B}$	$\dot{\varepsilon}$
Gravity acceleration	$m/s^2)$	g	g
Force	$kg \cdot m/s^2$	F	f
Strain		B	ε
Stress	$kg/m \cdot s^2$	Σ	σ
Duration of impact	s	T	t
Wave speed	m/s	c	c

The impact velocity is not changing while the kinetic energy is multiplied by β^3. The response time is multiplied by β. The equations are as follows:

Strain: $\varepsilon = \frac{\delta}{l} = \frac{\beta\Delta}{\beta L} = \frac{\Delta}{L}$

Stress: $\sigma = E\varepsilon$

Wave speed: $c = \left(\frac{E}{\rho}\right)^{1/2}$

Response time: $\frac{t}{T} = \frac{l}{c} \cdot \frac{C}{L} = \beta$

Velocity: $v = \frac{\beta\Delta}{\beta T} = V$

Energy: $\frac{mv^2}{2} = \beta^3 \cdot \frac{MV^2}{2}$

Acceleration: $1/\beta$

Dynamic force: $\frac{m\delta}{t^2} = \beta^2 \cdot \frac{M\Delta}{T^2}$

However, this scaling method cannot scale the gravity, fracture, the strain rate effect properly. The Cowper-Symonds constitutive equation for a strain-rate-sensitive material is as follow

$$\sigma_0' = \sigma_0[1 + (\frac{\dot{\varepsilon}}{Q})^{1/q}] \tag{4.1}$$

where σ_0 is the static yield stress, σ_0' is the dynamic yield stress, and Q and q are the coefficients. The strain rate should be invariable, however, as the following relationship,

$$\dot{\varepsilon} = \frac{\varepsilon}{t} = \frac{\varepsilon}{\beta T}$$

the strain rate in the model will become $1/\beta$ times larger. The relationship between prototype and model is summarized in Table 4-5 Relationships between the model and prototype with Jones' approach

Table 4-5 Relationships between the model and prototype with Jones' approach

	Prototype	**Model**
Linear dimensions	1	β
Impact mass	1	β^3
Impact velocity	1	1
Impact energy	1	β^3
Strain rate	1	$1/\beta$
Stress	1	1
Deformation	1	β
Force	1	β^2
Time for impact	1	β

Because of this conflict, Calladine (1983) suggested another way to construct the model. Instead of keeping the velocity the same, the new approach scales down the velocity and keeps the strain rate the same. By linearly scaling down the dimensions, the relationship between prototype and model is shown in Table 4-6. It is clear that this method preserves the consistency of the strain rate, but the mass and the linear dimensions have conflicts only if the material is changed. If the material is not changing, scaling the dimensions by β will consequently scale the volume by β^3 and therefore scale the mass by β^3. However, it is rather impossible to find a cheap material many times heavier than steel. Moreover, changing the material will consequently change the material property. Comparing these two schemes, in our case, the first one is chosen as the second one is not feasible.

Table 4-6 Relationships between the model and prototype with Calladine's approach

	Prototype	Model
Linear dimensions	1	β
Impact mass	1	β
Impact velocity	1	β
Impact energy	1	β^3
Strain rate	1	1
Stress	1	1
Deformation	1	β
Force	1	β^2
Time for impact	1	1

4.3.2 Impact Energy

Based on the scaling law of impact, the model test result can be scaled up. It needs to be remembered that the pipelines have slightly different scale factors and the overall scale factor has some approximation. The impact energy is scaled up by 2.38^3 or 2.14^3 times. The prototype energy is listed in Table 4-7.

Table 4-7 Model and prototype energy

	Model Potential Energy (J)	Model Kinetic Energy (J)	Prototype Potential Energy (J)	Prototype Kinetic Energy (J)
I-SPS2	6615	6038.9	$8.86*10^4$	$8.09*10^4$
I-PPSA2	6615	6424.4	$8.86*10^4$	$8.61*10^4$
I-PPSB2	6615	6244.4	$6.44*10^4$	$6.08*10^4$

The prototype energy shown here is almost in the same range of the energy that is plotted in Figure 3-27. The highest energy here, $8.61*10^4$ J, is about 19133 kg mass moving at 3 m/s. The trawl gear is not that heavy therefore the impact energy here is much larger than in reality. The deformation in this impact test is much larger than in reality.

In the impact test, only the bottom deflection is measured. The energy in Figure 3-27 of prototype of quasi-static indentation tests is re-plotted here against the bottom deflection. The impact energy of I-SPS2 is about $8.09*10^4$ J.

According to the figure, when the impact energy is equal to 8.09*10^4 J, the bottom deflection is about 115 mm and the indenter displacement is about 210 mm. Those numbers are larger comparing to the data listed in Table 4-3. The reason for that is because the boundary conditions of the quasi-static indentation tests and the impact tests are different. The comparison between them will be illustrated in the following chapter.

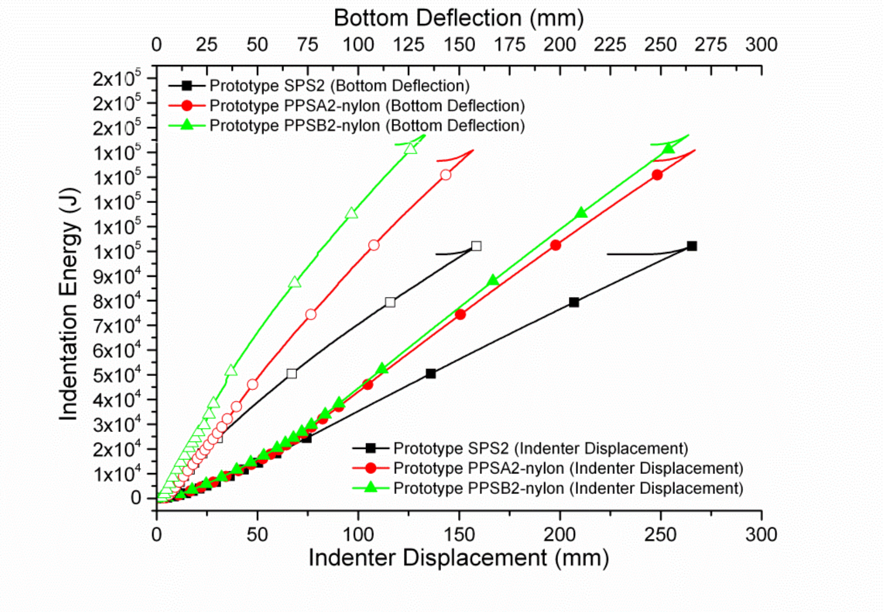

Figure 4-21 Indentation Energy versus indenter displacement and bottom deflection

4.4 Summary

In this chapter, the impact experiments are described. Three impact tests have been conducted. The motivation for the impact analysis is to determine the difference between quasi-static response and dynamic response. However, because of the boundary condition difference, the impact tests and the quasi-static indentation tests cannot be compared directly.

The different scaling laws of impact have been studied. Jones’ method is selected as it is more feasible for this test. The model test results are scaled up according to this scaling law. The impact energy and indentation energy cannot be directly compared as the boundary conditions are different.

Finite element models will be used for the comparison. The impact test results can be used to validate the FE models. The next chapter will show the development of the FE models and the comparison between the quasi-static response and the impact response.

5 Finite Element Modelling and Further Analysis

5.1 Single Wall Pipe Quasi-static Indentation Model

A pipe can be simulated by shell elements or solid elements. The advantage of shell element is that it is more computationally efficient and it is easier to change the shell thickness during parametric study. It is reasonable to treat a pipe as a shell structure, and to use shell elements in simulations. The shell element is built on a reference surface and the thickness is defined through the section property definition, which can be easily changed in ABAQUS/CAE. On the other hand, because of this, the interaction with other surface is not so accurate when it has to consider the thickness and thickness changing in ABAQUS/explicit. For example, shell elements create a penetration problem as Figure 5-1 and Figure 5-2 show. Solid elements can be used to resolve this problem. A solid element is a standard volume element. C3D8 is a linear brick element, whose accuracy significantly depends on the mesh density. Although a second-order element, such as C3D20R could give more accurate results and able to capture steep gradients in stress concentration areas, it cannot model complex contact conditions, impact or severe element distortions (Hibbitt et al., 2001). Therefore, second-order elements are not used for the impact analysis. For single wall pipes, a shell element is sufficient as interaction with the reference surface will not be influenced by the thickness if the outer surface is set to be the reference surface. For pipe-in-pipes, the interactions are more complicated and shell elements should be avoided. For comparisons with impact models, solid element C3D8 is used for consistency. If the accuracy of high gradient stress or strain is needed, second-order solid elements should be used.

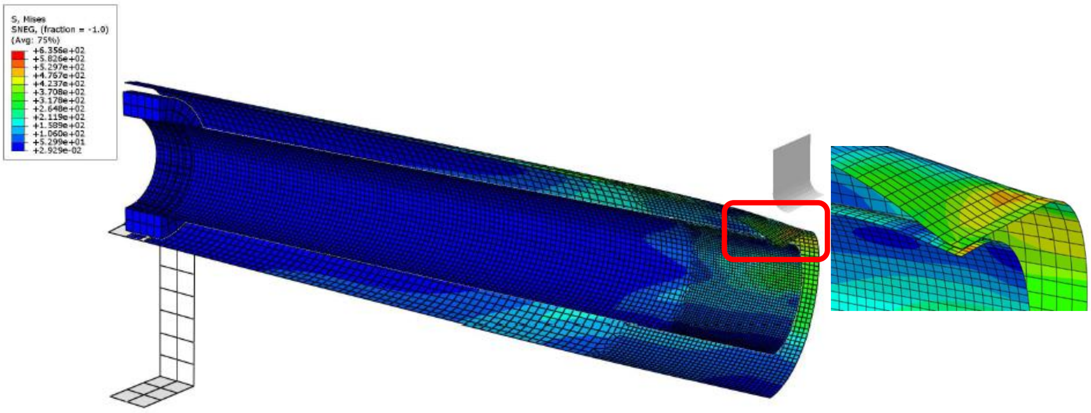
S, Mises
SNEG, (fraction = -1.0)
(Avg: 75%)
+6.356e+02
+5.826e+02
+5.297e+02
+4.767e+02
+4.237e+02
+3.708e+02
+3.178e+02
+2.648e+02
+2.119e+02
+1.589e+02
+1.060e+02
+5.299e+01
+2.929e-02

Figure 5-1 Deformed shape of PPSB2-nylon with shell element

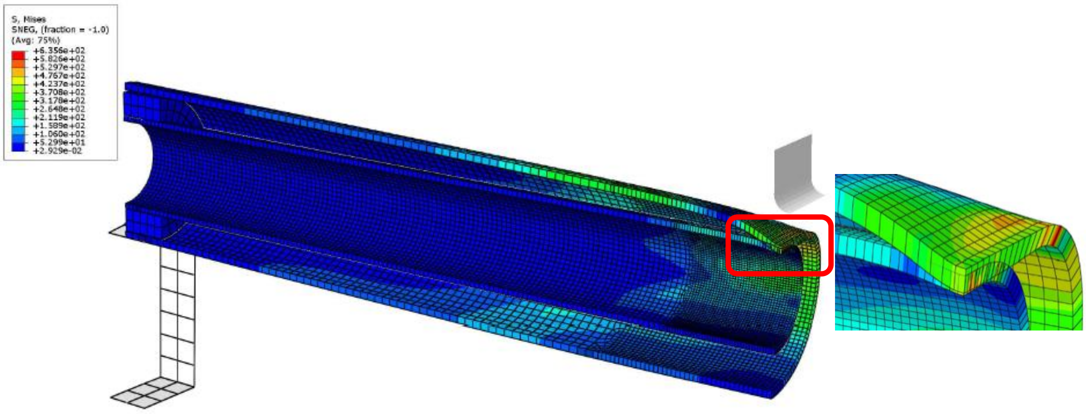
S, Mises
SNEG, (fraction = -1.0)
(Avg: 75%)
+6.356e+02
+5.826e+02
+5.297e+02
+4.767e+02
+4.237e+02
+3.708e+02
+3.178e+02
+2.648e+02
+2.119e+02
+1.589e+02
+1.060e+02
+5.299e+01
+2.929e-02

Figure 5-2 Deformed shape of PPSB2-nylon with shell element, thickness rendered

The indenter and supports are simulated by rigid bodies. There are two different rigid bodies: one is an analytical rigid body and the other is a discrete rigid body. An analytical rigid body can only simulate simple geometries, but it is more computationally efficient than a discrete rigid body. The indenter and the rigid bottom support are both simulated using an analytical rigid body and the support is treated as a discrete rigid body.

Coupon tensile tests are carried out to find the steel's material property. The test results are presented in Appendix C. Steel linear elastic behaviour is described by Young's modulus. The plastic behaviour is described by its yield point and hardening. The classical metal plasticity model in ABAQUS is adopted in the present simulation. This model uses the standard von Mises yield criteria with associated plastic flow and isotropic hardening definitions. The classical metal plasticity model approximates and smoothes a stress-strain curve of the material after the yield point with a series of straight lines joining the given data points. ABAQUS requires that the input stress-strain points should be true stress and true strain. Therefore, data of the coupon tensile tests have to be transformed to true stress and true strain for FE modelling material input. The input data are listed in Appendix B.

The first step of the simulation is a loading step. The loading is added by moving the indenter. The nonlinear geometry option is enabled for geometric nonlinearity analysis. The maximum increment size is 0.02 step. The second step is an unloading step: the indenter moves back to the original position.

The contact condition between the indenter and the pipe is treated as a frictionless contact pair. The contact pair contains a master surface and a slave surface. Generally, the master surface should be chosen as the surface of the stiffer body, or as the surface with the coarser mesh if the two surfaces are on structures with comparable stiffness. Therefore, the indenter is modelled as a rigid body and set as the master surface as it is stiffer. Hard contact is applied, which minimizes the penetration of slave nodes into the master surface and does not allow the transfer of tensile stresses. The details are listed in Table 5-1. Before any force is imposed on the finite element model, the clearance between all surfaces is zero. In order to save computational cost, only a quarter model is built based on the symmetrical character of the problem. The geometric model follows the actual size of the specimen and set-up.

Table 5-1 Contact definitions in quasi-static indentation FE models

FE model	*No.*	*Contact/Tie*	*Master Surface*	*Slave Surface*
SPS	1	Frictionless contact	Outer surface of indenter	Outer surface of pipe
	2	Tie (Set-up II)	Outer surface of support	Outer surface of pipe
	3	Frictionless contact	Floor (Set-up I)	Outer surface of pipe
Pipe-in-pipe	1	Frictionless contact	Outer surface of indenter	Outer surface of pipe
	2	Frictionless contact	Inner surface of outer pipe	Outer surface of inner pipe
	3	Frictionless contact	Inner surface of outer pipe	Outer surface of nylon spacer
	4	Tie	Outer surface of inner pipe	Inner surface of nylon spacer
	5	Tie	Outer surface of support	Outer surface of pipe

For single wall pipe specimens, there are two different set-ups. The FE model of set-up I is shown in Figure 5-3, including the shell element model, solid element C3D8 model and solid element C3D20R model. Both the YZ plane and the XY plane are planes of symmetry. The pipe's end is restricted in all rotational degrees of freedom. The indenter is only allowed Y axis translation. It is controlled to move to the expected displacement in loading step, and moved back to the original position in the unloading step. The floor does not have any degree of freedom.

The FE model of set-up II is presented in Figure 5-4. The pipe is sitting on the saddle supports as in the experiment. Both the YZ plane and the XY plane are planes of symmetry. The saddle support is only allowed X axis rotation and the Z axis translation. In set-up II, there is another contact condition that the pipe is tied to the saddle support. This setting aims to simulate the situation when the pipe was sitting on the saddle support during the test. It was observed that the friction prevented the pipe slipping on the saddle support during the test. Therefore, it is reasonable to tie the pipe’s ends to the saddle support.

The mesh is fine around the indentation area, and coarser at the end as shown. The mesh density needs to be sufficient to obtain a smooth force - displacement curve and the correct deformation pattern. The convergence is checked. Solid element C3D8 needs a higher mesh density than the other two. The three different element types are compared in Figure 5-5. The comparison shows all three elements can be used for modelling, and they create little difference. However, as mentioned before, the shell element S4 is not suitable for pipe-in-pipe modelling, and the second-order solid element C3D20R is not able to simulate the impact response. Therefore, for the further analysis, if not specially mentioned, C3D8 is used.

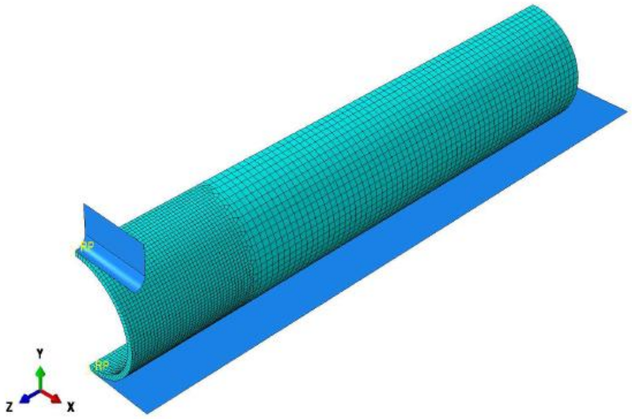

(a) Shell element S4

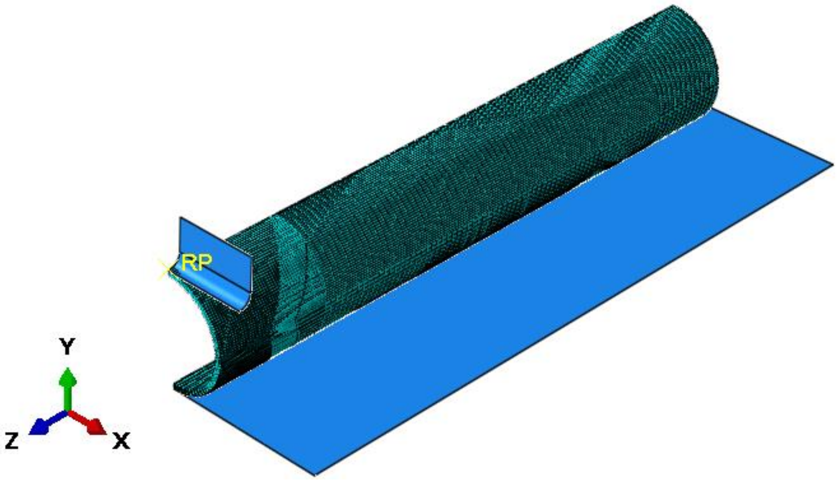

(b) Solid element C3D8

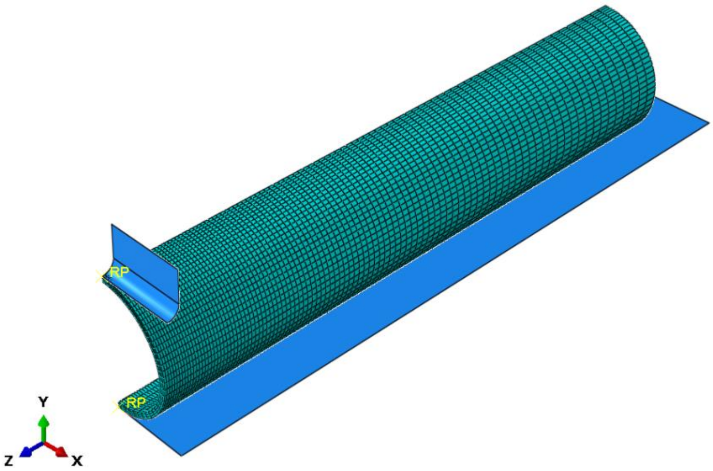

(c) Solid element C3D20R

Figure 5-3 Single wall pipe quasi-static indentation FE model under set-up I

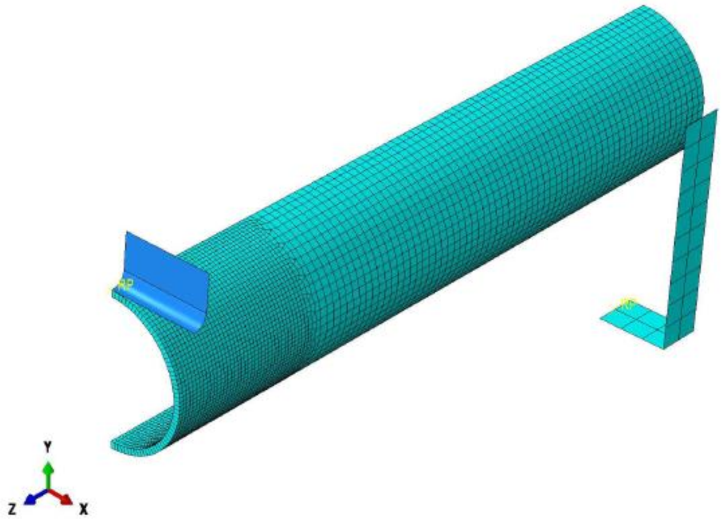

(a) Shell element S4

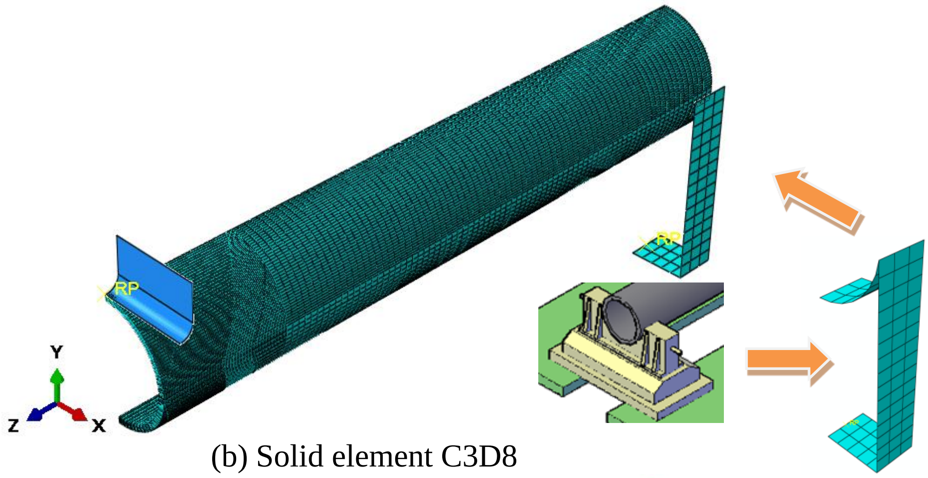

(b) Solid element C3D8

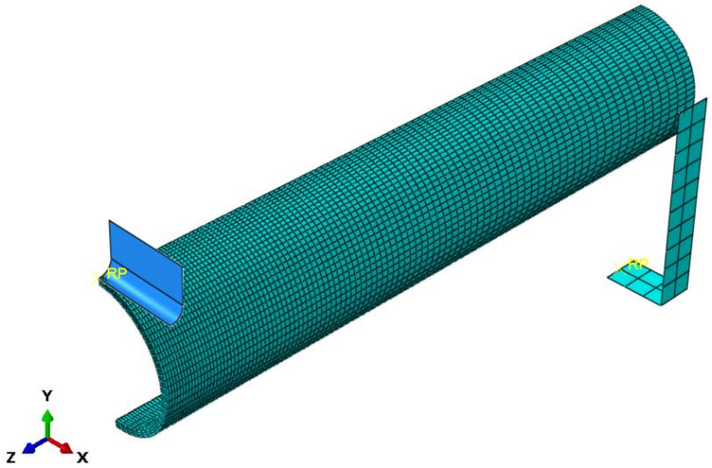

(c) Solid element C3D20R

Figure 5-4 Single wall pipe quasi-static indentation FE model under set-up II

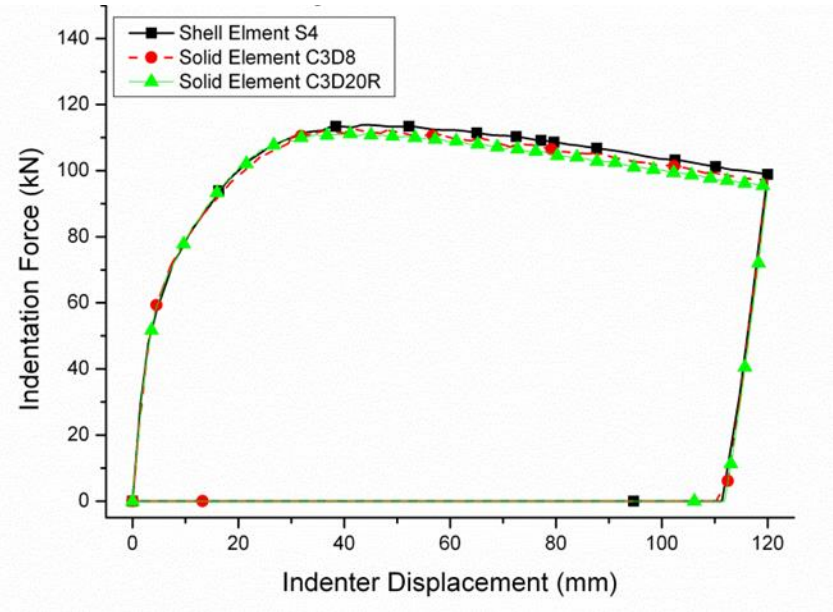

Figure 5-5 Comparison among different elements of SPS4

SPS4 is chosen to illustrate the comparisons as it is the only specimen type which has been used in both set-ups. The comparisons are shown in Figure 5-6 to Figure 5-9, and the differences between the finite element results and the experiment results are within 10%.

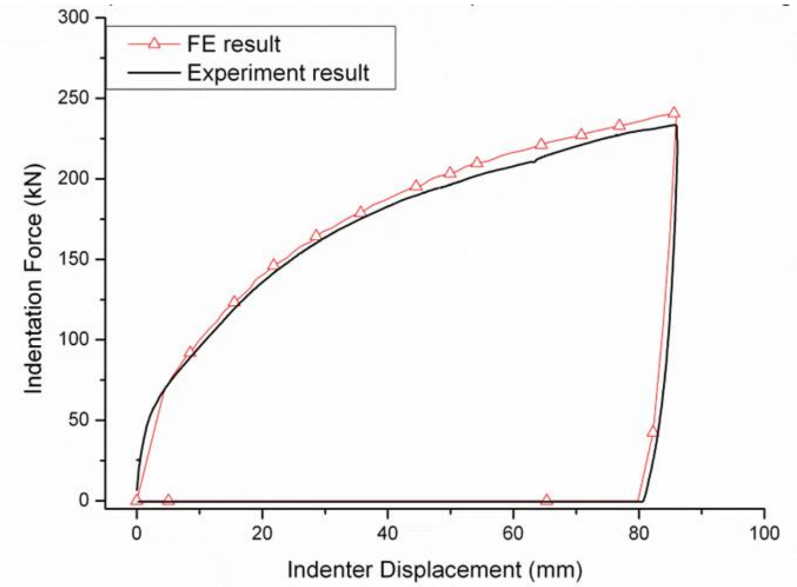

Figure 5-6 Comparison of SPS4-BCrigid between FE and experiment results

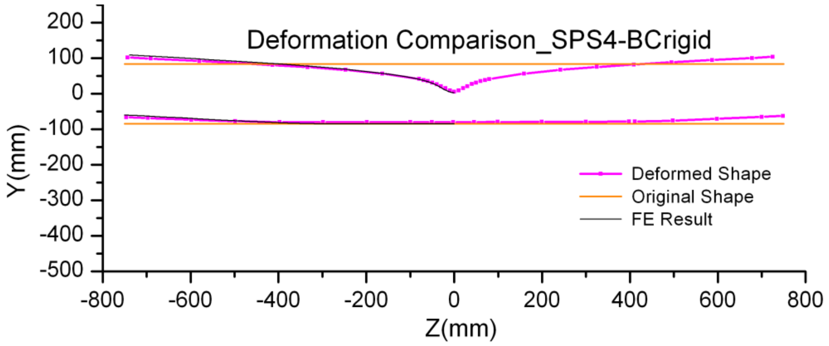

Figure 5-7 SPS4_BCrigid failure shape comparison

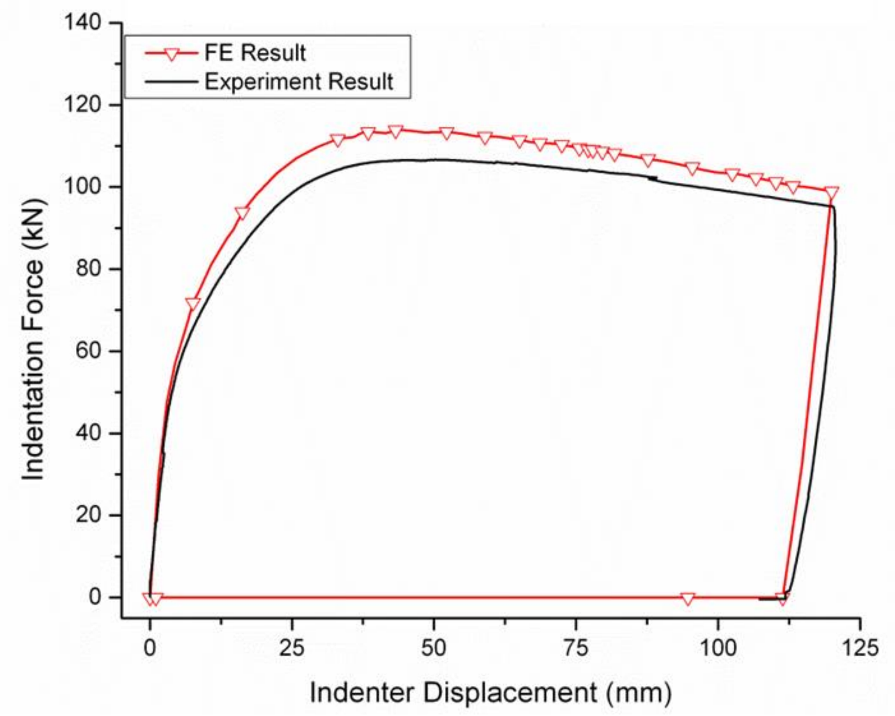

Figure 5-8 Comparison of SPS4 between FE and experiment results

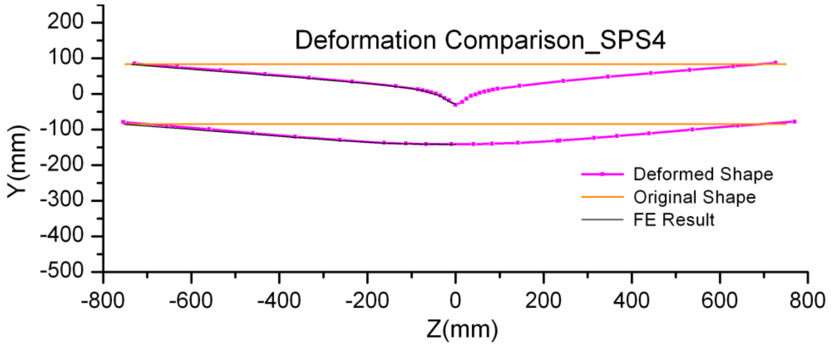

Figure 5-9 SPS4 failure shape comparison

Based on the modelling methodology, the FE models for other single wall pipes are developed, and the comparisons show good agreement. Figure 5-10 to Figure 5-12 show the comparison between the FE models and the experiment results for SPS1, SPS2 and SPS3. (SPS1 and SPS3 do not have profile comparisons, because SPS1 and SPS3 are loaded to a large displacement, and whole set-up collapses. The FE model is not intended to capture that.) The deviations are listed in Table 5-2 .The comparisons increase confidence level of the single wall pipe indentation FE model, and further analysis can be processed based on it.

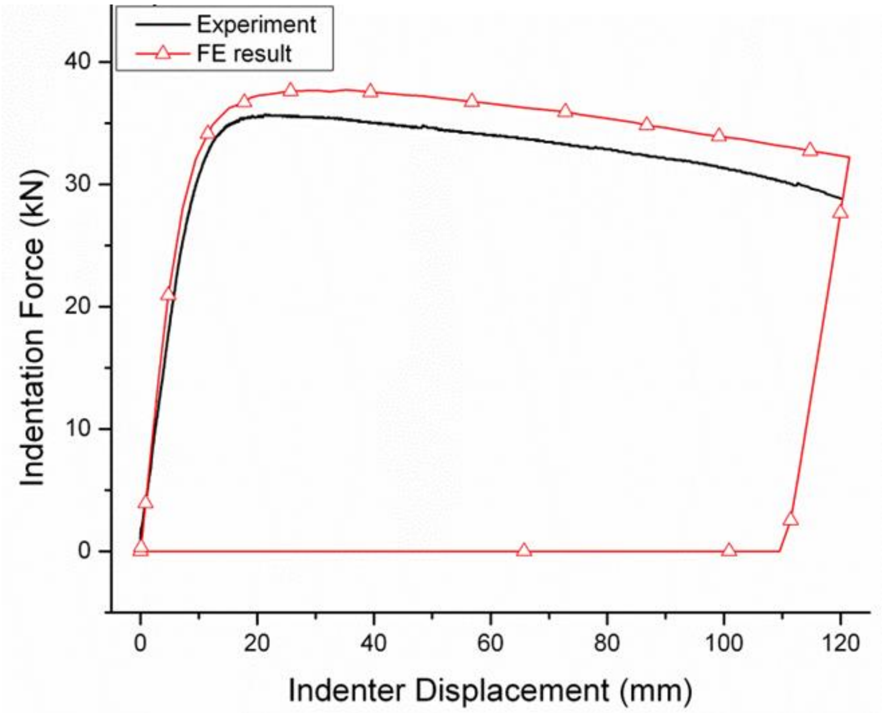

Figure 5-10 Comparison of SPS1 between FE and experiment results

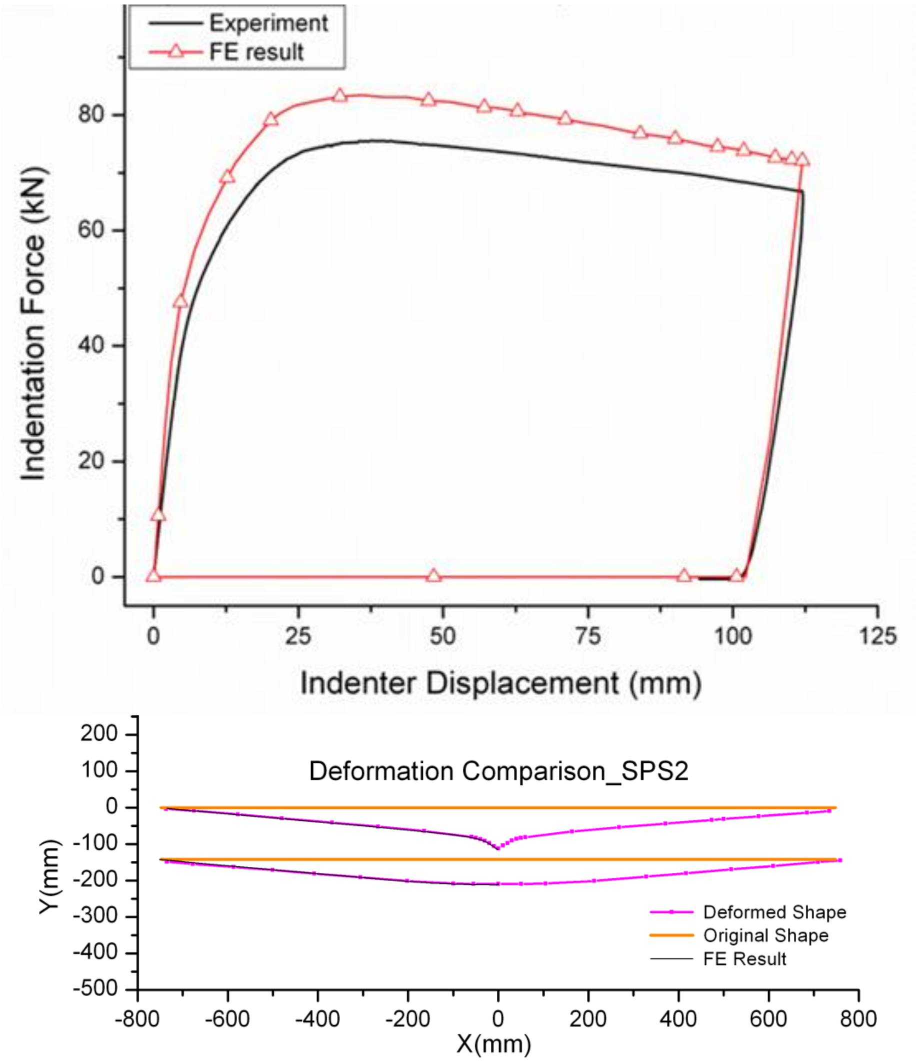

Figure 5-11 Comparison of SPS2 between FE and experiment results

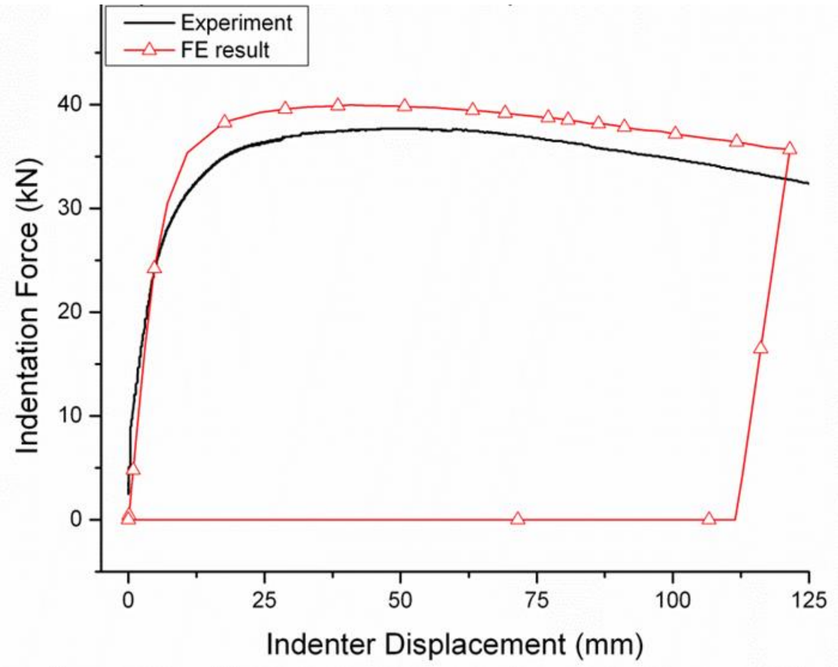

Figure 5-12 Comparison of SPS3 between FE and experiment results

Table 5-2 Deviations between experimental data and FE results of single wall pipes

Cases	**Maximal Force (kN)**		**Deviation**
	Experimental Data	Finite Element Result	
SPS4_BCrigid	233.4	240.9	3.2%
SPS1	35.6	37.7	5.9%
SPS2	75.6	83.5	10.2%
SPS3	37.7	39.8	5.6%
SPS4	106.6	113.7	6.7%

5.2 Pipe-in-Pipe Quasi-static Indentation Model

The difference between the single wall pipe FE model and the pipe-in-pipe FE model is the model of the pipe structure. The set-up of pipe-in-pipe indentation tests is the same as the set-up II of single wall pipe indentation tests.

The pipe-in-pipe has an outer pipe and an inner pipe, and in between there are spacers. During the manufacture process, the spacers are installed on the inner pipe first, and then the inner pipe with spacers installed is pulled into the outer pipe. The spacers sit freely on the outer pipe, and support the inner pipe in the centre. The FE model complies with this process. The spacers are modelled by solid elements, and tied to the inner pipe. The spacer sits on the inner surface of outer pipe with frictionless contact. Figure 5-13 shows the FE model of pipe-in-pipe from different directions. The pipe sits on the saddle supports as in the experiment. The indenter is simplified as a rigid body and is displacement controlled. Both the YZ plane and the XY plane are the symmetric planes.

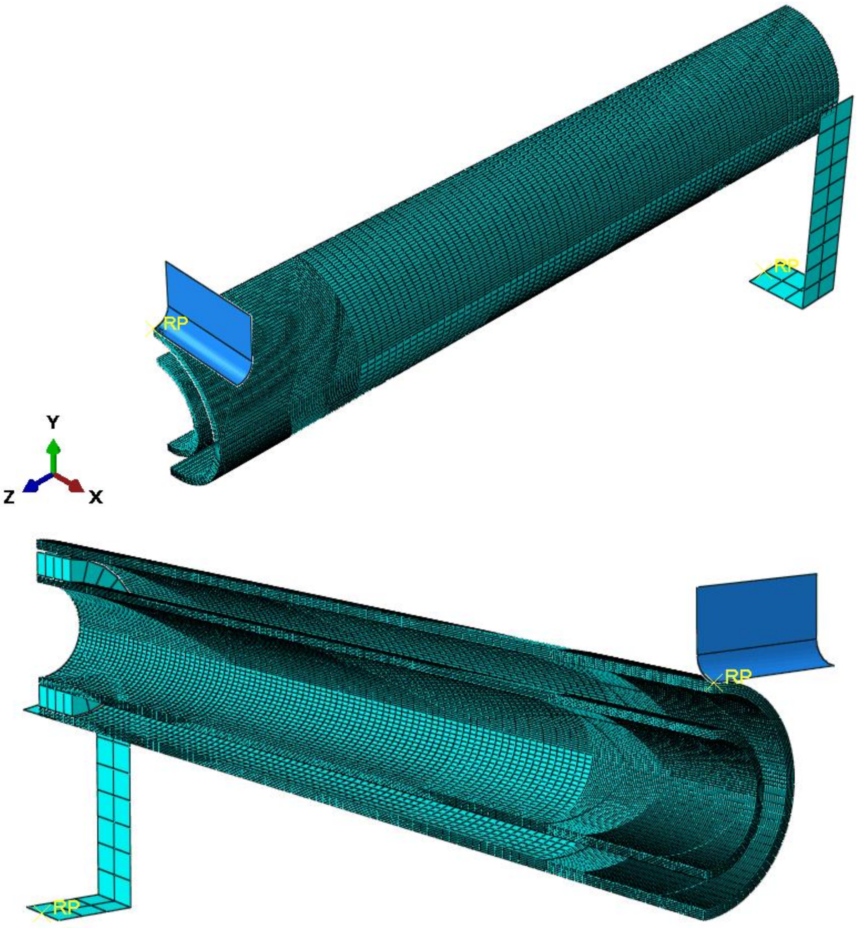

Figure 5-13 Pipe-in-pipe quasi-static indentation FE model under set-up II

In order to install the inner pipe with spacers on easily, the spacer outside diameter is slightly smaller than the inner diameter of the outer pipe.

Therefore, there is a small gap between the spacer and the outer pipe at the top.

There are altogether three contact pairs. All of them are frictionless contacts and are summarized in Table 5-1. The spacer's inner surface is tied to the outer surface of the inner pipe, and the outer surface of the outer pipe is tied to the support. The saddle support isfree to rotate about the X axis and translate about the Z axis. One node of the spacer is restricted the Y axis rotation and Z axis rotation. There are two kinds of spacers, one is made of rubber and another one is made of nylon. A few experiments are conducted to determine material properties of the rubber and nylon.

Rubber is one of the hyper-elastic materials. For these materials, ABAQUS allows six kinds of test data for simulations, including uniaxial tensile test data, uniaxial compression test data, biaxial tensile test data, biaxial compression test data, planar tensile test data and planar compression test data. Because the spacers are always under compression during the test, uniaxial compression test is carried out. The test set-up is illustrated in Figure 5-14. The displacement of the hydraulic ram and the force are recorded. The normal stress and normal strain are calculated and input into ABAQUS material module. C3D8RH is used to simulate rubber spacer. Enhanced hourglass control and distortion control are both used to avoid divergence. However, this may not succeed every time. The alternative scheme is to use ABAQUS/explicit to avoid divergence induced by the heavy distortion. Two pipe-in-pipe specimens used rubber spacers. Both ABAQUS/standard and ABAQUS/explicit are used for these two cases and comparisons between them are made. The comparison of case PPSA2-rubber is shown in Figure 5-15. The comparison of case PPSB2-rubber is shown in Figure 5-16. Because the specimen of PPSB2-rubber was cut into pieces after the test, the profile comparison is not available here.

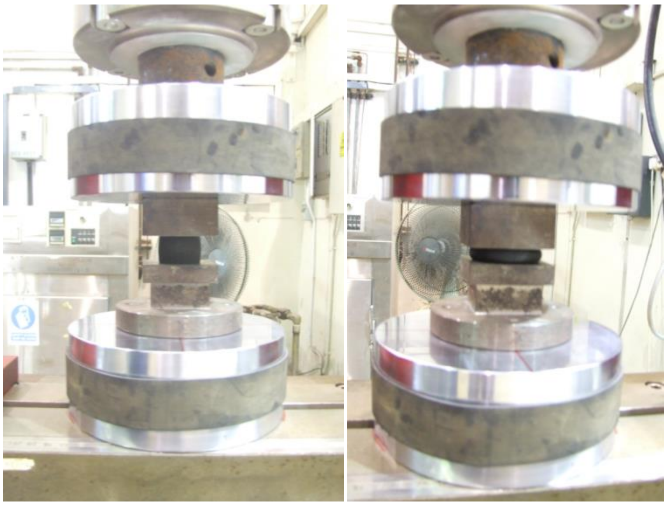

Figure 5-14 Uniaxial compression test of rubber

It can be concluded that the comparisons show acceptable agreement. Results from ABAQUS/standard and ABAQUS/explicit have their own features. The results from ABAQUS/standard are smooth curves, while the results from ABAQUS/explicit have dynamic response. This is because the quasi-static simulation in ABAQUS/explicit is achieved by a small loading rate; therefore, although the influence on the results can be ignored, this is still a dynamic response. The limitation of ABAQUS/standard is the difficulty of convergence. These two cases converge only when the elements of the rubber spacers are large enough to accept the distortion. The large elements bring inaccuracy. However, as the rubber spacer is not the part we are most interested in, the effect can be ignored.

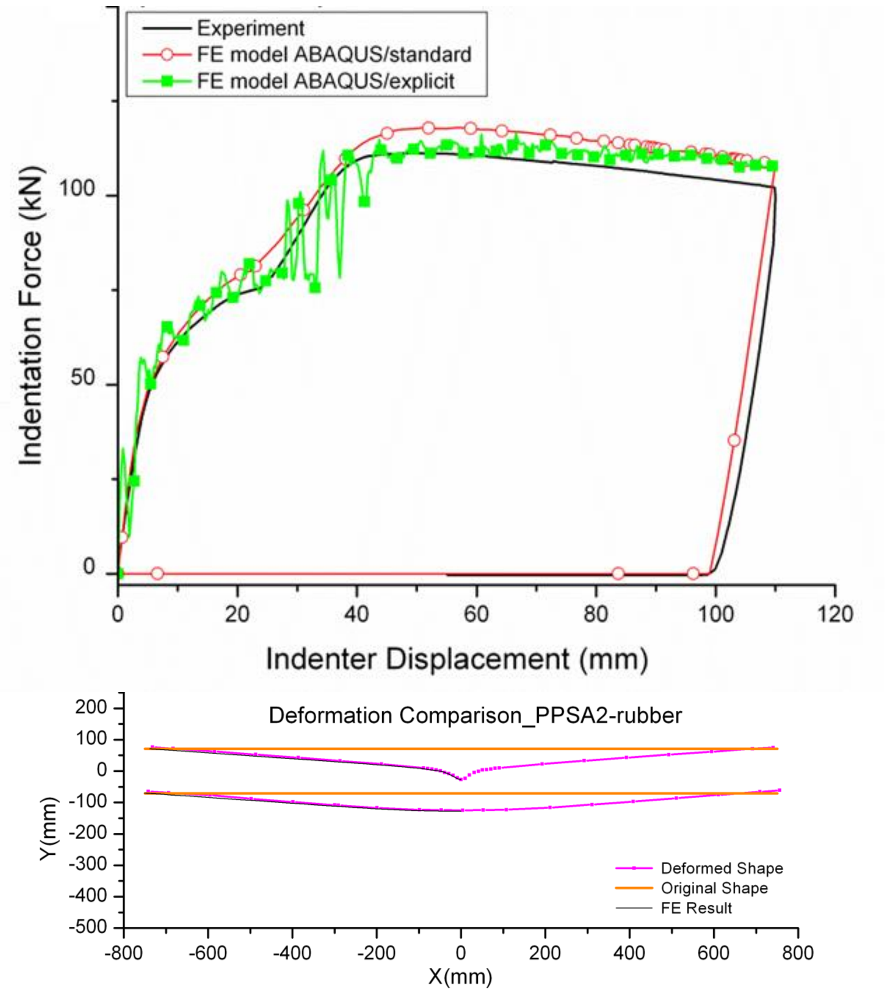

Figure 5-15 Comparison between test result and FE results of PPSA2-rubber

Nylon is treated as an elastic / plastic material. Tension and compression tests are used to determine the elastic and plastic properties, as Figure 5-17 shows. For the nylon spacers, ABAQUS/standard is used. Altogether four pipe-in-pipes used the nylon spacer. The comparison of the PPSAs-nylon is shown in Figure 5-18 to Figure 5-20. The spacing distance of PPSA1, PPSA2 and PPSA3 are different. The comparison of PPSB2-nylon is shown in Figure 5-21. All the comparisons show agreement between the test results and FE results, the deviations are listed in Table 5-3.

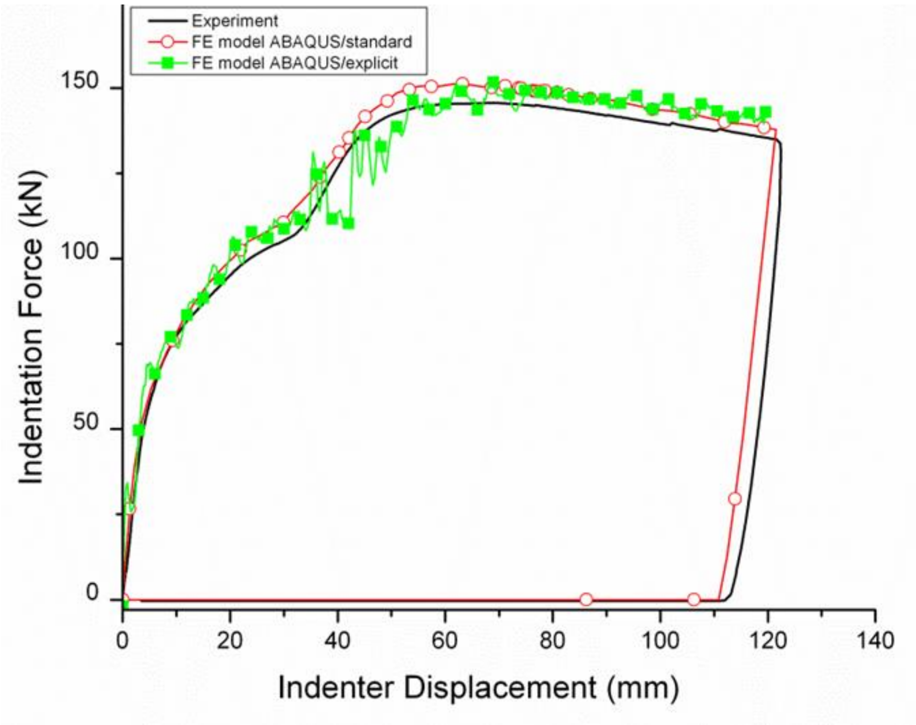

Figure 5-16 Comparison between test result and FE results of PPSB2-rubber

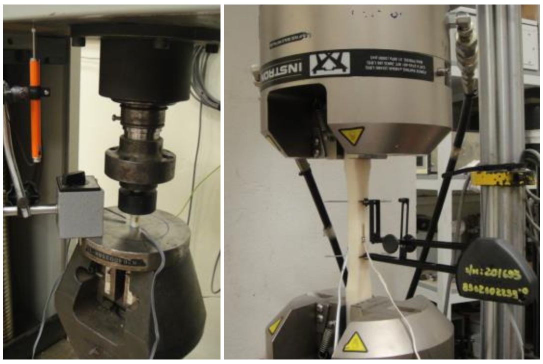

Figure 5-17 Nylon compression and tension test

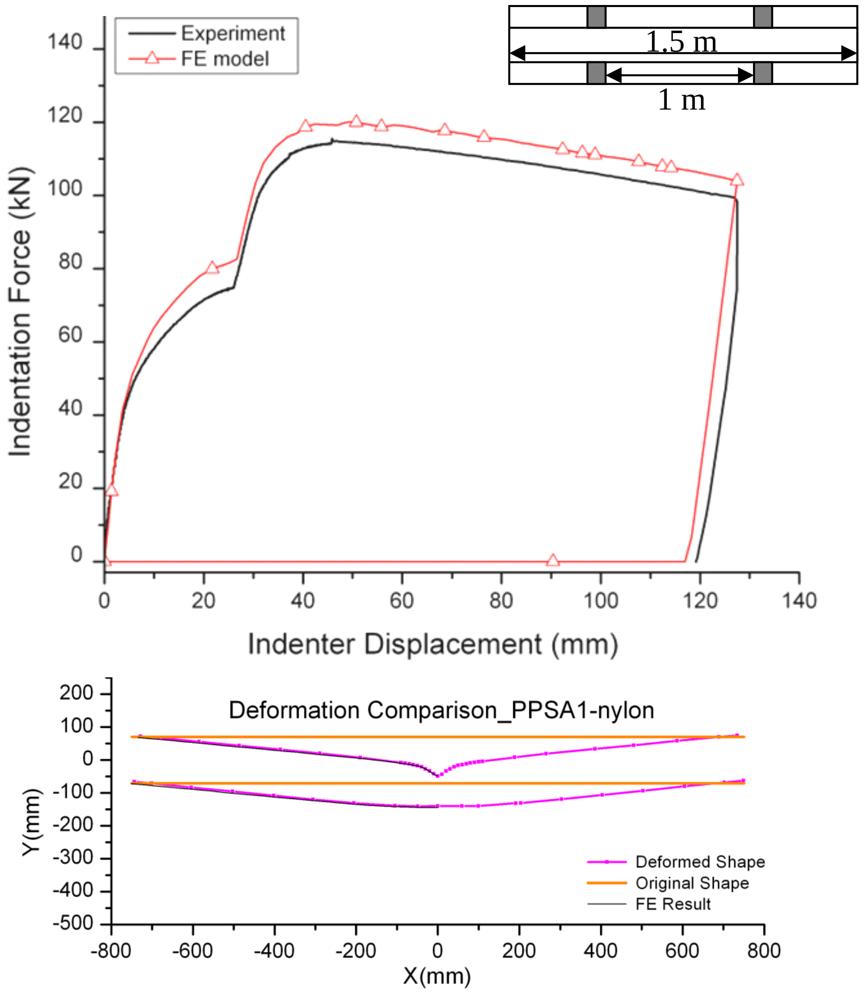

Figure 5-18 Comparison between test results and FE results of PPSA1-nylon

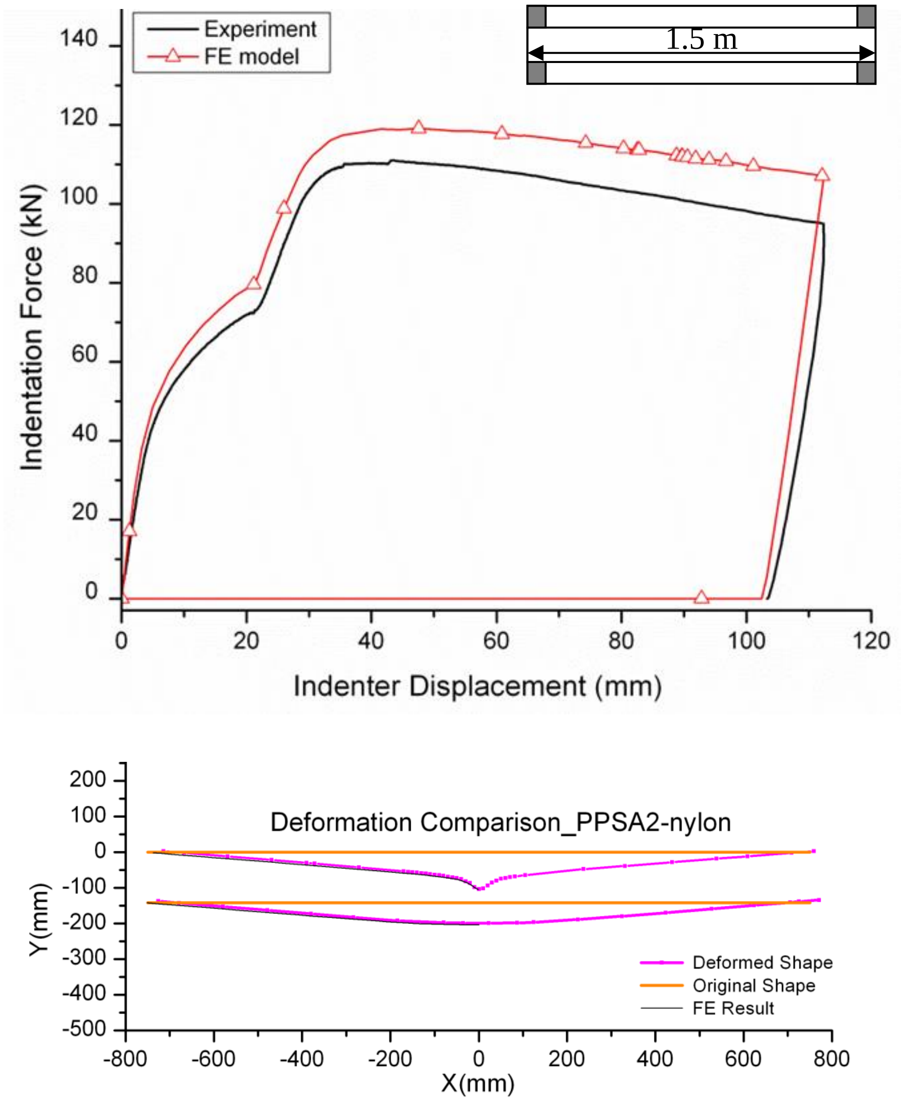

Figure 5-19 Comparison between test results and FE results of PPSA2-nylon

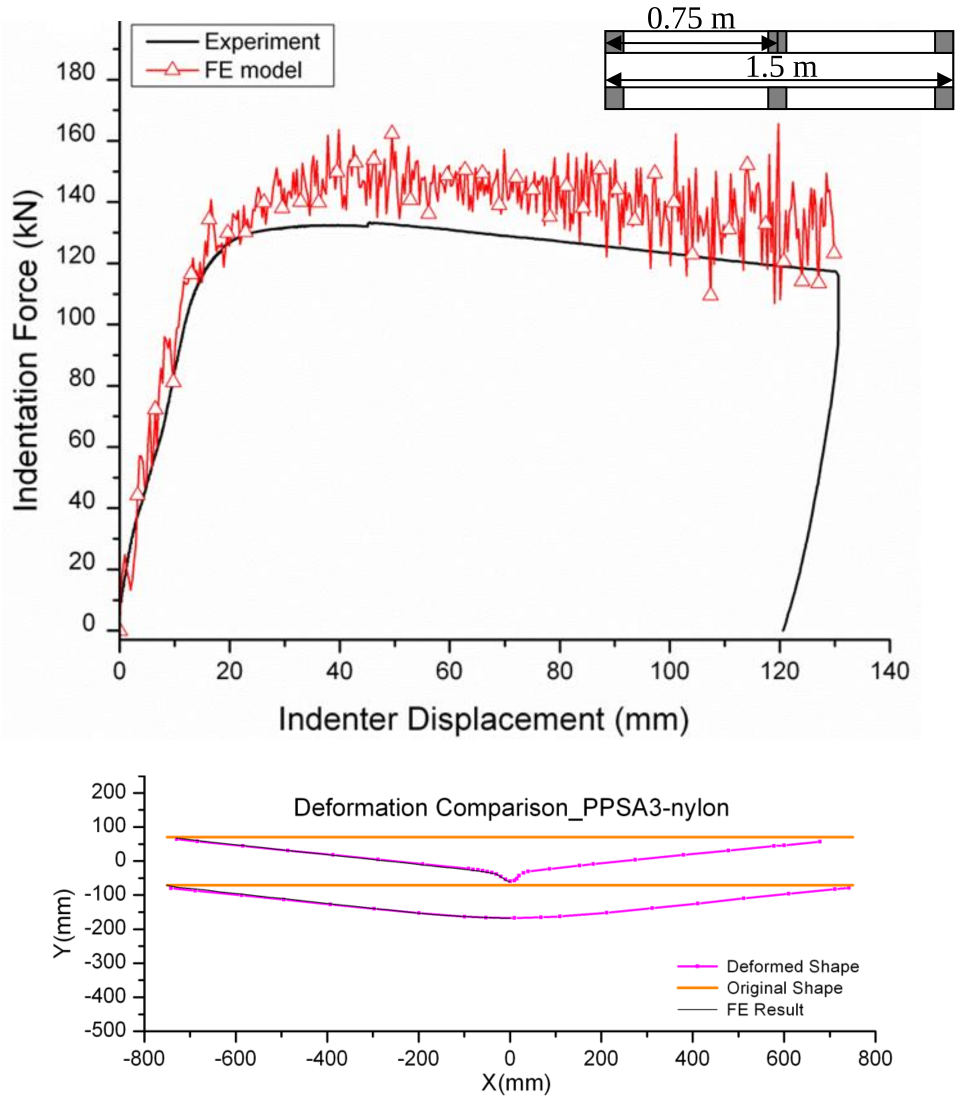

Figure 5-20 Comparison between test results and FE results of PPSA3-nylon

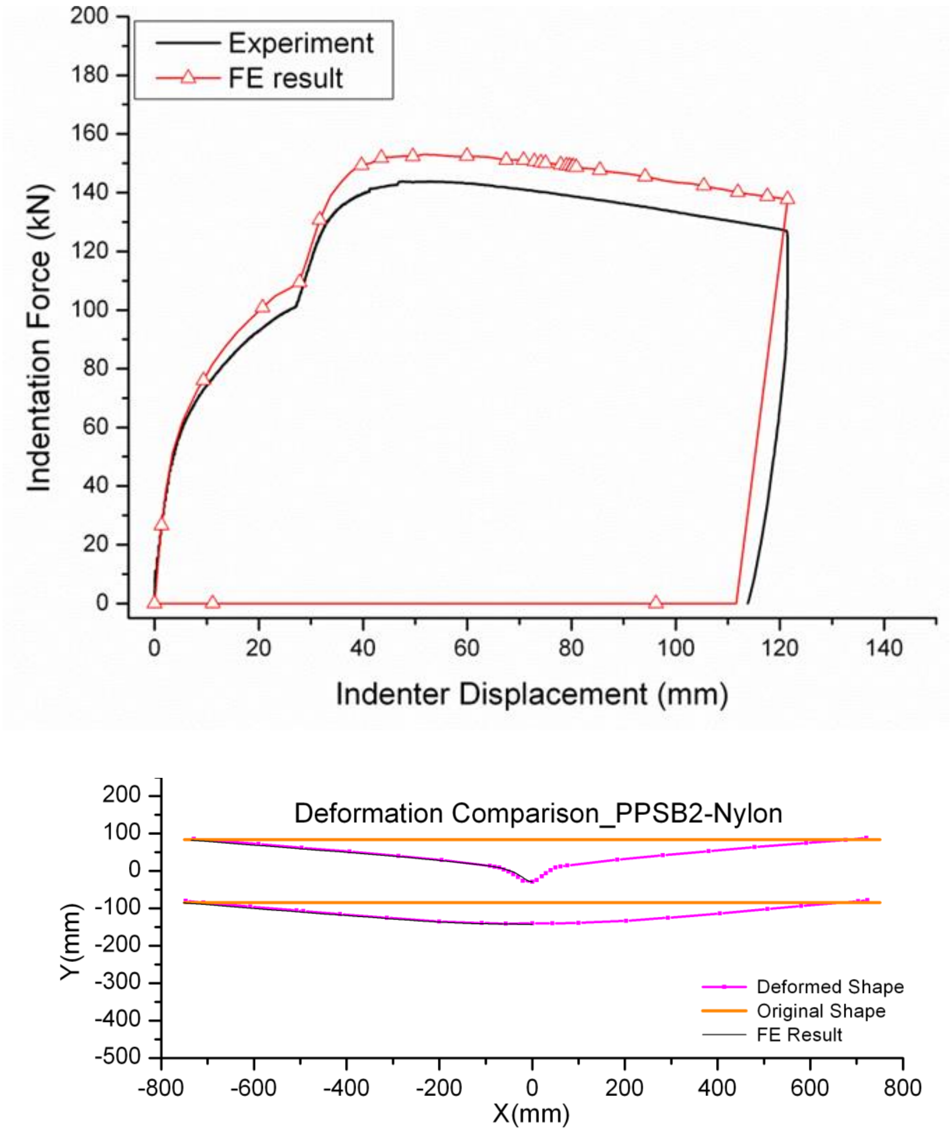

Figure 5-21 Comparison between test result and FE result of PPSB2-nylon

Table 5-3 Deviations between experimental data and FE results of pipe-in-pipes

Cases	Maximal Force (kN)		Deviation
	Experimental Data	Finite Element Result	
PPSA2-Rubber	111.2	118.0	6.12%
PPSA1-Nylon	114.7	120.0	4.62%
PPSA2-Nylon	110.5	119.0	7.69%
PPSA3-Nylon	132.7	146.0	10.02%
PPSB2-Rubber	145.7	151.3	3.84%
PPSB2-Nylon	143.7	152.6	6.19%

5.3 Summary of the Finite Element Model of Quasi-static Indentation

FE models for both inner pipes and outer pipes are developed for quasi-static indentation tests. Three elements are studied, and all of them can be used to model this problem with restrictions. As shell element S4 is not suitable for pipe-in-pipe modelling, and second-order solid element C3D20R is not able to simulate the impact response, for consistency solid element C3D8 is used unless otherwise specified. The comparisons between FE results and experimental results show good agreement, which validates the FE models. The FE models can be used for further analysis with different diameter and thickness pipes.

5.4 Impact FE Models

FE models of the single wall pipe and the pipe-in-pipe are shown in Figure 5-22 and Figure 5-23. There are five differences between the quasi-static FE model and the impact FE model.

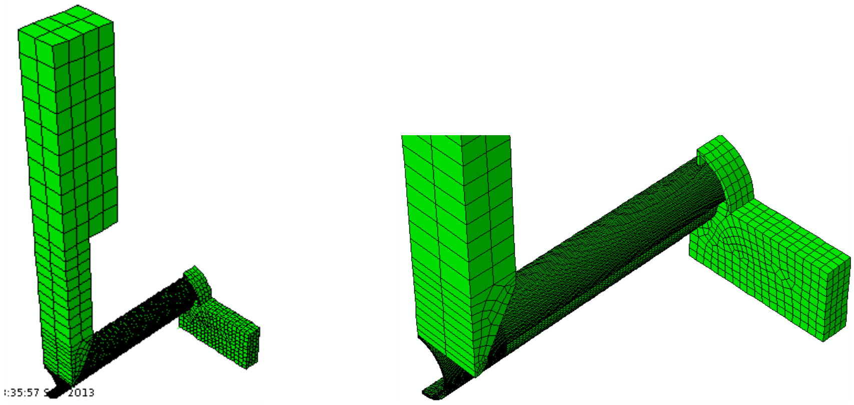

Figure 5-22 Impact FE model of single wall pipe

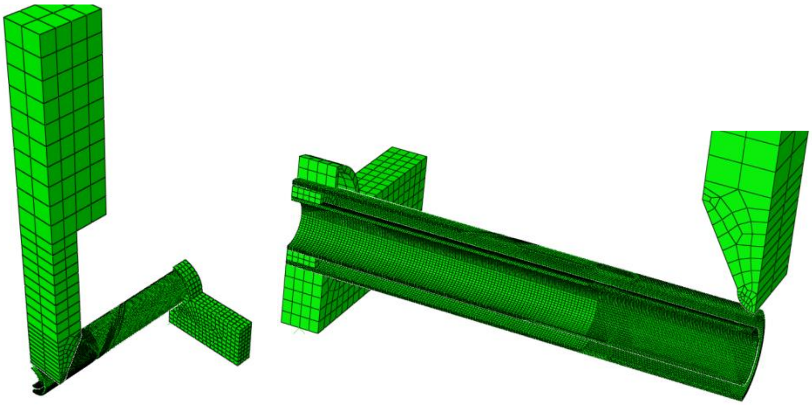

Figure 5-23 Impact FE model of pipe-in-pipe

1. First of all, ABAQUS\explicit is used to simulate the impact experiments instead of ABAQUS\standard.
2. Secondly, all of the contact settings change to explicit ones. The pipe is no longer bonded to the support, but changes to a friction contact. The details are shown in Table 5-4.

Table 5-4 Contact definitions of impact FE models

FE model	*No.*	*Contact/Tie*	*Master Surface*	*Slave Surface*
I-SPS2	1	Frictionless contact	Outer surface of indenter	Outer surface of pipe
	2	Friction (factor 0.4) contact	Outer surface of support	Outer surface of pipe
	3	Frictionless contact	Inner surface of Omega clamp	Outer surface of Pipe
I-PIPE-IN-PIPE	1	Frictionless contact	Outer surface of indenter	Outer surface of pipe
	2	Friction (factor 0.4) contact	Outer surface of support	Outer surface of pipe
	3	Frictionless contact	Inner surface of Omega clamp	Outer surface of Pipe
	4	Frictionless contact	Inner surface of outer pipe	Outer surface of inner pipe
	5	Frictionless contact	Inner surface of outer pipe	Outer surface of nylon spacer

3. The third change is that the indenter is built with exact geometries by solid element C3D8, and the front radius is 30 mm. It is no longer displacement controlled. In the experiment, the indenter is dropped from a specified height. In the FE model, the indenter is placed on the pipe surface, with an assigned predefined velocity which equals to the impact velocity in the experiment. The impact velocity is obtained from the laser lights data. The results are presented in Table 4-2.

4. The boundary condition in the FE model has to be changed, because the right hand support is no longer moveable. Therefore both of the saddle supports in the impact FE model are only allowed X axis rotation. Although both saddles supports are still idealized as rigid bodies, they are built as solid with less idealised geometries.
5. Last but not least, the strain rate effect treated by a Cowper-Symonds model that can be directly used in ABAQUS is added.

$$\dot{\varepsilon} = Q(\frac{\sigma'_0}{\sigma_0} - 1)^q \tag{5.1}$$

Where $\dot{\varepsilon}$ is the strain rate, Q and q are the parameters, σ_0 is the yield stress on static condition and σ'_0 is the dynamic yield stress.

There are three ways to obtain the coefficients. The first is to use the coefficients which Symonds gave for mild steel: Jones(Jones, 2012) stated the two coefficients of Cowper-Symonds model as Q=40.4 /s and q=5 for mild steel.

Another way is to use another model to calculate the parameters. Another relationship developed by L. Javier Malvar(1998) considers different strain rate effects with different grade steels, with yield stresses ranging from 290 to 710 MPa. Strain rates of these data are from 0.0001 to 2 (1/s). The proposed model fits the various data reasonably as Malvar claimed. The model is as follows

$$\mathrm{DIF} = \frac{\sigma_0^{'}}{\sigma_0} = (\frac{\dot{\varepsilon}}{10^{-4}})^{\alpha} \tag{5.2}$$

$$\alpha = 0.074 - 0.040\frac{\sigma_0}{414} \tag{5.3}$$

where σ_0 is the static yield stress in MPa. DIF is the ratio of the dynamic yield stress to the static yield stress, and stands for dynamic increase factor.

This model is able to calculate different DIF at different strain rates. All these data points can be then used to fit the curve of the Cowper-Symonds model and therefore obtain the parameters.

The third way is to conduct experiments using the same material in the impact experiment. In order to get higher strain rate with the same pulling speed, a smaller gage length 10 mm is chosen. The specimen is shown in Figure 5-24.

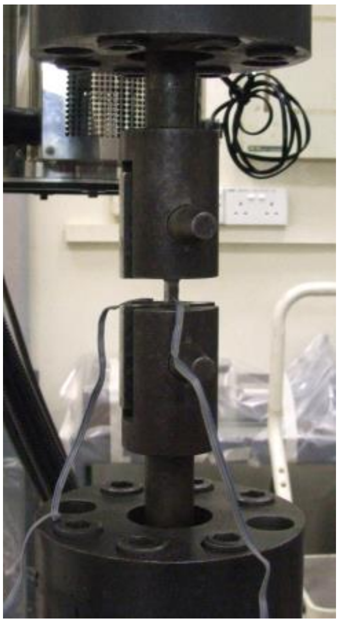

Figure 5-24 Test specimen on the test machine

The test results are given in Table 5-5. There are not sufficient experiments to generate regression coefficients which are significance for the material. The results are also compared in Figure 5-25 with Cowper and Symonds and Malvar’s models. The comparison shows that the Cowper Symonds model gives the upper bound of the strain rate effect. It gives a higher strain rate effect than the actual situation. If the analysis using Cowper and Symonds model with Q=40.4 S-1 and q=5 shows the strain rate effect does not influence the final result much, and because Cowper and Symonds model gives the upper bound of the strain rate effect, it can be conclude that in current experiment with current steel the strain rate effect can be ignored. Therefore, for the impact FE models, the Cowper and Symonds model is used with the parameters R=40.4 s^{-1} and q=5.

Table 5-5 Dynamic coupon tensile test

strain rate (S^-1)	**yield stress (MPa)**	$\boldsymbol{\frac{\sigma'_0}{\sigma_0}}$
0.0002	321	1
0.0218	346	1.08
0.0725	379	1.18
0.2172	366	1.14
1.7375	448	1.40

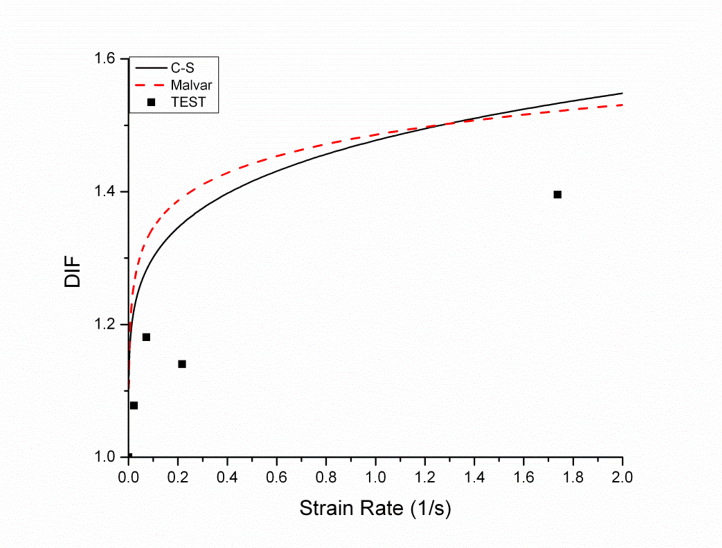

Figure 5-25 Strain rate sensitivities according to different models

Based on all these changes, the new FE impact model is developed. The FE impact responses are compared with the experiment results as the follows. Figure 5-26 and Figure 5-27 shows the FE results of I-SPS2, as well as comparisons with the experiment results. The comparisons show good agreement

. The FE result of the impact force is somewhat lower than the measured force. The reason is that during the test, the pipe is fully pushed down by the Omega clamps, whereas in the FE simulation, the pipe's position is only limited by the geometry of the support and there is no other force to push it down. Because of this, the whole pipe is more likely to slide and jump up. However, this is a very small amount, which can be ignored. The difference in the displacement time history in the beginning part is because during the test, the displacement potentiometer slipped off the little screw hole and made the displacement a little larger than it should be. As the maximum force is associated with the collapse phenomenon, the maximum force is decided by the pipe's structure, dimensions, the material and the boundary condition if the energy is more than the critical energy (the collapse energy). On the other hand, the reaction time and the deformation are more related to the total energy. The friction between the pipe and the support is critical too as this consumes energy and therefore influences the response time and deformation. All these factors have to be carefully studied and decided in the FE models. Figure 5-28 shows the final shapes of I-SPS2, both for experimental measurement and FE result. The comparison shows acceptable agreement. The FE results of I-PPSA2 and I-PPSB2 are shown in Figure 5-29 to Figure 5-34.

Because of the dynamic noise and the shortness of the response time, it is not possible to see any sudden change on the force time history curve at the moment when the inner pipe got indented. Comparisons with experimental data show acceptable agreement, although the deformation of the FE result is less than the experiment result. To sum up, the impact and the dynamic process are much more complicated than the static case; as a result, the FE result is not as close as to the experiment result, though the impact FE model shows acceptable agreement.

The maximum forces show good agreement. However, the response time in the FE model is smaller compared to the experimental data. This might be because that the linear elements make the pipe a bit stiffer. The maximum load is decided by the pipe size and the boundary condition, and in the experiment this maximum load is the buckling load. The bottom displacements in the experiment and in the FE model are within an acceptable difference. To sum up, the impact and the dynamic process are much more complicated than in the static case; as a result, the FE result is not as close to the experiment result, though the impact FE model shows acceptable agreement.

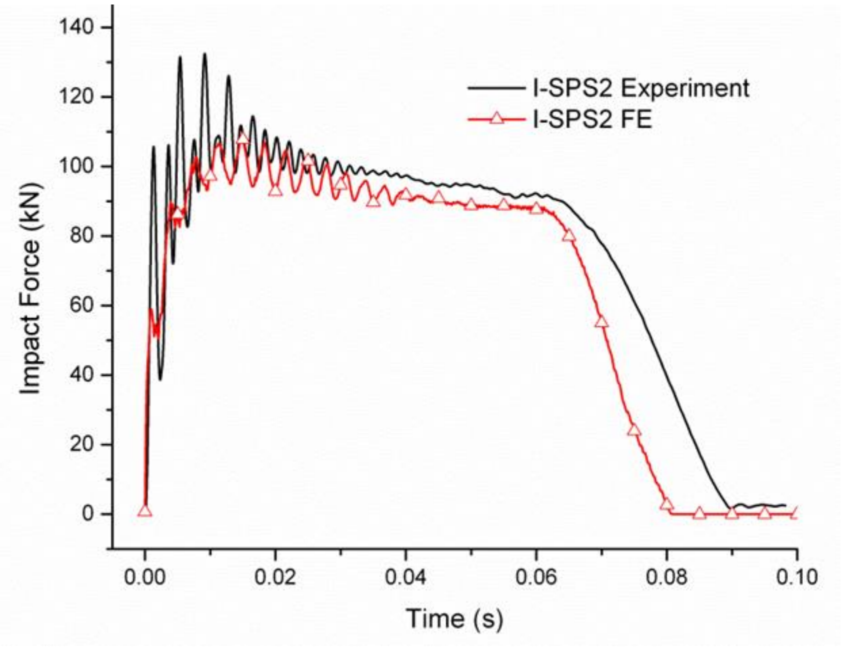

Figure 5-26 Impact force time history of I-SPS2

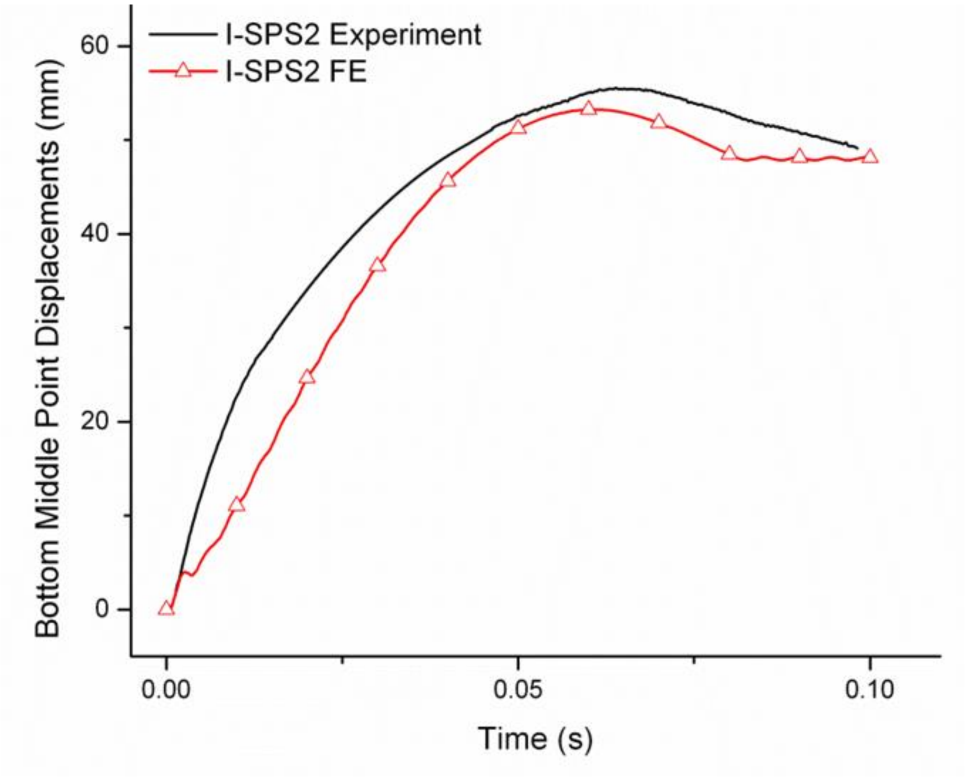

Figure 5-27 Displacement Time History I-SPS2

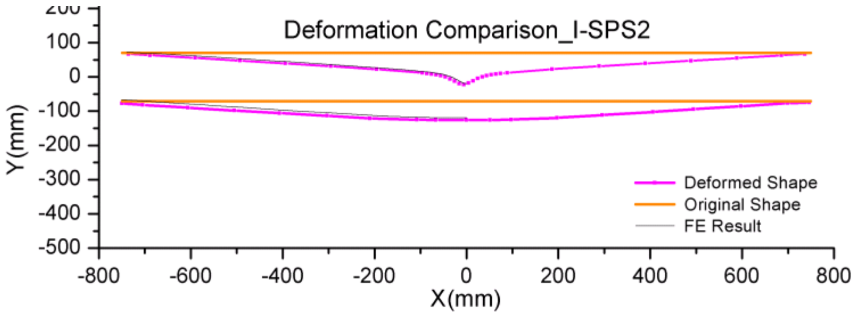

Figure 5-28 Final shape of I-SPS2

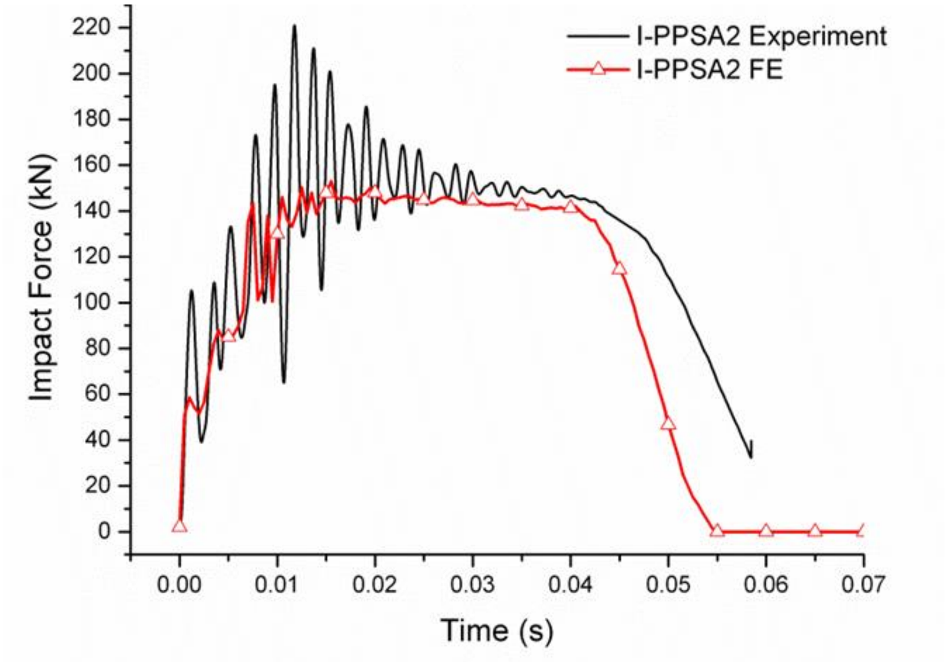

Figure 5-29 Impact force time history of I-PPSA2

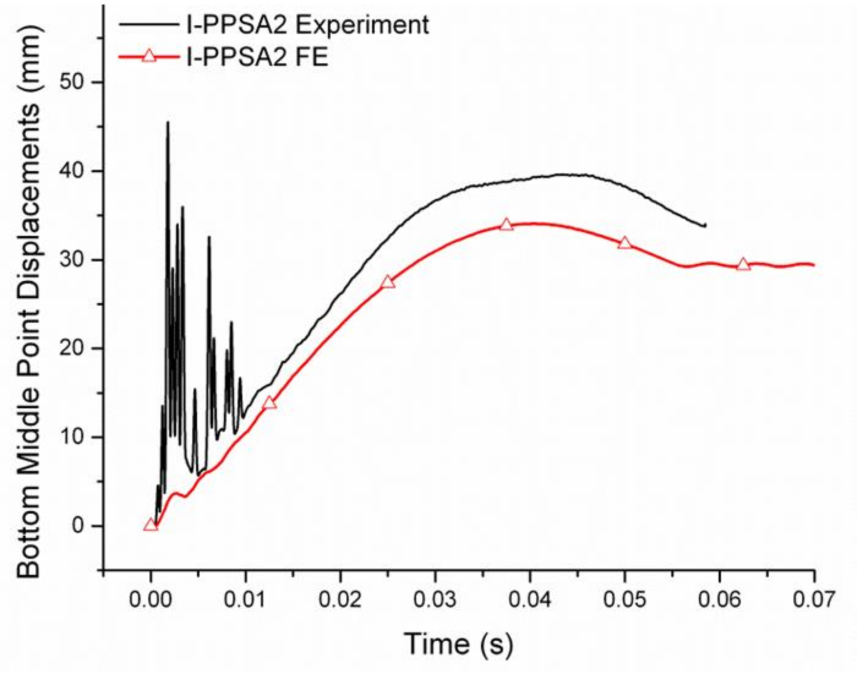

Figure 5-30 Displacement time history of I-PPSA2

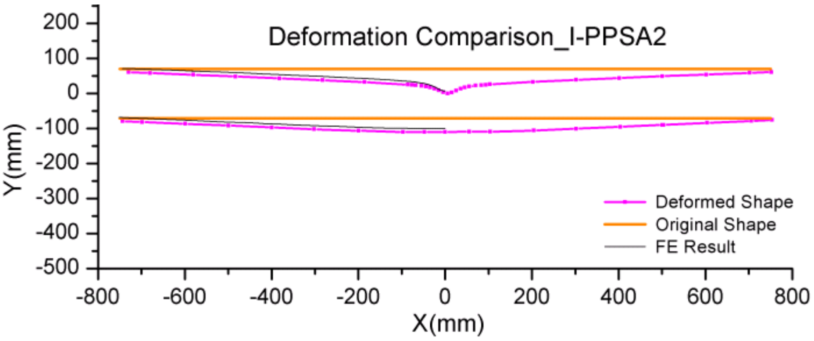

Figure 5-31 Final shapes of I-PPSA2

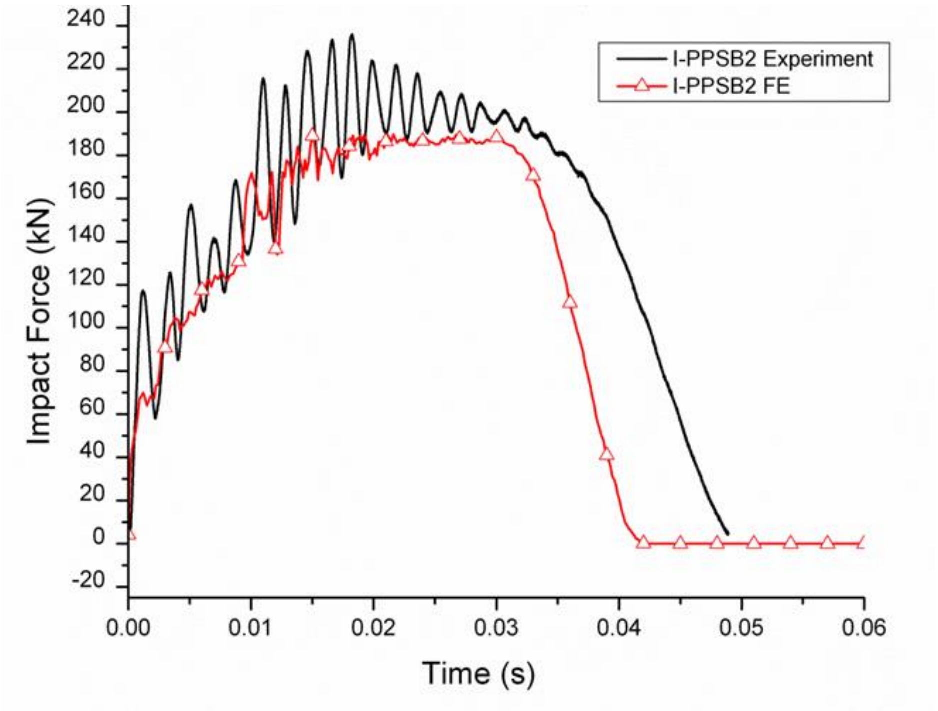

Figure 5-32 Impact force time history of I-PPSB2

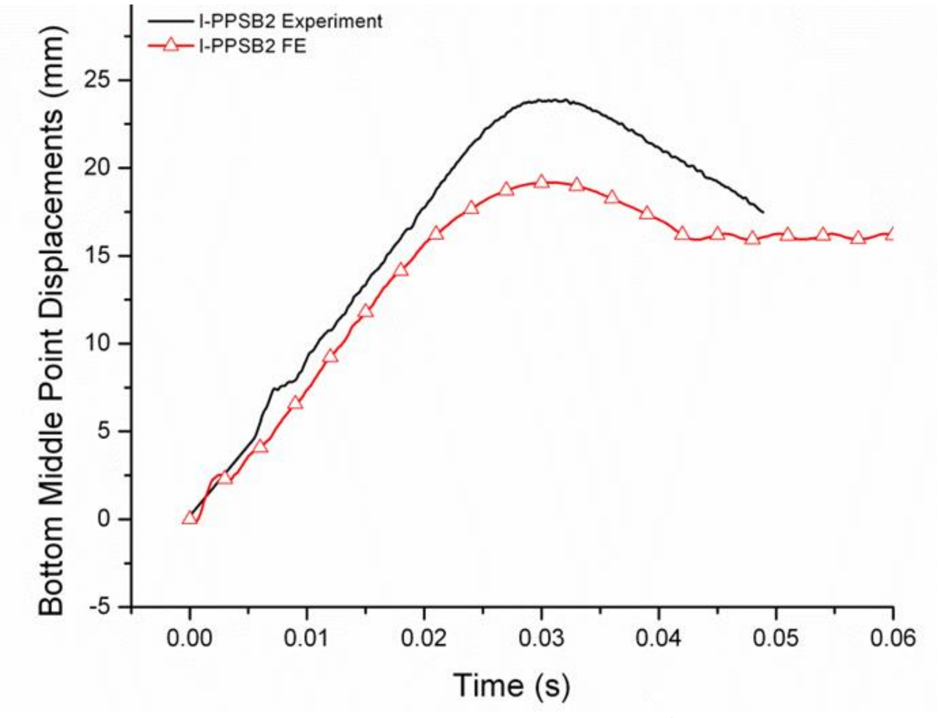

Figure 5-33 Displacement time history of I-PPSB2

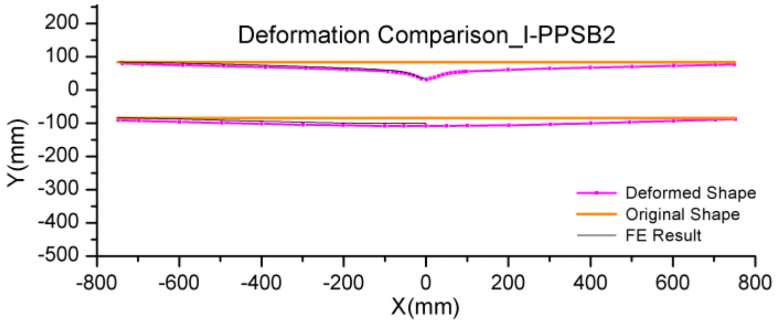

Figure 5-34 Final shapes of I-PPSB2

To sum up, in this section, impact FE models are described, and the comparisons between the finite element results and experiment results show acceptable agreement. These FE models can be used for further analysis.

5.5 Quasi-static Indentation & Dynamic Impact

Shen(Shen and Jones, 1991) concluded that a quasi-static procedure can be used to investigate the dynamic plastic response for the cases that the structures are struck by a heavy mass travelling at a low speed. The comparison between the quasi-static indentation test and the impact test is able to identify if this case falls into this category as Shen suggested. If the comparison does not show much difference between the impact and quasi-static indentation, the further analysis of this issue can be simplified as a quasi-static problem and consequently reduce its complexity.

The comparison between quasi-static response and impact response is conducted using FE models, because the boundary conditions in these two experiments are not exactly the same. The boundary condition of the quasi-static indentation test is shown in Figure 5-35 and the boundary condition of the impact test is shown in Figure 5-36. At the right hand side, the first one is able to move sideways, but the second one could not move.

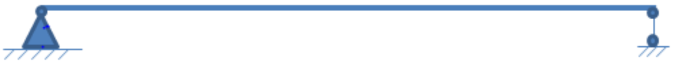

Figure 5-35 Boundary condition of quasi-static indentation test

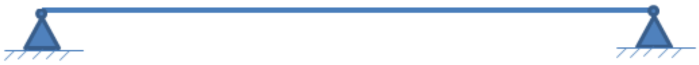

Figure 5-36 Boundary condition of impact test

5.5.1 Quasi-static Response & Impact Response

As the FE model for both the quasi-static indentation test and the impact tests are verified by the test data, the most direct way to compare them is to calculate the quasi-static response under the impact test boundary condition, and then compare it with the impact test data. Moreover, as it is too difficult to measure the indenter’s displacement in the impact test, only the displacement of the bottom centre point is available, and therefore the displacement used for the comparison will be the bottom deflection.

The comparison is given in Figure 5-37. The dashed line is the quasi-static response from the experiment, and the line with circles is the quasi-static response with the impact boundary condition. The solid line is from the impact experiment data. It is clear that the different boundary conditions change the response. Beside this, with the same boundary condition, the quasi-static response and impact response are within the same range; and does not show a big difference. The reason is that the strain rate only influences a small area and does not change the overall response much. The details of strain and strain rate analysis are described in the next section.

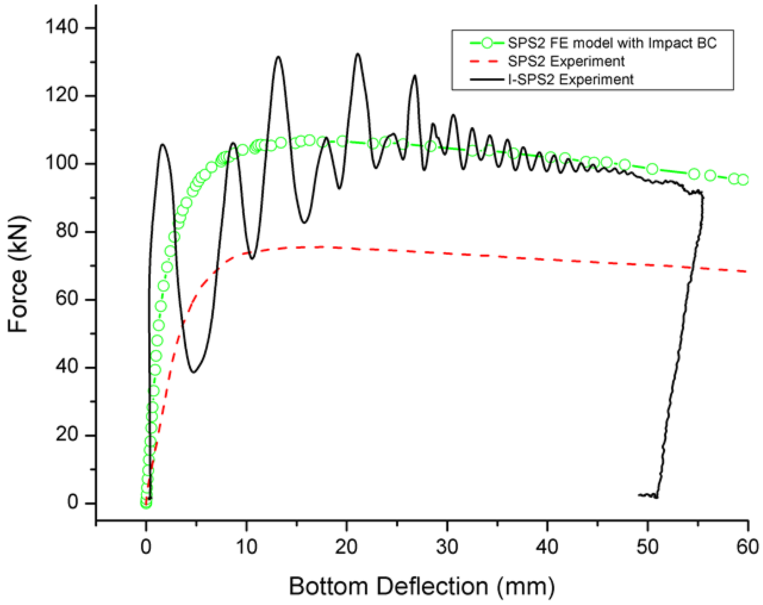

Figure 5-37 Comparison of the quasi-static response and impact response

5.5.2 Strain Rate Effect

One way to investigate the strain rate is to look into the strain time history. In experiments, the strain is measured by strain gauges. However, difficulties arise in the contact area of the indenter and the pipe, where the strain gauges will be damaged. Even outside this range, the strain gauges can only measure the strains in a limited range and will be damaged when the strain exceeds the limit. Moreover, the glue used to install the strain gauge will also be damaged at a large strain. The experiments used Tokyo Sokki Kenkyujo YEF series Post-yield strain gauge whose strain limit is 10-15%.

The measurements and analysis are shown in Figure 5-38 to Figure 5-40, where ε_0 represents the strain in the 0 degree direction, ε_{90} represents the strain in the 90 degree direction, γ_{45} represents the shear strain calculated by the rosette strain gauge data, $\varepsilon_{\max}$ is the calculated maximum principal strain, $\varepsilon_{\min}$ is the calculated minimum principal strain, and $\varepsilon_{\text{bottom}}$ is the strain at the centre of the bottom in the 0 degree direction. It is obvious and expected that the strain is much larger at the indentation point. However, a strain gauge at that point was broken soon on impact. Strain decreases quite quickly when the point is further away. The strain at the middle cross-section is not as large as the strain on the top and bottom side overall. The strain measurements on the impact test I-SPS2 are limited and only the strain at the bottom can be compared with the SPS2 one, as Figure 5-41 shows. Despite the error from the experiment, the strain on the bottom of SPS2 and I-SPS2 is comparable and the bottom is deformed in the same way.

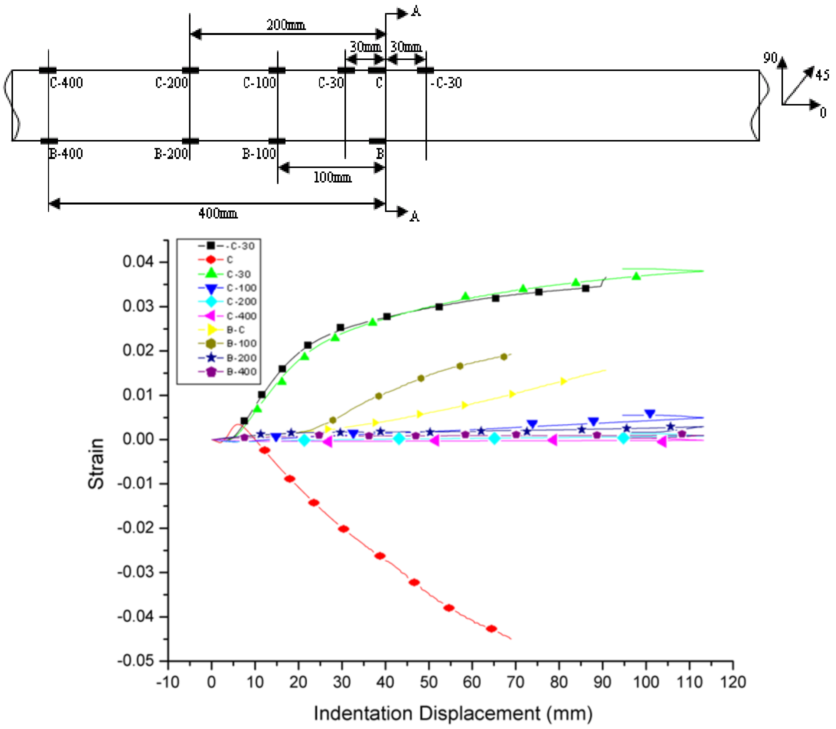

Figure 5-38 Comparison of Strains on the top and bottom for SPS2

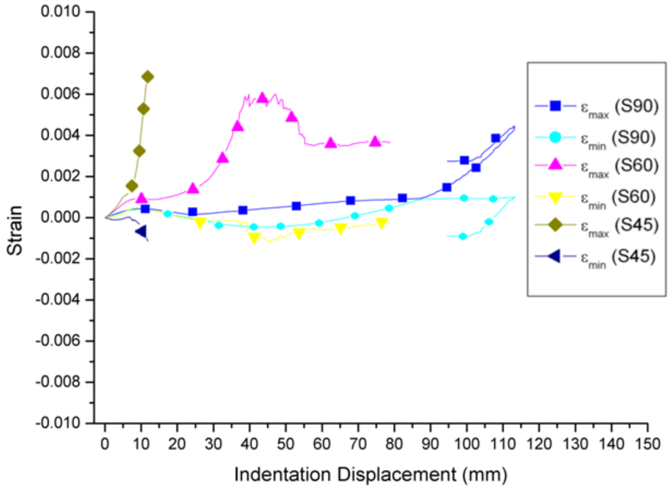

Figure 5-39 Comparison of strains on the middle cross section for SPS2

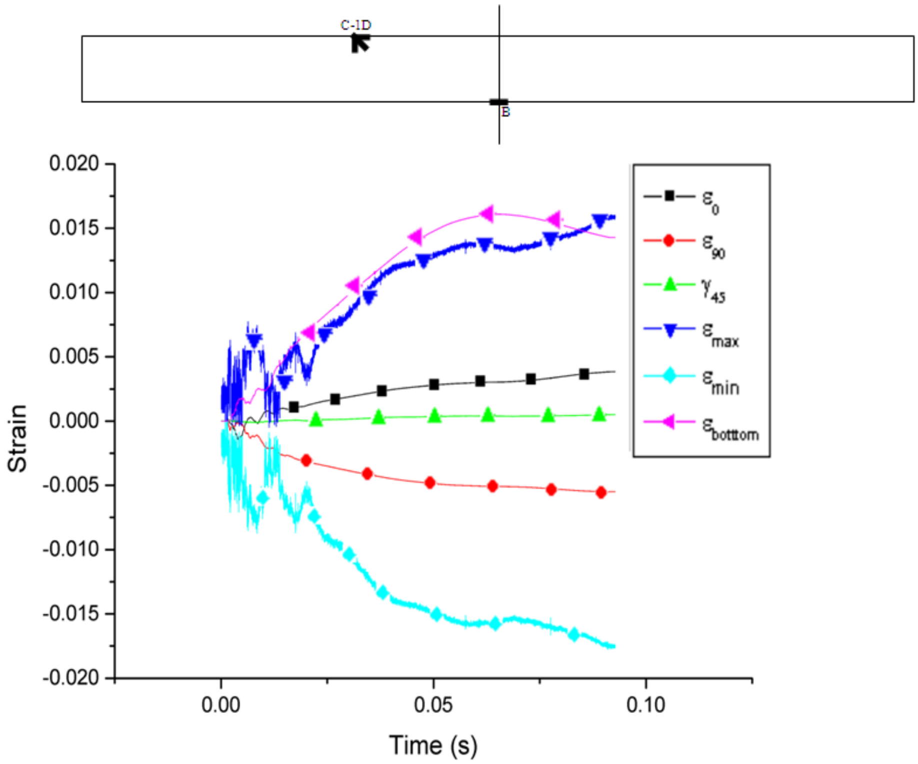

Figure 5-40 Strain measurements of I-SPS2

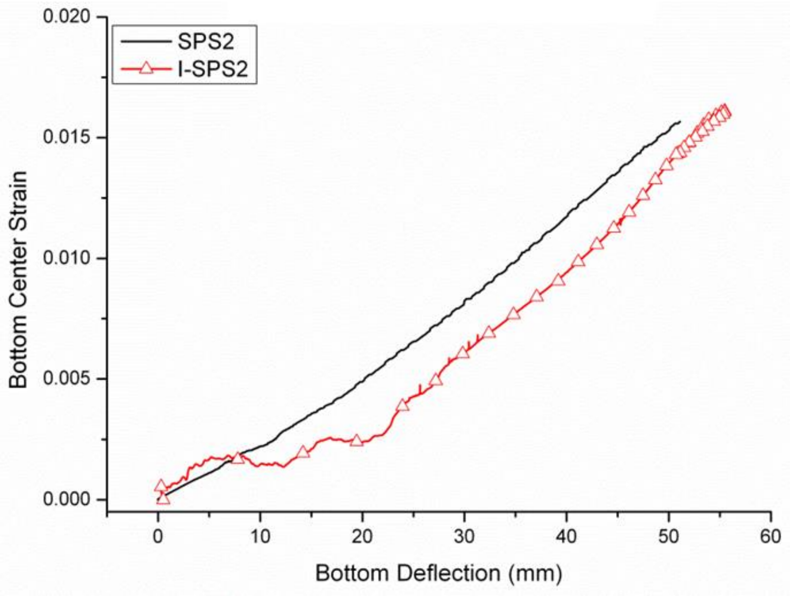

Figure 5-41 Bottom strain - deflection comparison between impact and quasi-static

With the assistance of the FE model, the strain time history can be obtained. Randomly choose one node in the middle cross-section, and plot the strain time history as Figure 5-42 shows. It can be observed that the strain rate is higher at the beginning, and reduces accordingly to the reduced impact velocity. The change is not linear. The strain distributions for SPS2 under such deformation are illustrated in Figure 5-43. The strain at the middle of the top is large, but most of the readings are very small. The conclusion is that the strain is very large only at the middle cross-section, and especially at the top. According to this analysis, the strain rate effect is mainly happening in the middle part, a small area, and the overall effect of strain rate is negligible according to the force-displacement response comparison.

To sum up, the comparison between the quasi-static and the impact shows that: as the strain rate only influences a very small area and the strain rate is small comparing to high speed impact problems, the response does not change much. This conclusion is very useful because it makes it possible to use the quasi-static procedure rather than to analyze the dynamic interference. The impact response lasts only hundredths of a second, which makes it more difficult to investigate the mechanical behaviour. Especially for pipe-in-pipe, the point when the inner pipe being indented is clear in the quasi-static case, but it is difficult to locate that point in the impact test data.

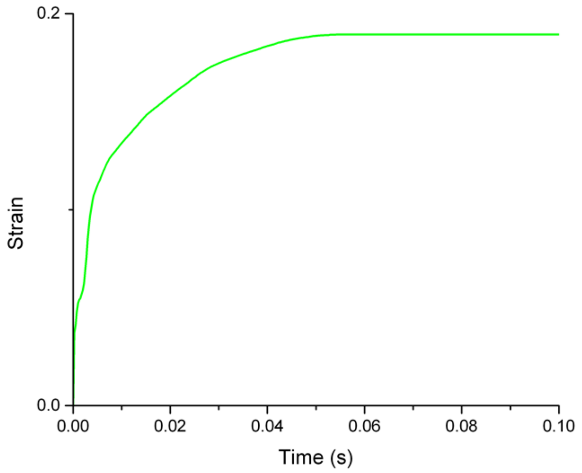

Figure 5-42 Strain time history from the I-SPS2 FE result

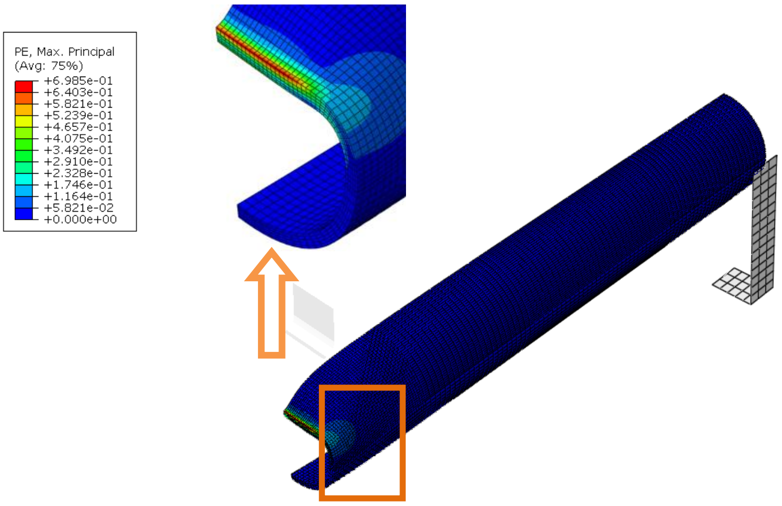
PE, Max. Principal
(Avg: 75%)
+6.985e-01
+6.403e-01
+5.821e-01
+5.239e-01
+4.657e-01
+4.075e-01
+3.492e-01
+2.910e-01
+2.328e-01
+1.746e-01
+1.164e-01
+5.821e-02
+0.000e+00

Figure 5-43 Maximum Principal Strain of SPS2

5.6 Prototype Comparisons

5.6.1 Impact Energy

As mentioned in 4.3.2, because of the boundary condition difference, the quasi-static indentation tests and impact tests are not able to compare directly. In this chapter, the FE models for the quasi-static indentation tests and the impact tests are built. The boundary conditions can be changed in the FE model. As shown in Figure 5-37, the quasi-static FE model with Impact BC of SPS2 is calculated. Scaling up this curve and integrating the area below it, we can plot the indentation energy of this case. Together with the results shown before, the energy is plotted in Figure 5-44. The impact energy of I-SPS2 is about 8.09*10^4 J, and according to the figure, the bottom deflection is about 73 mm and the indenter displacement is about 150 mm. The errors between the experimental data and FE results come from the errors of the measurements, especially for the maximum indenter displacement which was measured by the video, and also from the error of the FE model.

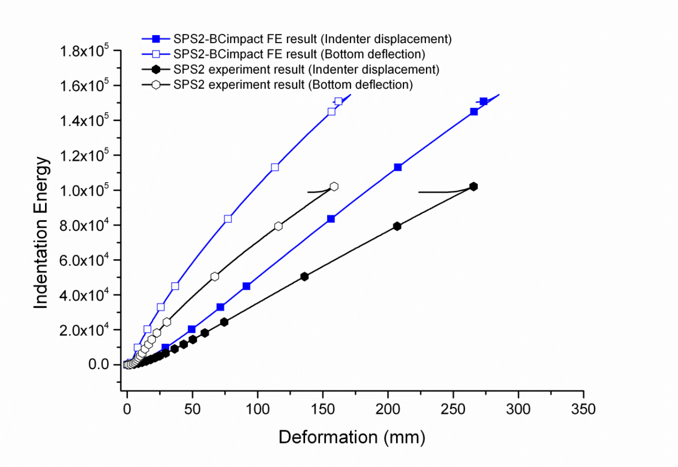

Figure 5-44 Indentation Energy of SPS2 and SPS2-BC impact

5.6.2 PIP12 & PIP14

PIP12 and PIP14 are the major concern as they are less than 16 inch (406.4 mm) in diameter, and both attractive in the applications in the field. Because the test pipes are not perfectly scaled from PIP12 and PIP14, the dimensions of prototypes of the test specimens are slightly different from PIP12 and PIP14, as well as the results. FE method is used to build the model of PIP12 and PIP14. PIP12 and the prototype of PPSA2-nylon are compared in Figure 5-45. The first part of prototype of PPSA2-nylon is larger than the PIP12, and that is because the outer diameter and thickness of the outer pipe of PIPA2-nylon (prototype) are larger than those of PIP12. But as the inner pipe of PIPAB-nylon (prototype) is smaller than the PIP12, the difference decreases in the second part of the curve. The dimension can be checked in Table 3-2. The same situation applies to the case of the prototype of PPSB2-nylon and PIP14, which is shown in Figure 5-46. Because the dimensions are closer, the response difference between the prototype of PPSB2-nylon and PIP14 is much smaller.

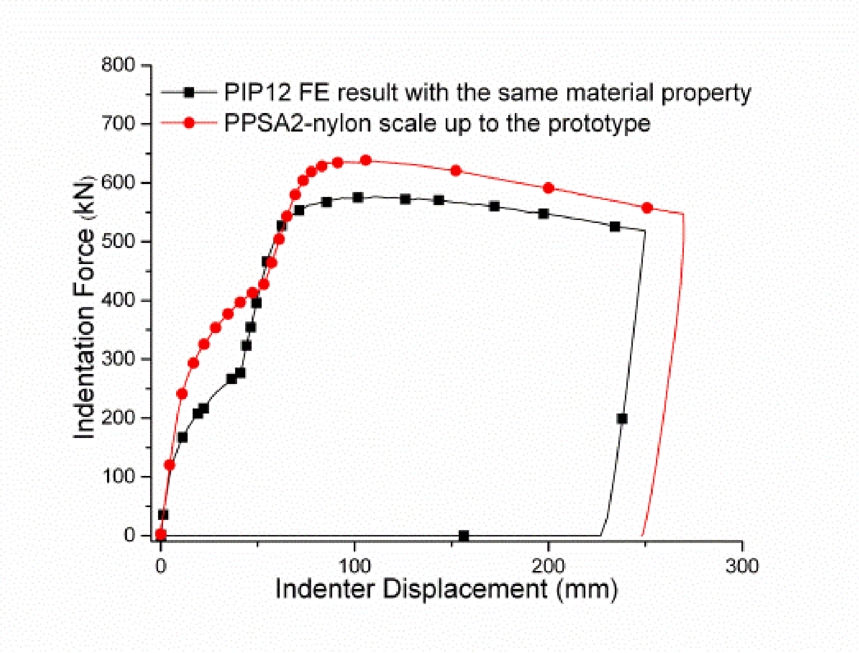

Figure 5-45 Prototype of PPSA2-nylon and PIP12

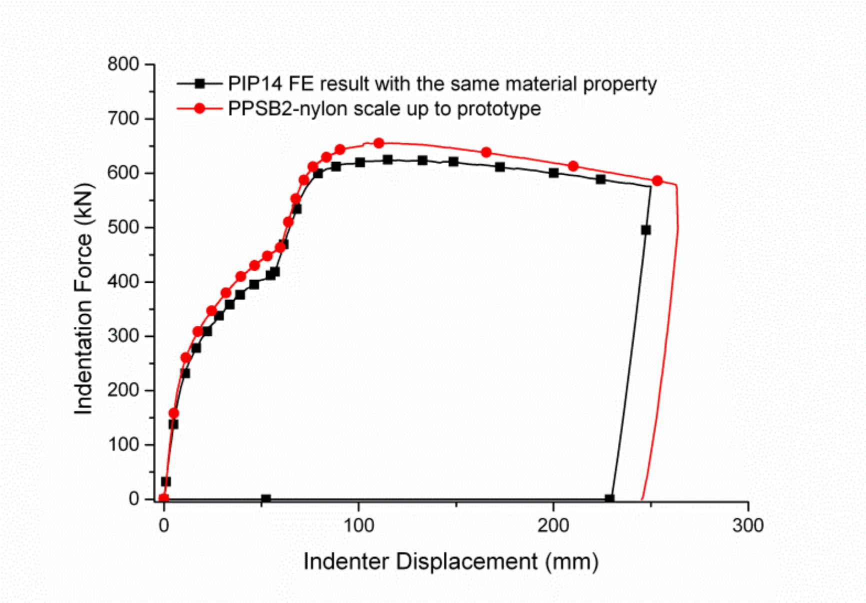

Figure 5-46 Prototype of PPSB2-nylon and PIP14

To make a trenching decision is complicated, and is a case-by-case consideration. A comparison among PIP12, PIP14 and a typical 16 inch (406.4 mm) single wall pipe (SP16) is conducted as this may be able to throw light on the overtrawlability of the pipe-in-pipe. The reason it was decided to make a comparison with a typical 16 inch (406.4 mm) single wall pipe is that based on research carried out between 1974 and 1980, the industry reached a consensus that pipelines over 16 inches need not be trenched. Therefore, if the pipe-in-pipe's overtrawlability is comparable to a typical 16 inch (406.4 mm) pipe, the pipe-in-pipe is highly likely to be able to be left on the seabed without trenching. The responses of the pipe-in-pipe and the 16 inch (406.4 mm) single wall pipe are calculated using the quasi-static FE model established earlier.

The dimensions of PIP12, PIP14 and SP16 are decided as Table 5-6 shows. The 16 inch (406.4 mm) single wall pipe (SP16) is a benchmark for the comparison. According to DNV-RP-F111(DNV, 2010), the failure criteria are shown in Table 5-7. Those failure criteria are a combination of considerations of fatigue life, burst pressure, collapse, pigging processes, safety factors and the frequency of trawl gear impact in that area. This is recommended by DNV who develops guidelines and standards for this industry. The frequency is classified into three classes: "High" represents an impact frequency more than 100 /year /km; "Medium" represents an impact frequency between 1 to 100 /year /km and "Low" represents an impact frequency less than 1 /year /km. In these three different categories, the acceptable dent depths are different, as Table 5-7 shows. Based on these criteria, if we choose the "Medium" class, the critical dent depth and correspond indenter displacement can be calculated for the PIPs and SP16. The acceptable dent depth is 6.10 mm for 16 inch (406.4 mm) single wall pipe and 3.29 mm for the inner pipe of the PIP12 and the PIP14 as Table 5-8 shows. If the outer pipe of the pipe-in-pipe is not restrained by the criteria, because it is not holding any internal pressure or subjected to pressure cycles, the total dent depth for the pipe-in-pipe is more than 3.29 mm, and that allows the pipe-in-pipe to absorb more energy before the failure than the single wall pipe. One should notice that the indenter displacement is different from the dent depth. Their relationship is shown in Figure 3-24. If the ovalization is ignored, the *d* and *b* add up to the indenter displacement (u). The indenter displacements in Table 5-8 are obtained from the FE analysis when the dent depth is the critical dent depth.

Table 5-6 Dimensions of PIP12, PIP14 and SP16

	Pipe-in-Pipe	*D (mm)*	*t (mm)*	*D/t*	*Length*	*Material*
PIP12	Inner pipe	219.1	14.30	15.30	3.44 m	X65
	Outer pipe	323.9	12.70	25.50	3.44 m	X60
PIP14	Inner pipe	219.1	14.3	15.30	3.44 m	X65
	Outer pipe	355.6	14.3	24.90	3.44 m	X60
SP16	SWP	406.4	26.56	15.30	4.32 m	X65

Table 5-7 Failure Criteria (DNV, 2010)

Frequency class	*Dent depth (% of D)*
High (>100)	0
Medium (1-100)	1.5
Low (<1)	3.5

Table 5-8 Acceptable indenter displacement for PIP12, PIP14 and SP16

	D (mm)	*Dent depth (% of D)*	*Critical Dent Depth d (mm)*	*Indenter Displacement u (mm)*
PIP12	219.1 (inner pipe)	1.5	3.29 (inner pipe)	65
PIP14	219.1 (inner pipe)	1.5	3.29 (inner pipe)	86
SP16	406.4	1.5	6.10	17

Figure 5-47 shows the indentation force and indenter displacement relationship for PIP12, PIP14 and SP16. It is clear that the SP16 with larger diameter and thickness can resist a higher indentation force. However, if the same criteria are applied to the single wall pipe and the inner pipe of the pipe-in-pipe, the pipe-in-pipe is allowed to be dented more. The outer pipe is not pressure-containing, and therefore the criteria applied to the inner pipe do not necessarily need to be applied to the outer pipe. The relationships between energy and the dent depth or the indenter displacement are shown in Figure 5-49. With the same criteria apply to the inner pipe and the single wall pipe, the pipe-in-pipe can absorb more energy than the single wall pipe, as much as about 300% more.

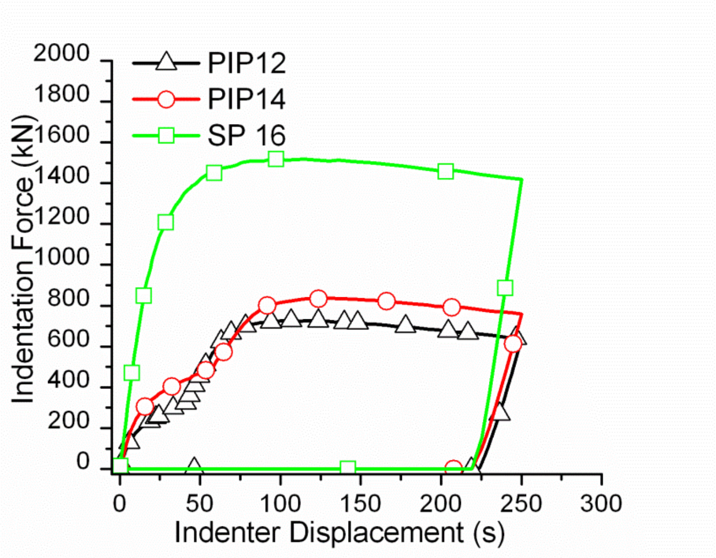

Figure 5-47 Comparison among PIP12, PIP14 and SP16

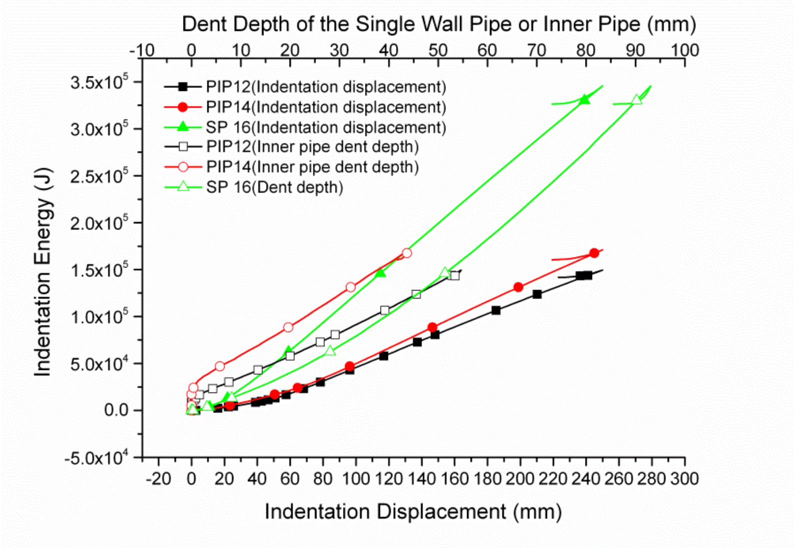

Figure 5-48 Energy versus indenter displacement or dent depth (displacement up to 240 mm)

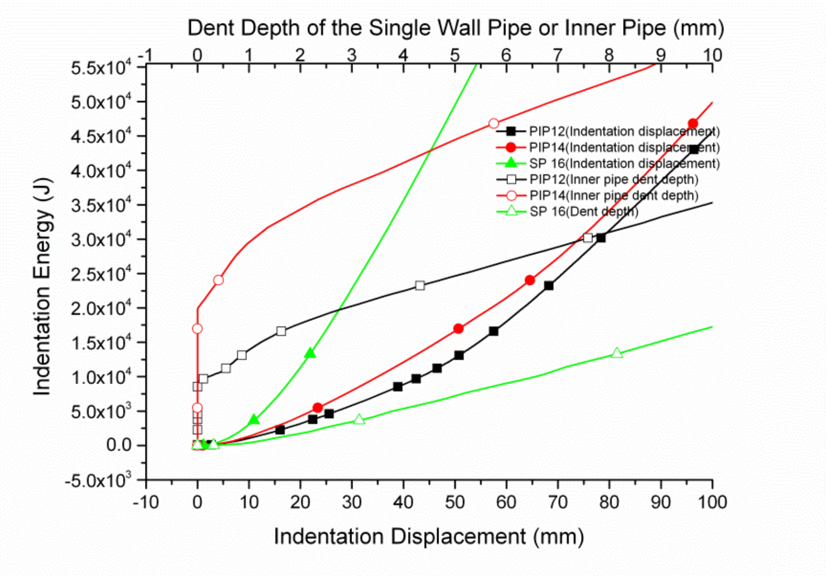

Figure 5-49 Energy versus indenter displacement or dent depth (displacement up to 100 mm)

5.7 Parametric Analysis and Empirical Relationship

When a pipeline's overtrawlability is to be assessed, engineers prefer a simple design equation as it is one of the most effective way to resolve this issue in a very short time. Many researchers have devoted themselves to looking into this problem and to find out a simple closed form equation, by pure theoretical method or semi-empirical method. In this section, a semi-empirical model to describe the relationship between indentation force and displacement is developed based on the validated FE model and the achievements of other researchers.

As shown in Chapter 3, the De Oliveira's theory gives much higher maximum indentation force as that does not consider the global bending. In this section, parametric study is carried out to find out the relationship between the maximum indentation force with outer diameter, thickness, length, and yield stress. Three dimensions (diameter D, thickness t and length L) and one material property (yield stress Y) highly influence the load and deformation during impact phase, and eventually the maximum force. The FE models developed and validated in the previous chapter are used for parametric study here.

From the experimental data it is noticed that every simply supported pipe reaches a maximum force. The maximum force is decided by the collapse mechanism, and both the local deformation and global deformation lead to that limitation. Either bending or denting can make the tube collapse.

If the pipe is perfectly round, the full plastic moment of the cross-section $\mathrm{M_{0c}}$ is given by (5.4).

$$M_{0c} = \sigma_0 D^2 t \tag{5.4}$$

For three-point bending, if the bending goes beyond the elastic range, with a rigid-rigid-plastic material, the collapse load for a simply supported beam is shown as equation (5.5). The collapse load for a fixed ends beam is shown as equation (5.6).

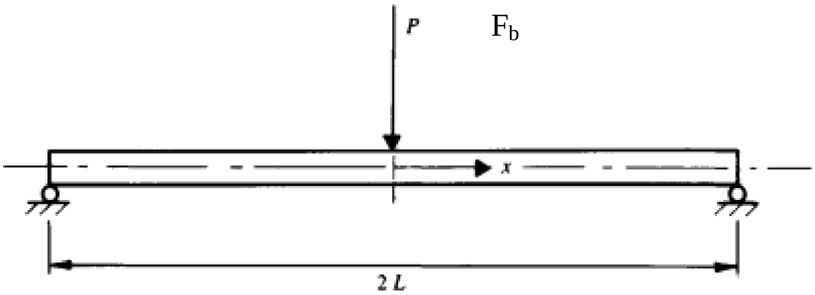

Figure 5-50 Beam under a concentrated load

$$F_b = \frac{2M_{0c}}{L}$$

(5.5)

$$F_b = \frac{4M_{0c}}{L}$$

(5.6)

However, mainly because of the local deformation, the full plastic moment is decreasing. The decreasing relates to the dimensionless group D/t which represents the stiffness of the local denting, and also relates to the dimensionless group L/D which represents the stiffness of the global bending. The two dimensionless groups can be written as equation (5.7).

$$\frac{L}{D} * \frac{t}{D}$$

(5.7)

A model as equation (5.8) can be used to explain this relationship that the ratio of the maximum force over the full plastic bending force is a function of $(\frac{L}{D} * \frac{t}{D})$ and which accounts for the ration of bending capacity and denting capacity.

$$\frac{F_{max}}{2\sigma_0 t D^2/L} = f\left(\frac{Lt}{D^2}\right)$$

(5.8)

The function *f* should have the capacity to describe two trends: first of all, if L is very long, bending will dominate and then the maximum force will equal to the full plastic bending force; secondly, if L is very short, the ratio $\left(\frac{Lt}{D^2}\right)$ will be small, and denting will dominate. Therefore, the maximum value of function f is 1and minimum value is 0. Based on that, the function is chosen as Equation (5.9).

$$f\left(\frac{Lt}{D^2}\right) = 1 - \exp(z * \frac{Lt}{D^2})$$

(5.9)

where z is empirical factor.

In order to determine the empirical factor z, altogether 24 cases of FE models are built and calculated. The details of all the cases are shown in Table 5-9. Experiment data of SPS1 to SPS4 are also included. Moreover, geometries of case 2 are the same as SPS1, geometries of case 5 are the same as SPS3, geometries of case 8 are the same as SPS2, and geometries of case 11 are the same as SPS4. The first set of FE models is with strain hardening effect, while the second set of FE models is not with strain hardening effect. When considered the strain hardening effect, the FE results are closer to the experimental results as expected. However, because the equation of the full plastic bending force does not considered the strain hardening effect, the FE results without strain hardening effect are more comparable. For example, with the strain hardening effect, the maximum force of case 3 is larger than the full plastic bending moment. _To consider the strain hardening is the correct attempt. But because F_{max} should be smaller than $2\sigma_0 tD^2/L$ and if considering the strain hardening, F_{max} might be larger than $2\sigma_0 tD^2/L$, then the equation could not be solved. Moreover, using the FE results without strain hardening effect, the estimation of the maximum force will be conservative, and which is desirable. According to Figure 5-51, the semi-empirical equation is as Equation (5.10).

$$\frac{F_{max}}{2\sigma_0 tD^2/L} = 1 - \exp(-\zeta * \frac{Lt}{D^2})$$

(5.10)

where when ζ=*3.4*, the equation gives a conservative result which does not consider the strain hardening effect; when ζ=*5.35*, the equation considers the strain hardening effect.

As the data are limited, the empirical formula only applies to the pipes whose D/t is around 14 to 25, and the L/D is around 4 to 18. More cases can be done to study if the range can be extended in the future if necessary.

Table 5-9 Details of 24 cases

Case	***D (m)***	***t (m)***	***L (m)***	***yield stress (MPa)***	***Max F(N)***	$\frac{Lt}{D^2}$	$\frac{F_{max}}{2\sigma_0 tD^2/L}$	$1-\frac{\boldsymbol{F_{max}}}{2\sigma_0 tD^2/L}$	$ln(1-\frac{F_{max}}{\frac{2\sigma_0 tD^2}{L}})$
					Finite Element Result with strain hardening				
Case1	0.0889	0.00478	0.75	342.38	31575	0.454	0.915	0.085	-2.470
Case2	0.0889	0.00549	0.75	342.38	38270	0.521	0.966	0.034	-3.383
Case3	0.0889	0.00635	0.75	342.38	46851.3	0.603	1.023	-0.023	#NUM!
Case4	0.1016	0.00478	0.75	342.38	37962.5	0.347	0.843	0.157	-1.849
Case5	0.1016	0.00574	0.75	342.38	4931.2	0.417	0.913	0.087	-2.440
Case6	0.1016	0.00635	0.75	342.38	56398.2	0.461	0.942	0.058	-2.854
Case7	0.1413	0.00556	0.75	342.38	72216.3	0.209	0.713	0.287	-1.247
Case8	0.1413	0.00655	0.75	342.38	91321.2	0.246	0.765	0.235	-1.447
Case9	0.1413	0.00714	0.75	342.38	103461	0.268	0.795	0.205	-1.584
Case10	0.1683	0.00635	0.75	342.38	108829	0.168	0.663	0.337	-1.087
Case11	0.1683	0.00711	0.75	342.38	127765	0.188	0.695	0.305	-1.187
Case12	0.1683	0.00792	0.75	342.38	148970	0.210	0.727	0.273	-1.299

Case	***D (m)***	***t (m)***	***L (m)***	***yield stress (MPa)***	***Max F(N)***	$\frac{Lt}{D^2}$	$\frac{F_{max}}{2\sigma_0 t D^2/L}$	$1-\frac{\boldsymbol{F_{max}}}{2\sigma_0 t D^2/L}$	$ln(1-\frac{F_{max}}{\frac{2\sigma_0 t D^2}{L}})$
Case13	0.2191	0.0127	1.75	342.38	212474	0.463	0.891	0.109	-2.213
Case14	0.2191	0.01427	1.75	342.38	246633	0.520	0.920	0.080	-2.527
Case15	0.2191	0.01509	1.75	342.38	264697	0.550	0.934	0.066	-2.716
Case16	0.3238	0.01113	1.75	342.38	301072	0.186	0.659	0.341	-1.077
Case17	0.3238	0.0127	1.75	342.38	365005	0.212	0.701	0.299	-1.206
Case18	0.3238	0.01427	1.75	342.38	429398	0.238	0.733	0.267	-1.322
Case19	0.3556	0.0127	1.75	342.38	408088	0.176	0.649	0.351	-1.048
Case20	0.3556	0.01427	1.75	342.38	483118	0.197	0.684	0.316	-1.153
Case21	0.3556	0.01509	1.75	342.38	527321	0.209	0.706	0.294	-1.225
Case22	0.1683	0.00711	0.375	323.85	165152	0.094	0.475	0.525	-0.644
Case23	0.1683	0.00711	1.5	323.85	70412	0.377	0.810	0.190	-1.659
Case24	0.0269	0.0016	0.2	375	3342	0.442	0.770	0.230	-1.469
Finite Element Result without strain hardening									
Case1	0.0889	0.00478	0.75	342.38	25837.8	0.454	0.749	0.251	-1.383
Case2	0.0889	0.00549	0.75	342.38	32047.3	0.521	0.809	0.191	-1.655
Case3	0.0889	0.00635	0.75	342.38	38389.8	0.603	0.838	0.162	-1.819
Case4	0.1016	0.00478	0.75	342.38	32488.2	0.347	0.721	0.279	-1.277
Case5	0.1016	0.00574	0.75	342.38	41307	0.417	0.764	0.236	-1.442
Case6	0.1016	0.00635	0.75	342.38	47179.9	0.461	0.788	0.212	-1.553
Case7	0.1413	0.00556	0.75	342.38	61153.5	0.209	0.603	0.397	-0.925
Case8	0.1413	0.00655	0.75	342.38	76676.5	0.246	0.642	0.358	-1.028
Case9	0.1413	0.00714	0.75	342.38	86210.7	0.268	0.662	0.338	-1.086
Case10	0.1683	0.00635	0.75	342.38	91033.3	0.168	0.554	0.446	-0.808
Case11	0.1683	0.00711	0.75	342.38	106666	0.188	0.580	0.420	-0.868
Case12	0.1683	0.00792	0.75	342.38	124142	0.210	0.606	0.394	-0.932
Case13	0.2191	0.0127	1.75	342.38	183739	0.463	0.770	0.230	-1.471
Case14	0.2191	0.01427	1.75	342.38	213466	0.520	0.796	0.204	-1.591
Case15	0.2191	0.01509	1.75	342.38	229377	0.550	0.809	0.191	-1.657
Case16	0.3238	0.01113	1.75	342.38	259076	0.186	0.567	0.433	-0.838
Case17	0.3238	0.0127	1.75	342.38	310506	0.212	0.596	0.404	-0.906
Case18	0.3238	0.01427	1.75	342.38	364737	0.238	0.623	0.377	-0.976
Case19	0.3556	0.0127	1.75	342.38	349414	0.176	0.556	0.444	-0.812
Case20	0.3556	0.01427	1.75	342.38	410079	0.197	0.581	0.419	-0.869
Case21	0.3556	0.01509	1.75	342.38	442533	0.209	0.593	0.407	-0.898
Case22	0.1683	0.00711	0.375	323.85	141832	0.094	0.408	0.592	-0.524
Case23	0.1683	0.00711	1.5	323.85	63684	0.377	0.732	0.268	-1.318
Case24	0.0269	0.0016	0.2	375	3355.904	0.442	0.773	0.227	-1.483
Experimental Data									
SPS1	0.0889	0.00549	0.75	342.3	35708.4	0.521	0.902	0.098	-2.319

Case	***D (m)***	***t (m)***	***L (m)***	***yield stress (MPa)***	***Max F(N)***	$\frac{Lt}{D^2}$	$\frac{F_{max}}{2\sigma_0 tD^2/L}$	$1-\frac{F_{max}}{2\sigma_0 tD^2/L}$	$ln(1-\frac{F_{max}}{\frac{2\sigma_0 tD^2}{L}})$
SPS2	0.1413	0.00655	0.75	341.98	75580	0.246	0.634	0.366	-1.004
SPS3	0.1016	0.00574	0.75	275.58	37572.3	0.417	0.863	0.137	-1.987
SPS4	0.1683	0.00711	0.75	323.85	106650	0.188	0.613	0.387	-0.950

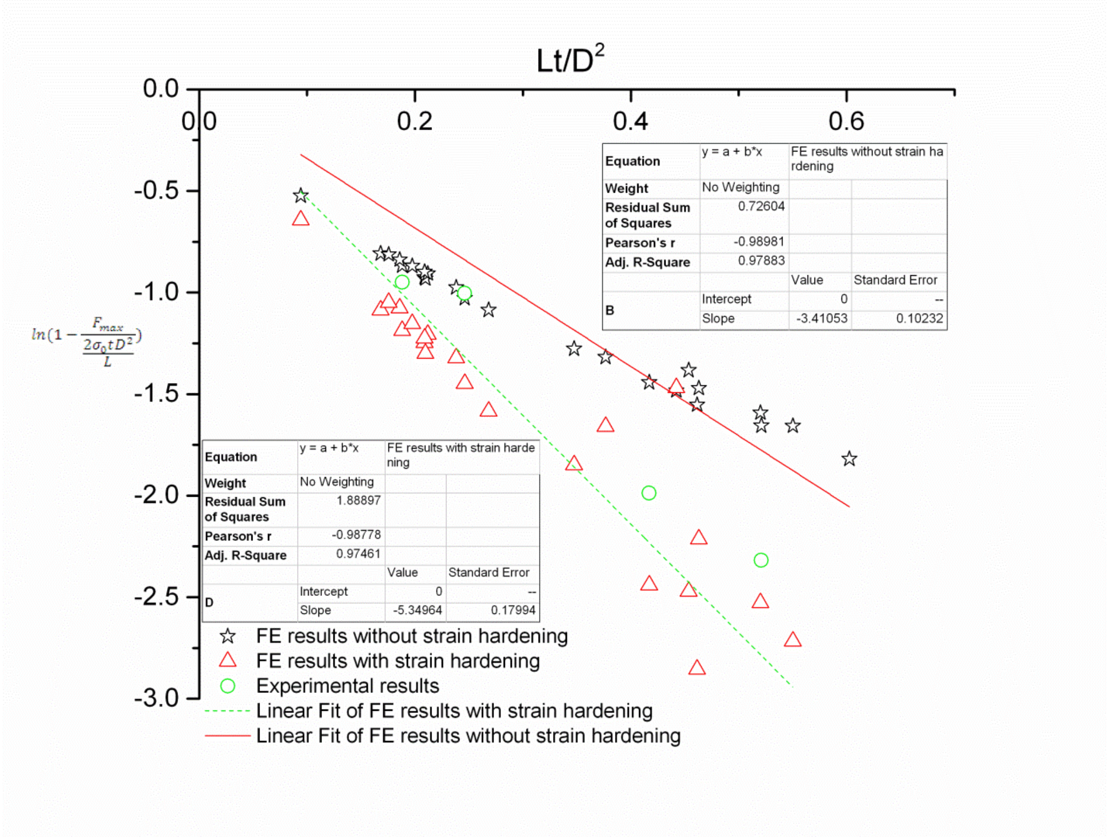

Figure 5-51 Maximum force of 24 cases and linear fitting curve

5.8 New Model of Indentation Force and Displacement

The equation developed in the previous section provides a convenient way of calculating the maximum force, however, in reality, especially for the over trawl problem, the criteria might not allow the pipe to deform so much, so the behaviour before the maximum indentation force is also of interest

In this section, firstly, developed theories are reviewed again to find out which theory applies to such pipes over long spans. The comparisons have been made in Chapter 3, but because the material in the theories is idealized to rigid-plastic, or the BCrigid boundary condition in the test is not perfect, these theories are compared again with finite element models which can eliminate the differences and make the data more comparable.

A new FE model is built for this purpose. It changes the SPS4-BCrigid FE model's boundary condition to fully fixed at both ends, and it is named as SPS4-denting. The comparison between the FE result of SPS4-denting and other theory results is shown in Figure 5-52.

According to the comparison, the FE result is not very different from the test result. Equation DO, WS1 and DNV all agree well with the FE result. They are all based on the theory that De Oliveira (1982) developed. Wierzbicki (1988) improved the relationship by restoring the cross-section back to the circular one, and DNV (2010) used many simulation results to develop this relationship into a semi-empirical one. According to the comparison, both Equation DO and WS are suitable for the specimens studied in this program. Further studies will be based on them.

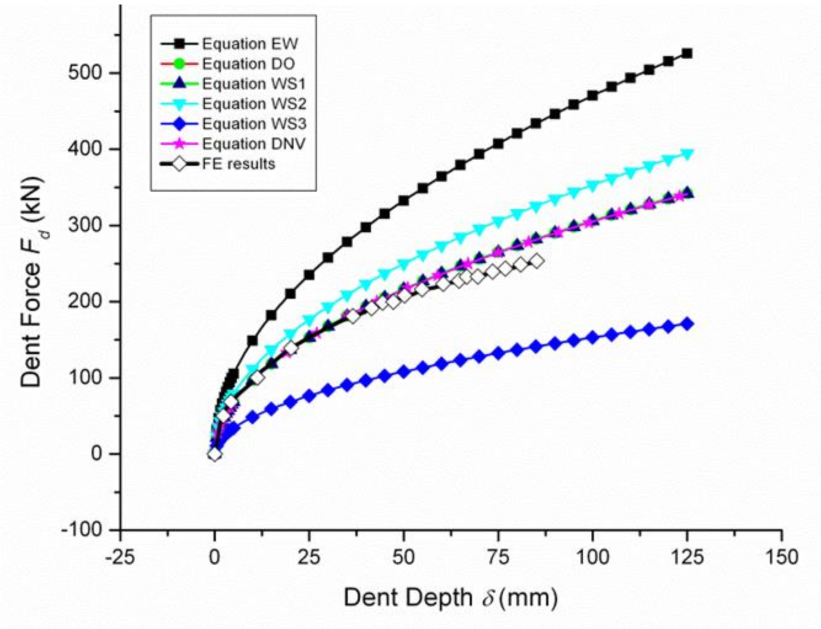

Figure 5-52 Comparison betweenSPS4-denting FE result and theories of pure denting

Moving on to the bending theories, it will be interesting to study the plastic moments of different cross-sections, as De Oliveira did (Figure 2-12), as this is the key parameter to find out the influence on bending. The comparison is shown in Figure 5-53. M_{0c} is the full plastic moment of the undeformed cross-section. Ellinas (1983) and De Oliveira (1982) gave the plastic moment of deformed cross-section. Ellinas' theory treated the denting and bending phase totally separately, and therefore the dent depth in their equation should be the maximum dent depth when the denting phase ceases. Here, if assume the dent depth can change continuously, the plastic moment reaches zero when the dent is about 0.6 the outer diameter, in the Ellinas' theory. Moreover, the deformed shape of Ellinas' theory shown in Figure 2-9 is not as realistic as Oliveira's shape as Figure 2-10 shows. Therefore, for the bending part, the author decided to adopt De Oliveira's theory.

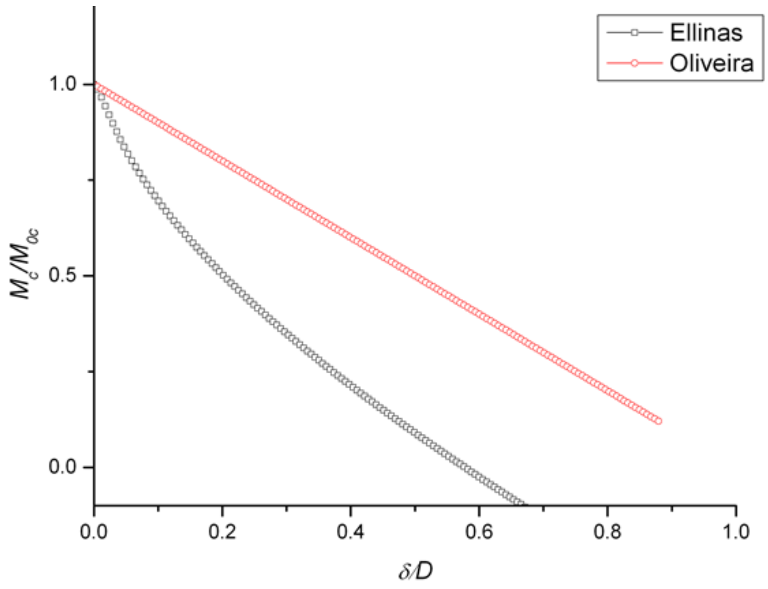

Figure 5-53 Different theories of plastic moment of deformed cross-section

The similar comparison is conducted between the FE model of SPS4 with rigid-plastic material and De Oliveira’s theory. The same conclusion can be drawn that the maximum force calculated by De Oliveira’s theory is much higher than the FE result, according to Figure 5-54.

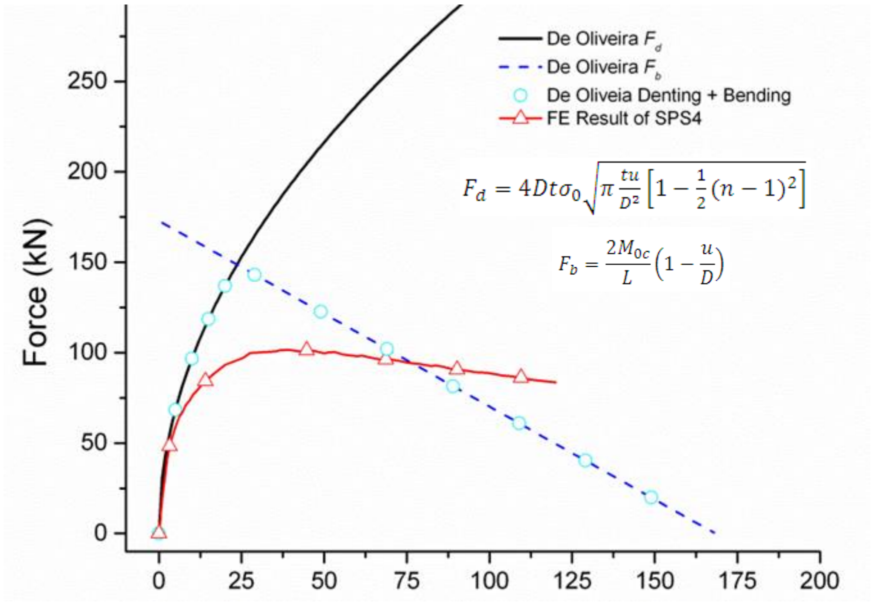

Figure 5-54 Denting and bending alone compare with the FE result of SPS4

To sum up, Wierzbicki and Suh's denting model and the Oliveira's bending model are suitable for the pipes in this research program, and these two theories are used to develop a new model to describe the response of the pipe. However, to treat the denting and bending as two separate phases is not suitable for the pipes studied in current program and the pipes with similar D/t ratio and span length. For this reason, a new model is proposed and trying to find out the relationship between denting and bending and their interference.

As stated in chapter 3, the maximum force calculated by De Oliveira's theory is much higher than the FE result and the test result is because the denting process is influenced by the bending process from the beginning of the deformation, which has not been accounted. On the other hand, the bending capacity decreases much faster in the theory because u is used as dent depth in the equation but it is larger than the real dent depth. Therefore, a new equation (5.11) is proposed to consider three effects: first of all, the denting and bending are developed from the beginning till the end. Secondly, it uses the cross-section deformation d instead of the top centre displacement u to calculate the F_d and F_b, which is more accurate. Last but not the least, the coefficients α and β are used to consider the interaction between denting and bending.

$$F = \alpha \cdot F_d(d) + \beta \cdot F_b(d) \tag{5.11}$$

d is the displacement of the centre of the top of the pipe minus the displacement of the centre of the bottom of the pipe. Most of this deformation comes from the denting process and a small amount of it comes from the bending. Most of this deformation comes from the bending process, but the ovalization and local deformation also influence it to some extent. The ratio of d and b is always changing when the indenter displacement u is increasing. d will be increasing slower while b will be increasing faster.

Reid and Goudie (1989) also observed that “the relationship between the local deformation and the global deformation clearly depends on both the plastic collapse mechanism operating in the dented region and the elastic bending stiffness of the entire tube”. They considered this response as two springs in series, one of stiffness $K_{1,}$ representing the denting stiffness and the other one of stiffness $K_{2,}$ representing the elastic stiffness of the entire tube.

The springs in series theory cannot apply to this problem because the total force should equal to the sum of the forces which develop the dent and the deflection, but the idea is valuable. The current model considers the deformation relates to the respective stiffness, and higher stiffness brings smaller deformation. The stiffness is always changing according to the deformation, and only the deformation at that moment which is Δd and Δb relates to the stiffness at that moment. The stiffness of denting is derived from Wierzbicki and Suh’s equation (2.11) and shown as equation (5.12), assuming u is the denting deformation. The stiffness of bending is derived from De Oliveira’s equation (2.10), as equation (5.13), where u is assumed to be the denting deformation.

$$K_d = \frac{F_d}{u} = 16\frac{M_{0t}}{u}\sqrt{\frac{\pi}{3}}\sqrt{\frac{D}{t}\frac{u}{R}}\sqrt{1-\frac{1}{4}\left(1-\frac{0}{N_P}\right)^3} = 16M_{0t}\sqrt{\frac{\pi}{2tu}}$$

(5.12)

$$K_b = \frac{F_b}{u} = 2\frac{M_{0c}}{Lu}(1-\frac{u}{D})$$

(5.13)

However, u is not the denting deformation when there is global bending. When there is global bending, the measurable parameters *b* and *d* calculated by *d*=*u*-*b* relates to the stiffness. Also, considering *u* is much larger than actually dent depth, the bending stiffness is adjusted by adding a factor $\frac{M_{0c}\left({}^{u}/_{D}\right)}{Lu}$. The ratio of Δd and Δb relates to the respective stiffness, and has the relationship as equation (5.14). To calculate *b* and *d*, Equation (5.15) is used.

$$\frac{\Delta d}{\Delta b} = \frac{(2M_{0c}\left(1-{}^{u}/_{D}\right)+M_{0c}\left({}^{u}/_{D}\right))/(Lu)}{16M_{0t}\sqrt{\pi/(2tu)}} = \frac{M_{0c}\left(2-{}^{u}/_{D}\right)/(Lu)}{16M_{0t}\sqrt{\pi/(2tu)}}$$

(5.14)

$$d_i = d_{i-1} + \Delta d = d_{i-1} + \Delta d\% * \Delta u$$

$$b_i = b_{i-1} + \Delta b = b_{i-1} + \Delta b\% * \Delta u$$

$$\Delta d\% = {}^{\Delta d}/_{(\Delta d + \Delta b)} = {}^{\Delta d}/_{\Delta u}$$

$$\Delta b\% = {}^{\Delta b}/_{(\Delta d + \Delta b)} = {}^{\Delta b}/_{\Delta u}$$

(5.15)

where *b* is the displacement of the centre of the bottom.

This relationship is compared for the cases SPS1 to SPS4. To achieve a better comparison, FE models of SPS1 to SPS4 with rigid-plastic material are used. The comparisons achieve acceptable agreement. There is a discrepancy at the beginning because of the neglect of the elastic deformation.

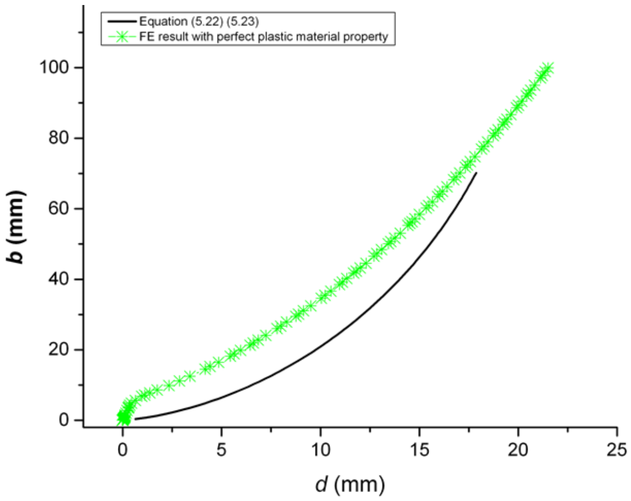

Figure 5-55 Relationship *b*-*d* of SPS1

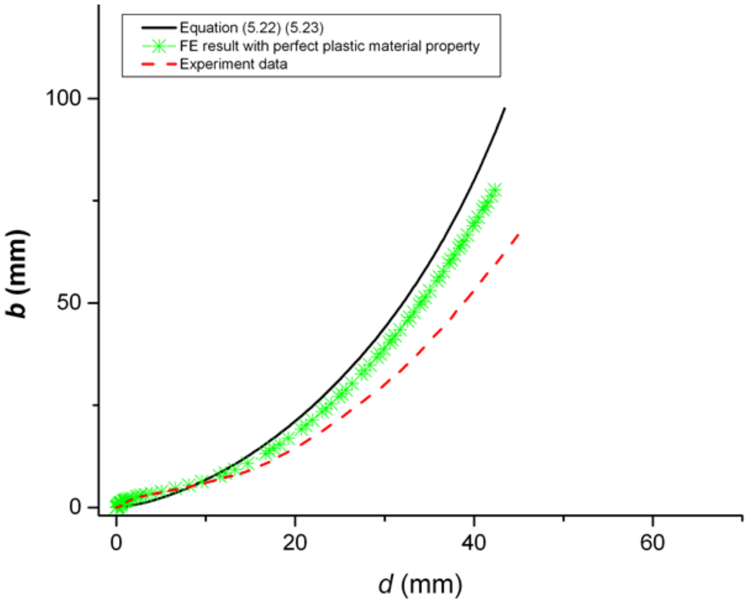

Figure 5-56 Relationship *b*-*d* of SPS2

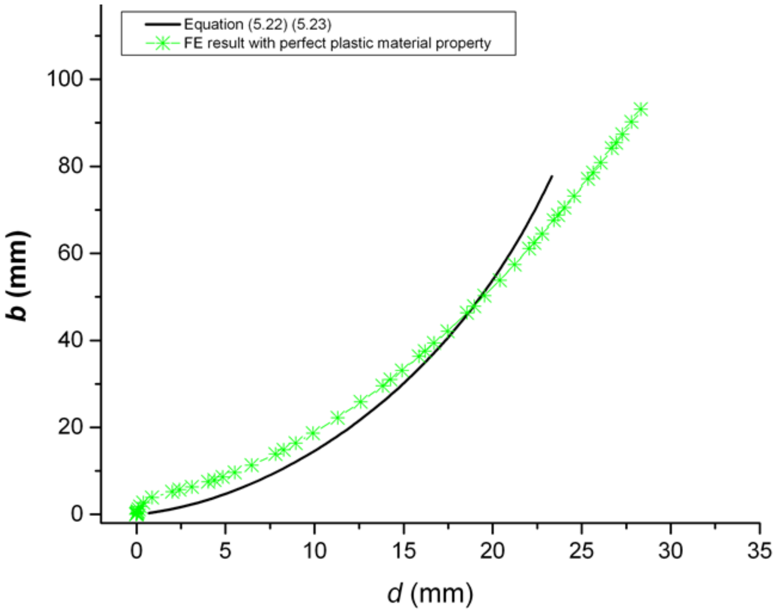

Figure 5-57 Relationship *b*-*d* of SPS3

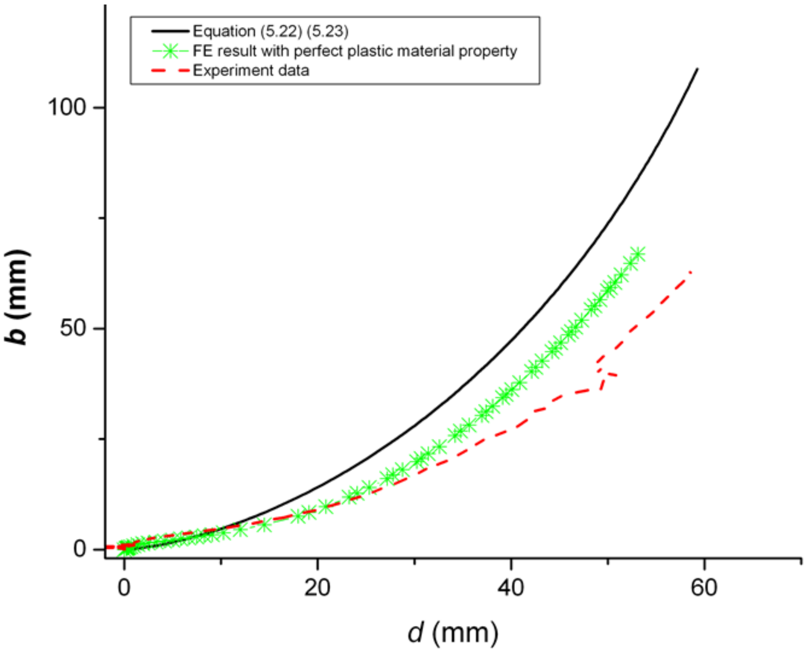

Figure 5-58 Relationship *b*-*d* of SPS4

α and β in equation (5.11) also relate to the deformation of d and b. d and b relates to the denting and bending, but they are not the dent depth and the pure bending deflection, which are not measurable. The development of the bending deformation decreases the capacity to resistant the denting, and this factor count as α. It influenced by $\Delta d\%$ and counts the bending influence. On the other hand, the development of the denting also reduces the bending capacity, and this factor β is shown in equation (5.16), where 0.5 is an empirical factor. The semi-empirical relationships for the coefficients of α and β are written as equation (5.16).

$$\alpha = \frac{M_{0c}\left(2 - {}^{u}\!/_{D}\right)/(Lu)}{16M_{0t}\sqrt{\pi/(2tu)} + M_{0c}\left(2 - {}^{u}\!/_{D}\right)/(Lu)}$$

$$\beta = \frac{0.5 * 16M_{0t}\sqrt{\pi/2tu}}{16M_{0t}\sqrt{\pi/(2tu)} + M_{0c}\left(2 - {}^{u}\!/_{D}\right)/(Lu)}$$

(5.16)

Based on that relationship, the indentation force - indenter displacement curve can be drawn. The curve based on the equation (5.11) is compared with FE results and experiment data as shown in Figure 5-59 to Figure 5-62. The FE result calculates based on the rigid-plastic material property. The comparison shows acceptable agreements. One discrepancy is at the beginning which is again because of the elastic response. If a higher accuracy is required, the elastic response of bending at the beginning can be considered. SPS1 is taken as an example as the discrepancy there is the largest. The curve with considering the elastic response is shown in Figure 5-59, which eliminates the discrepancy to some extent. Again, a higher accuracy can be achieved by considering more factors such as the elastic response of denting and the relationship of denting and bending of the elastic part.

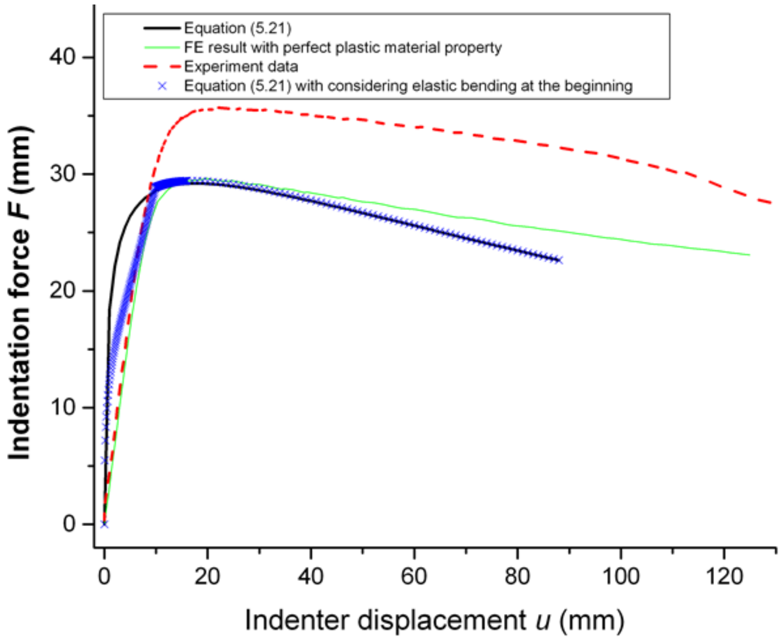

Figure 5-59 Indentation force *F* - indenter displacement *u* of SPS1

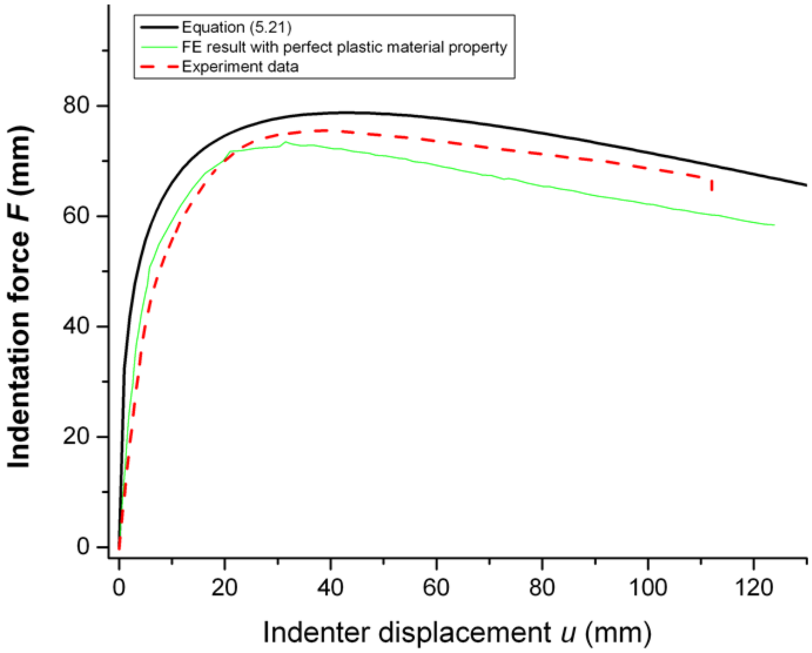

Figure 5-60 Indentation force *F* - indenter displacement *u* of SPS2

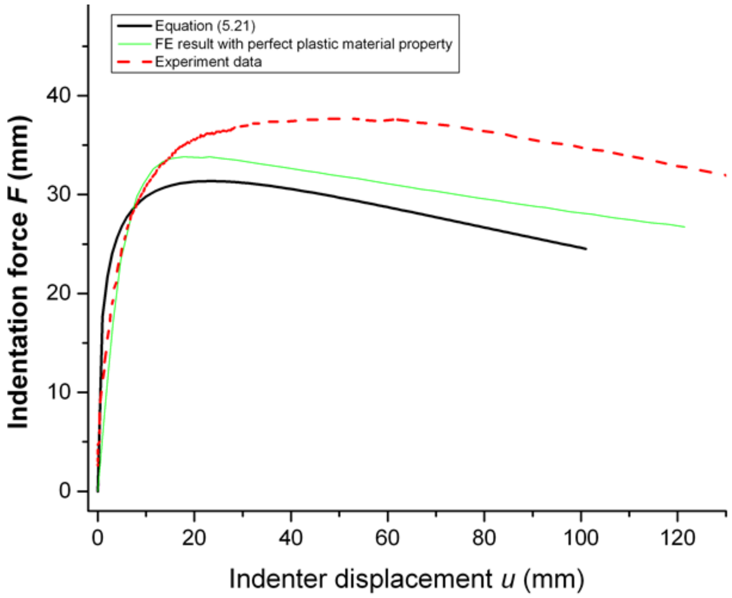

Figure 5-61 Indentation force *F* - indenter displacement *u* of SPS3

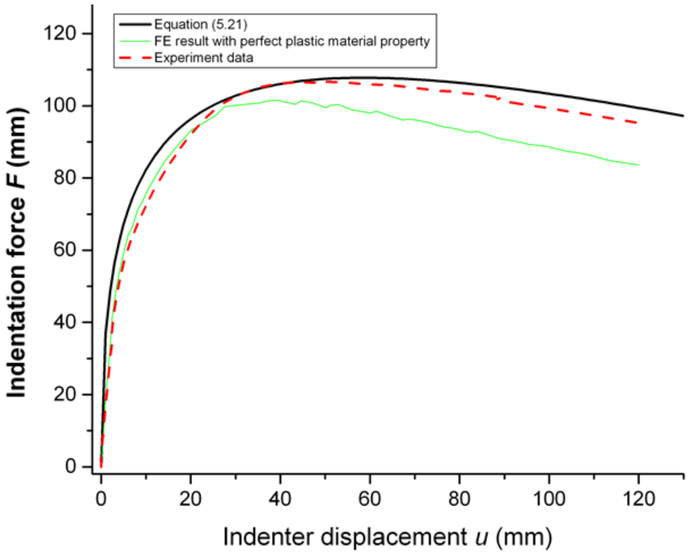

Figure 5-62 Indentation force *F* - indenter displacement *u* of SPS4

5.9 Theories for Pipe-in-Pipes

After understanding the mechanical behaviour of pipe-in-pipe, new theories can be developed for pipe-in-pipes based on the theories for single wall pipes. The main mechanical behaviours that have been recognized in the current research are summarized as follows:

1. The inner pipe is not deformed before the outer pipe actually touches the inner pipe, unless the indentation is applied directly over the spacer.
2. If the indentation is not applied directly over the spacer, the behaviour of the pipe-in-pipe is the sum of the behaviours of the two single wall pipes, and the maximum force equals to the sum of the two maximum forces of the two single wall pipes.
3. If the indentation is applied directly over the spacer, the inner pipe deforms together with the outer pipe, and it requires a higher indentation force.
4. The spacers do have an effect on the result as they will be deformed as well, but the effect is minor.

Based on these observations, theories of the maximum force and the indentation force and displacement relationship of pipe-in-pipe are discussed.

When a pipe-in-pipe is simply supported, according to the semi-empirical relationship developed in section 5.7, if the indentation is not applied directly over the spacer, the maximum force is the sum of the two maximum forces of the two single wall pipes. The equation changes to (5.17).

$$F_{max} = F_{max}^{i} + F_{max}^{o}$$

$$= \frac{2\sigma_0^o t^o {D^o}^2}{L} * \left(1 - \exp\left(\zeta * \frac{Lt^o}{{D^o}^2}\right)\right) + \frac{2\sigma_0^i t^i {D^i}^2}{L} * \left(1 - \exp\left(\zeta * \frac{Lt^i}{{D^i}^2}\right)\right)$$

(5.17)

where the superscripts indicates parameters of the inner pipe (i) or the outer pipe (o).

When the indentation is not applied directly over the spacer, the pipe-in-pipe deforms as a single wall pipe with a higher indentation resistance. The maximum force is larger than the sum of the maximum forces of the two single wall pipes. According to the current experimental results, the force is about 20% higher. The Equation (5.17) still can be used as it gives the conservative estimation. Additionally, impact over the indentation is less likely to happen comparing the other case.

Similarly, when the indentation is not applied directly over the spacer, the relationship of the indentation force and the indenter displacement can be separated into two parts. If the boundary conditions are fixed ends plus the rigid bottom which only allow the pipe to gain local deformation, as demonstrated before, Wierzbicki and Suh's model can be used to develop the model for pipe-in-pipes. Assume the annulus space is a, and that $a = (D^o - 2 * t^o - D^i)/2$. The relationship will be as Equation (5.18). The same idea also applies to the other models, such as De Oliveira's model and DNV's model which have been demonstrated that they are suitable for such pipes.

$$\begin{cases} F = 16M_{0t}^{o}\sqrt{\frac{\pi}{3}}\sqrt{\frac{D^o}{t^o}\frac{u}{R^o}}\sqrt{1-\frac{1}{4}\left(1-\frac{N^o}{N_0^o}\right)^3} & when\, u \le a \\ F = 16M_{0t}^{o}\sqrt{\frac{\pi}{3}}\sqrt{\frac{D^o}{t^o}\frac{u}{R^o}}\sqrt{1-\frac{1}{4}\left(1-\frac{N^o}{N_0^o}\right)^3} + 16M_{0t}^{i}\sqrt{\frac{\pi}{3}}\sqrt{\frac{D^i}{t^i}\frac{u-a}{R^i}}\sqrt{1-\frac{1}{4}\left(1-\frac{N^i}{N_0^i}\right)^3} & when\, u \ge a \end{cases} \tag{5.18}$$

If the boundary condition is simple support which allows both local and global deformations, the model shown as Equation (5.9) can be developed to fit pipe-in-pipes. When the indentation is not applied directly over the spacer, the model is shown as Equation (5.19).

$$\begin{cases} F = \alpha^o \cdot F_d^o(d^o) + \beta^o \cdot F_b^o(d^o) & when\, u \le a \\ F = \alpha^o \cdot F_d^o(d^o) + \beta^o \cdot F_b^o(d^o) + \alpha^i \cdot F_d^i\left(d^i\right) + \beta^i \cdot F_b^i\left(d^i\right) & when\, u \ge a \end{cases} \tag{5.19}$$

where

$$F_d = 4Dt\sigma_0 \sqrt{\pi \frac{td}{D^2}\left[1 - \frac{1}{2}(n-1)^2\right]}$$

$$\frac{F_b}{2M_{0c}/L} = (1 - \frac{d}{D})$$

$$\alpha^o = \frac{M_{0c}^o\left(2 - {}^{u}/_{D^o}\right)/(Lu)}{16M_{0t}^o\sqrt{\pi/(2t^o u)} + M_{0c}^o\left(2 - {}^{u}/_{D^o}\right)/(Lu)}$$

$$\beta^o = \frac{0.5 * 16M_{0t}^o\sqrt{\pi/2t^o u}}{16M_{0t}^o\sqrt{\pi/(2t^o u)} + M_{0c}^o\left(2 - {}^{u}/_{D^o}\right)/(Lu)}$$

$$\alpha^i = \frac{M_{0c}^i\left(2 - {}^{(u-a)}/_{D^o}\right)/(L(u-a))}{16M_{0t}^i\sqrt{\pi/(2t^i(u-a))} + M_{0c}^i\left(2 - {}^{u}/_{D^i}\right)/(L(u-a))}$$

$$\beta^i = \frac{0.5 * 16M_{0t}^i\sqrt{\pi/(2t^i(u-a))}}{16M_{0t}^i\sqrt{\pi/(2t^i(u-a))} + M_{0c}^i\left(2 - {}^{(u-a)}/_{D^i}\right)/(L(u-a))}$$

$$d_i^o = d_{i-1}^o + \Delta d^o = d_{i-1}^o + \Delta d^o\% * \Delta u$$

$$\Delta d^o\% = {\Delta d^o}/{(\Delta d^o + \Delta b^o)} = {\Delta d^o}/{\Delta u}$$

$$\frac{\Delta d^o}{\Delta b^o} = \frac{M^o_{0c}\left(2 - {u}/{D^o}\right)/(Lu)}{16 M^o_{0t}\sqrt{\pi/(2t^o u)}}$$

$$d^i_i = d^i_{i-1} + \Delta d^i = d^i_{i-1} + \Delta d^i\% * \Delta u$$

$$\Delta d^i\% = {\Delta d^i}/{(\Delta d^i + \Delta b^i)} = {\Delta d^i}/{\Delta u}$$

$$\frac{\Delta d^i}{\Delta b^i} = \frac{M^i_{0c}\left(2 - {(u-a)}/{D^i}\right)/(L(u-a))}{16 M^i_{0t}\sqrt{\pi/(2t^i(u-a))}}$$

The theories shown here and corresponding FE results and experimental results are compared as shown in Figure 5-63. It can be seem the semi-empirical models are close to the test result and which can be applied to such pipe-in-pipes with restrictions.

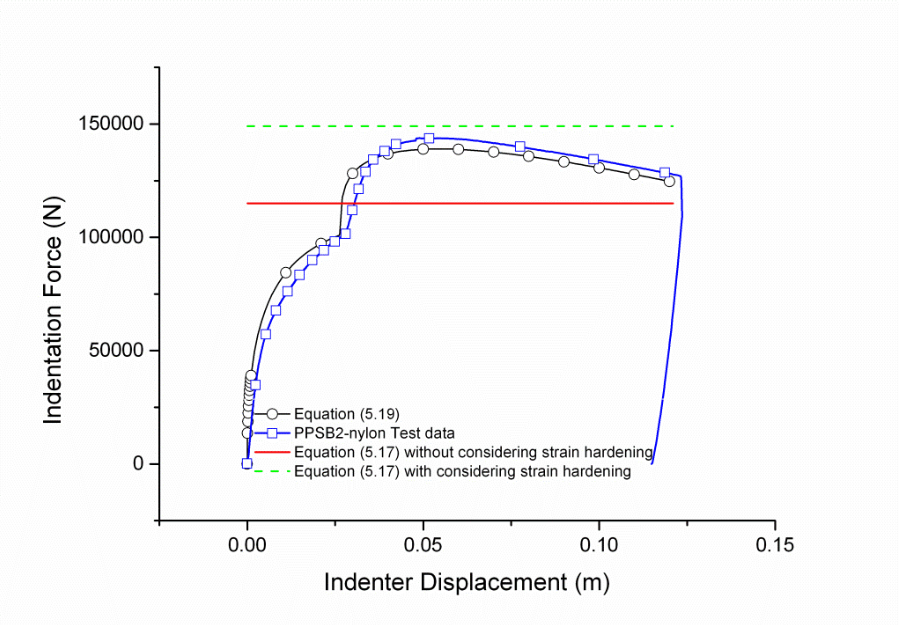

Figure 5-63 Comparison of semi-empirical models of pipe-in-pipes and test data

5.10 Summary

Both the quasi-static indentation FE models and impact FE models have been built for single wall pipes and pipe-in-pipes. The comparisons between the test results and finite element results show acceptable agreement. With the FE models, more comparisons are carried out. The followings are the main findings of this chapter.

1. FE models have been developed and verified against test data. It can be used for further analysis with different parameters and the methodology can be applied to similar problems.
2. The quasi-static response of SPS2 and the impact response of I-SPS2 have been compared in this chapter, including the strain rate effect, and dynamic effect. The comparison shows little difference in the overall response. The author demonstrates that the quasi-static analysis can be used for this problem instead of impact analysis. The quasi-static indentation FE models have closer results to the test data. They are easy to build and to simulate with computational efficiency.
3. The impact energy and indentation energy have been compared. With the FE model, the difference of the boundary condition can be eliminated. The difference between them comes from errors in the FE analysis and errors in the experiment measurements.
4. The prototypes of the test pipes and their corresponding original prototypes PIP12 or PIP14 have been compared. The comparisons show reasonable results which are consistent with the difference of the geometries. The comparison of PIP12, PIP14 and SP16 illustrates the

overtrawlability of pipe-in-pipe. If the design criteria of the outer pipe can be relaxed, the pipe-in-pipe can absorb more energy before it fails.

5. The semi-empirical relationships have been developed to estimate the maximum indentation force and the relationship of the indentation force and indenter displacement for single wall pipe and pipe-in-pipe. The local and global deformations are both considered in this model instead of treating them separately.

On one hand, the outer pipe is not pressure-containing and not subject to pressure cycle; one the other hand, it might suffer from other failure mode which associates with low internal pressure and big dents. The most possible failure mode is collapse. External pressure tends to push the wall inward. Because of that interaction, an impact under external pressure dents the pipeline more severely than the same impact with no external pressure. In addition, with a high external pressure and an imperfect geometry, collapse happens much more easily than it does for a round pipe containing a high internal pressure. This part of the work is summarized in Chapter 6.

6 Interaction between External Pressure and Indentation

The possibility to relax the criteria for pipe-in-pipe depends on the feasibility of applying different criteria to the outer pipe. The outer pipe of pipe-in-pipe gives the inner pipe extra protection, and it is not required to resist internal pressure and can accommodate a greater level of indentation than a single-wall pressure-containing pipe. Moreover the acceptable dent depth level is also limited by pigging; the outer pipe does not have the pigging procedure. From this point of view, it is possible to relax the criteria. On the other hand, the outer pipe is under a larger external pressure as the internal pressure is zero or very low. This situation may be more dangerous than for a single wall pipe because as the pipe might collapse and the collapse might propagate.

External pressure is a key factor to be considered in the design of subsea pipelines. However, all the theories and experiments the author described in the previous chapters deal with pipelines in the air, not in water. To consider the possibility to relax the criteria for the outer pipe, external pressure must be considered together with the denting. Kyriakides (2007a) has pointed out that the pipe with imperfection (ovality, a dent etc.) is much easier to collapse or buckle, and the indentation creates significant imperfection. Park (1996) has investigated the dented pipe under external pressure, and found the dent decreases the pipe’s capacity against the external pressure, and they developed a curve to be the “Universal Collapse Resistance Curve” (UCRC) to look into the collapse pressure for dented tube. But this is not exactly the case of trawl gear impacting the pipeline because the impact is taking place under external pressure, instead of the pipeline being impacted first and then collapsing under external pressure. Quite a bit of experimental and numerical work has been conducted on the denting of pressurized pipe.

This chapter develops a FE methodology to analyze the pipeline under both of the indentation and external pressure. As external pressure changes the relationship of indentation force and dent depth, this chapter will fill the gap left by models with no external pressure, and considers the criteria for the outer pipe case by case.

6.1 FE Modelling Methodology and Validation

The strategy to develop the FE model of denting with the existence of external pressure is to establish and validate the FE model of denting and FE model of external pressure respectively, and then combine them together to create the new model. The validation of the FE model of denting is addressed in Chapter 3, and the validation of the FE model of external pressurizing is achieved by comparison with published results, including both numerical results and experiment results.

6.1.1 FE Model of External Pressure

Kyriakides at the University of Texas at Austin has worked on the collapse and buckling of pipelines for several years, and published a book “Mechanics of Offshore Pipelines” (Kyriakides and Corona, 2007b). In his book, several models related to pipeline collapse and buckling under different loading combinations have been established by theoretical work, experimental work and numerical work. Kyriakides’ results will therefore be a good choice and sufficient to verify the FE model of external pressure. The validation consist two steps: the first step is to build the FE model of collapse of an undamaged pipe under pure external pressure and validated against a published numerical result, and then, the FE model of collapsing a dented pipe under pure external pressure will be built and validated against published experimental and numerical results.

Hydrostatic fluid element F3D4 is used to simulate the external pressure rather than apply a constant pressure to the structure. The advantage of this is that the hydrostatic fluid element is able to simulate the interaction between the deformation of the structure and the pressure change. One more advantage is that the hydrostatic fluid element is able to simulate the collapse and buckle, as well as post-buckle behaviour as the boundary condition can be applied as displacement control method. The Riks method could also use to simulate collapse and buckling; however, this method creates the problem to simulate the possible collapse under both the external pressure and the indentation force.

The hydrostatic fluid elements F3D4 in ABAQUS can be used to define surfaces and the surfaces can be used to form a cavity. The cavity can be any shape, but has to be sealed. Within the cavity, there is fluid. By defining the fluid’s behaviour, the pressure at different steps can be defined. If the cavity’s elements share the same nodes with the structure’s elements, the deformation of the structure will also change the shape of the cavity and consequently change the volume of the cavity. If the fluid was not defined as fixed pressure, the pressure will change accordingly with the volume change; therefore simulating the fluid-structure interaction. The cross-section of the model is shown in Figure 6-1. The cross-section of the cavity can be rectangle, circular or any other shape. The pipe's wall has two boundaries: the inner surface touches the inner fluid, and the outer surface contacts the outer fluid. Therefore, the outer boundary is also the cavity and which shares the same node with the structure elements. The change of the pipe wall will change the volume of the cavity. Changing the fluid volume or pressure will have an effect on the structure.

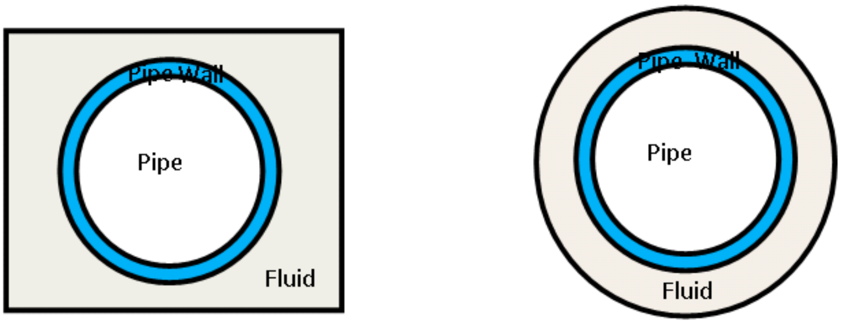

Figure 6-1 Cross-section of the structure and cavity

In Chapter 4 of "Mechanics of Offshore Pipelines" (Kyriakides and Corona, 2007b), a nonlinear formulation is introduced and solved by a numerical method. A custom program BEPTICO was developed based on this, which was validated by the experimental results (Kyriakides and Corona, 2007b). One of the results calculated by BEPTICO and shown in Figure 4.8 in the book will be used here to validate the first case: a pipe collapse under pure external pressure. The pipe is an X52 pipe. X52 indicates the material yield stress is 52 ksi, which is 359 MPa. The stress-strain curve is represented by the Ramberg-Osgood model $\varepsilon = \frac{\sigma}{E}(1 + \frac{3}{7}(\frac{\sigma}{\sigma_y})^{n-1})$ with fitting parameters n=13 and $\sigma_y = 317$ MPa. The diameter over thickness ratio is 20 and ovality is 0.2%. Ovality is one measure of the cross-section's out-of roundness of pipe, defined as $\frac{D_{max}-D_{min}}{D_{max}+D_{min}}$. The FE model built by the author is illustrated in Figure 6-2. The hydrostatic fluid elements are indicated. The geometry of the cavity is a conical shell. The reason to choose this geometry is to eliminate the end effect as the end cap area is small while the middle section has a large space. The structure elements can be shells element or solid elements. Here solid element C3D20R is used in order to seek higher accuracy. Some of the hydrostatic fluid elements share the same nodes with the solid element on the outer surface. The result is compared and presented in Figure 6-3. The comparison shows acceptable agreement.

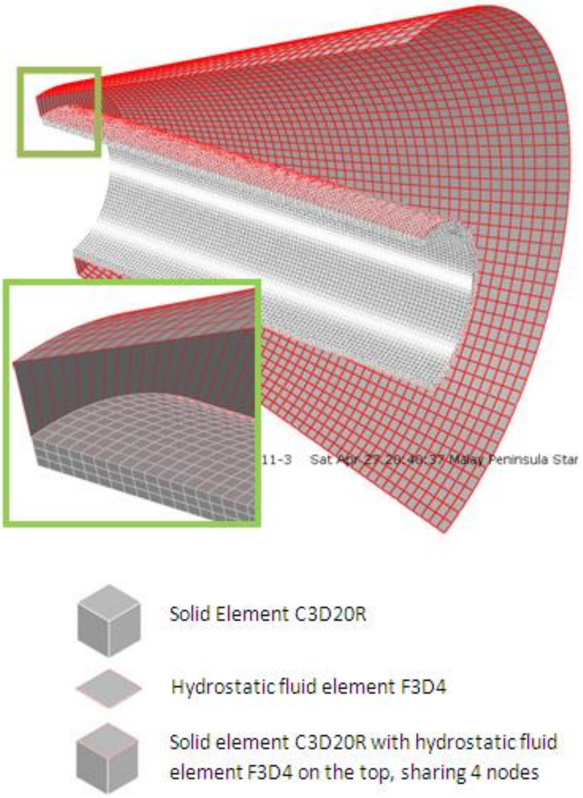
11-3 Sat Apr 27 20:40:37 Malay Peninsula Star
Solid Element C3D20R
Hydrostatic fluid element F3D4
Solid element C3D20R with hydrostatic fluid element F3D4 on the top, sharing 4 nodes

Figure 6-2 FE model of the pipe collapse under pure external pressure

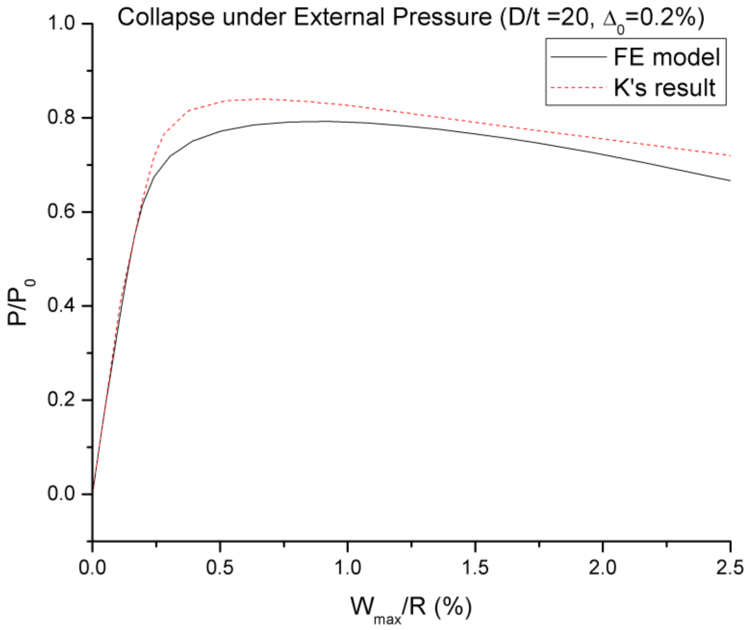

Figure 6-3 Result of FE model and Kyriakides' BETPICO result (material X52, ovality 0.2%)(Kyriakides and Corona, 2007a)

After validation of the FE model of the pipe collapse under external pressure using hydrostatic fluid element, the second step is to change the pipe into a dented pipe and collapse it. Park (1996) has studied the collapse of dented pipe by experiments and the FE method. One case in his paper is selected to be reproduced using the hydrostatic fluid element. The geometric and material parameters of this case are shown in Table 6-1, where *D* is the outer diameter of the pipe, *t* is the pipe thickness, *d* is the diameter of the spherical head indenter, δ_0 is the maximum dent depth after unloading, σ_0 is the stress corresponding to a 0.2% strain offset and considered as the yield stress . P_{CO} is the collapse pressure and P_o is the yield pressure of the pipe (Park and Kyriakides, 1996).

Table 6-1 Geometric and material parameters of dented tubes with *D/t= 24.2* together with their measured collapse pressures (Park and Kyriakides, 1996)

Normal $\frac{D}{t} = 24.2$								
D in (mm)	$\frac{D}{t}$	$\frac{d}{D}$	$\frac{\delta_0}{D}$	Δ_{od}	σ_0 *MPa (ksi)*	$\frac{P_{CO}}{P_O}$	σ_y *MPa (ksi)*[a]	*n*[a]
1.2484 (31.71)	23.62	0.4	0.0492	0.0261	372.9 (54.08)	0.539	344.7	12.6

[a]: Ramberg-Osgood fitting parameters of strain-stress response.

The FE results are compared with Park's data in Figure 6-4. The compared data are taken from Figure 13 in his paper (Park and Kyriakides, 1996), which contains both Park's experimental results and FE results. The indenters were different as he indicated as d/D 0.4 to 1.6, the FE models simulated more indenters with d/D from 0.16 to 1.6. The pipes were dented first, and then the ovality Δ_{od} was measured after unloading. After the indentation, all the dented pipes were collapsed in the pressure vessel and the collapse pressures were recorded as P_{co}. The same procedure is adopted in the FE analysis. The results of current FE model are shown in Table 6-2 and marked in Figure 6-4 as cross star marks. The comparison shows that the results of hydrostatic fluid element are close to Park's test results and FE results.

Table 6-2 Collapse pressure of dented pipe by hydrostatic fluid element

δ_0 *(mm)*	Δ_{od}	$\frac{P_{CO}}{P_O}$
1	0.0105	0.731
5	0.0925	0.438
7	0.1460	0.368
10	0.2365	0.306

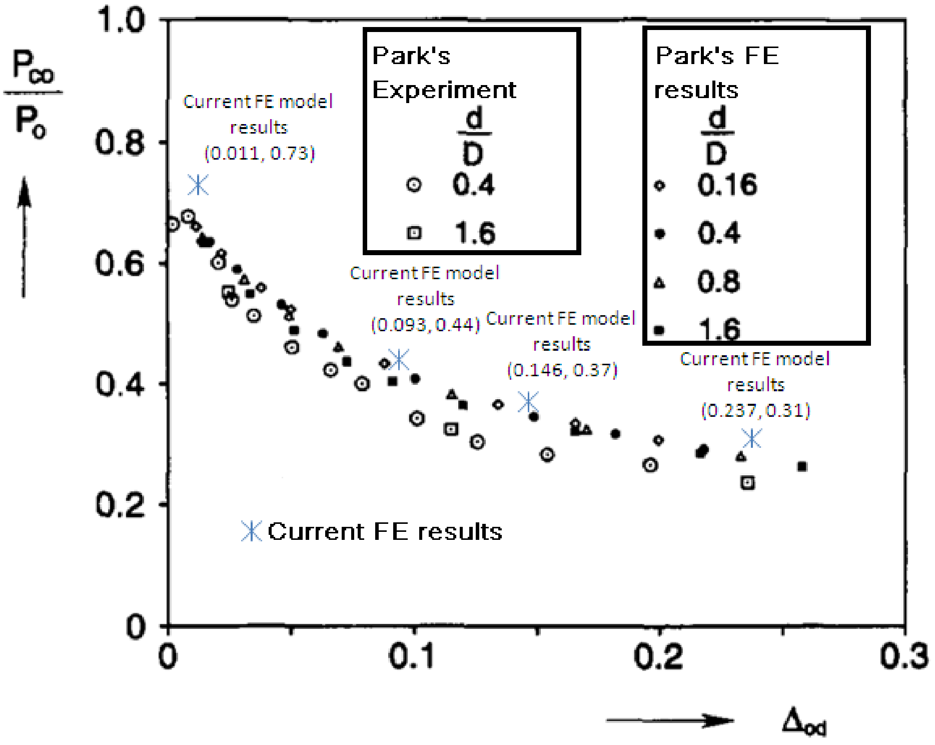

Figure 6-4 Comparison with Park's result (Figure 13. Comparison of measured and calculated collapse pressures of tubes as a function of dent ovality for various indentor diameters (D/t = 24.2)) (Park and Kyriakides, 1996)

6.1.2 FE model of Denting with Existence of External Pressure

Based on the validation of the indentation model and the collapse model under external pressure, a FE model of pipe under both the external pressure and the indentation process has been developed. In this model, the two forces, indentation and external pressure will act at the same time, which is the main difference compared to the FE model of the collapse of the dented pipe. The new model has three steps: pressurizing, holding the pressure and denting, holding the pressure and unloading. The first step is to add the pressure to a certain level, and then the second step is to keep the pressure constant and indent the pipe. The final step is unloading. ABAQUS/Standard is used to analyze this model. This model can calculate up to the collapse point.

Specimen SPS4 is selected to illustrate this model. Based on the dented model SPS4 and SPS4-BCrigid, different FE models are built as Figure 6-5 and Figure 6-6 shows. The geometry of the cavity is joined by two conical shells, and only a quarter model is built. The reason to choose this geometry is to eliminate the end effect. There are some intersections between the cavity and rigid bodies in the model, however as the rigid bodies have no contacts or interaction settings with the cavity; the intersections will not influence the model and the results. Basically the FE program will treat them as two totally independent objects.

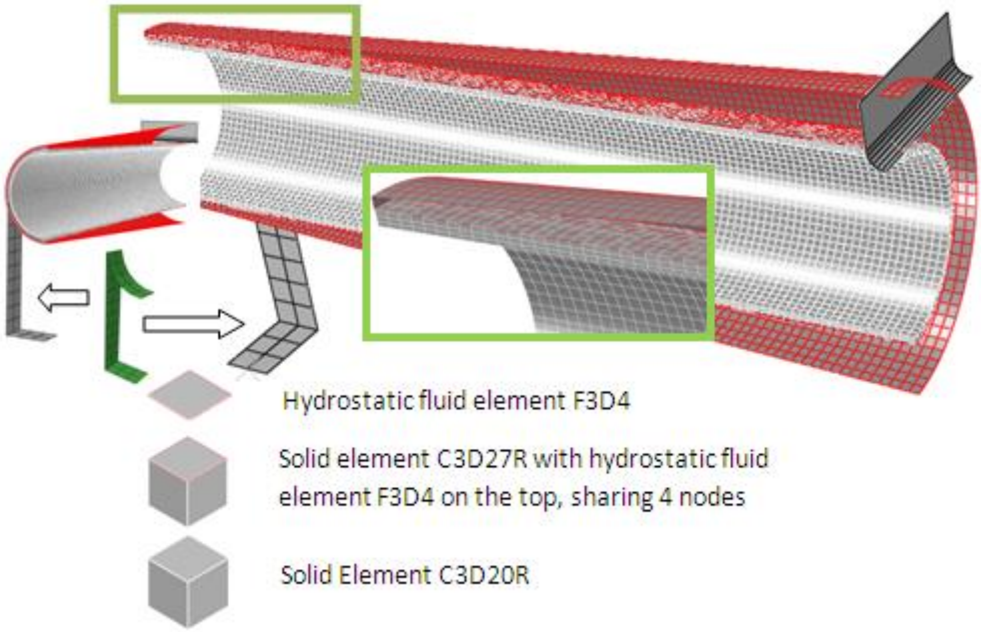
Hydrostatic fluid element F3D4
Solid element C3D27R with hydrostatic fluid element F3D4 on the top, sharing 4 nodes
Solid Element C3D20R

Figure 6-5 FE model of denting pipe with simply supported boundary condition and the existence of external pressure

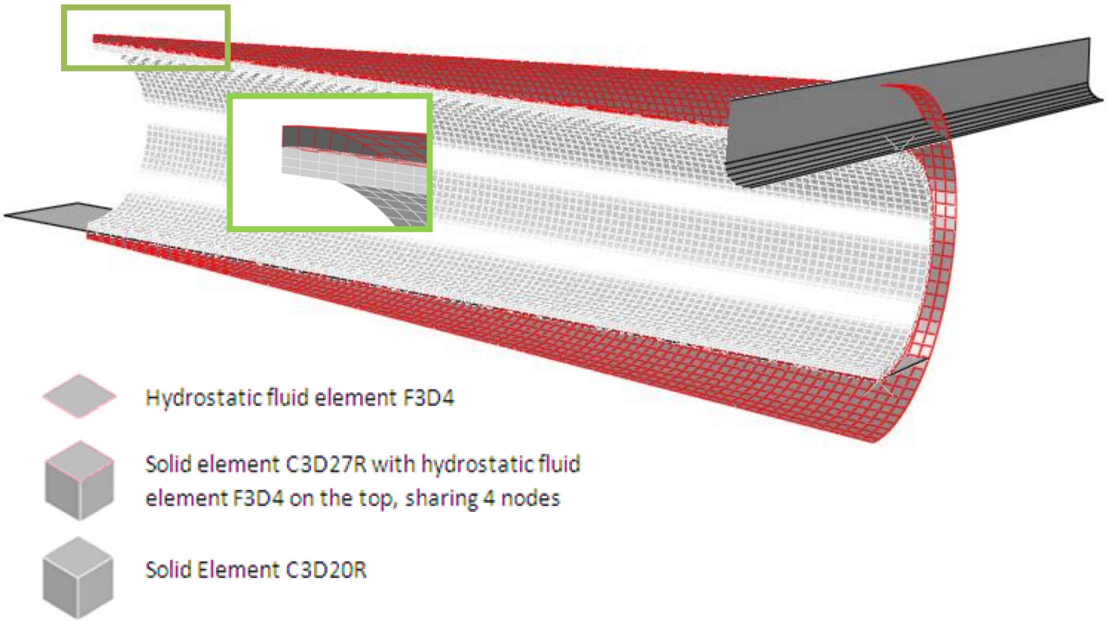
Hydrostatic fluid element F3D4
Solid element C3D27R with hydrostatic fluid element F3D4 on the top, sharing 4 nodes
Solid Element C3D20R

Figure 6-6 FE model of denting pipe with rigid boundary condition and the existence of external pressure

Under an external pressure (EP) of 4 MPa, the FE results are shown in Figure 6-7 and

Figure 6-9. The indentation force decreases about 10% for the simple support boundary condition case, while it decreases about 50% with the rigid boundary condition. Figure 6-8 and Figure 6-10 compares the geometry after unloading between the experiments and FE data for the two different boundary conditions. For SPS4, the local deformation and global deformation are clearly shown. The external pressure is trying to make the pipe’s bottom go inwards according to Figure 6-8. In SPS4-BCrigid, the pipe jumps up when there is no external pressure. When there is 4 MPa external pressure, the end stays on the floor and does not jump up, but the bottom of the middle cross-section tends to go inwards, which is the sign of collapse.

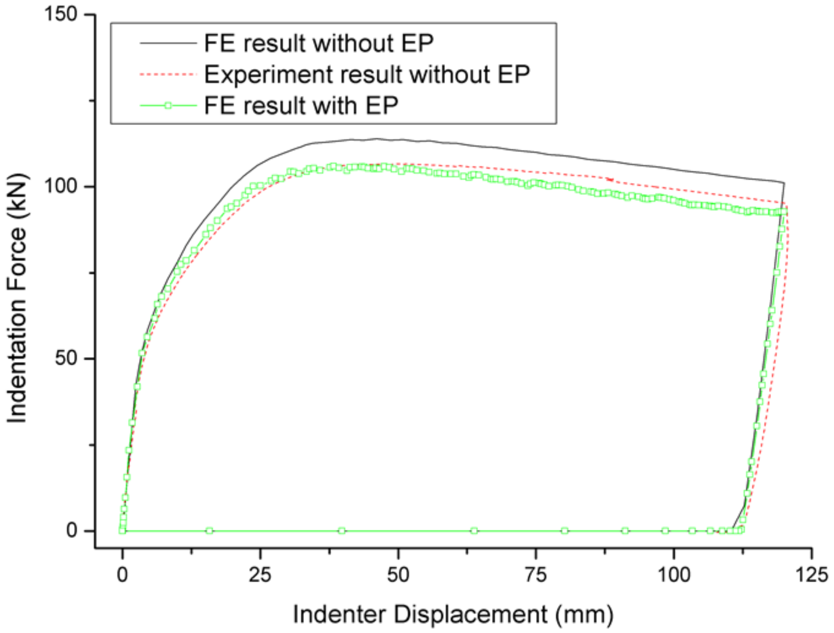

Figure 6-7 Comparison between FE results and experiment result of SPS4 (EP 4 MPa)

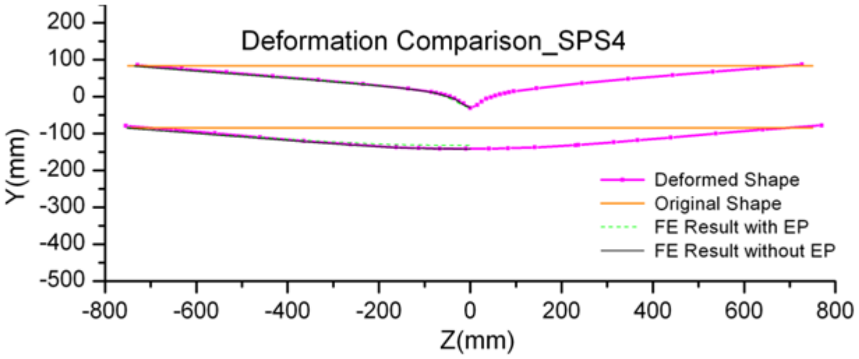

Figure 6-8 Deformation Comparison of SPS4 with or without external pressure (EP 4 MPa)

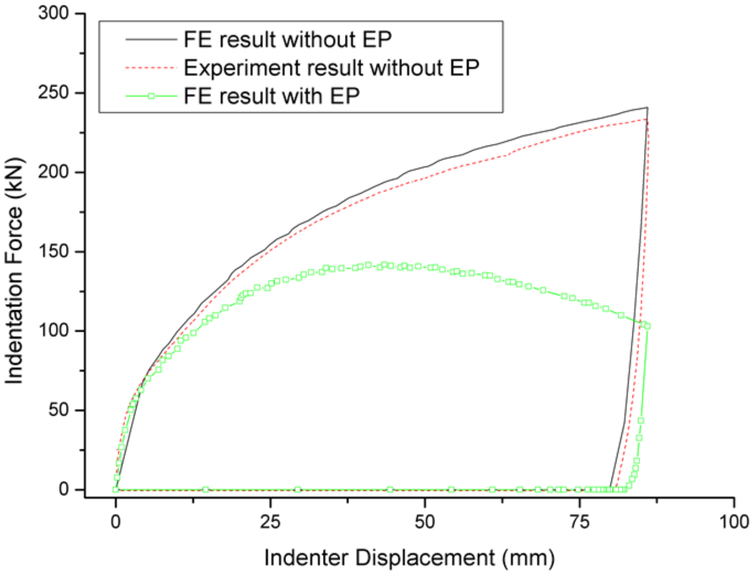

Figure 6-9 Comparison between FE results and experiment result of SPS4-BCrigid (EP 4 MPa)

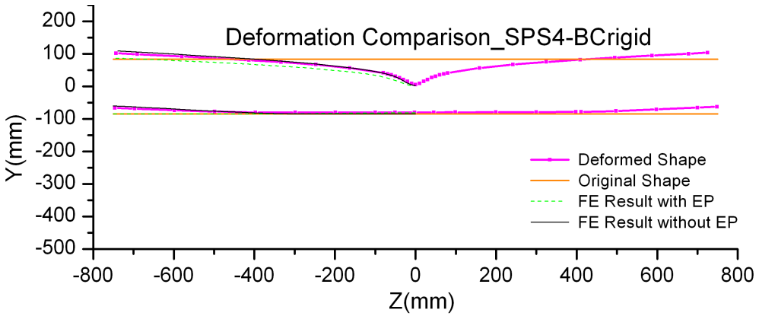

Figure 6-10 Deformation Comparison of SPS4-BCrigid with or without external pressure (EP 4 MPa)

6.2 Effect of External Pressure

A parametric study of different external pressure is carried out to investigate the external pressure effect. The comparisons are shown in Figure 6-11 and Figure 6-12. The collapse force is dropping with the increasing of the external pressure. Moreover, the difference between maximum indentation forces of different boundary conditions is decreasing as Figure 6-13 shows.

In Figure 6-12, the DNV formula 3.5 (DNV, 2010) is compared with the experimental data. The DNV formula is conservative when the pipe only has local deformation under indentation force. However, if there is external pressure or the pipe will have global deformation, it no longer conservative and more analyses are required.

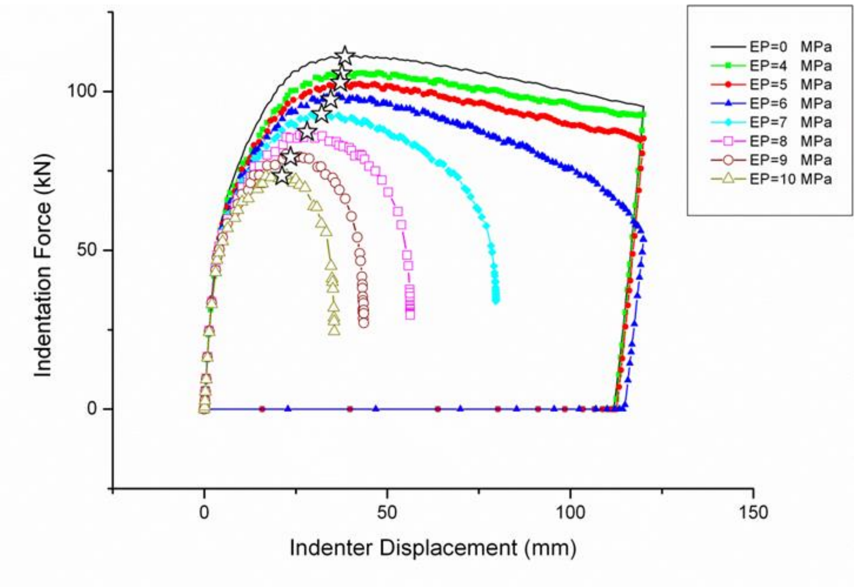

Figure 6-11 Parametric study of SPS4 under different external pressure

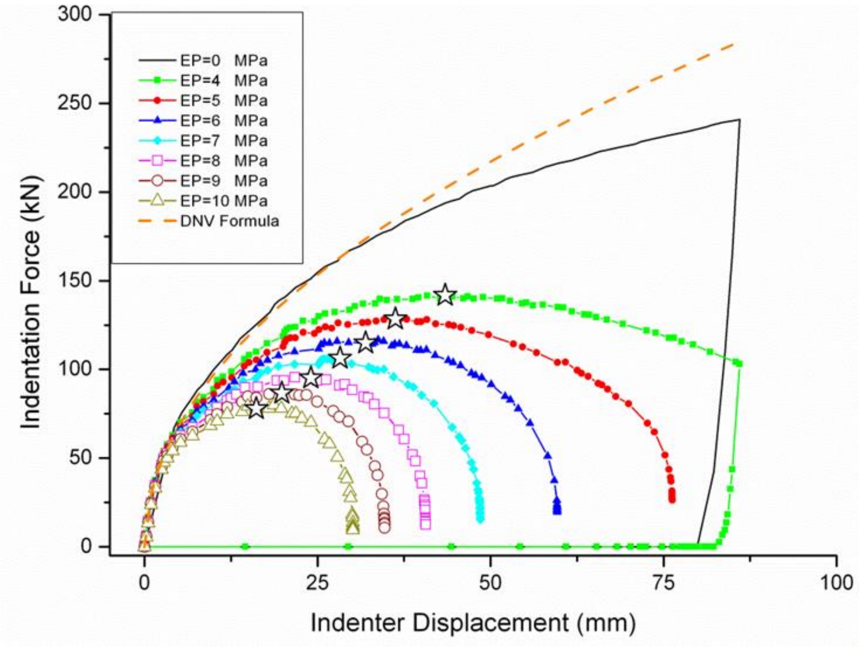

Figure 6-12 Parametric study of SPS4-BCrigid under different external pressure

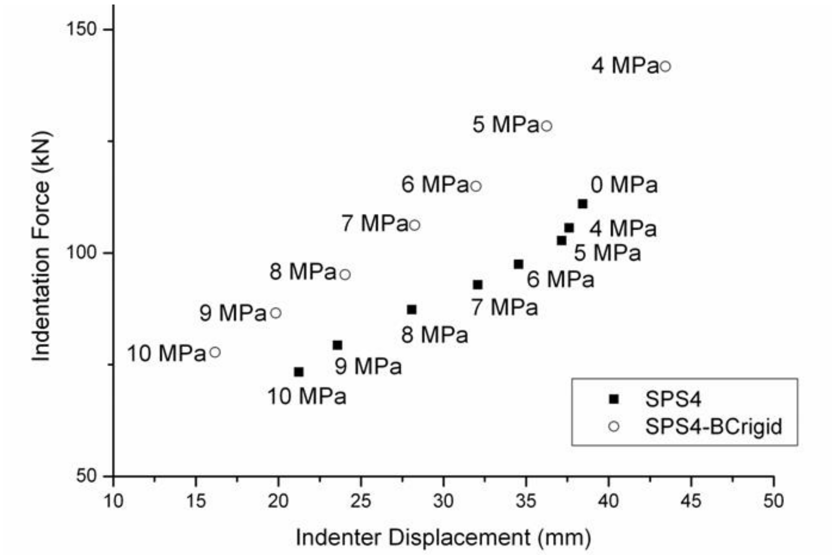

Figure 6-13 Collapse points under different boundary conditions and external pressure

When the pipeline is in use, it is almost always with internal pressure which balances the external pressure. In that situation, the external pressure effect and the global deformation effect may not be so severe depending on the difference between the internal pressure and the external pressure. However, for pipe-in-pipe systems, the carrier pipe may not have any internal pressure or have a lower internal pressure. The external pressure effect could not be balanced out and has to be considered.

6.2.1 Pipe-in-Pipe FE model of Denting with Existence of External Pressure

This section extends the previous work of single wall pipes to pipe-in-pipes and analyzes the pipe-in-pipe's response under external pressure and indentation force by FE models. The FE methodology is basically the same, but only the pipe's model is changed to a pipe-in-pipe model as Figure 6-14 shows. Contact settings and boundary settings are the same as the FE model PPSB2-nylon; the hydrostatic fluid elements do not have contact properties with the support and the indenter.

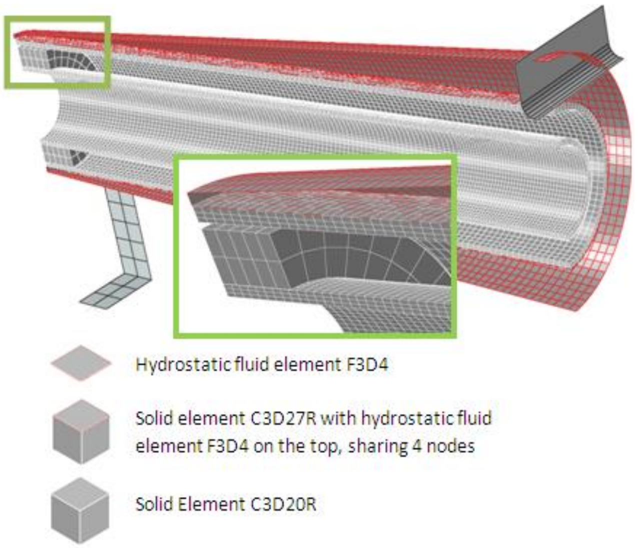
Hydrostatic fluid element F3D4
Solid element C3D27R with hydrostatic fluid element F3D4 on the top, sharing 4 nodes
Solid Element C3D20R

Figure 6-14 FE model of PPSB2-NYLON with hydrostatic fluid elements

Figure 6-15 shows the comparison between experimental and FE results with and without external pressure. According to the comparison, external pressure 4 MPa decreases the maximum indention force about 13%. It only influences the outer pipe before the outer pipe touches the inner pipe, and beyond that it affects both the outer pipe and the inner pipe.

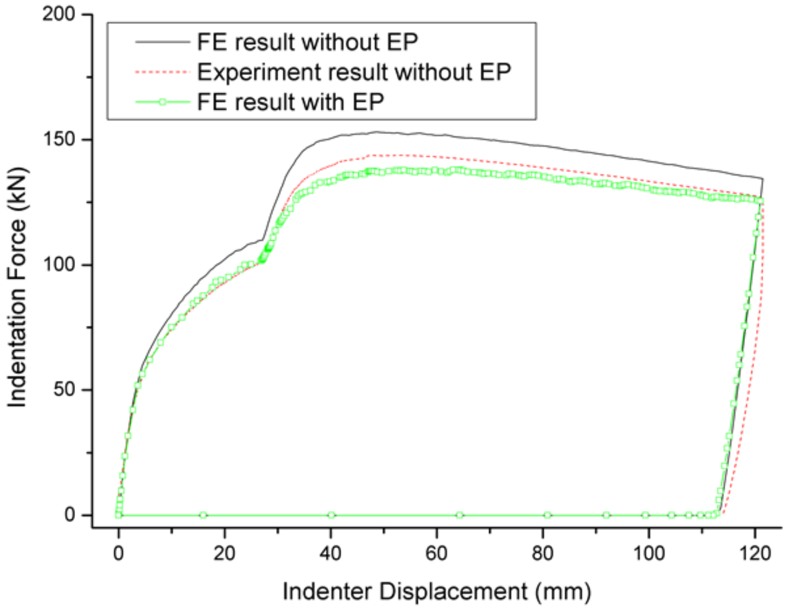

Figure 6-15 Comparison between FE results and experiment result of PPSB2-nylon

A parametric study of different external pressure level is carried out and shown in Figure 6-16. With water depth up to 1000 m, the buckling of the outer pipe will not propagate before the outer pipe touches the inner pipe. Then both the outer pipe and the inner pipe will buckle together and the buckling will propagate at some point later.

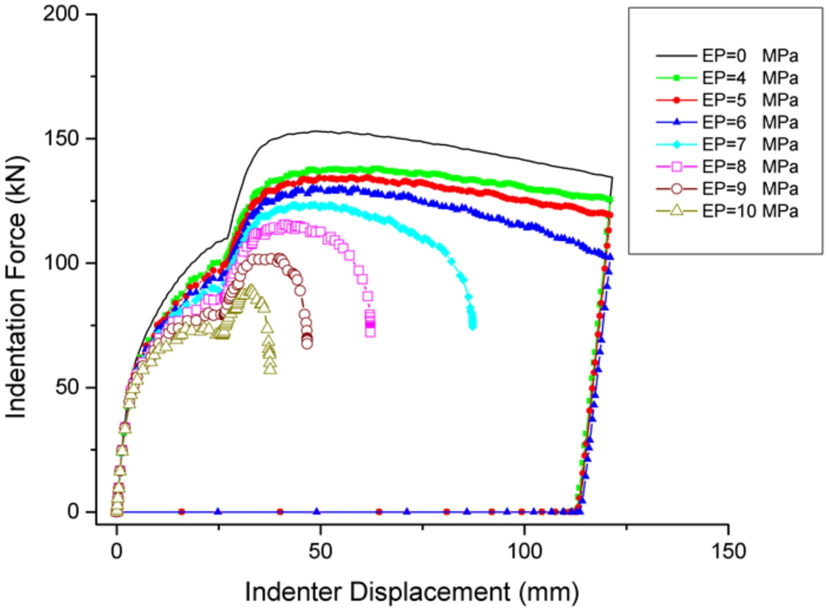

Figure 6-16 PPSB2-nylon under different external pressure

Figure 6-17 show the comparison between single wall pipe SPS4 and pipe-in-pipe PPSB2-nylon indented under different external pressure level. Under external pressure (EP) 4 MPa, the indentation force decreases about 10% for SPS4 and 13% for PPSB2-nylon. It only affects the outer pipe until the outer pipe touches the inner pipe, and beyond that it affects both the outer pipe and the inner pipe. From this point of view, if the annulus is larger, the outer pipe can absorb more energy before the inner pipe being damaged. This brings less damage to the inner pipe, and therefore protects the inner pipe. However, if the annulus is too big, the buckling of the outer pipe will propagate before the outer pipe touches the inner pipe. In that case, the internal pressure of the inner pipe which could help to enhance the capacity and avoid the propagation will be wasted. For example, with water depth up to 1000 m, the buckling of the outer pipe will not propagate before the outer pipe touches the inner pipe, and then both the outer pipe and the inner pipe will deform together and this requires a higher force. A buckle will propagate at some later point. An optimized design of the annulus space can be able to balance these two aspects, not too large to make the outer pipe be alone and not too small to make the inner pipe being indented too early.

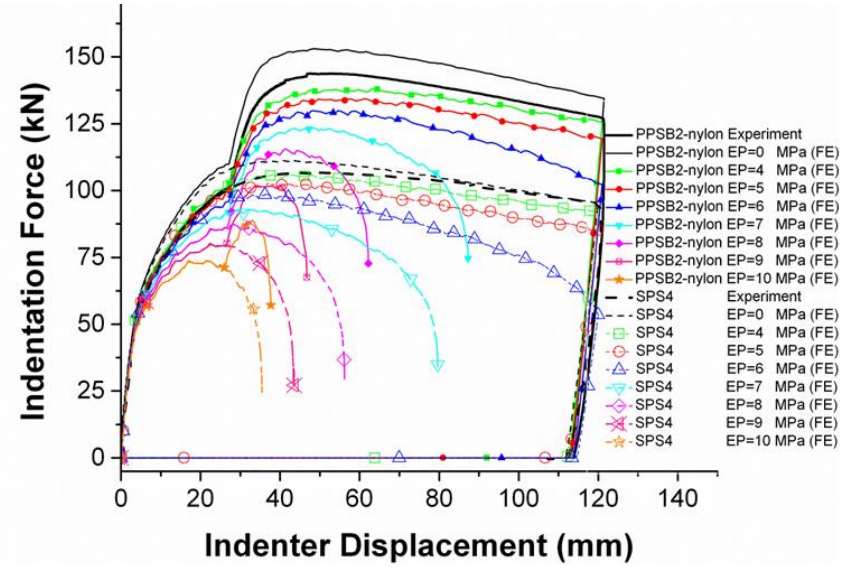

Figure 6-17 Comparison between PPSB2-nylon and SPS4 under different external pressure

6.3 Combination of Internal Pressure, External Pressure and Indentation

The previous sections developed the method to analyse the indentation response when the pipe is under water. The external pressure does influence the indentation response indeed. At the same time, the internal pressure is also important as it counterbalances the external pressure. Therefore, in this section, the internal pressure will be considered in the FE model together with the external pressure and indentation.

When the subsea pipeline is in operation, the pipeline will not only be under external pressure, but also under internal pressure. If the external pressure exceeds the internal pressure, it can be treated as if the external pressure equals the difference of the external pressure and the internal pressure, and the internal pressure is set to zero. If the internal pressure is higher, there is no need to consider the external pressure effect. However, the internal pressure might drop at some point for some reasons. For example, after the pipeline is hit by the trawl gear, possibly an inspection has to be carried out and possibly the pipeline has to be shut down for this purpose or has to be shut down after the inspection. It might also happen that the pipeline collapses and a buckle propagates when the internal pressure drops. To avoid that, analysis is needed to consider whether the internal pressure can be decreased and at what level it can be. This section develops the FE model specifically for this purpose.

For the single wall pipes, the developed model is able to simulate external pressure and internal pressure by only simulating the difference between them. For example, if the water depth is 2000 km and the operation internal pressure is 16 MPa, the difference of the internal pressure and the external pressure is 4 MPa. This can be simulated by a model of an empty pipe with 4 MPa external pressures. The pipe will be indented under this condition. Referring to Figure 6-17, the buckle will not propagate even when it is indented to 120 mm. However, if the internal pressure is reduced, which is equivalent as increasing the external pressure in the FE model, the collapse will propagate. The process is shown in Figure 6-18. The first step is to increase the external pressure to 4 MPa. Steps 2 and3 are the indentation of the pipe and unloading of the indenter, while the external pressure is kept the same. The indentation force and indenter displacement curve is the same as in Figure 6-17. Step 4 increases the external pressure to represent the decrease in the internal pressure. According to the pressure at different steps, the pipe collapses at 9 MPa. The final shape is shown in Figure 6-18, and clearly collapse can be seen. This FE model offers a tool for the engineers. They can calculate the response before they reduce the internal pressure which may lead to collapse or buckle propagation. According to the analysis result, they can find out how far the internal pressure can be reduced to. It might be that they should not reduce the internal pressure at all without other protection methods.

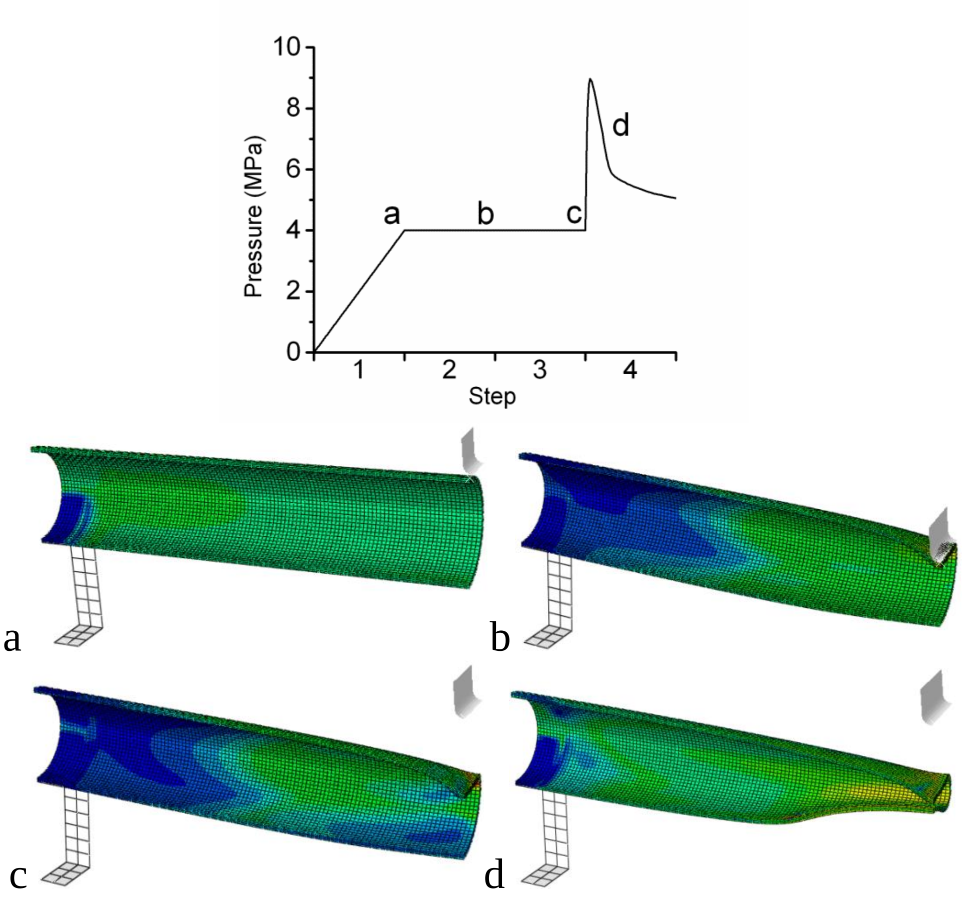

Figure 6-18 Process of reducing internal pressure simulation Final shape: collapsed pipe

The FE model of pipe-in-pipe to simulate internal and external pressure is not as simple as the single wall pipe. The internal pressure of the pipe-in-pipe is within the inner pipe, and the external pressure is outside the outer pipe. They could not counterbalance each other directly as the single wall pipe case does. Therefore, a new model with two independent cavities is built to simulate the internal pressure and external pressure respectively. The FE model is shown in Figure 6-19. The difference is that another layer of hydrostatic fluid element added to the inner surface of the inner pipe. The normal direction points to the pipe axis and which can simulate the inner pressure in the inner pipe.

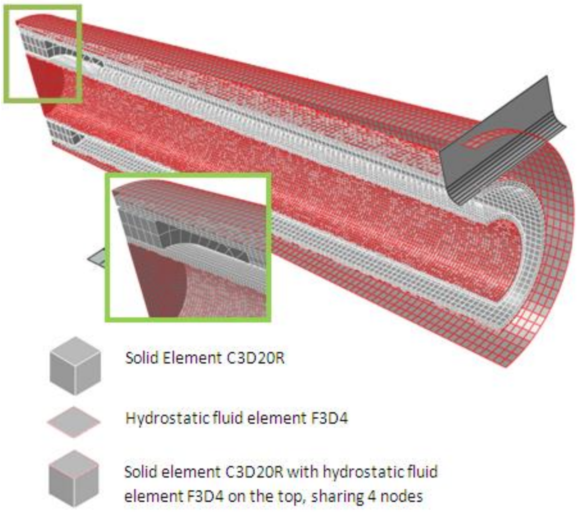
Solid Element C3D20R
Hydrostatic fluid element F3D4
Solid element C3D20R with hydrostatic fluid element F3D4 on the top, sharing 4 nodes

Figure 6-19 FE model of PPSB2-NYLON with hydrostatic fluid elements

The simulation procedure includes four steps. The first step is to add the internal pressure and the external pressure up to a certain level. The second step is to indent the pipe to a certain distance. The third step is unloading the indentation force. The final step is to decrease the internal pressure. The pressure at different steps of the internal pressure cavity and the external pressure cavity are shown in Figure 6-20. The indentation force versus indenter displacement curve is given in Figure 6-21. It also shows the comparison between the response with external pressure 10 MPa and with no internal pressure. The first part relates to the outer pipe is almost the same, and the inner pipe with internal pressure is better able to resist the indentation according to the second part of the curve. The internal pressure increases the pipe’s resistance to indentation.

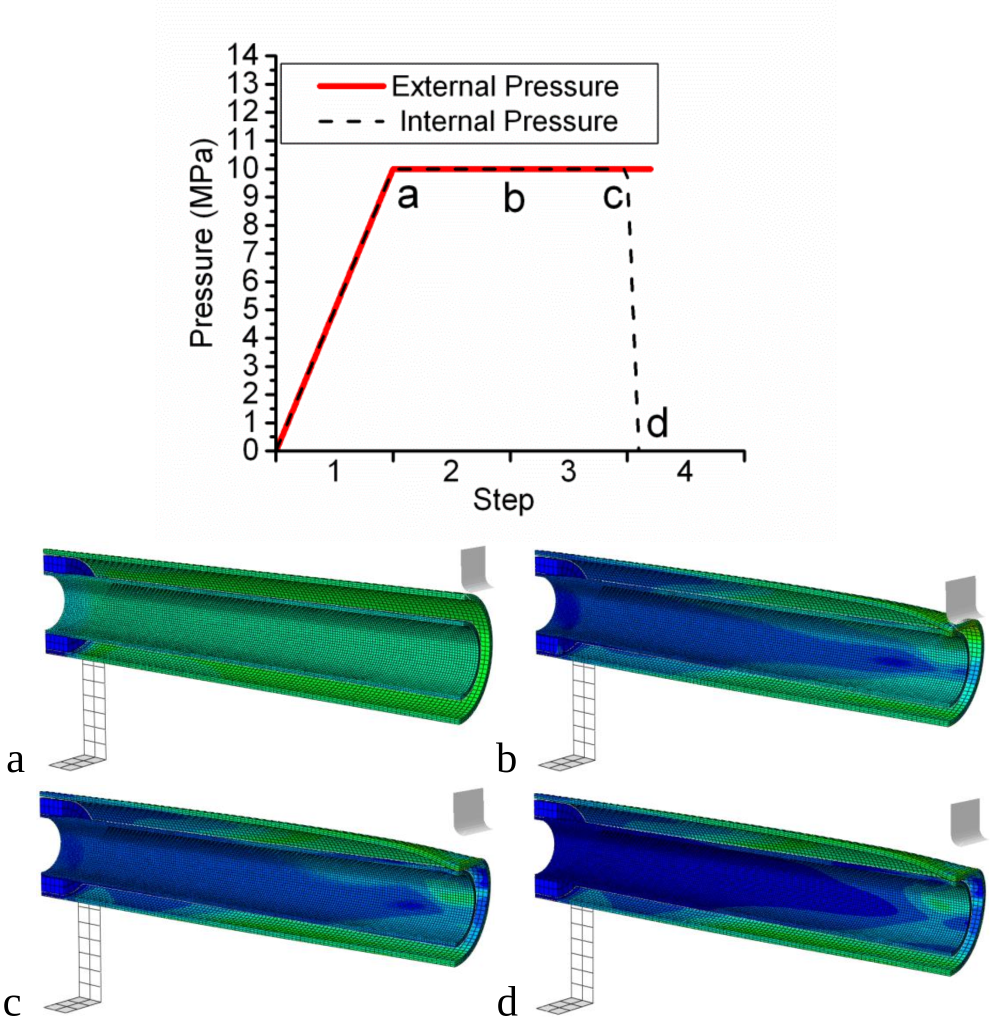

Figure 6-20 External pressure and the internal pressure at different steps as well as the deformation of the pipe

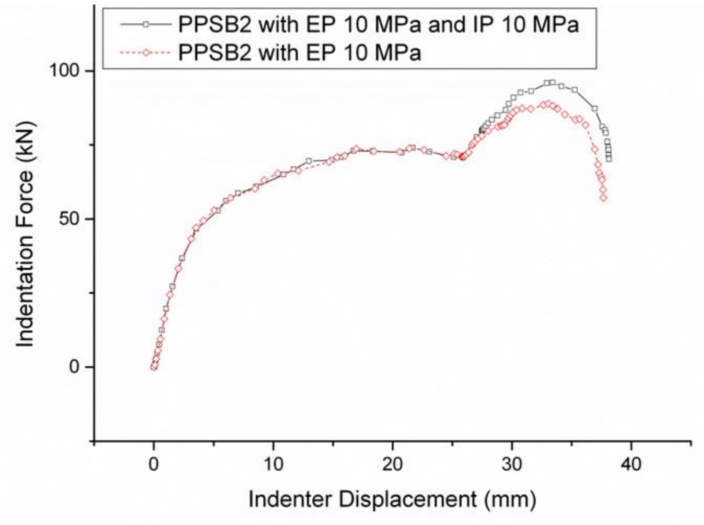

Figure 6-21 Comparison between PPSB2-nylon with or without internal pressure (IP)

If the indenter displacement is smaller than the collapse and propagation point, the pipe will maintain the deformed shape after the unloading of the indentation force. For this case, when the indenter displacement is 38 mm, the indenter can be unloaded and the collapse will not propagate after decreasing the internal pressure. For single wall pipe, as shown earlier, with decreasing the internal pressure, the collapse will propagate. This is because the inner pipe is not exposed to the external pressure except at the point where the inner pipe is touched by the deformed outer pipe. This is one advantage of the pipe-in-pipe, that the inner pipe is not as sensitive to external pressure as a single wall pipe.

6.4 Conclusion

This chapter presents the external pressure effect on the denting process of the pipeline by using FE method. The validation of this FE model contains two parts: first to validate the indentation FE model by comparing with indentation experiments and then to validate the external pressure model by repeating a FE model of collapse of a dented pipe. The comparisons with the experiments and with Park's result (Park and Kyriakides, 1996) show acceptable agreement. This model is a valid representation of the real situation in the field, and will improve the accuracy of design or repair analysis.

Based on the validated FE model, the indentation with and without external pressure is compared with two different boundary conditions. Moreover, parametric study of different external pressure is conducted. The study reveals that the external pressure has an effect on the denting process of pipelines, regardless of the boundary condition. Secondly, external pressure reduces the maximum indentation force at different levels according to the boundary condition. With increasing external pressure, the maximum indentation force is decreasing and the maximum indentation forces with different boundary conditions tend to be the same with the increasing of the external pressure. The comparison with DNV formula shows that if the external pressure is higher than the internal pressure, external pressure effect on denting needs to be considered. This method also applies to the pipe-in-pipe models. The external pressure will not influence the inner pipe until the outer pipe touches the inner pipe during the indentation process. This model is a valid representation of the real situation in the field, and will improve the accuracy of design or repair analysis.

The modelling methodology can be used to simulate the interaction of internal pressure and external pressure. The internal pressure will counterbalance the external pressure and increase the capacity to resist the indentation. However, if the pipe already has the dent or imperfection, to reduce the internal pressure might be dangerous as the pipe might collapse and the buckle might propagate. The new model can be used to analyse these cases with combined internal pressure, external pressure and indentation. Two case studies show that collapse induced by reducing the internal pressure has a high possibility to happen for single wall pipe, but because of the annular space between the inner pipe and outer pipe, the inner pipe is not so sensitive to the external pressure and therefore a buckle is less likely to propagate because of reducing internal pressure.

7 Pull-over Test Program

After the impact, the trawl gear requires some force to cross the pipeline, and this is the second phase, the pull-over phase. This phase lasts longer than the impact phase, about 1 to 10 seconds. This pull-over force is mostly responsible for global response of the pipe. Additionally, not only is the pipeline's integrity a concern, but also the fishermen's safety. The pull-over force not only acts on the pipeline, but also pulls the ship. If unfortunately, trawl gear is hooked, the pull-over force will greatly increase and possibly break the warp line and consequently put the fishing vessel and the fishermen in danger. Therefore, an analysis must be conducted to ensure the new pipeline on the seabed will not be an increased hazard compared to existing pipelines, as well as to ensure that the trawl gear will not damage the pipeline.

The interaction between the pipeline and the trawl gear is a very complicated process. There is no standard method to estimate the pull-over force, the pipeline's response and the possibility of hooking. Normally, a model test trial will be conducted to increase the confidence level as the other methods are not mature enough. A model test is less costly than a field test, which is time consuming, difficult to control and hard to measure. On the other hand, a model test has limitations, such as the size and scaling issues.

7.1 Motivation and Purpose

Many pull-over model tests have been done as described in Chapter 2. Based on the accessible information, the model tests were mainly for pipes with diameter more than 16 inch. Moreover, most of the test data are not published. It is difficult to use FE methods to analyse it because it is difficult to access existing experiment data and therefore difficult to validate the FE model against experiment data. It is also difficult to start with the theoretical work as the mechanical behaviour is not clear. In addition, the scaling law used in the previous model tests is Froude scaling law which might not be the proper way to scale the pipeline and trawl gear interaction.

Therefore, a pull-over model test program is designed for the following purposes:

1. To investigate the pipe-in-pipe's pull-over response, and to look into the overtrawlability of pipe-in-pipe by comparing it with the response of single wall pipes.
2. To understand the mechanical behaviour of the pull-over response, and to find out the important parameters of the system.
3. To investigate whether the Froude scaling Law is suitable for this model test.
4. To look into the effect of velocity in the pull-over process.

Based on these objectives, the experiment is designed.

7.2 Experiment Design

When the trawl gear crosses a pipeline, the interaction involves four dynamic systems, i.e. the fishing vessel, warp-line, trawl gear and the pipeline. The free body diagram is shown in Figure 7-1. Consequently, in the model test, the four dynamic systems should all be properly scaled and modelled. The experiment was conducted in the wave basin in the Hydraulic Engineering Laboratory, Department of Civil & Environmental Engineering, National University of Singapore. The dimension of the wave basin is 8*22*0.7 m. The scale factor is chosen within the limitations imposed by those dimensions.

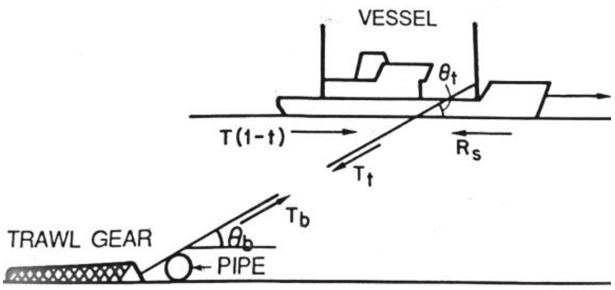

Figure 7-1 Free body diagram of the system (G. Horenberg and Guijt, 1987)

7.2.1 Model Pipeline Design

The objective and scope of the pull-over test program is to investigate the response of a pipe-in-pipe whose outer diameter is less than 16 inch, and compare it to a 16 inch (406.4 mm) single wall pipe, because 16 inch (406.4 mm) pipes will not normally be damaged by the trawl gear crossing. The prototype is shown in Table 7-1. The outer diameter of the pipe-in-pipe is either 12 inch (323.85 mm) or 14 inch, and the inner pipe is 8 inch (219.08 mm) in diameter. The indentation and impact test specimens have a scale factor of 1 over 2.2. Pull-over brings more global response to the pipeline compares to the indentation response; therefore, a smaller scale factor should be chosen in order to represent a longer pipe section in this 8 m wide wave basin. A set of pipes has been found in the Singapore market which is suitable for use in this experiment. Their details are located in Table 7-1. Comparing to the prototype, the pull-over specimens are about 1/8.3 times smaller; and comparing to the indentation specimens, the pull-over specimens are 1/4 times smaller. As the length of the specimen is 7 m, the specimen is simulating a 58.1 m long prototype pipe, with L/D about 170.

Table 7-1 Details of specimens

Pull-over Specimen (PS)				**Prototype (P)**					**Indentation Specimen (IS)**				
	OD	***t***	***OD/t***		***OD***	***t***	***D/t***	***D_P/D_{PS}***		***D***	***t***	***D/t***	***D_{IS}/D_{PS}***
SPS A	26.9	1.6	16.81	***Inner***	219.1	14.3	15.3	8.14	***SPS 1***	88.9	5.49	16.19	3.30
									SPS 3	101.6	5.74	17.70	3.78
SPS B	42.5	1.9	22.36	***Carrier II***	355.6	14.3	24.9	8.37	***SPS 4***	168.3	7.11	23.67	3.96
SPS C	42.5	2.6	16.34										
SPS D	48.4	2.9	16.68	***16 inch***	406.4	26.6	15.3	8.40					
				Carrier I	323.9	12.7	25.5		***SPS 2***	141.3	6.55	21.57	

Based on the pipe size in Table 7-1, four single wall pipe specimens and four pipe-in-pipe specimens are set up as Table 7-2 shows. Table D-1 and Figure 7-2 show the details of the specimens.

Table 7-2 Details of pull-over specimen

Test Specimen	**Specimen**	**Spacing (m)**	
SPSA	Pipe A		Single wall pipe
SPSB	Pipe B		Single wall pipe
SPSC	Pipe C		Single wall pipe
SPSD	Pipe D		Single wall pipe
PIPAB	Pipe A,B	0.5	Pipe-in-pipe
PIPAC	Pipe A,C	0.5	Pipe-in-pipe

Test Specimen	Specimen	Spacing (m)	
PIPAD	Pipe A,D	0.5	Pipe-in-pipe
PIPAB-S	Pipe A,B	0.25	Pipe-in-pipe

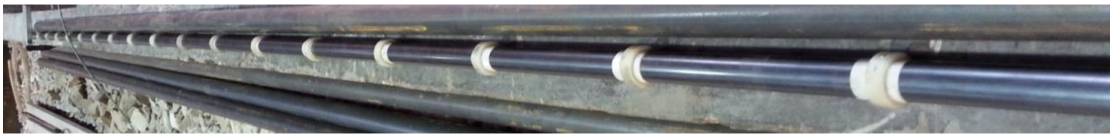

Figure 7-2 Spacers installed on the inner pipe

The pipe is placed on the top of a fine sand layer. There is a 70 mm fine sand layer on the bottom, and the particle size distribution of the sand is shown in Figure 7-3. There are three kinds of boundary conditions. One boundary condition is a simply supported pipe (S), and another one is fixed ends (F). Additionally, to investigate the effect of different length, a shorter pipe section of 3 m in the middle is clamped to the foundations. This boundary condition is named as SF, which stands for a short fixed end boundary condition.

Because it is not permitted to drill holes to fix anything on the wave basin floor, two heavy foundations are placed in the wave basin to offer the supports for the pipe. The two foundations sit on the bottom and are covered with sand. Two connectors are welded on the foundations, one for each. There are hooks on the connector, and also on the pipe ends. For the simply supported pipe, the two hooks are connected together by shackles. The connection is shown in Figure 7-4. The boundary condition of fixed ends is illustrated in Figure 7-5. Pipe ends connect to steel plates, and the steel plates connect to connecters by four screws. At the left side, a load cell is installed between the pipe and the plate to measure the tension. Beside these two major boundary conditions, a shorter pipe section is clamped to the wave basin floor as Figure 7-6 shows.

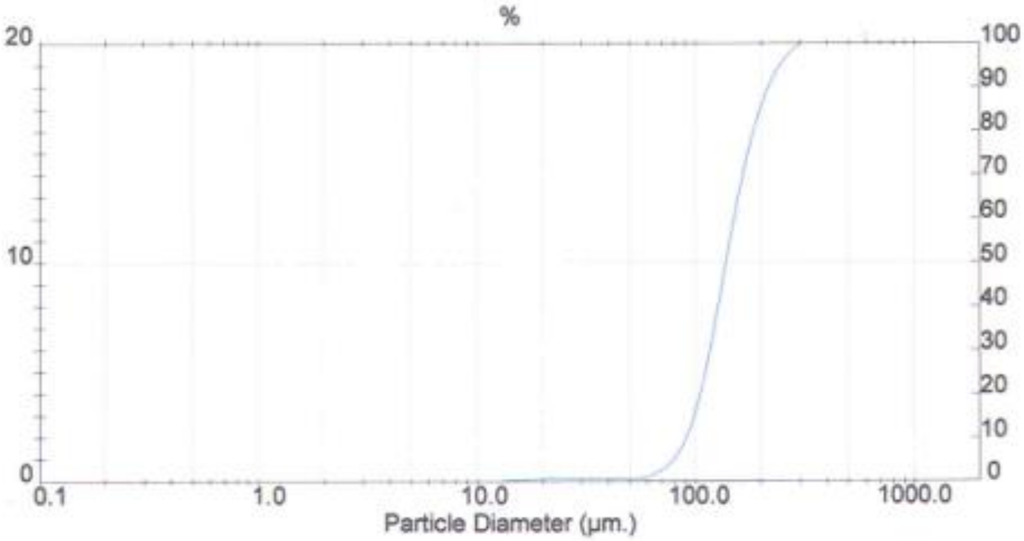

Figure 7-3 Sand property

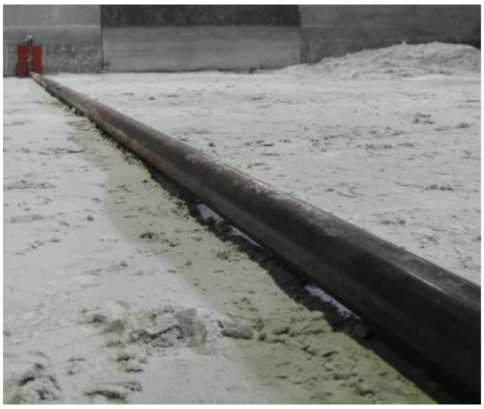

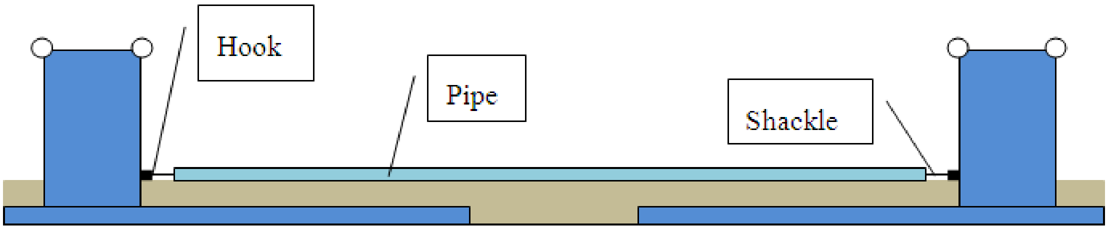
Hook
Pipe
Shackle

Figure 7-4 Boundary Condition of the Pipe

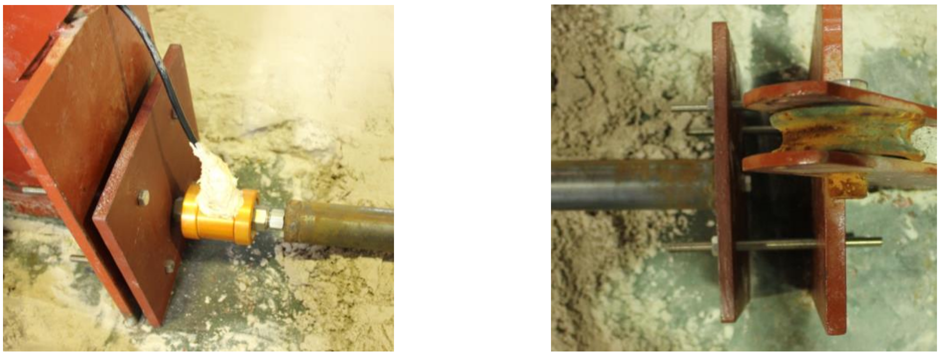

(a) (b)

Figure 7-5 Fixed ends boundary condition (a) Left End (b) Right End

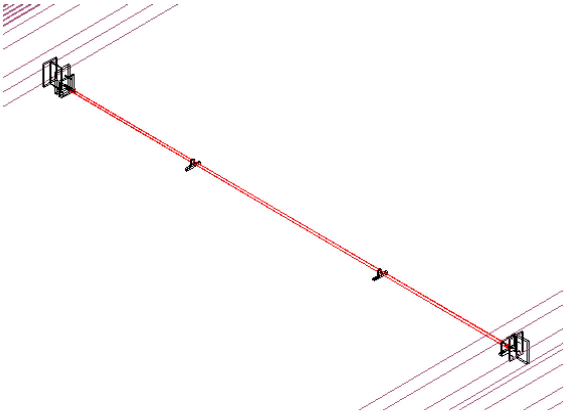

Figure 7-6 Fixed ends boundary condition with a shorter pipe section

7.2.2 Trawl Gear Design

The trawl gear is designed based on the prototype size and the scale factor 1/8.3 as decided in the previous section. According to the records in DNV-RP-F111, the largest beam trawl gears in use in the North Sea and the Norwegian Sea in 2005 have the mass up to 5500 kg and beam trawl length up to 17 m. The “Guidelines for Trenching Design of Submarine Pipelines” gives the largest dimension of trawl gear shoes. However, there is no information of the detail designs. A small scale trawl gear was borrowed from the UK SEAFISH authority. The SEAFISH trawl gear is measured and the details are given in Figure E-1. The strategy is first to confirm some key geometry parameters of the prototype based on the information of the largest beam trawl according to the DNV-PR-F111 and “Guidelines for Trenching Design of Submarine Pipelines”, and then scale down these key parameters with the scale factor 1:8.3. The key parameters are shown in Figure 7-7. After that, refer to the SEAFISH trawl gear design, and design the small scale beam trawl for the current test. The trawl shoe is designed as Figure E-2 shows. The beam is 1.8

m long, and the height of the trawl shoe is 95.98 mm. The height of the warp-line connecting point is 52.37 mm.

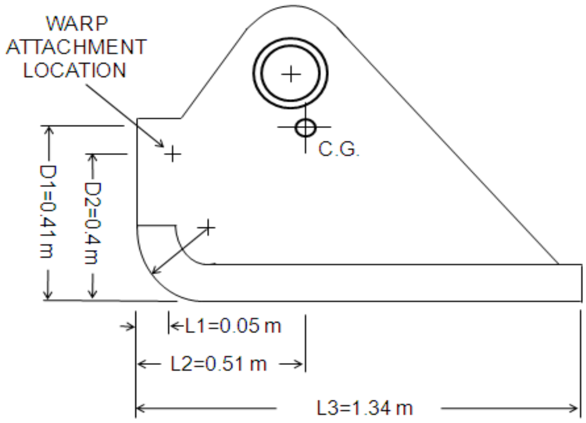

Figure 7-7 Largest dimensions of trawl gear shoes

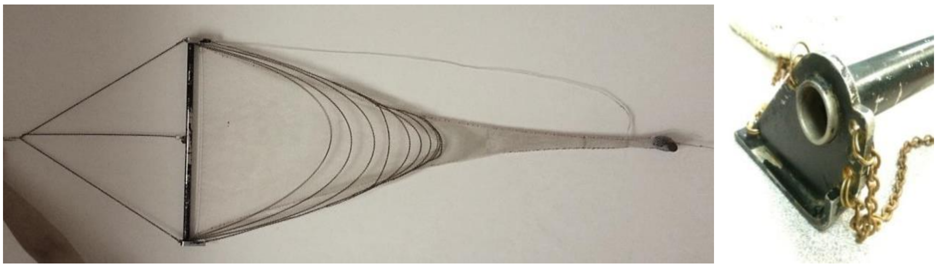

Figure 7-8 Trawl gear borrowed from SEAFISH Authority

If it obeys the Froude's law of scaling, the dimension of the trawl gear should be linearly scaled by β, and weight will be scaled by β^3. For that case, the geometry of the beam is shown in Figure E-3, and named as F beam. Together with the shoes, the total weight of F beam trawl is 9.36 kg as shown in Figure 7-9. Considering the weight of the entrance water in the beam, the total weight is 11.65 kg.

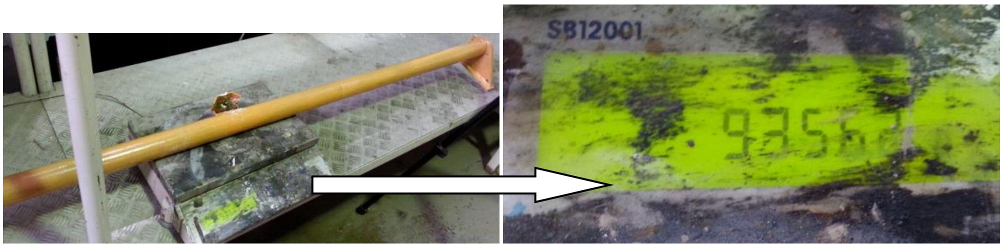

Figure 7-9 Weight of F beam trawl

If the hollow beam section is changed to a solid beam section, the weight of the beam trawl is 27.34 kg as Figure 7-10 shows. This one is named as Solid (S) beam trawl.

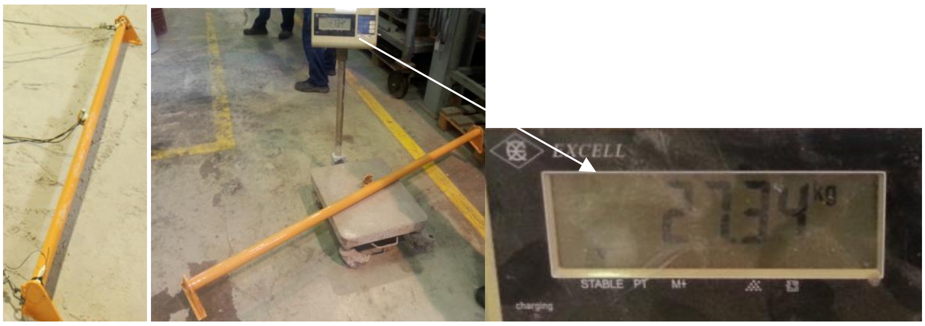

Figure 7-10 Solid beam trawl (S)

7.2.3 Warp-line Design

The trawl gear is connecting to the fishing vessel by a warp-line. Generally the warp-line is a standard 6*19 configuration steel wire rope with diameter between 28 and 34 mm. (G. Horenberg and Guijt, 1987) The warp-line length is approximately 2 to 4 times the water depth(DNV, 2010), and the warp-line will then have an angle of 18 to 20 degrees to the seabed(G. Horenberg and Guijt, 1987). If the water depth is 100 m, based on the scale factor 1/8.3, the scaled water depth should be 12 m and this is impossible to achieve with the current lab facility. Alternatively, only the bottom section of the warp-line is simulated, which means only the angle to the seabed and the warp-line stiffness is scaled and simulated. DNV gives a method to calculate the stiffness of the warp-line with diameter 32 to 38 mm as equation (7.1) shows. Scaling down the warp-line in diameter and length, consequently the stiffness is scaled down by 68.68 times. The scaled stiffness is achieved by a spring. There are two springs prepared as given in Table 7-3. They represent water depths of 30 m and 100 m respectively. The spring is installed in the warp-line as Figure 7-11 shows. Load cells are connected in between the spring and the warp-line to measure the pull-over force.

$$K = \frac{3.5 \cdot 10^7}{L_w} \tag{7.1}$$

Table 7-3 Details of the springs

No.	Stiffness (kN/m)	Represented Water Depth
Spring 1	55.05	30
Spring 2	14.47	100

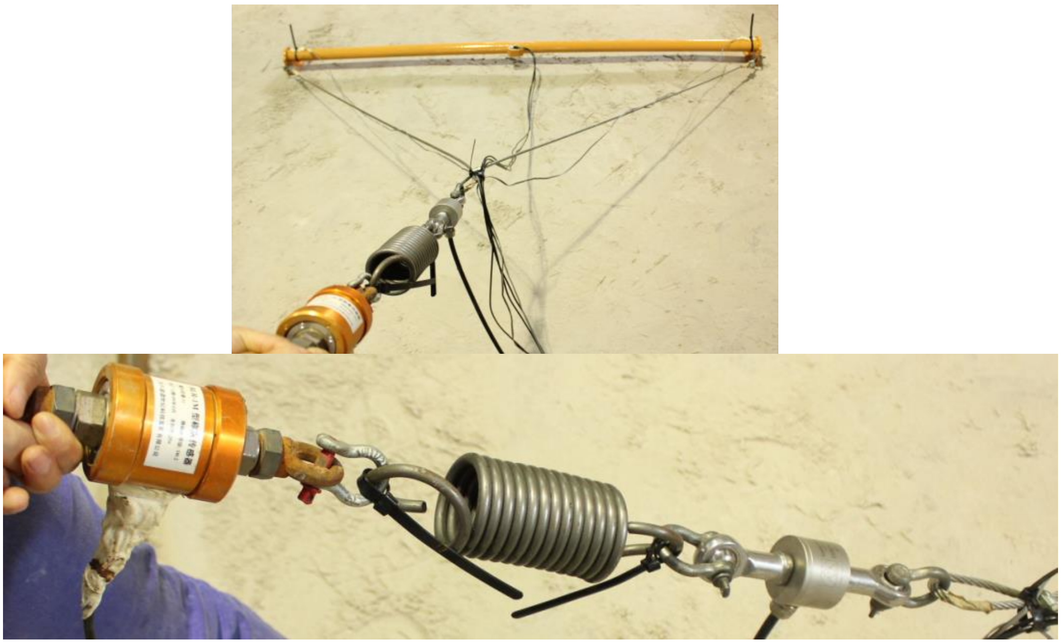

Figure 7-11 Load Cells in between the warp line

A rubber boat is used to keep the warp-line angle constant as shown in Figure 7-12. The warp-line is connected between the stern of the rubber boat and the trawl. The total length of the warp-line is 2.4 m which is about 3 times the water depth. The height can be adjusted by changing the water level. In these tests, the water level is about 400 mm, and from the water level to the warp-line end is about another 400 mm.

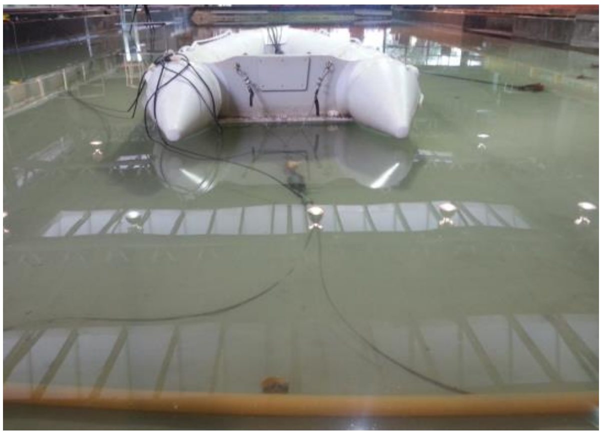

Figure 7-12 Scaled Warp-line

7.2.4 Driving Force System Design

A driving force system has to be designed to pull the rubber boat to move at a constant velocity. Various possibilities were considered, and finally a winch system was chosen as it is more feasible. A winch with velocity range of 1 m/s to 3 m/s is preferred; however, such a high velocity winch is not sold in the market and has to be customized. Separate parts are purchased or manufactured, including the motor, pulleys, the gear box and the drum. The motor is running at 1500 revolutions/min, which is the input for the pulley system. With different diameters of pulleys, the output rotation speed changes accordingly and is input to the gearbox. The gearbox reduces the rotation speed further by 20 times, and this is the rotation speed of the drum. The drum’s diameter is 955 mm, and then the circumference is calculated as 3 m. The winch is assembled as Figure 7-13 shows. At the side of the pulley, a speed sensor is installed to measure the speed of the drum. Different pulley sets and corresponding pull speeds are shown in Table 7-4.

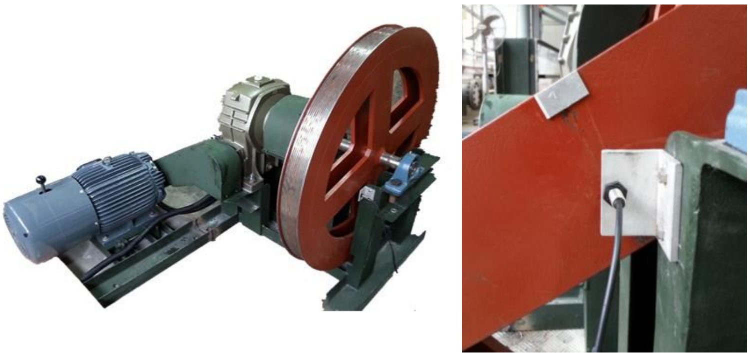

Figure 7-13 (a) Winch (b) Speed sensor installed on the Winch

Table 7-4 Different pulley set and corresponding pull speed

Series	**Motor Speed (RPM)**	**Pulley diameter (motor side)**	**Pulley diameter (gear box side)**	**Input for the gear box**	**Output of the gear box**	**Pull speed**
1	1500	3 inch	9.5 inch	473.7 RPM	23.7 RPM	1.18m/s
2	1500	4 inch	7.5 inch	800 RPM	40 RPM	2 m/s
3	1500	4 inch	5 inch	1200 RPM	60 RPM	3 m/s

7.2.5 Pull-over Test Set-up in the Wave Basin

All parts are designed and installed in the wave basin as Figure 7-14 shows. The positions matter. The pipeline should in the middle to ensure that the trawl gear has enough space to accelerate and enough space to decelerate. The wire rope length should be carefully calculated. The pipe is placed horizontally at an angle. In this program, the author studies the crossing at 90 degree, 60 degree, 45 degree and 30 degree. The set-up for 60, 45 and 30 degree is shown in Figure 7-15.

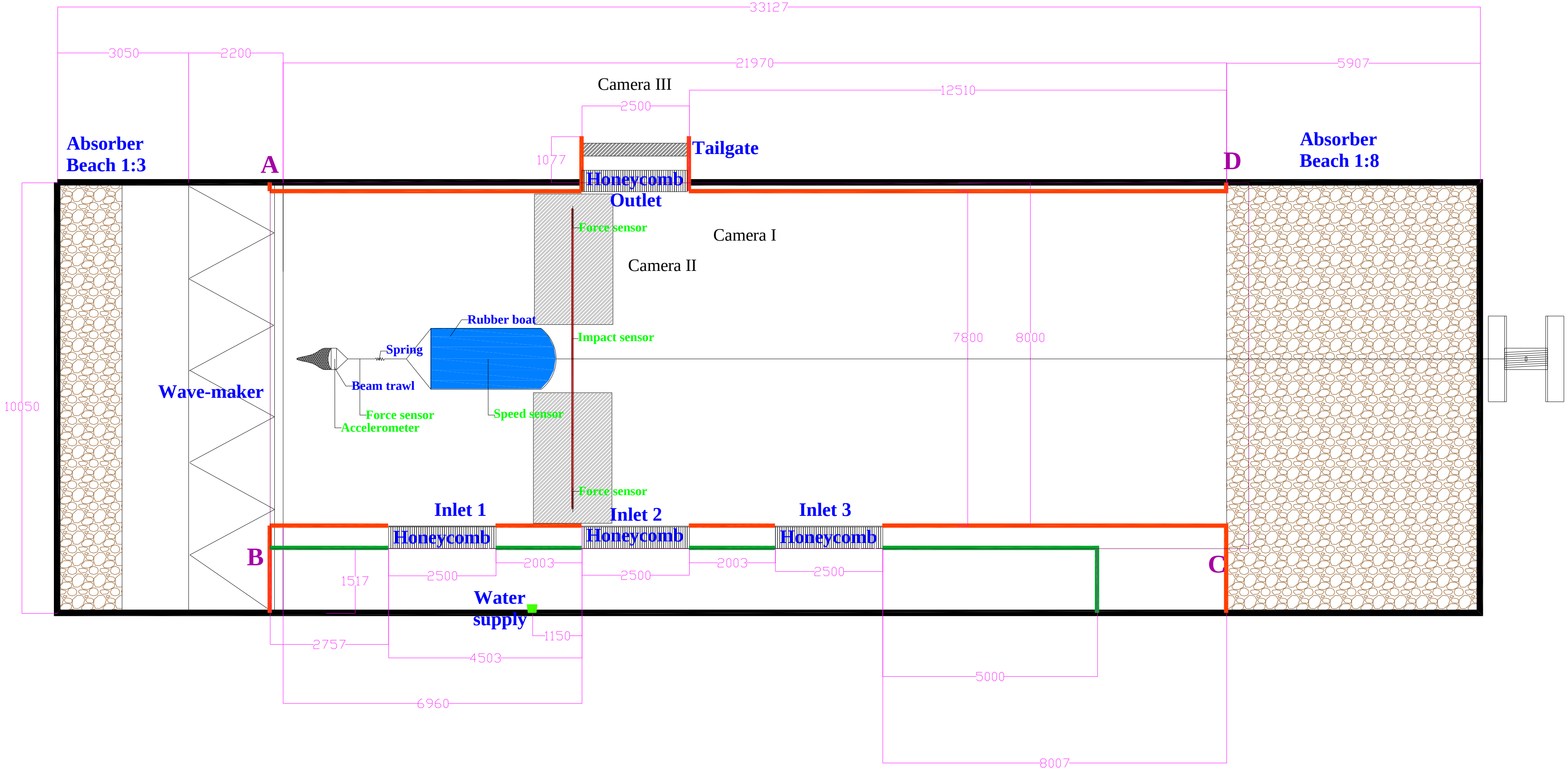
33127
3050
2200
21970
5907
12510
Camera III
2500
1077
Tailgate
Absorber
Beach 1:3
A
Honeycomb
Outlet
D
Absorber
Beach 1:8
Force sensor
Camera I
Camera II
Rubber boat
Spring
Impact sensor
7800
8000
Beam trawl
Wave-maker
10050
Force sensor
Accelerometer
Speed sensor
Force sensor
Inlet 1
Inlet 2
Inlet 3
Honeycomb
Honeycomb
Honeycomb
B
C
2003
2003
1517
2500
2500
2500
Water
supply
1150
2757
4503
5000
6960
8007

(a) Plane view

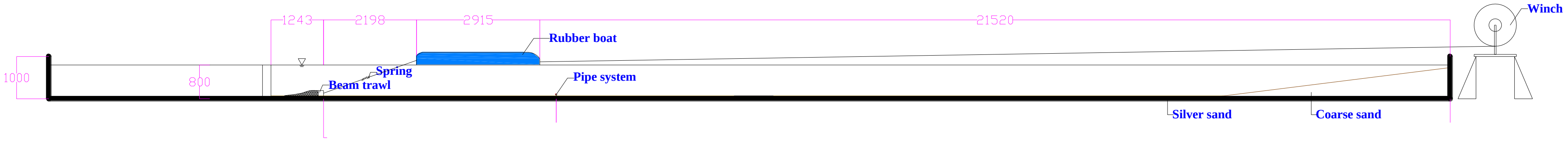
1243
2198
2915
21520
Winch
Rubber boat
1000
800
Spring
Beam trawl
Pipe system
Silver sand
Coarse sand

(b) Side view
Figure 7-14 Experiment Design

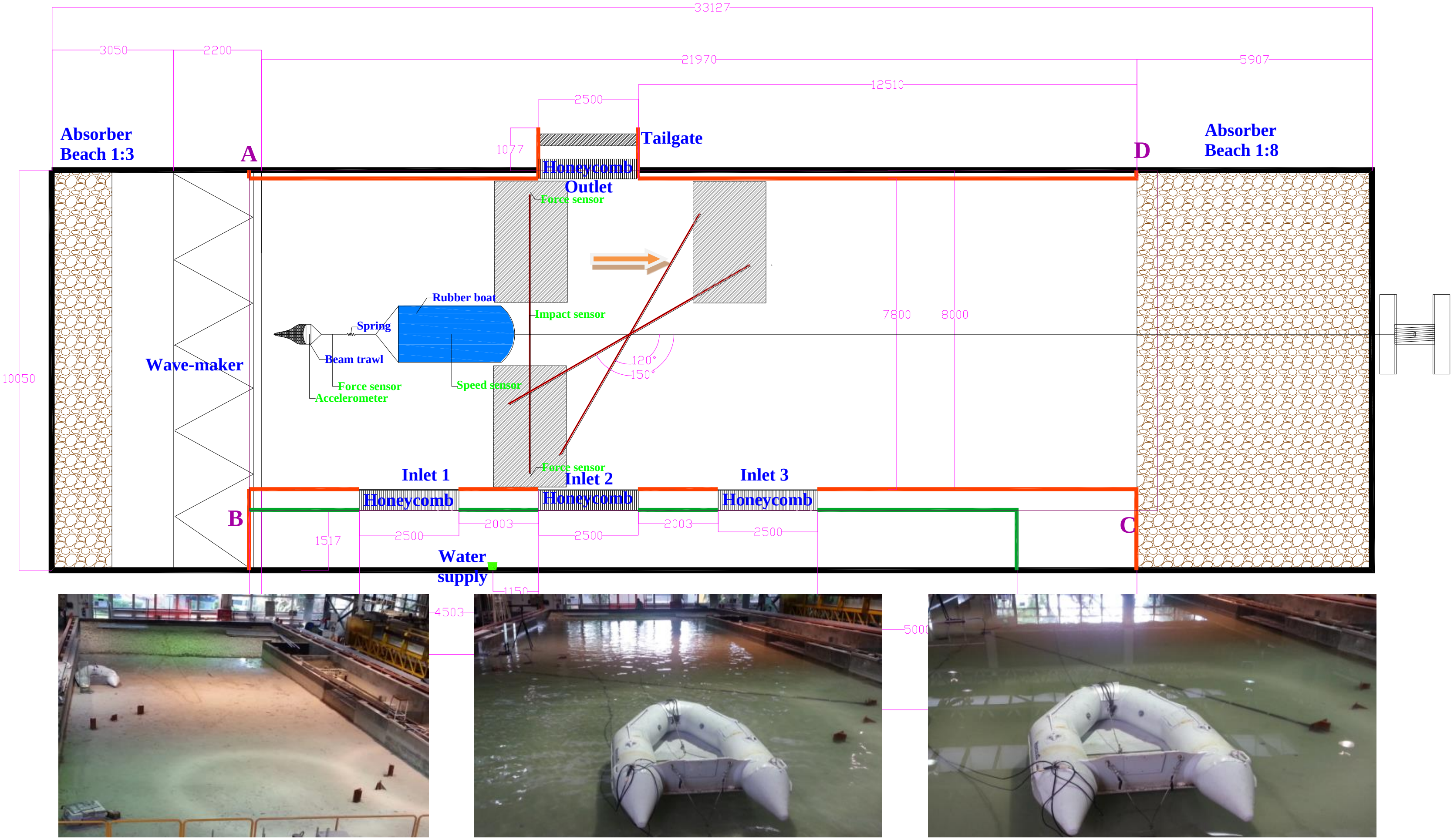
33127
3050
2200
21970
5907
12510
2500
1077
Absorber
Beach 1:3
A
Honeycomb
Outlet
Tailgate
D
Absorber
Beach 1:8
Force sensor
Rubber boat
Spring
Impact sensor
Beam trawl
Force sensor
Accelerometer
Speed sensor
Wave-maker
10050
7800
8000
120°
150°
Force sensor
Inlet 1
Inlet 2
Inlet 3
Honeycomb
Honeycomb
Honeycomb
B
C
1517
2500
2003
2500
2003
2500
Water
supply
1150
4503
5000

Figure 7-15 Set-up for different angles

7.2.6 Experiment Data Collection and Analysis

The sensors used in the experiment and the corresponding measurements are shown in Table 7-5.

Table 7-5 Sensors and corresponding measurements

Chanel	Sensors	Measurements	Position
1	Displacement-1200	Displacement d_C	Figure 7-16 middle one
2	Displacement-600	Displacement d_A	Figure 7-16 left one
3	Displacement-600	Displacement d_B	Figure 7-16 right one
4	Speed sensor	Drum RPM	On the drum (Figure 7-13)
5	Load Cell DUT #17	Pull-over force F_p	On the warp line (Figure 7-11)
6	Load Cell I	Pull-over force F_p	On the warp line (Figure 7-11)
14	Accelerometer	Accelerometer a_1	On the beam trawl centre of gravity (Figure 7-17)
15	Accelerometer	Accelerometer a_2	
16	Accelerometer	Accelerometer a_3	
	Camera I	Video under water	The positions marked in Figure 7-14
	Camera II	Video under water	
	Camera III	Video outside water	

It is straightforward for most sensors to be mounted and to measure. The load cells are connected in the warp-line and the accelerometer is glued to the trawl gear. One difficulty is to mount the displacement sensor. The sensors aim to measure the displacement of the impact points and the middle point of the pipe. However, the wire of the wire displacement sensor will block the trawl gear’s movement. The solution is to use a soft wire to connect the measuring point on the pipe and the sensor, and if the soft wire blocks the trawl gear’s movement, the soft wire will be easily broken and give way to the trawl gear. This protects the sensor. The sensor is mounted as Figure 7-16 shows.

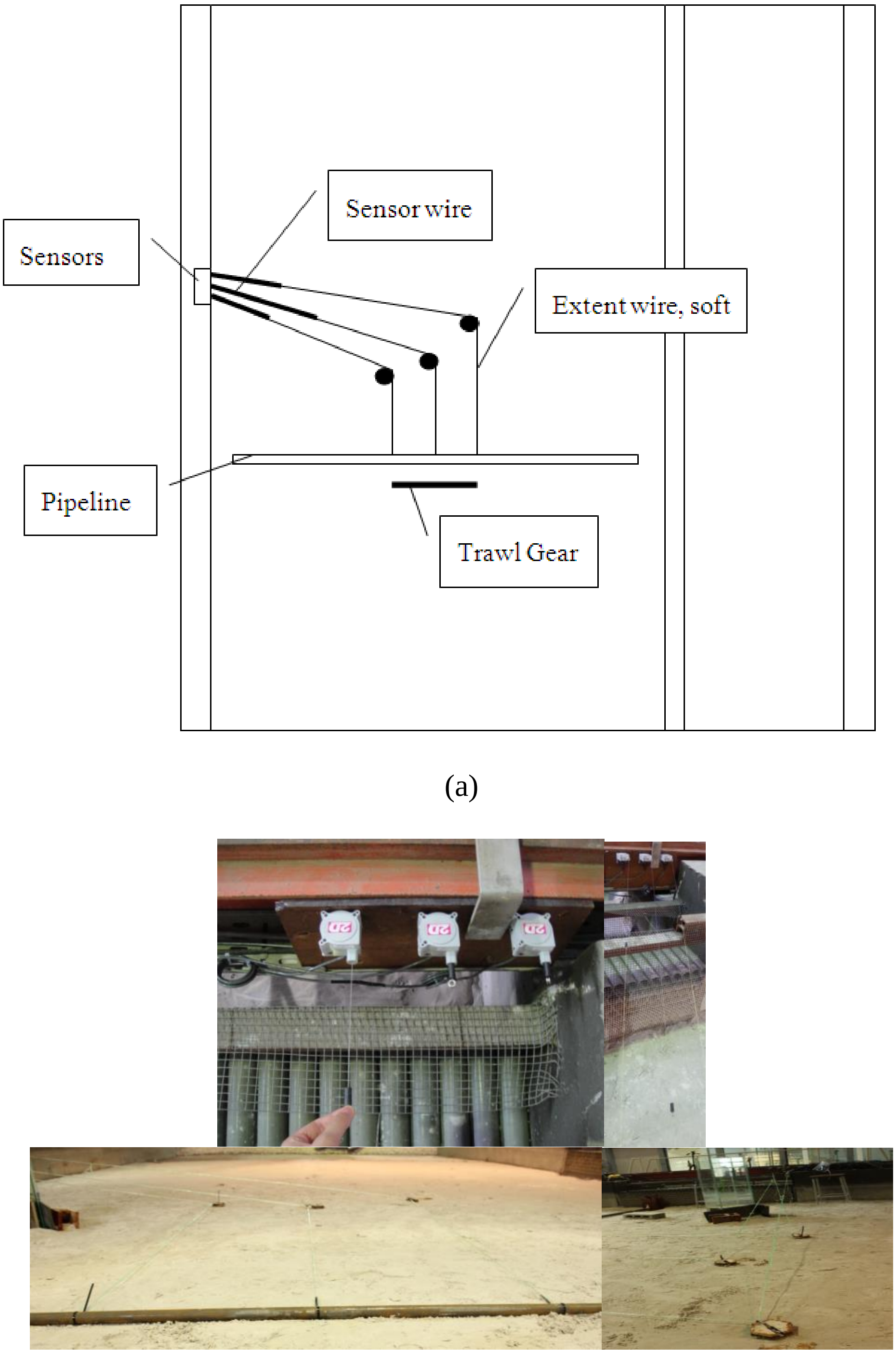
Sensor wire
Sensors
Extent wire, soft
Pipeline
Trawl Gear

(a)

(b)

Figure 7-16 Wire potentiometer connection (a) Sketch (b) Set-up

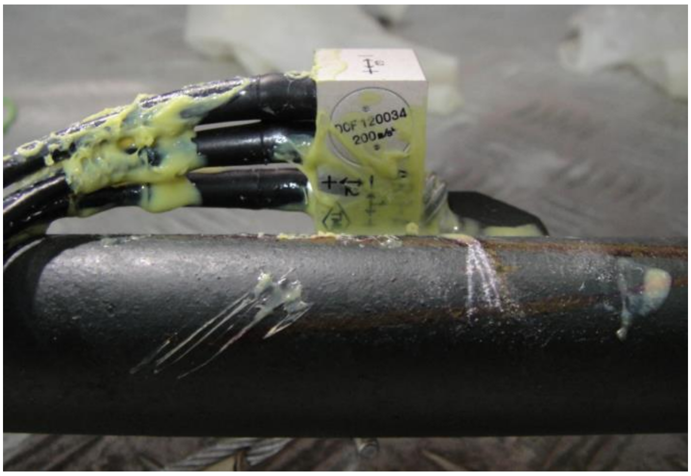

Figure 7-17 3-Axial Accelerometer on the beam trawl

Three cameras capture the trawl gear movement and impact. Camera I is put in a waterproof glass tank fixed on the steel plate. The camera in the glass tank is under the water level. Camera II is a water-proof camera and it is placed in water to video the pull-over. Camera III is outside the water, and by the side of the wave basin. The positions are marked in Figure 7-14 (a).

7.2.7 Test Program Design

To sum up, there are altogether eight different specimens, three different boundary conditions, two different springs represent two different water depths, two different trawl gear, three different velocities and four different crossing angles. Specimen details are shown in Table 7-2, and details of other parameters of the tests are shown in Table 7-6.

Based on all these parameters and different combinations, altogether 100 tests are conducted as summarized in Table F-1. The test name of every test reflects the conditions. The first part is the specimen name, and is followed by a dashed line. The first letter after the first dashed line represents the boundary condition, the second one is the water depth or the spring stiffness, the third one is the trawl gear type and the last number is the pulling speed. After the second dashed line, a number represents the test repeat time. The last part is the crossing angle.

Table 7-6 Summary of Parameters

	Abbreviation	**Stands for**	**Remarks**
Boundary Condition	S	Simply support	
	F	Fixed ends	
	SF	Short section fixed ends	
Water depth / Spring stiffness	S	Shallower water	Represent 30 m, and the spring stiffness is 55.05 kN/m
	D	Deeper water	Represent 100 m, and the spring stiffness is 14.47 kN/m
Trawl gear	F	Froude trawl gear	can be applied to the Froude scaling
	S	Solid trawl gear	change the hollow beam to solid
Moving Speed	1	1.18 m/s	
	2	2 m/s	
	3	3 m/s	
Crossing angle	90	90 degree crossing	the crossing angle is the angle between the pulling direction and the pipe axis
	60	60 degree crossing	
	45	45 degree crossing	
	30	30 degree crossing	

7.3 Test Results and Analysis

The pull-over force, the pipeline displacement, the velocity and accelerations are recorded by an oscilloscope. Here the case PIPAB-FDF1-1-90 is randomly taken as an example to explain the original data. The pull-over force time history is shown in Figure 7-18. The pull-over force is measured by two load cells, one with range of 0 to 10 kN and the other 0 to 3 kN. In the data analysis, the data recorded by the smaller range one are used, and the data recorded by the larger range load cell are used to double check. The frequency of the data acquisition is 10^4 /s. The data are filtered with a low pass filter at a frequency of 100 Hz, and are plotted in the same figure for validation. The pull-over force curve has five phases, the acceleration phase, the stabilization phase, the interaction phase with the pipeline, the re-acceleration phase and the deceleration phase. In this case, the maximum force is 0.491 kN, and the time of the pull-over force to increase to the maximum is 0.131 s. This information of other tests is listed in Table F-2. All the pull-over force time history for other cases is plotted in Appendix E.

As suggested by Jee (2003), the force in the warp-line before the trawl gear hit the pipeline is defined as the baseline force. The baseline force is associated with the hydrodynamic drag and the friction force. In this case, the baseline force is 0.12 kN. The delta force is defined as the difference between the maximum force and the baseline force, and is 0.371 kN.

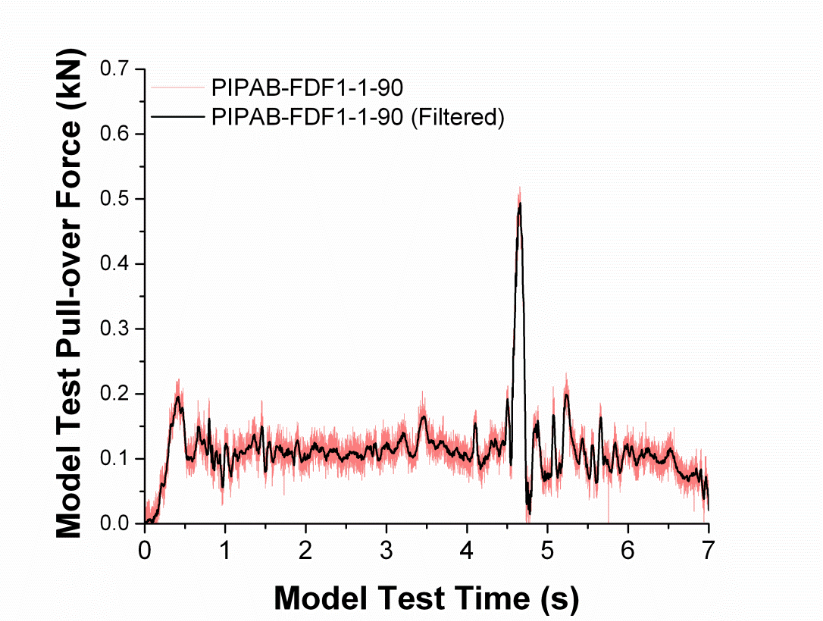

Figure 7-18 Pull-over force time history of PIPAB-FDF1-1-90

Three displacement wire sensors measure the displacement of the pipe at three points. For the case PIPAB-FDF1-1-90, the displacement is shown in Figure 7-19. From the figure, the maximum displacement is 32 mm. All the maximum displacements for all other tests for 90 degree crossing are read and listed in Table F-2.

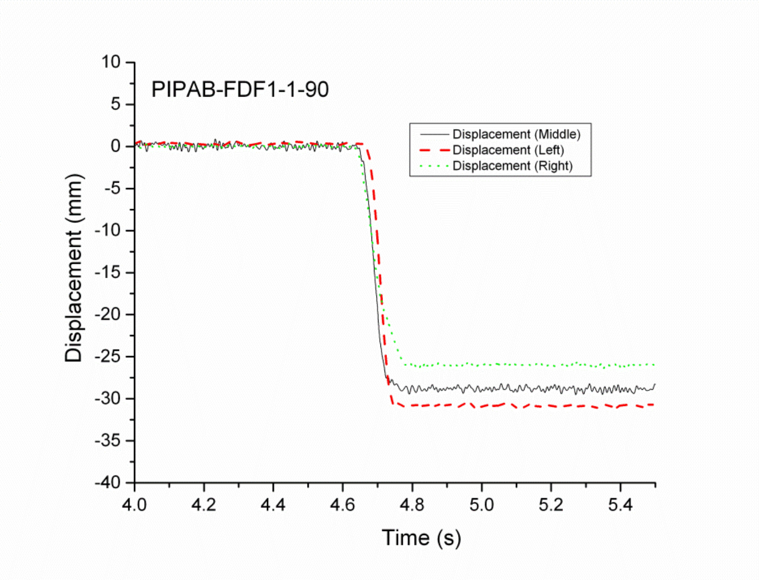

Figure 7-19 Displacement time history of PIPAB-FDF1-1-90

The tension measured by the load cell at the pipe end is shown in Figure 7-20. The maximum tension for this case is 2 kN. Similarly, other tensions from other 90 crossing cases are all read and listed in Table F-2. The tension has a linear relationship to the maximum deflection as Figure 7-21 shows.

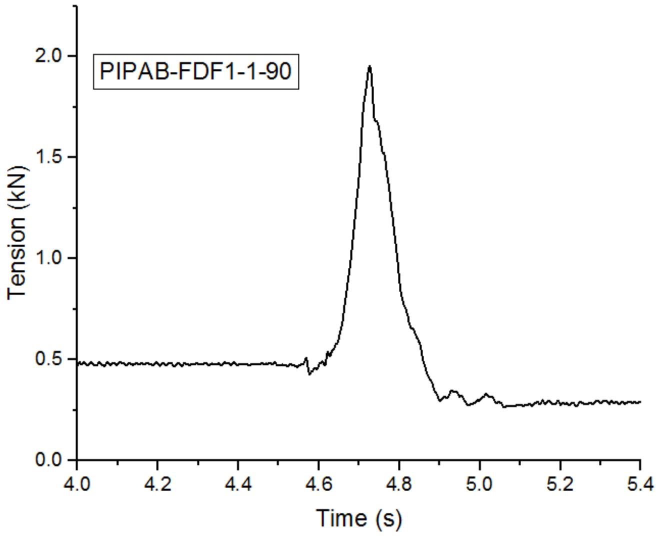

Figure 7-20 Tension time history of PIPAB-FDF1-1-90

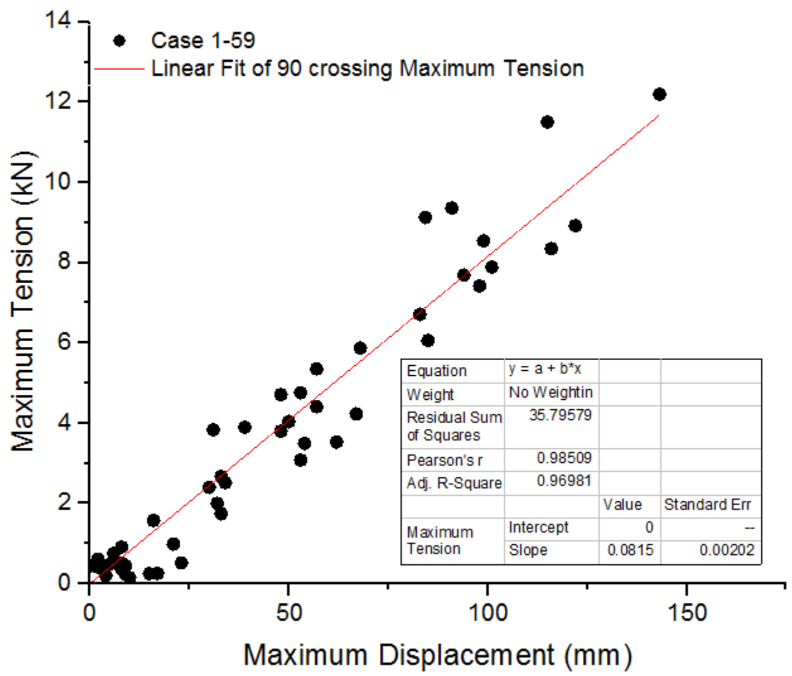

Figure 7-21 Liner relationship of maximum tension & maximum displacement

The accelerations measured by the three-axial accelerometer are plotted in Figure 7-22. Direction 1 is the vertical direction, and Direction 3 is the trawl gear moving direction. Direction 2 is the trawl beam axis direction. The moving direction and the vertical direction have larger accelerations compared to direction 2. The data are sensitive to small motions and difficult to analysis. Unfortunately, as there are so many impacts, the accelerometer was broken at a late stage.

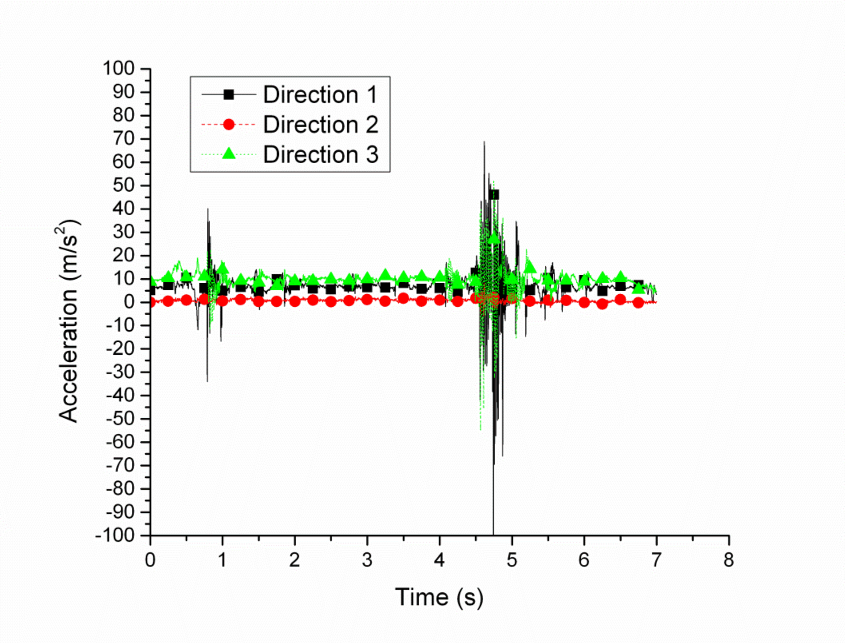

Figure 7-22 Acceleration time history of PIPAB-FDF1-1-90

7.4 Different Crossing Angles

In the field, the trawl gear does not always cross the pipeline at 90 degrees. Just the opposite, as the fisherman likes to trawl the fish along the pipe, the trawl gear always crosses the pipeline at a small angle. In this program, the crossings at 60 degree, 45 degree and 30 degree are all conducted. For the crossings at other angles, the displacement could not be measured because it is more difficult to set up. Take the case SPSD-FSF1-1-60 as an example to illustrate the results. Figure 7-23 shows the pull-over force time history of SPSD-FSF1-1-60. Unlike the 90 crossing case, the pull-over force curve has two peaks in addition to the starting one, although one is larger and one is smaller. This is because one of the trawl shoes impacts the pipe, and pulls the pipe, then the other trawl shoe impacts the pipe at a later time. The time interval is dependent on the crossing angle as well as the velocity. In this case, the maximum pull-over force is 0.464 kN, and the time for the trawl gear to cross the pipe is 1.1205 s.

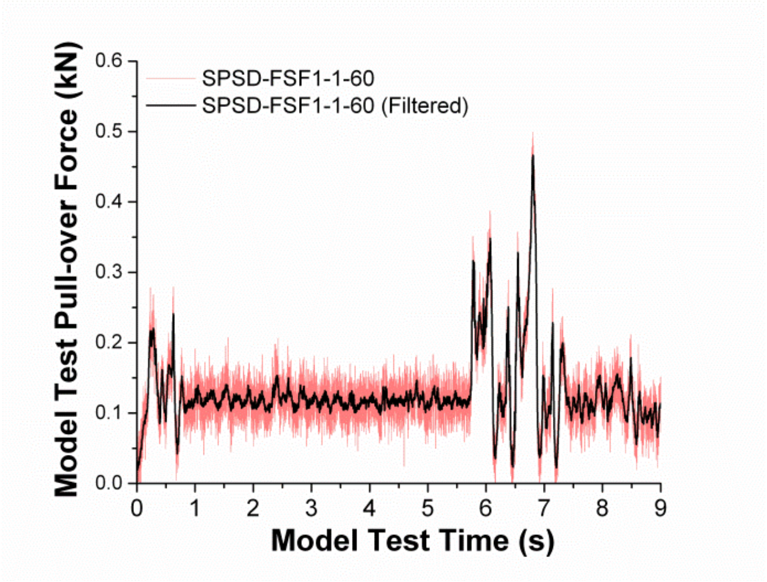

Figure 7-23 Pull-over force time history of SPSD-FSF1-1-60

Tension time history of SPSD-FSF1-1-60 is shown in Figure 7-24. The tension also shows two peaks, corresponding to the pull-over force time history. The maximum tension is 2.37 kN at the second crossing.

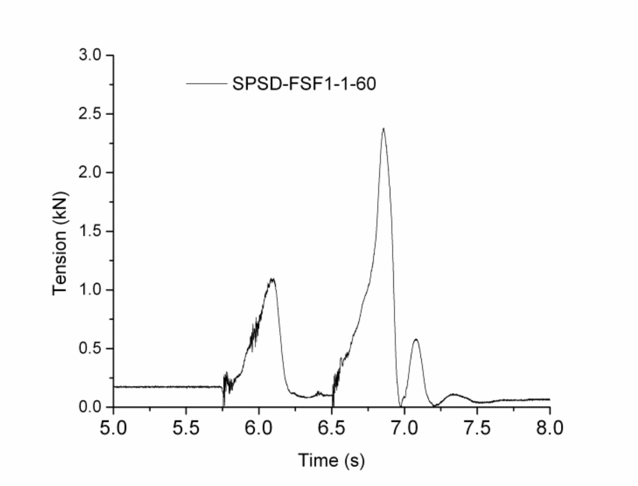

Figure 7-24 Pull-over force time history of SPSD-FSF1-1-60

7.4.1 90 Degree Crossing vs. Smaller Degree Crossing

Comparisons among different crossings under different conditions are shown in Figure 7-25 and Figure 7-26. Unlike the 90 degree crossing, the other degree crossings have two peaks of the pull-over force other than a single one. This is because the trawl shoes cross the pipeline one by one with a time interval for other angle crossings. It should be noticed, that the pull-over force is much larger for the 90 degree crossing than for crossings at other angles, and almost twice as large. This conclusion is convenient for the engineers, as they do not need to calculate pull-over forces for all angles and the pull-over force at 90 degree crossing will be a conservative estimate. The maximum pull-over forces, the time for trawl gear to cross the pipe, the maximum tension for the crossing at other angles are listed in

Table F-3.

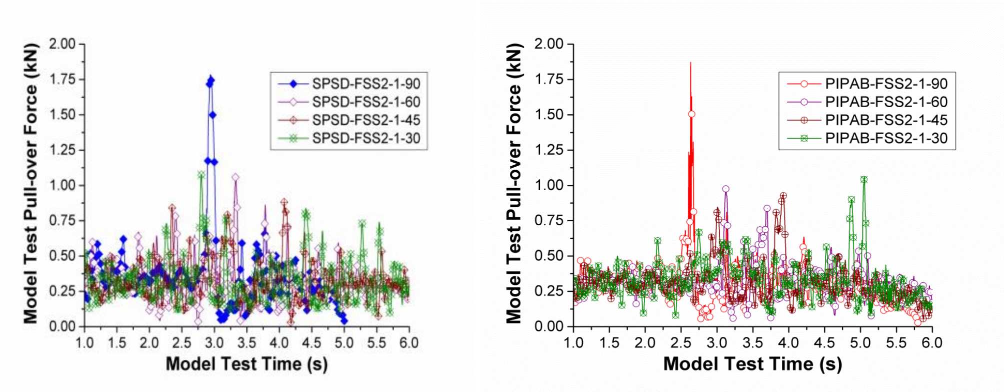

Figure 7-25 Crossing at different angles under FSS2 condition

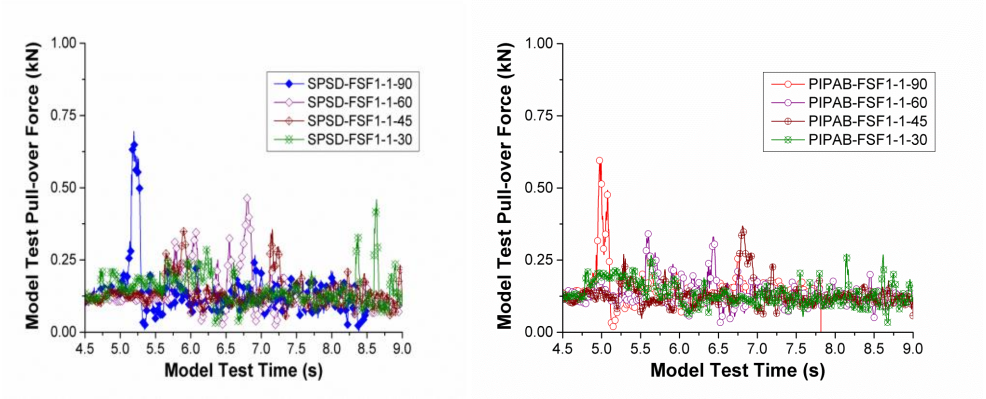

Figure 7-26 Crossing at different angles under FSF1 condition

7.4.2 Sliding at Low Crossing Angle

Although the pull-over force is smaller at other angles than 90 degrees, a unique behaviour happens when the crossing angle is so low that the trawl gear slides along the pipe for some distance before it crosses the pipeline. This increases the possibility of hooking and makes the situation more complicated, and therefore needs more attention.

Take PIPAB-FSF1-1-30 as an example to demonstrate the behaviour of the sliding. As shown in Figure 7-27, firstly the right shoe impacts the pipe, and then it slides along the pipe. After it crosses the pipe, the beam slides on the pipe, and finally the left shoe crosses the pipe. There are two stages of sliding behaviour in the whole process: the first is when the right shoe slides along the pipe, and the second is when the trawl beam slides on the pipe.

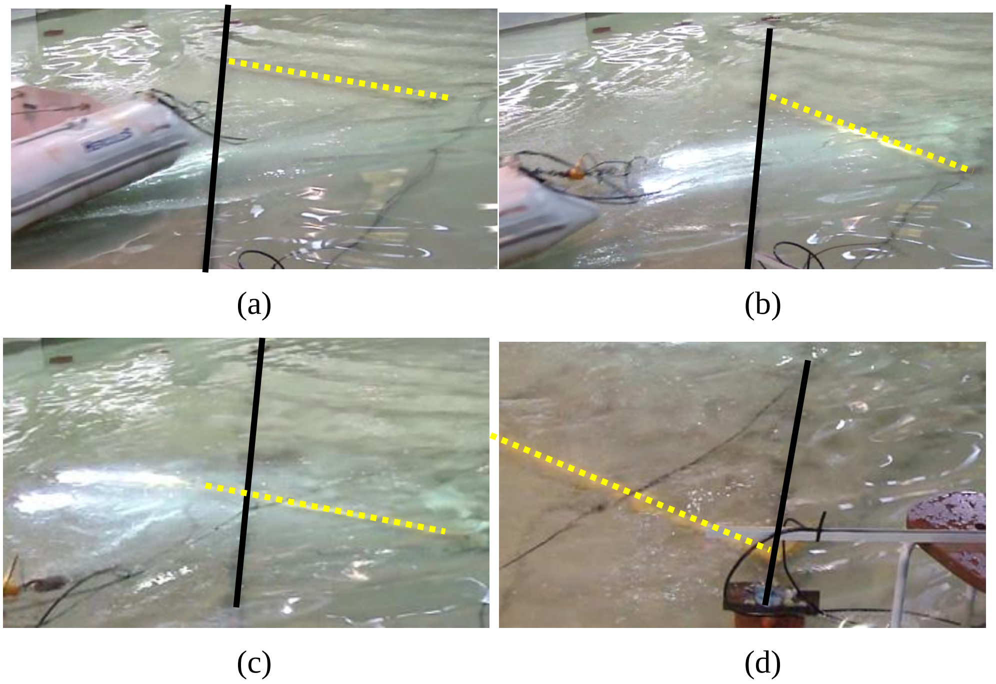
(a) (b)

(c) (d)

Figure 7-27 PIPAB-FSF1-1-30 sliding along the pipe (a) the right shoe impacts the pipe (b) the right shoe slides along the pipe (c) the trawl beam slides on the pipe (d) the left trawl shoe cross the pipe (Black solid line: pipe, Yellow dash line: trawl beam)

Condition FSF1 and FSF2 are compared in order to study the effect of the velocity. From the recorded videos, PIPAB-FSF2-1-30 has almost no sliding behaviour whereas PIPAB-FSF1-1-30 does slide along the pipeline as Figure 7-27 shows. PIPAB-FSF1-1-30 slides further in both sliding stages (the first when the right shoe slides along the pipe, and the second when the trawl beam slides on the pipe) than in the other one.

For the S trawl gear, the condition FSS1, FSS2 and FSS3 are compared. The sliding distance of the stage one of FSS1 is larger than the sliding distance of FSS2, and larger than FSS3. However, the sliding distance of the stage two of FSS3 is much larger than that of FSS2. Therefore, the sliding distance of the case of FSS3, both in stage one and stage two is the longest. The left trawl shoe crosses nearer to the end in this case.

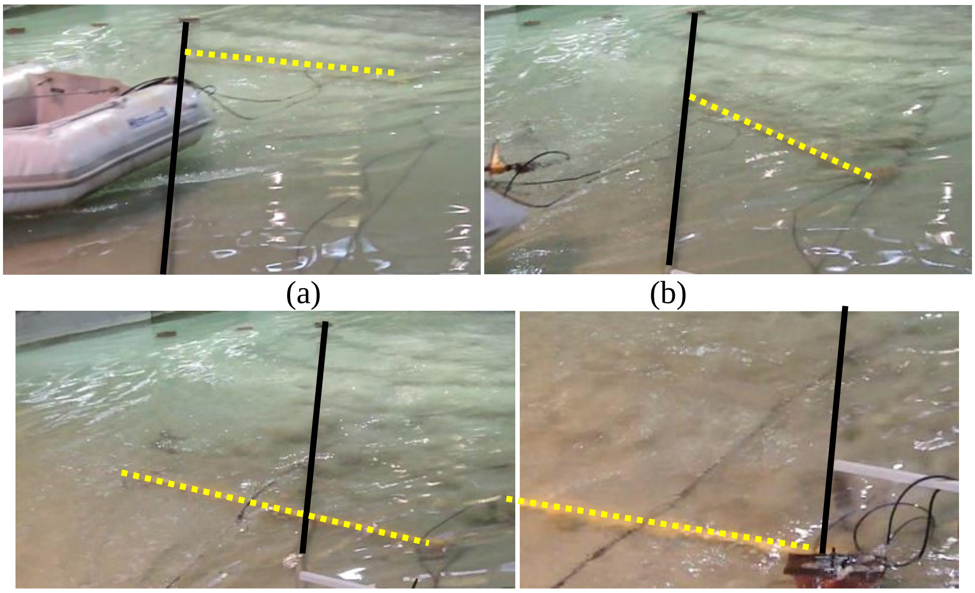

(a) (b)

(c) (d)

Figure 7-28 SPSD-FSS1-1-30 (a) Right shoe impacts (b) Right shoe slides (c) Trawl beam slide (d)Left shoe blocked by the connector (Black solid line: pipe, Yellow dash line: trawl beam)

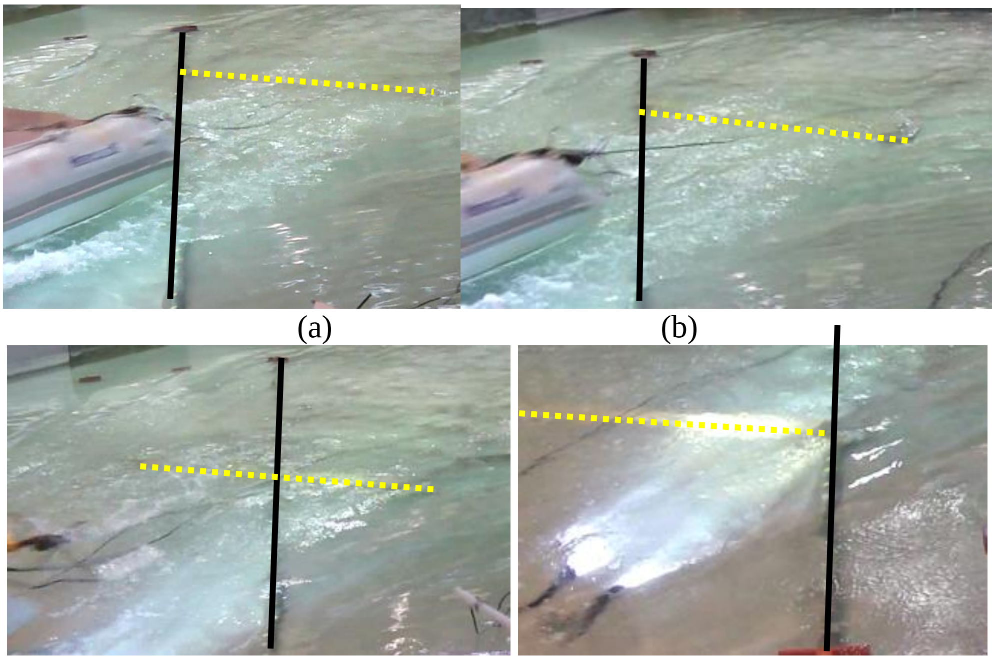

(a) (b)

(c) (d)

Figure 7-29 SPSD-FSS2-1-30 (a) Right shoe impacts (b) Right shoe slides (c) Trawl beam slide (d)Left shoe crosses the pipe (Black solid line: pipe, Yellow dash line: trawl beam)

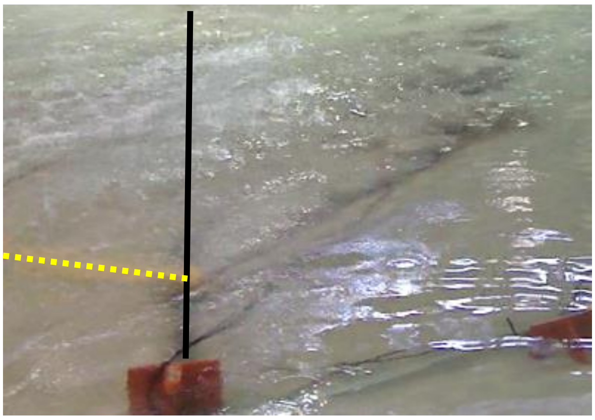

Figure 7-30 SPSD-FSS3-1-30 left shoe crosses the pipe (Black solid line: pipe, Yellow dash line: trawl beam)

The pipeline geometries also have an impact on the sliding behaviour. The comparison is between SPSD-FSS1-1-30 and PIPAB-FSS1-1-30. The total sliding distance of SPSD-FSS1-1-30 is so long that the trawl gear cannot cross the pipe and is finally blocked by the connector. The trawl gear just crosses the pipe at the end in the case PIPAB-FSS1-1-30.

To sum up, the sliding behaviour directly relates to the difficulty level of crossing and the velocity. The first crossing relates to the difficult level, which relates to the vertical force ratio and the ratio of the pipe’s geometry and the trawl gear’s. The more difficult it is to cross, the more likely it is to slide, and the further it will slide. The second crossing relates to the friction and the velocity. When the trawl gear is heavier, the friction is larger, and when the velocity is large, such as in the case of FSS3, the second sliding phase is long.

7.5 Summary

In this chapter, the pull-over test program is described, and the test results are summarized. From the beginning of planning to do this experiment, through the experiment design, sensors purchasing till the end, the total process costs almost two years. The major contributions of this chapter are:

1. A model test has been designed. The way to design the specimen, the beam trawl gear, the warp-line, the boundary conditions and the winch are all clearly described here. The set-up is feasible, functional and affordable. The set-up can be a good reference to other similar experiments.
2. In this test program, several parameters are studied, including single wall pipes and pipe-in-pipes, different pipe diameters and thicknesses, different spacing, different boundary conditions, different pulling speeds, different trawl gear, different warp-line stiffness and different crossing angle, in order to achieve the objective.
3. Altogether 100 tests have been conducted. These large amounts of raw data are valuable for the research on this subject. The raw data include the pull-over force data, the response time, the displacement, the tension and video data.
4. The analysis of the raw data with crossings at 90 degree is explained, and all information is listed in the table. The global deformation of the pipeline proportionally relates to the tension measured by the load cell installed at the end boundary. The behaviour of the sliding has been studied. The sliding behaviour relates to the crossing angle, the crossing difficulty level and the velocity.

8 Analysis of Pull-over Model Test

The previous chapter presents the design and results of the pull-over model tests. In this chapter, the results will be analysed in order to achieve the four objects stated at the beginning of Chapter 7. Firstly, the overtrawlability of pipe-in-pipe is investigated by comparing responses of pipe-in-pipes with responses of single wall pipes. Then the parametric study is conducted to study the mechanical behaviour of pull-over. Based on that, the two most important questions of the velocity effect and the scale law of this problem are discussed. Finally, a new model is proposed.

8.1 Overtrawlability of Pipe-in-Pipe

The Overtrawlability is the immediate question that this research wants to answer. Pull-over response is one aspect of the pipe's overtrawlability. The pull-over response of pipe-in-pipe is studied in this section. Moreover, comparisons between pipe-in-pipe and single wall pipe illustrate the difference of pull-over response between them.

8.1.1 Comparison between Single Wall Pipe and Pipe-in-Pipe

The objective of this test program is to investigate the pipe-in-pipe's pull-over response, and find out how it compares to a single wall pipe. As mentioned in the beginning, generally, the overtrawlability of a 16 inch (406.4 mm) single wall pipe is sufficient for the pipe to stay on the seabed without trenching.

Here the specimen SPSD is the scaled model of a 16 inch (406.4 mm) pipe. The pipe-in-pipes with a smaller diameter than 16 inch (406.4 mm) are represented by specimens PIPAB and PIPABS. The spacer number of PIPABS is two times that of PIPAB. Comparisons among them are produced as Figure 8-1 and Figure 8-2 show. Both comparisons show the same trend, that the pull-over force of SPSD is larger than the pull-over force of PIPAB, and that both of them are smaller than the pull-over force of PIPABS. The reason that the pull-over force of SPSD is larger is because the outer diameter is larger, and the reason that the pull-over force of PIPABS is larger is because of the larger bending stiffness, a result of the spacers and the closer spacing. The reason that the pull-over force of PIPAB is smallest is that its outer diameter is smaller, and additionally the spacers are fewer in number and spacing is two times longer. PIPAB behaves more like a single pipe. It can be seen by adjusting the spacers and spacing it is able to change the global response of the pipeline and therefore achieve a satisfactory level of overtrawlability.

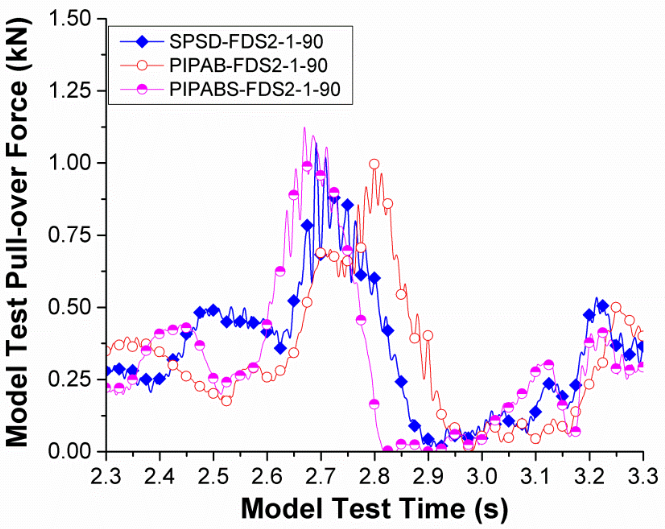

Figure 8-1 Comparison among SPSD, PIPAB and PIPABS at FDS2 condition

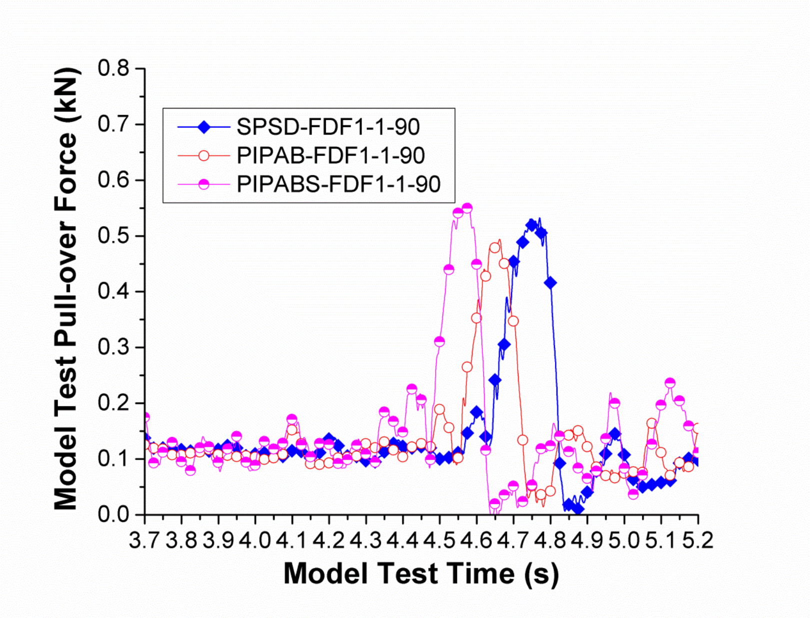

Figure 8-2 Comparison among SPSD, PIPAB and PIPABS at FDF1 condition

The maximum tensions measured by the load cell at the end of the pipe and the pipe's deflection are given in Table F-2. The tension is proportional to the pipe's deflection. According to the data, the deflection of a pipe-in-pipe with a smaller diameter is not necessarily larger than the deflection of a larger diameter single wall pipe. This is because the pipe-in-pipe's structure makes the pipe stiffer than a single wall pipe with the same outer diameter. For single wall pipes, though the pull-over force is smaller, the deflection might be too large and the pipeline might therefore need to be buried.

8.1.2 Prototype Scale Up

Scaling laws are important in model tests. They guide engineers to scale down the field to a lab scale, and they offer a method to scale up the model test results to a prototype value. Which scaling law is more suitable for this problem is a question that needs to be considered. It is difficult for this problem as the interaction involves too many parameters and is therefore complicated. The dimensions are all linearly scaled down; however, the scaling law to deal with the pull velocity is unclear. Some research institutes adopted the Froude's scaling law. With this scaling law, the scaling factors are given in Table 8-1.

Table 8-1 Scaling Factors based on Froude's law

Parameter	**Scaling Factors**	**Unit**
Length	β	m
Velocity	$\beta^{0.5}$	m/s
Time	$\beta^{0.5}$	s
Force	β^{3}	N

According to Froude scaling law, the velocity should scale down by 2.88 times. If the prototype velocity is 3.4 m/s, the model test velocity should be 1.18 m/s. This corresponds to the cases that F trawl gear whose dimensions are linearly scaled and is moving at 1.18 m/s. In the test program, the test names with the form "****-**F1-*-*" are scaled under the Froude's scaling law. According to the Froude scaling law, the prototype pull-over forces equal to the small scale pull-over forces multiplied by third power of the scale factor, that is, the cube of 8.3. Prototype forces of all corresponding cases are plotted in Figure 8-3. The scaled pull-over forces are in the same range as the calculated forces based on DNV's methods, and other model test results; this is discussed further below.

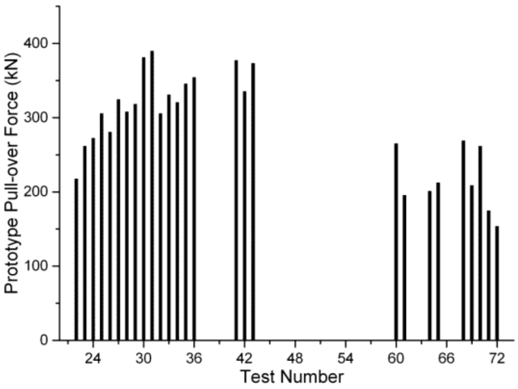

Figure 8-3 Prototype Force by Froude scaling

Table 8-2 Prototype Force by Froude scaling

	test series	*Prototype Pull-over Force*	*Prototype Time*	*Prototype Tension*	*Prototype Displacement*
22	SPSA-FDF1-1-90	217.85	0.39	563.78	174.30
23	SPSB- FDF1-1-90	261.88	0.29	1761.10	439.90
24	SPSC- FDF1-1-90	272.74	0.44	2229.97	323.70
25	SPSD- FDF1-1-90	305.91	0.39	1372.29	249.00
26	PIPAB- FDF1-1-90	280.75	0.38	1143.57	265.60
27	PIPAB-FDF1-2-90	324.78	0.50	280.75	66.40
28	PIPAB-FDF1-3-90	308.19	0.71	129.80	74.70
29	PIPABS-FDF1-1-90	318.49	0.44	289.32	66.40
30	PIPABS-FDF1-2-90	381.38	0.44	295.61	190.90
31	PIPABS-FDF1-3-90	389.96	0.47	522.04	66.40
32	PIPAC-FDF1-1-90	305.91	0.41	994.91	273.90
33	PIPAD-FDF1-1-90	331.06	0.57	142.95	124.50
34	PIPAD-FDF1-2-90	320.77	0.40	257.88	16.60
35	PIPAD-FDF1-3-90	345.93	0.31	251.59	16.60
36	PIPAD-FDF1-4-90	354.51	0.33	235.00	16.60
41	SPSD-FSF1-1-90	377.38	0.42	2693.12	398.40
42	PIPAB-FSF1-1-90	335.64	0.51	2521.58	473.10
43	PIPAD-FSF1-1-90	373.38	0.41	1000.63	273.90
60	SPS-FSF1-1-60	265.31	3.23	1355.14	N.A.
61	PIPAB-FSF1-1-60	195.55	2.66	301.90	N.A.
64	SPSD-FSF1-1-45	201.27	4.76	343.64	N.A.
65	PIPAB-FSF1-1-45	212.70	5.03	295.61	N.A.
68	SPSD-FSF1-1-30	269.31	8.77	268.17	N.A.
69	SPSD-FSF1-2-30	208.70	10.37	165.82	N.A.
70	SPSD-FSF1-3-30	261.88	11.29	226.43	N.A.
71	PIPAB-FSF1-1-30	174.97	8.97	264.17	N.A.
72	PIPAB-FSF1-2-30	153.81	9.75	230.43	N.A.

In the section 4.3 of DNV-RP-F111 (2010), it is stated that if the flexibility of potential free-spans is not dominating, then the method there can be used for 10 inch to 40 inch pipeline. This method is repeated in section 2.7.2.2 and used here to calculate the pull-over force.

Consider the prototype cases. The trawl gear is 5352 kg, moving at 3.4 m/s. C_F equals to 4.0. The added mass m_a is set to 0 for the comparison purpose. Assume the water depth is 100 m, and then the warp line stiffness k_w is about 140 kN/m. P can be calculated as 367.2 kN. The result is comparable to the results of the test program. The total time T_p is more than 1.189 s, and this is larger than 90 degree crossing and less than other degree crossing.

Moshagen (1980) reported the field tests and model tests results they conducted. Three main types of trawl boards and Dutch beam trawls were studied over pipelines of 16 inch (406.4 mm) and 36 inch. The model tests had the scale factor of 1:4, except one case was 1:5. The pull-over force was randomly distributed over a range. According to his experiments, the pull-over forces were generally between 100 kN to 200 kN. Figure 8-4 is the results of model tests and field tests for single wall pipes, which is suitable to compare with current test results. This field test was conducted in a sheltered coastal site, near Trondheim. The water depth is about 17 m to 20 m. The pipe is a 16 inch (406.4 mm) pipe. Total length is 300 m. The maximum field test pull-over force is about 230kN and the maximum model test pull-over force is about 250 kN. This is somewhat lower than the results in this test program. This might be because the beam trawl used in the field test is only about 1720 kg. The field data also illustrate that there is some randomness involved in the result, and in addition their pull-over forces are not linearly related to the velocity. For 16 inch (406.4 mm) pipes, the model test data are larger than the field test data. These phenomena will be discussed further later.

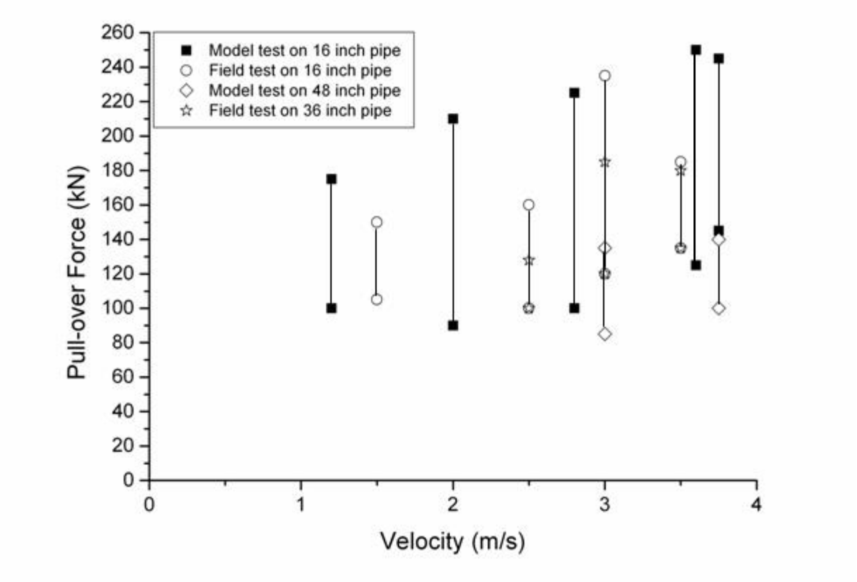

Figure 8-4 Replot data of Moshagen and Kjeldsen's

8.2 Parametric Study

In order to understand the mechanical behaviour better, the parametric study is conducted by changing various parameters in the test programs. The parameters are boundary conditions, pipe's geometries, warp-line stiffness and pulling velocities. This section investigates how these parameters influence the pull-over response. This creates the basis for further investigation.

8.2.1 Boundary Condition Effect

There are two boundary conditions in the test program for the 7 m pipeline. One is the simple support and another one is the fixed ends boundary condition. The comparison between them is shown in Figure 8-5. It shows that the boundary condition has little influence on the pull-over force. This is because when the pipeline is long enough, the boundary condition has little influence in the middle. The result shows it is reasonable to treat the boundary condition as fixed ends without considering the stiffness and damping effects at the end.

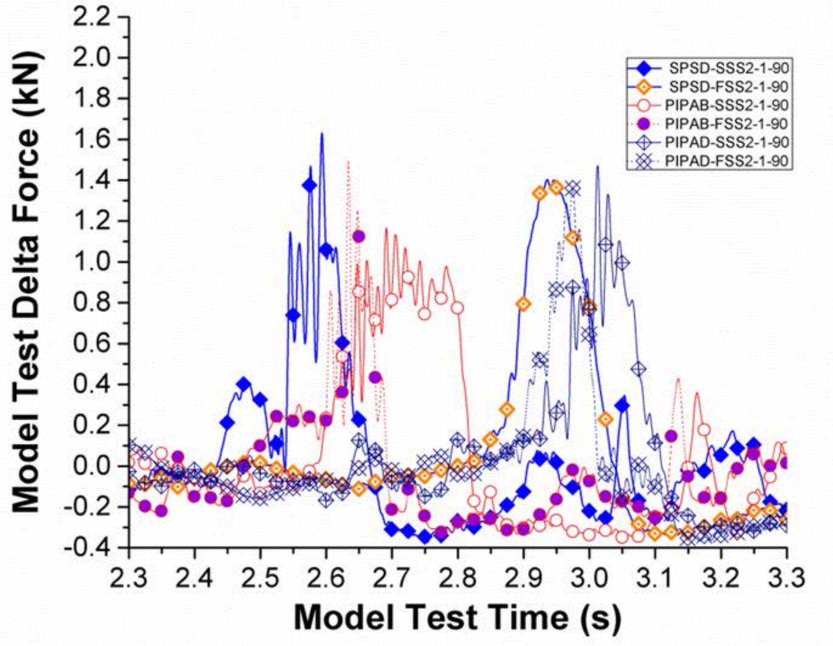

Figure 8-5 Pipe-in-pipes with different Boundary conditions

8.2.2 Pipeline Geometry Effect

There are four different single wall pipes and four different pipe-in-pipes among all the specimens. SPSA, SPSB, SPSC and SPSD are with four different diameters and wall thicknesses. Their delta forces are plotted in Figure 8-6, Figure 8-7 and Figure 8-8. Figure 8-6 shows the experiment results under SSS2 conditions. Figure 8-7 shows the results under FDS2 conditions. The conditions of the experiments shown in Figure 8-8 are FDF1. Among all these three figures, it can be observed that the delta force increases with the outer diameter. SPSB and SPSC have the same outer diameter but different wall thicknesses. According to the comparisons, the difference between results of SPSB and SPSC is minor. This means that the wall thickness does not much influence the delta force. This can be observed in the comparison among the pipe-in-pipes, as the Figure 8-9, Figure 8-10 and Figure 8-11 show. Especially in Figure 8-9, it is clearly that the delta forces of PIPAB and PIPAC are almost the same. It is also noticeable that no matter whether the pipe is single wall or pipe-in-pipe, if they have the same outer diameter, the forces are almost in the same range, as shown in Figure 8-12, Figure 8-13 and Figure 8-14, especially when the specimen is less in number. But it is not the case that only the diameter influences the delta force; the inner structure which changes the pipe's flexibility also influences the delta force. When there are twice as many spacers in the pipe, and the spacing distance is reduced to 0.25 m, the pipe becomes more rigid. The delta force is larger when the pipe is more rigid as Figure 8-15 shows. The same conclusion can be proved by the comparison between a short pipe section and longer pipe section. As shown in Figure 8-16, specimen of PIPAB-FDS-1 is 7 m, and the specimen of PIPAB-SFDS-1 is 3 m, the delta force is much larger for PIPAB-SFDS-1. This proves that when the pipe is more rigid, the delta force is larger.

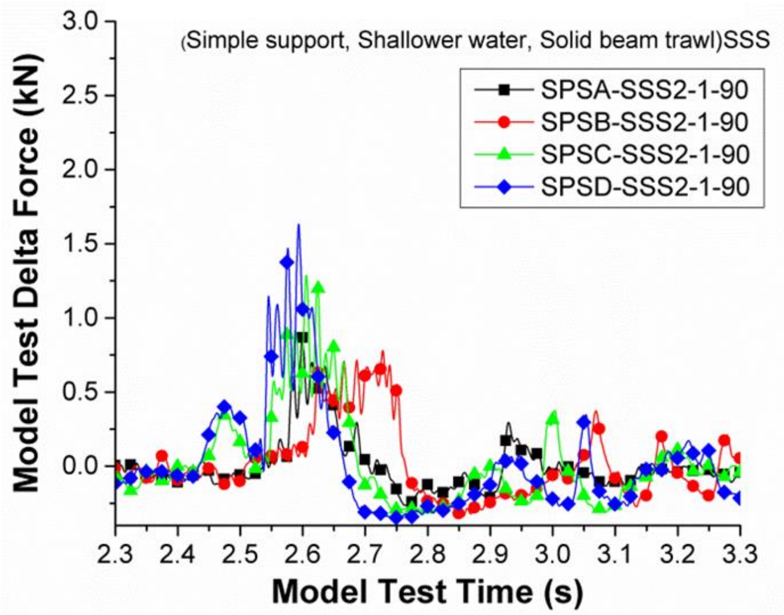

Figure 8-6 Single wall pipes with SSS2 conditions

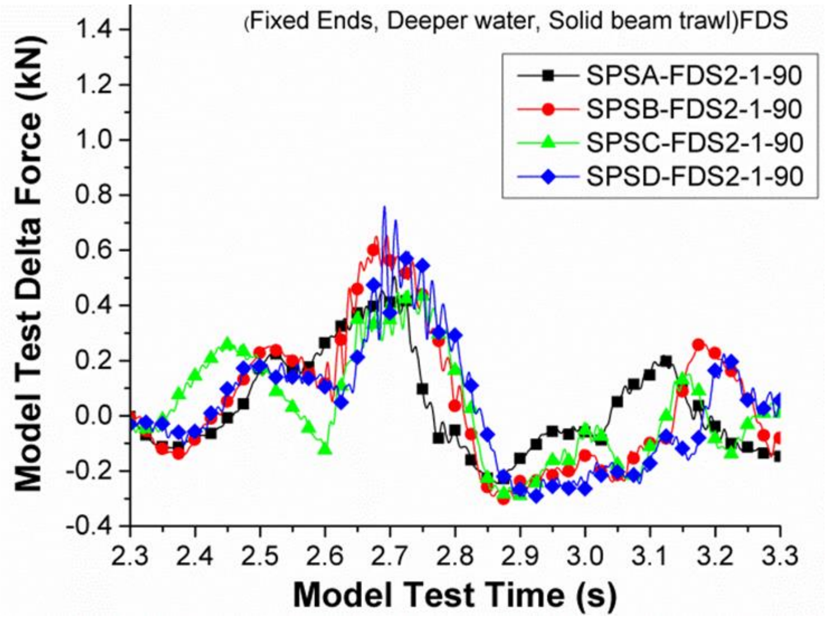

Figure 8-7 Single wall pipes with FDS2 conditions

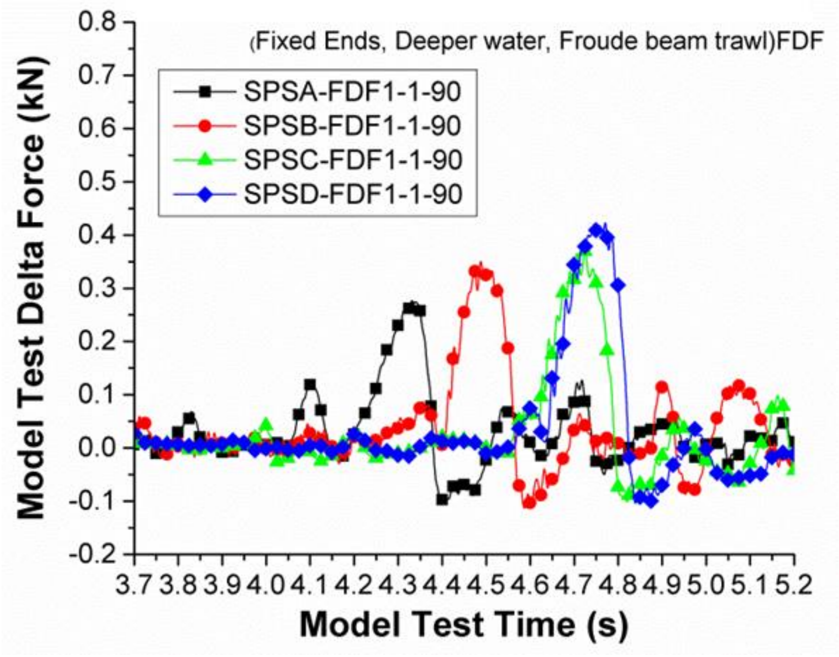

Figure 8-8 Single wall pipes with FDF1 conditions

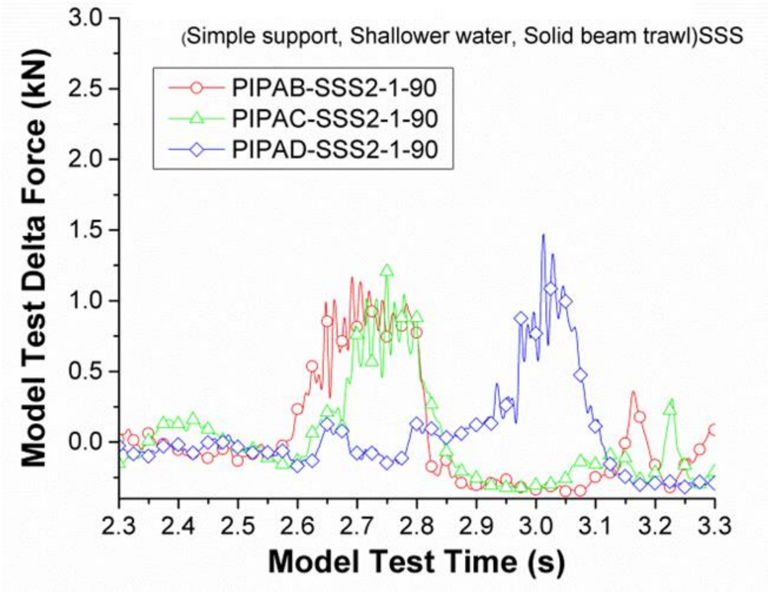

Figure 8-9 Pipe-in-pipe with SSS2 conditions

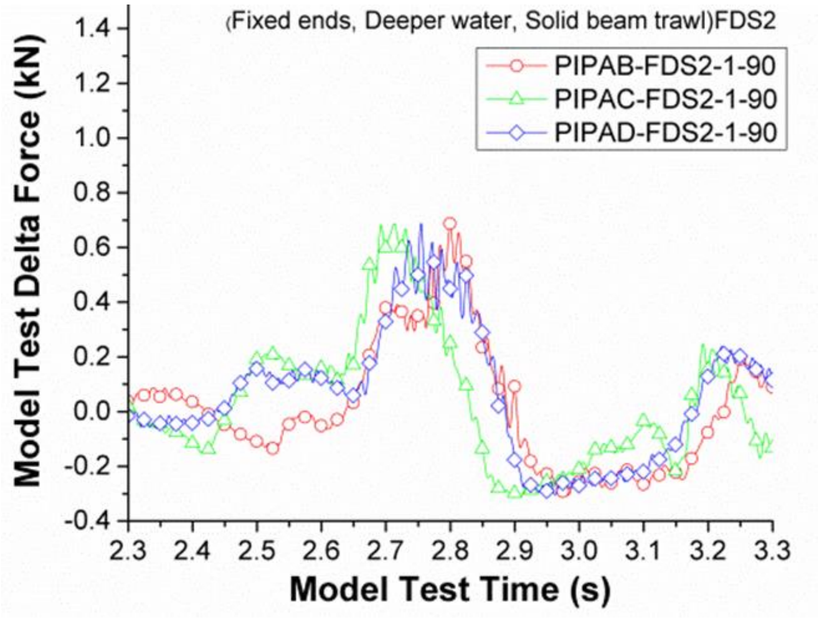

Figure 8-10 Pipe-in-pipe with FDS2 conditions

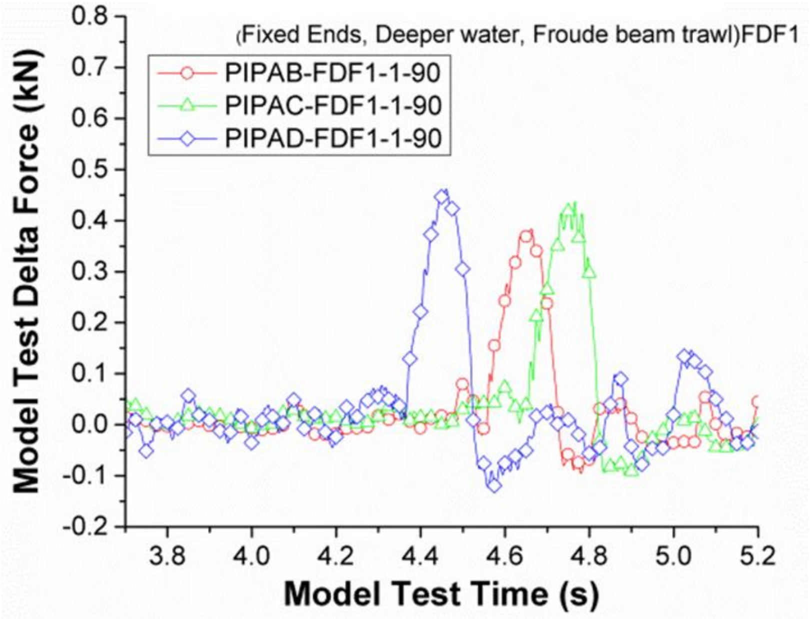

Figure 8-11 Pipe-in-pipes with FDF1 conditions

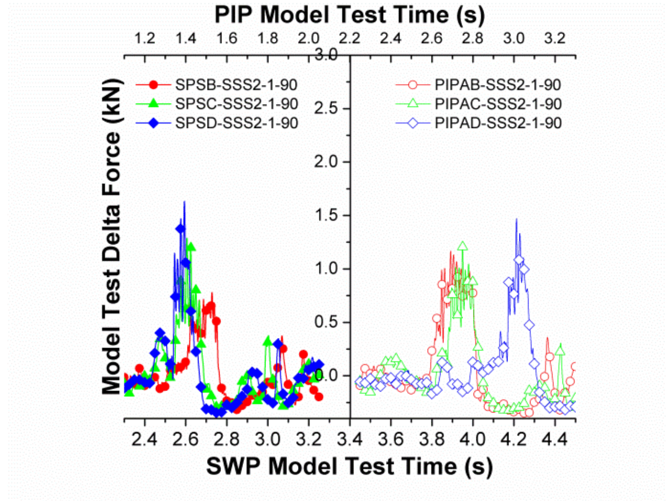

Figure 8-12 Single wall pipe & pipe-in-pipe with SSS2 conditions

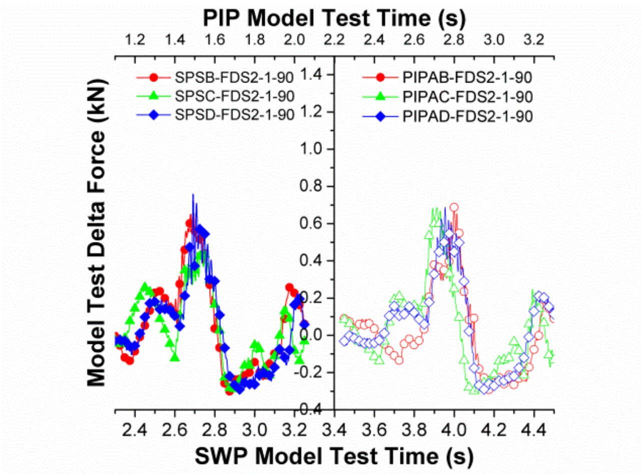

Figure 8-13 Single wall pipe & pipe-in-pipe with FDS2 conditions

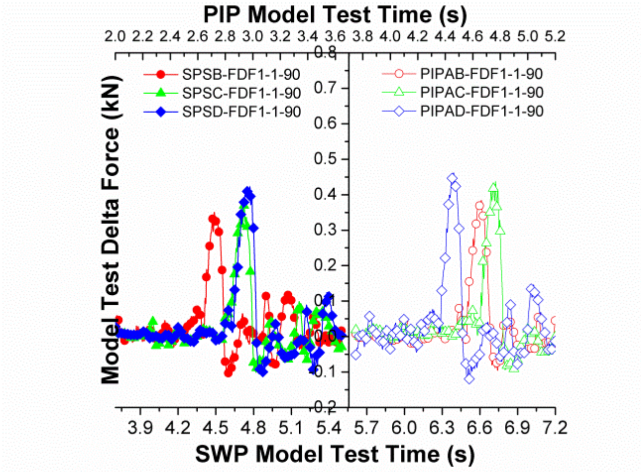

Figure 8-14 Single wall pipe & pipe-in-pipe with FDF1 conditions

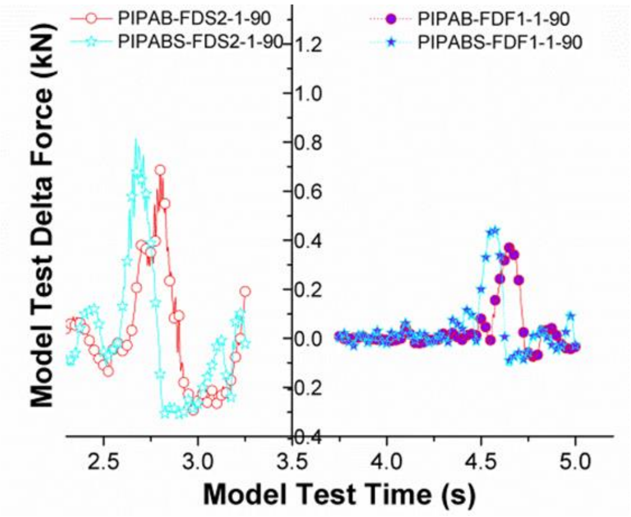

Figure 8-15 Pipe-in-pipe with different spacing

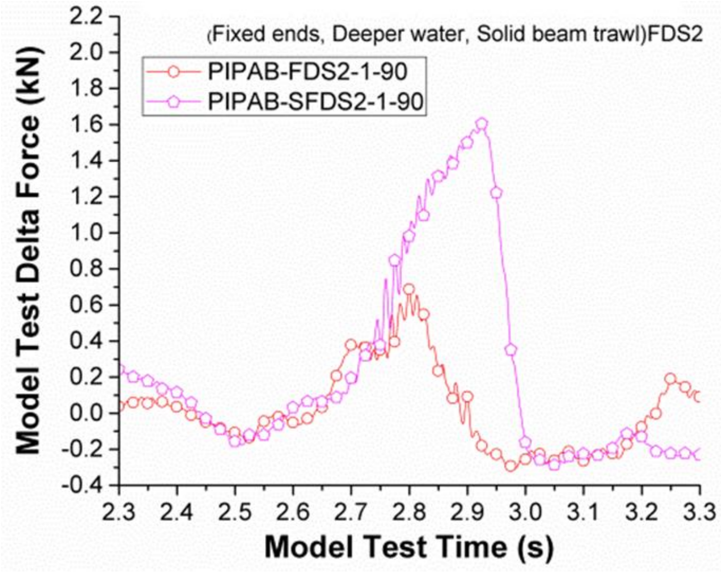

Figure 8-16 Pipe-in-pipes with different length

To sum up, the pull-over force relates to the pipeline diameter (*D*), the pipeline length (*L*) and the pipeline flexibility (*EI*). If the diameter is larger, the pipeline length is shorter or the pipeline is stiffer, the pull-over force is larger.

8.2.3 Water Depth Effect

The water depth factor is reflected in the warp line stiffness. Two types of stiffness are listed in Table 7-3. One represents a shallower water depth around 30 m, and the other one represents a deeper water depth around 100 m. Beam trawls are generally working in shallow water. The comparisons are shown in Figure 8-17 and Figure 8-18. The deeper the water depth is, the more flexible the warp line is, and the less pull-over force the warp line suffers. Moreover, the warp-line stiffness influences the heavier trawl gear much more than the lighter trawl gear.

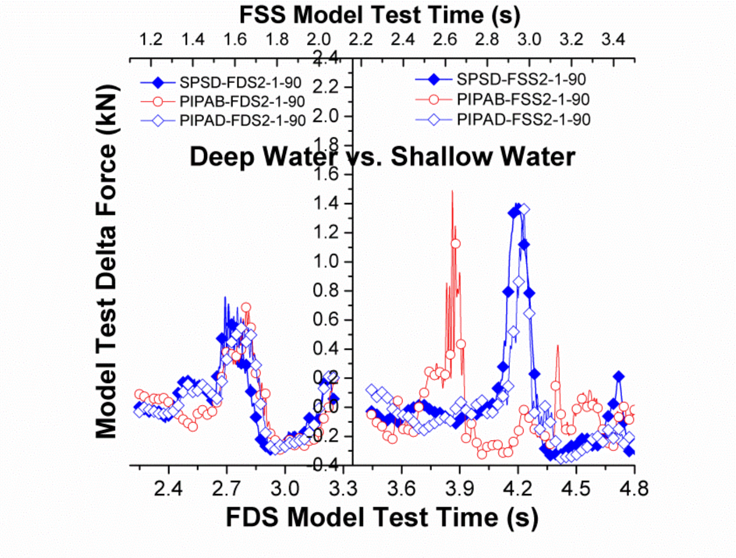

Figure 8-17 Pipe-in-pipes with different water depth (S trawl gear)

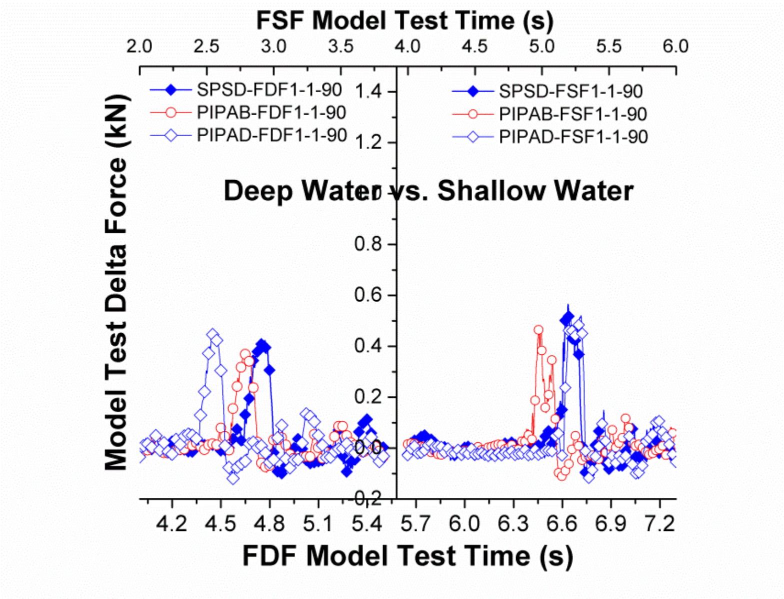

Figure 8-18 Pipe-in-pipes with different water depth (F trawl gear)

8.2.4 Kinetic Energy Effect

Kinetic energy influences the result a lot. The first comparison case is shown in Figure 8-19. The Solid trawl gear is 27.34 kg and is moving at 2 m/s, the kinetic energy is 54.68 J. The Froude trawl gear is 9.36 kg and moving at 1.18 m/s, and the kinetic energy of this case is 6.52 J. The difference of the kinetic energies are 48.16 J, the delta forces are not very different. On the other hand, the second comparison case shows a different conclusion. The solid trawl gear is 27.34 and moving at 1.18 m /s, for which the kinetic energy is 19.03 J, and the kinetic energy is almost the same as with the Froude trawl gear 9.36 kg moving at 2 m/s, when the kinetic energy is 18.72 J. The comparison between FDF2 and FDS1 is shown in Figure 8-20. Although the kinetic energy is almost the same, the pull-over forces are very different. The larger trawl gear moving at low velocity brings much larger pull-over force. This indicates the delta force does not linearly relate to the kinetic energy, which is very different from impact problems.

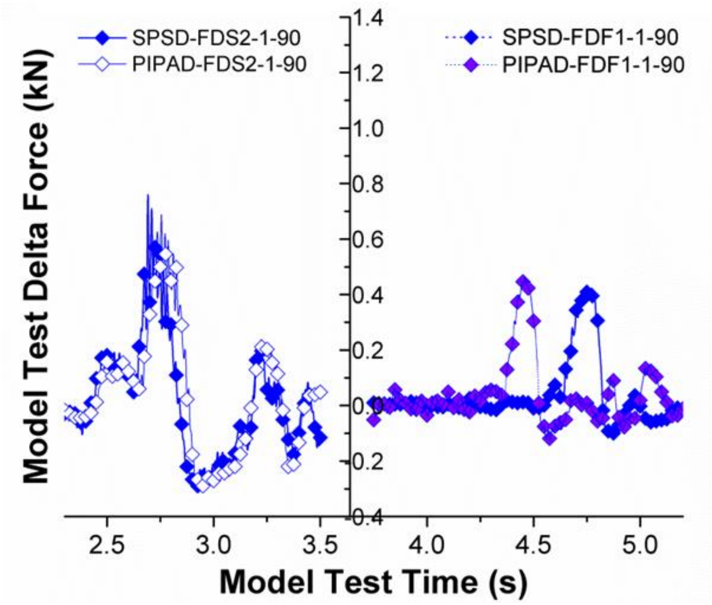

Figure 8-19 Pipe-in-pipes with different kinetic energy

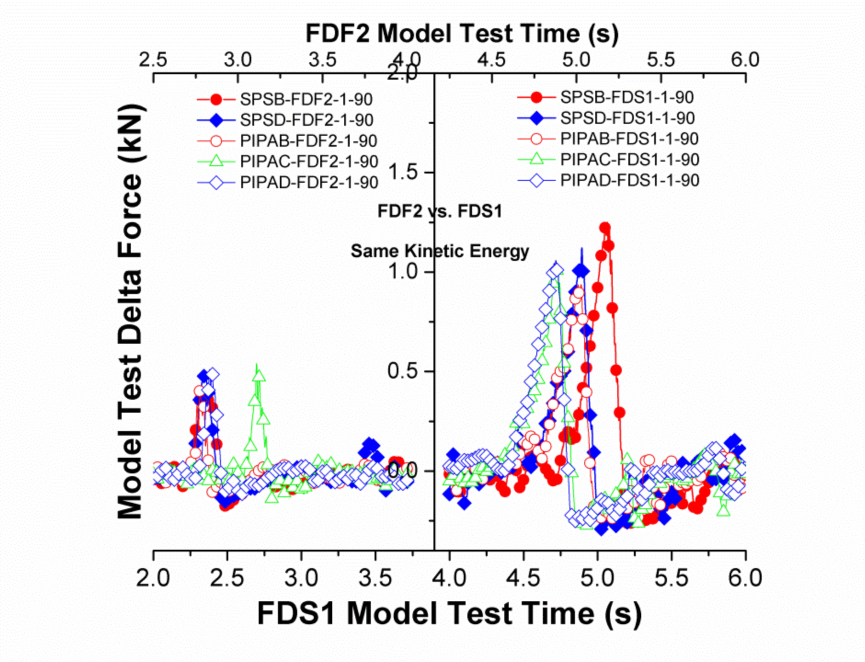

Figure 8-20 Pipe-in-pipes with same kinetic energy

8.3 Discussion of Froude Scaling Law

Velocity is a very crucial parameter in this dynamic system, and also the most controversial parameter in the scaling law. There are three different velocities in this program, 1.18 m/s, 2 m/s and 3 m/s. 3 m/s is in the range of the prototype velocity, and 1.18 m/s is scaled velocity based on the Froude scaling law. Both the F trawl gear and the S trawl gear are pulled at these three different velocities respectively, and the cases are compared in Figure 8-21 and Figure 8-25.

According to Figure 8-21, with a higher velocity, F trawl gear generates a little larger delta force. When F trawl gear moving at 3 m/s, it is not able to move firmly on the wave basin bottom. The velocity is so high that the trawl gear is already inclined and consequently it can easily cross the pipe and no obvious pull-over response are found as Figure 8-22 shows.

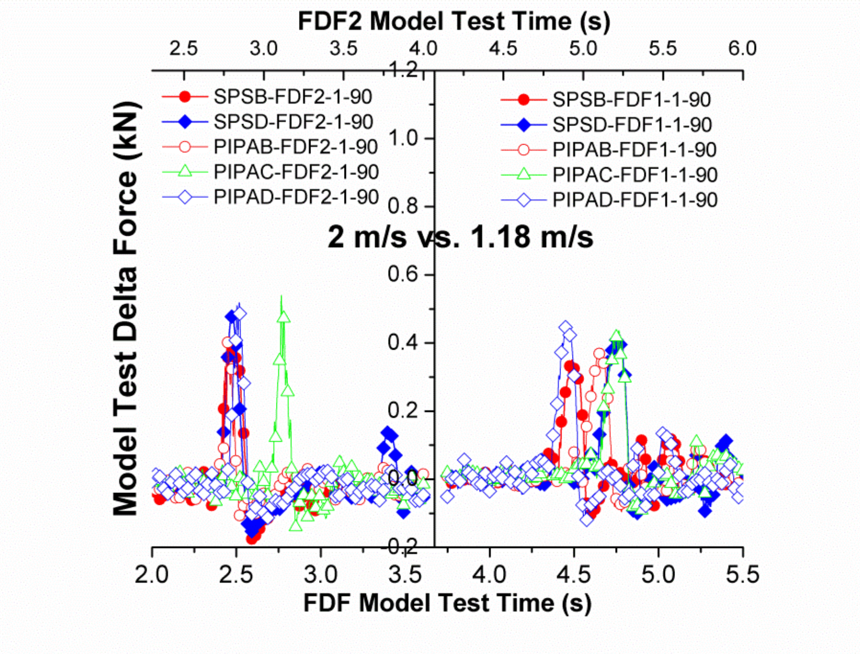

Figure 8-21 F trawl gear moving at different velocities

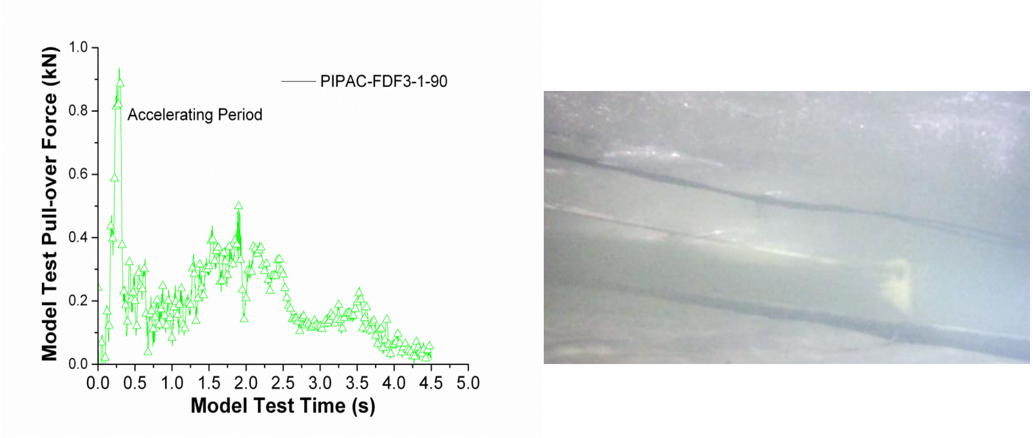

Figure 8-22 Pull-over force time history of PIPAC-FDF3-1-90

Whether the trawl gear is able to move firmly on the bottom relates to the ratio of the vertical forces. The free body diagram of the force on the trawl gear is shown in Figure 8-23. When the lift force and the buoyancy force together are larger than the gravity force, the trawl gear will leave the bottom. Therefore, to keep the trawl gear moving properly as well as to keep the difficulty level of the crossing the same, the ratios of the vertical forces should be kept the same. Most importantly, the ratio of the gravity force to the lift force should be kept the same as the geometries are scaled accordingly. If the ratio increases, trawl gear is “heavier” on the seabed, and it is more difficult to cross obstructions. If the ratio decreases, trawl gear is “lighter”, and possibly flies in the water. Some research institutes adopted the Froude scaling law, especially the fishing industry when they analysed the fishing net (Ward and Ferro, 1992). If the Froude number is kept the same, the moving behaviour will be similar for the trawl gear. Froude number maintains the ratio of the gravity over lift force as constant; therefore the model trawl gear will have the “same weight” as prototype. This ratio is derived as a dimensionless group as equation (8.1). It directly relates to the difficulty level of crossing. When the pull velocity increases, the ratio decreases towards zero. The smaller the ratio is, the easier the pipeline to cross. When the ratio decreases to a certain level, the trawl gear will not stay on the bottom.

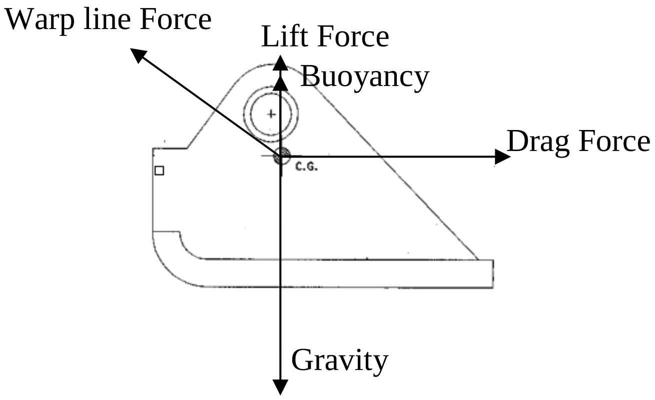

Figure 8-23 Forces on a moving trawl gear

$$\frac{Mg}{\rho V^2 h^2} \tag{8.1}$$

From this point of view, Froude scaling law is suitable as it preserves the trawl gear’s moving behaviour. However, the pull-over response does not only relate to the trawl gear’s movement, but also relate to the interaction between the trawl gear and the pipeline. According to Calladine (1983) and Jones (2012), to keep the similarity of the impact effect, the kinetic energy should be scaled by β^3. However, according to the Froude scaling law, the kinetic energy is scaled by β^4. This generates smaller response. On the other hand, though the response is smaller, according to the Froude scaling law, the model force is scaled up by β^3 instead of β^2 according to Calladine (1983) and Jones (2012).

8.4 Velocity Effect

As explained in previous section, the Froude scaling law is suitable to model the trawl gear's movement, but distorts the interaction with the pipeline. In order to look into this issue more deeply and find out how to scale the velocity, the effect of the pull velocity on interaction is studied.

DNV gives the method to calculate the maximum pull-over force from trawl boards and beam shoes is given as follows:

$$P = C_F V \sqrt{(M + M_a) * K} \tag{8.2}$$

where K is the warp line stiffness, V is the trawl velocity, M is the steel mass for the beam and shoes for beam trawls, M_a is the hydrodynamic added mass and mass of entrained water, C_F is the empirical coefficient of pull-over force based on laboratory and full-scale data.

Equation (8.2) indicates that the pull-over force relates to the velocity proportionally. However, according to the current test results, the proportional relationship between the maximum pull-over force and the velocity does not exist.

Firstly, the relationship between the baseline force and the velocity is studied. The baseline forces are the same if the warp-line stiffness (S, D), trawl gear (S, F) and moving velocities (1, 2, 3) are the same. Baseline forces of different combinations are plotted in Figure 8-24. Because of the hydrodynamic drag, the baseline forces are approximately proportional to the square of velocity. The fitted linear curve will not go through the origin as there is a friction force between the beam trawl and the seabed. The friction force of the S trawl gear is larger than the friction force of the F trawl gear as the data show. The effect of the warp-line stiffness relates to the baseline force. When the baseline force is small, the effect of warp-line stiffness is less.

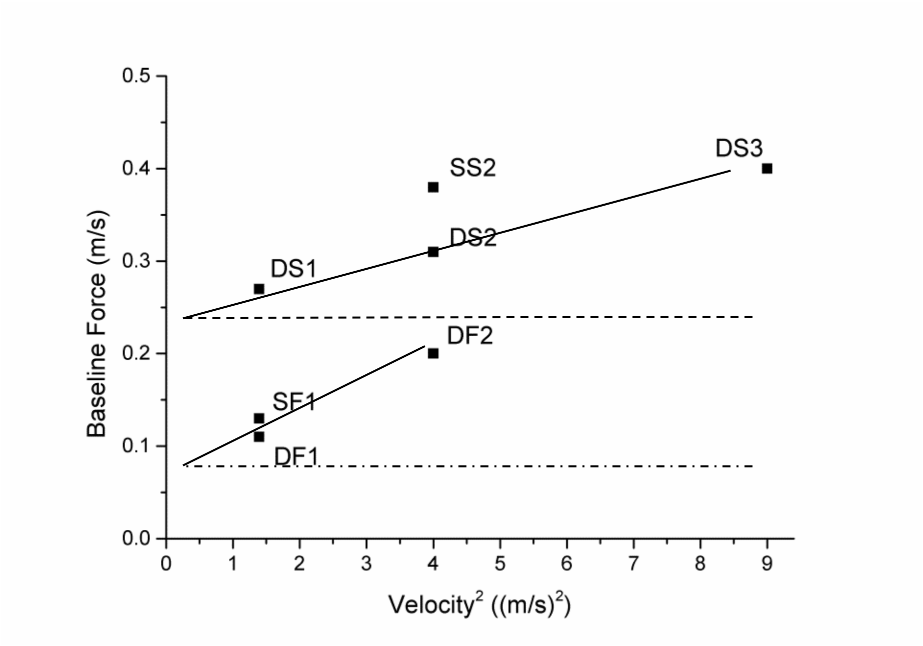

Figure 8-24 Baseline forces of different cases

The delta forces are investigated next. The comparison among three different velocities associated with S trawl gear is shown in Figure 8-25. S trawl gear is much heavier; therefore, it will remain on the bottom at 3 m/s. The delta force does not linearly relate to the trawl gear moving velocity. The delta force of 2 m/s is smaller than the delta force at 3 m/s, and it is also smaller than the delta force at 1.18 m/s although the velocity is larger than 1.18 m/s.

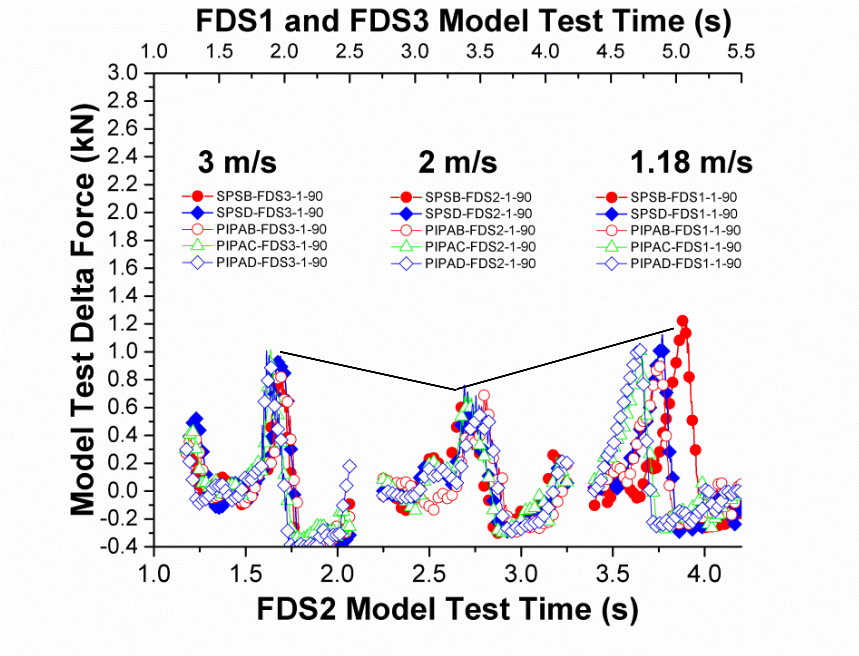

Figure 8-25 S trawl gear moving at different velocities

Altogether with other 90 degree crossing cases, the pull-over forces are shown in Figure 8-26, the maximum pull-over forces do not show a linear relationship with the velocity. Even if there is a velocity involvement, the effect is very small. Figure 8-27 shows the delta forces versus the velocity, and shows even less velocity effect. The proportional relationship that DNV suggested does not exist. The same conclusion is also reached by another source of test for trawl board conducted by JEE Ltd (JEE Ltd, 2003). One of the comparisons is shown in Figure 8-28. It shows the delta force is not affected by the change in velocity, and the peak pull-over force increases with velocity because of the baseline force.

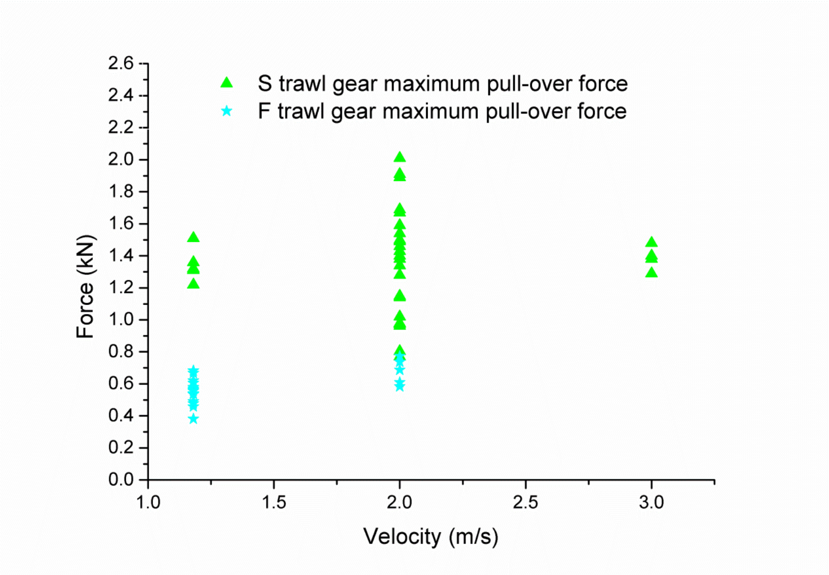

Figure 8-26 Maximum pull-over force versus velocity

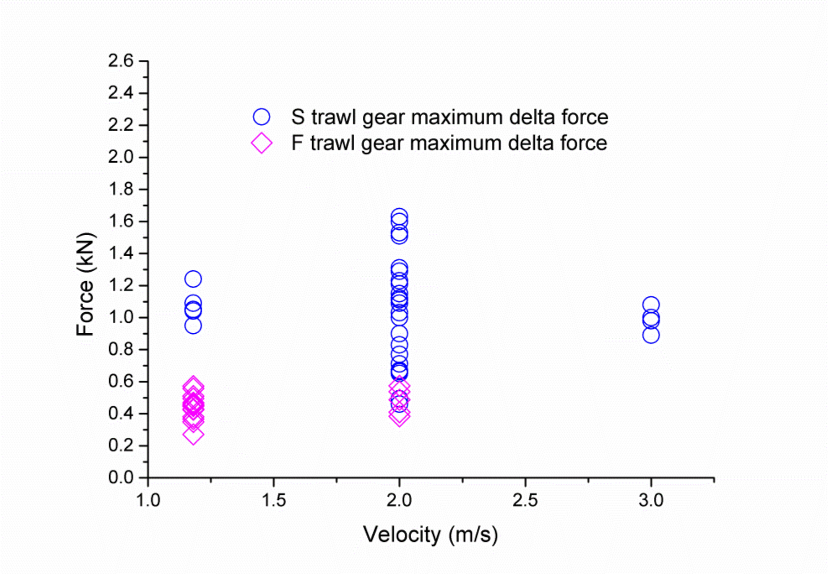

Figure 8-27 Maximum delta force versus velocity

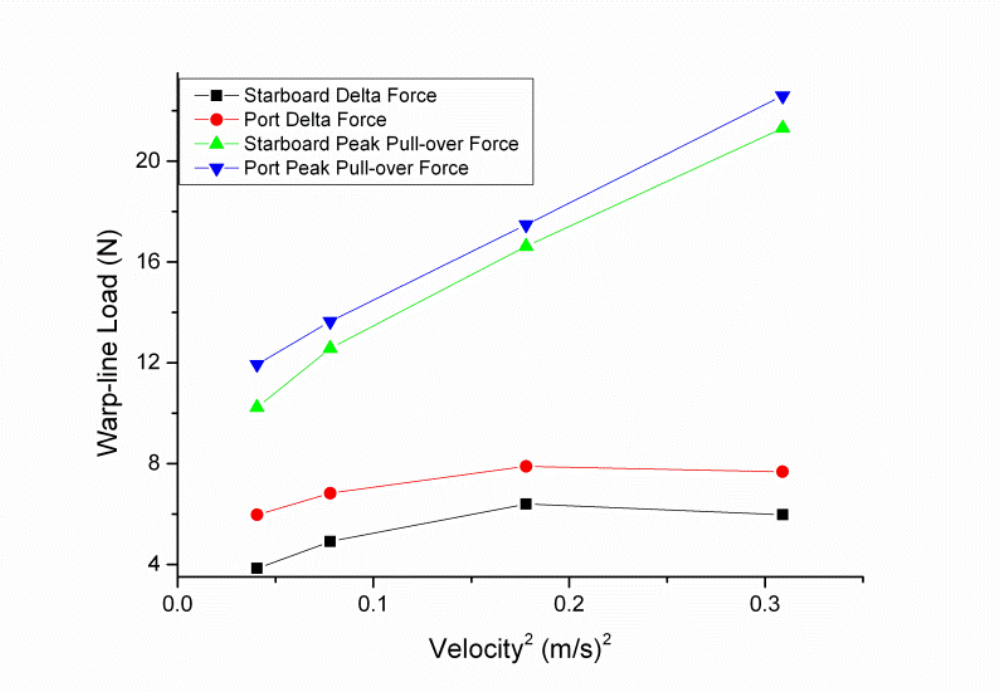

Figure 8-28 Warp force for Perfect door as a function of velocity^2 (JEE Ltd, 2003)

8.5 Parameter *V(MK)*$^{0.5}$

Together with the velocity *V*, the warp-line stiffness *K* and the trawl gear mass *M*, Verley (1992) suggested that the maximum pull-over force is proportional to $V\sqrt{MK}$. This is also the basis for the DNV formula (equation (8.2)). Palmer and Zheng (2014) pointed out “those equations predict that pull-over force is proportional to impact velocity, so that if the velocity is infinitesimally small, the pull-over force is also infinitesimally small. If the towing warp is very long, the warp stiffness *K* is very low and the pull-over force becomes small, another difficulty because it does not explain how the trawl gear “knows” the length of the warp that is pulling it. The coefficient C_F given in the RP is between 3 and 4 for beam trawls with hoop bars and between 3.5 and 5 without hoop bars, factors that are much greater than unity (which leaves unexplained where the additional kinetic energy that generated the increased force can have come from)”. C_F factor included here is to match the test data and however makes the forces predicted by the equations generally over-conservative.

The current test data are plotted in Figure 8-29. Maximum pull-over forces do show an increase manner versus the dimensionless group $V(MK)^{0.5}$. But this is seriously misleading.

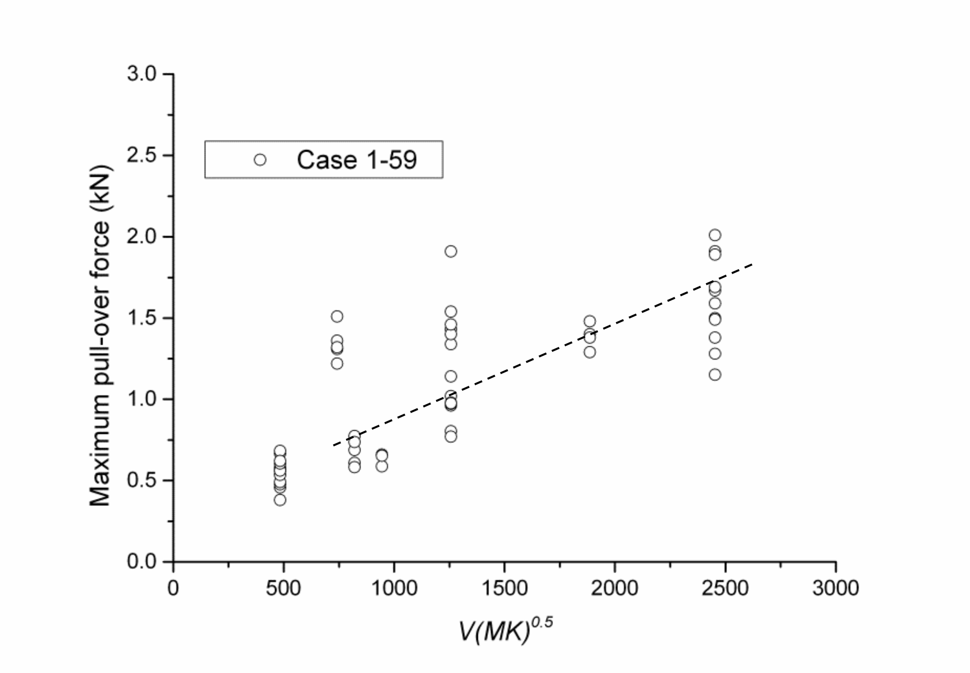

Figure 8-29 Maximum pull-over force versus $V(MK)^{0.5}$

The figure is re-drawn by separating the F trawl gear data and S trawl gear data as Figure 8-30 shows. For S trawl gear only or F trawl gear only, there is little increase trend shown. The increase shown in Figure 8-29 is mainly because of the weight of the trawl gear.

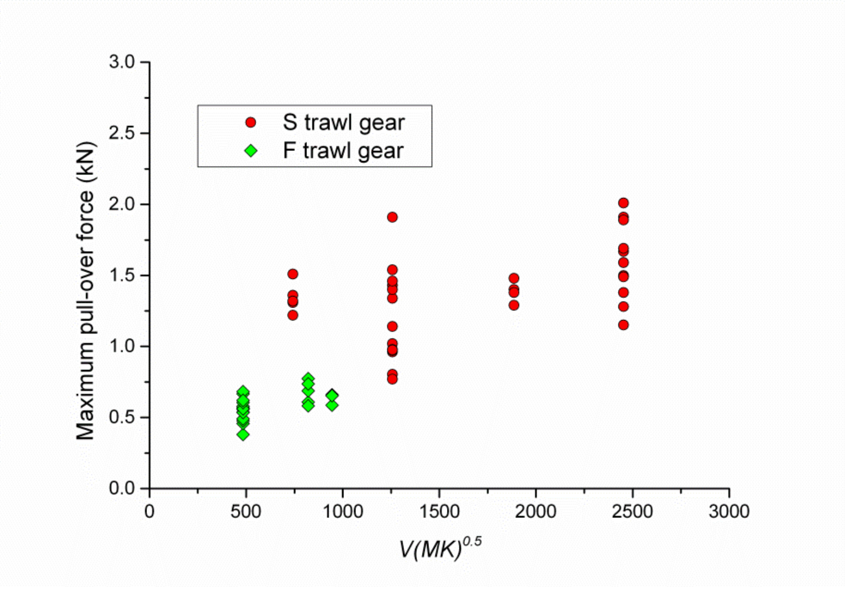

Figure 8-30 Maximum pull-over force versus $V(MK)^{0.5}$ of S and F trawl gear

A similar conclusion can be drawn from Figure 8-31. There is no indication of an increase of the delta force versus $V(MK)^{0.5}$ for S trawl gear or F trawl gear. As the only difference between the S trawl gear and the F trawl gear is the mass, the comparisons show the trawl gear weight is a critical parameter which largely influences the pull-over force.

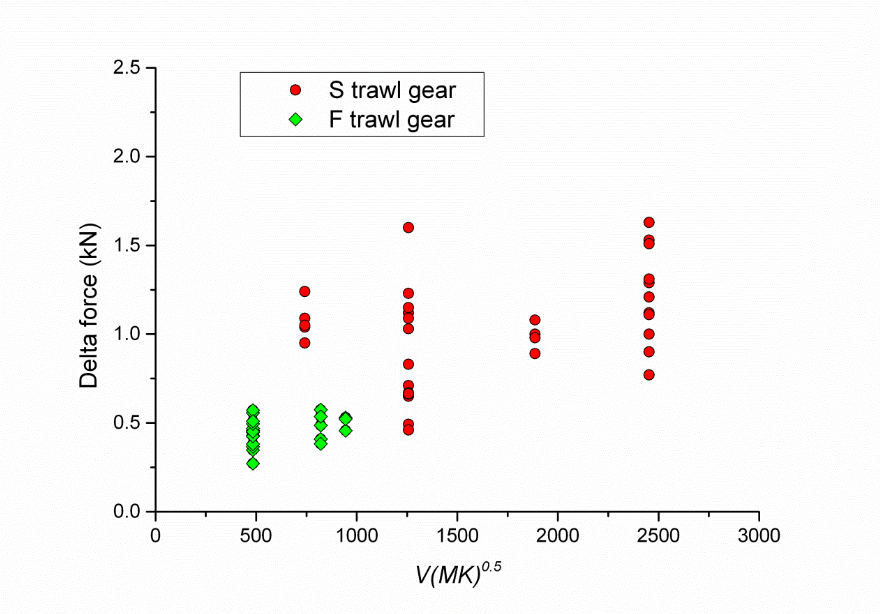

Figure 8-31 Delta force versus $V(MK)^{0.5}$ of S and F trawl gear

8.6 Proposed Model

8.6.1 Components of Warp-line Force

As mentioned in section 8.4.1, before the trawl gear impact the pipe, the warp-line force is the baseline force, which relates to the hydrodynamic force and the friction between the seabed and the trawl gear. When the trawl gear crosses the pipe, the warp-line force is the pull-over force, which is the sum of the baseline force and the delta force.

The delta force is complicated and consists of more than one component. The trawl gear impacts the pipeline first, and then is pulled over the pipeline. Though it is named “pull-over” force, the impact effect must inevitably be included in the delta force. As Palmer and Zheng (2014) indicated “If we idealise the collision as between a rigid mass moving with velocity *V* (representing the trawl gear) and a rigid, stationary and immovable pipeline, the effect is to generate an impulsive tension *F* in the towing warp, given by

$$F = V\sqrt{mK} \tag{8.3}$$

where m is the mass per unit length of the towing warp and *K* is the axial stiffness (axial force/axial strain) of the towing warp.

Note that *K* is not the same as the warp stiffness described in the RP, which has different dimensions. The impulsive increase of tension moves up the towing warp with velocity

$$c = \sqrt{\frac{K}{m}} \qquad (8.4)$$

……This corresponds to the impact component of the warp tension."

After impact, the trawl gear still needs to be lifted and rotated over the pipeline. As mentioned by Palmer and Zheng (2014), this component relates to the mass of the trawl gear, the dimensions of the trawl gear, the pipeline and the whole system. This component does not much relate to the velocity.

To sum up, there are at least three major components of the pull-over force. The first one is the baseline force, which includes the hydrodynamic force and the friction force, and is mainly velocity-dependent. The second component relates to the impact response, and it is velocity-dependent. The last component relates to the lift and rolling process, and it is not velocity-dependent. Though there are two components are velocity-dependent, it might not be a proportional relationship.

8.6.2 A Possible Scaling Law

As indicated in the previous section, there are three major components of the pull-over force, and they involve different mechanisms.

The baseline force is involved with the hydrodynamic force and the friction force, and associated with the period when the trawl gear does not interact with other obstacles. The fishing industry used the Froude scaling law to model the trawl gear and the fish nets. Ward (Ward and Ferro, 1992) studied the scaling law of trawl models, and compared a one tenth model with a full-scale prototype. The comparison showed there was a significant difference in the Reynolds number between the model and the full-scale for the net, but the Froude scaling law was still the most proper scaling law. The Froude scaling law can keep the model trawl gear moving the same way as the prototype. JEE Ltd (2003) did model tests on 1/10th scale mode and 1/18th scale model. The comparison of the baseline force between the two scale models showed the baseline force has scaled in accordance with expectation between 1/10th and 1/18th scale.

The last component relates to the lift and rolling process. It is little involved with velocity, and can be seen as velocity-independent. This is kind of a static response, and obeys the geometric similarity. When the model force is scaled up, the model force should be multiplied by λ^3. This is not distorted by the Froude scaling law if there is geometric similarity.

However, the component related to the impact will be distorted by the Froude scaling law. One possibility is to compromise and to maintain the most important factors. There are two most important factors: the impact energy and the ratio of the hydrodynamic force and gravity. The ratio of the hydrodynamic force and gravity is shown in Equation (8.5).

$$\frac{\frac{1}{2}\rho V^2}{Mg} = \frac{\frac{1}{2}\rho\beta^2 v^2}{mg} \tag{8.5}$$

The other factor is the kinetic energy. To keep the kinetic energy following the dimensional analysis, it has to follow the Equation (8.6).

$$\beta^3 \cdot \frac{MV^2}{2} = \frac{mv^2}{2} \tag{8.6}$$

In this test program, the maximum trawl gear is with the prototype mass M of 5351 kg, and the prototype velocity V of 3.4 m/s. The dimensions follow the scale factor β=*1/8.3*. When $v = 2\,m/s\ , m = 27kg$, Equations (8.5) and (8.6) are both satisfied. If the material is the same, the weight should be 9.36 kg instead of 27 kg. One way to change the weight but keep the geometries is to change the material, if the material property is not important. However, it is very difficult to find a material whose density is much larger than steel. For this case, keeping the dimension of the trawl gear but changing the weight is achieved by changing the hollow section beam to a solid bar. This corresponds to the case of the S trawl beam moving at 2 m/s. Then the prototype dynamic force changes in the following way.

Response time: $\frac{T}{t} = \frac{L}{c} \cdot \frac{c}{l} = \frac{1}{\beta}$

Dynamic force: $\frac{\frac{M\Delta}{T^2}}{\frac{m\delta}{t^2}} = \frac{M}{m} \cdot \beta * \frac{V}{v}$

The model test method changes to two steps: the first step is to scale the pull-over response by Froude scaling law, and scale up the baseline force based on Froude scaling law. Then do another set of tests based on the compromise scaling law, and scale the delta force based on that. The prototype pull-over force is the sum of the two parts.

This strategy had been applied to study the ship resistance by model tests. When a ship is moving in the water, the resistant force mainly contains two parts: the wave making resistance and the frictional resistance. The wave making resistance follows the Froude number, whereas the frictional resistance follows the Reynolds number. It is impossible to satisfy both. Therefore, the model test is based on the Reynolds number, and the wave making resistance force is separated and scaled up. The frictional resistance can be calculated and added together with the wave making resistance from the model test. This strategy has the same idea as the current proposed one, though the current model test is more complicated.

For example, for specimen PIPAB, the first set of the test is PIPAB-FDF1-1-90, PIPAB-FDF1-2-90 and PIPAB-FDF1-3-90. Their test data are shown in Figure 8-32. The average baseline force is 0.11kN, and prototype baseline force based on Froude scaling law is 62.90 kN. The average pull-over force is 0.53 kN, and the prototype pull-over force based on Froude scaling law is 304.57 kN.

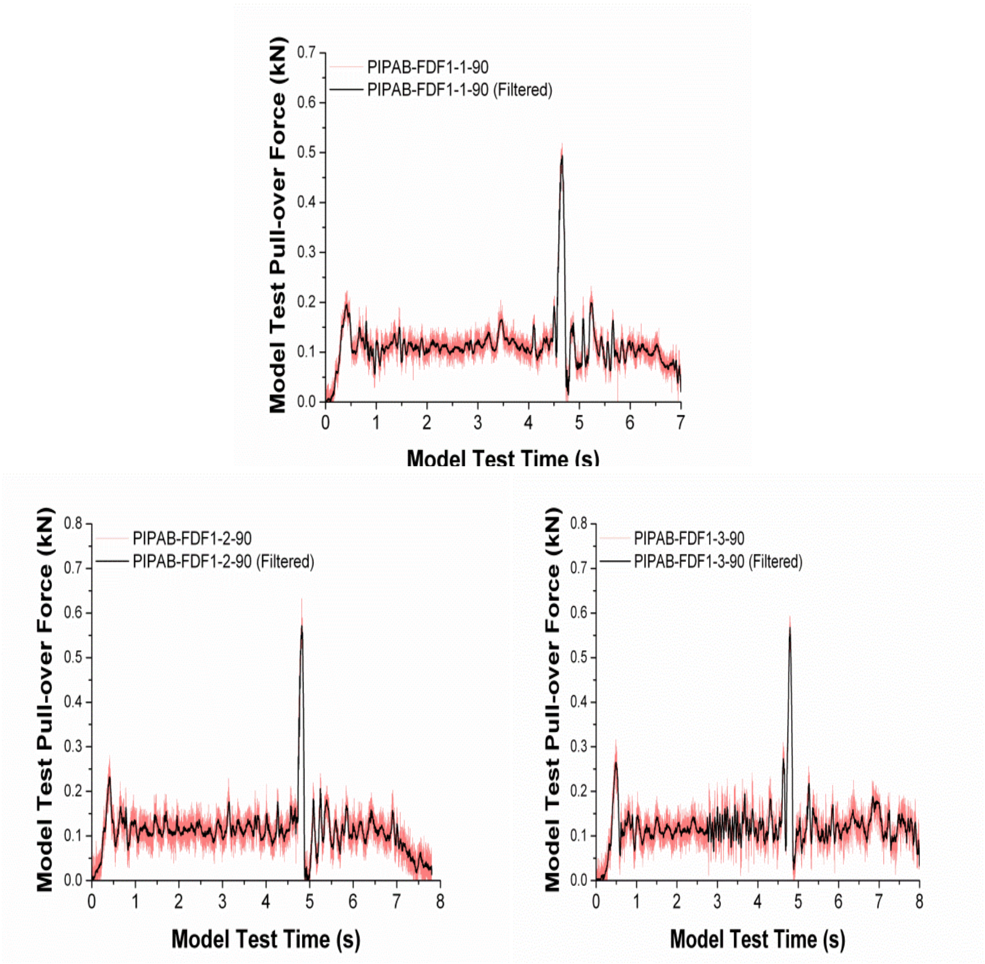

Figure 8-32 Model test of PIPAB scaled by Froude scaling law

Another set of test for PIPAB is PIPAB-FDS2-1-90, PIPAB-FDS2-2-90 and PIPAB-FDS2-3-90. Their test results are presented in Figure 8-33. The average delta force there is 2.812 kN, and the prototype delta force is 112.75 kN. Therefore, by adding the prototype baseline force 62.90 kN, the prototype pull-over force based on the compromised scaling law is 175.65 kN. This is 42% less than the prototype pull-over force scaled by the Froude scaling law. If this is right, it explains the reason why DNV’s method is conservative. However, a field test is needed to prove the result.

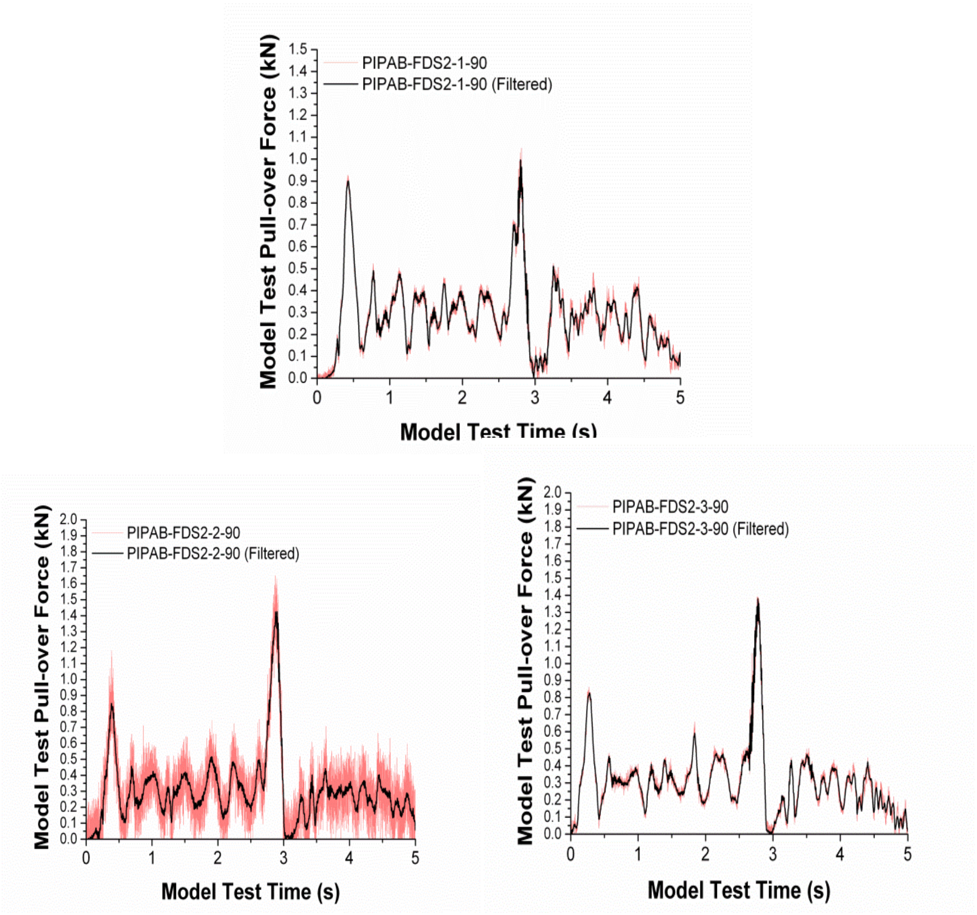

Figure 8-33 Model test of PIPAB scaled by Froude scaling law

8.7 Summary

In this chapter, the pull-over test results are analyzed, and the discussions based on the test data are presented The major contributions of this chapter are:

1. Pipe-in-pipes with 14 inch (355.6 mm)diameter has little difference compared to single wall pipes 16 inch (406.4 mm) in diameter. According to the test data, the 14 inch (355.6 mm) pipe-in-pipe and the 16 inch (406.4 mm) single wall pipe generate the pull-over forces in the same range. No obvious damages are found for both pipes. With different spacing, and different pipe's flexibility, the pull-over force

varies. The results increase the possibility of laying a 14 inch (355.6 mm) pipe-in-pipe on the seabed.

2. Though no one can fully convince people that Froude scaling law is absolutely correct, it is still the conventional way used in the industry. In order to compare with other works, prototype pull-over forces are calculated based on Froude scaling law. Comparison between DNV-RP-F111 and some field test data shows the test results are in a reasonable range, as they are all based on Froude scaling law.
3. Parametric studies show that the pull-over force will increase when the trawl gear mass increases, the warp-line stiffness increases, the pipe's diameter increases, or the pipe's stiffness increases.
4. The Froude scaling law is a proper way to scale the trawl gear's movement, but it is not suitable for the response of interaction of trawl gear and pipeline. In other words, the baseline force can be scaled and calculated by the Froude scaling law, but not the delta force.
5. The pull-over force has a more complicated relationship with the pulling velocity, and the maximum pull-over forces or the delta forces do not show a proportional relationship to the velocity, which is different from DNV-RP-F111.
6. The theory that the pull-over force consists of three major components is proposed. The three major components include the baseline force component, the component relates to the impact response and the component relates to the trawl gear to be lifted and roll over the pipeline. The three components relate to different mechanisms

respectively, and therefore should be scaled differently. If scaled by the Froude scaling law, the component relates to the impact response is distorted. Therefore, the Froude scaling law should be used with great caution.

7. A possible scaling law is proposed, which is a compromise between the Froude scaling law and the impact scaling law. This requires a different treatment of the weight of the trawl gear, and sometimes it is not feasible.

9 Conclusion and Future Work

9.1 Conclusion

The main contribution of this research is the development of new methodologies that can be applied to analyze the overtrawlability of pipe-in-pipes, a topic that has not been studied or included in any of the design codes. A correct estimate of overtrawlability is important because a rational trenching decision is based on it. The overtrawlability of pipe-in-pipes can be analyzed by the semi-empirical relationships, the newly developed FE models, and model tests. In this study, a pipe-in-pipe with 14 inch (355.6 mm) outer diameter and a pipe-in-pipe with 12 inch (323.85 mm) outer diameter are studied, and the conclusion is that the pipe-in-pipe with outer diameter less than 16 inch (406.4 mm) can be laid on the seabed without trenching. This conclusion offers the opportunity to avoid unnecessary trenching and eliminate over-conservatism.

Beside the methods that are developed for pipe-in-pipe, the methods for the single wall pipe are also improved in this research. The external pressure is considered in the indentation process by newly developed FE models, which have not been considered before. The external pressure not only decreases the pipe’s resistance to the indentation force, but also alters the failure mode. The combination of the internal pressure, external pressure and indentation is studied as well by using the new FE models, which offer methods for the engineer to make informed critical decisions. In addition, semi-empirical methods are improved. The maximum force can be estimated for three-point loading on a simply supported tube. The understanding of the relationship between indentation force and displacement is improved by considering local deformation and global deformation together instead of treating them separately. Moreover, the method of the pull-over model test has been investigated, and possible improvements of the experimental method and the scaling law are suggested.

Parts of the work have already been published as listed:

1. ZHENG, J., PALMER, A. C., LIPSKI, W. & BRUNNING, P. Impact damage on pipe-in-pipe systems. Twenty-second International Offshore and Polar Engineering Conference, 2012 Rhodes, Greece.
2. ZHENG, J., PALMER, A. & BRUNNING, P. 2013. Overtrawlability and Mechanical Damage of Pipe-in-Pipe. Journal of Applied Mechanics, 81, 031006-1-031006-11.
3. Zheng, J., Palmer, A.C., Brunning, P., Gan, C. T. (2014). "Indentation and external pressure on subsea single wall pipe and pipe-in-pipe." Ocean Engineering 83(0): 125-132.
4. Zheng, J., Palmer, A.C., et al. (2014). Method to Assess the Overtrawlability of Pipe-in-Pipe. Offshore Technology Conference Asia. 2014 Kuala Lumpur.
5. Palmer, A.C., Zheng, J., et al. (2014). "Fishing trawl pull-over across pipelines." Journal of Pipeline Engineering 13(1).

9.2 Future Work

The current research shows the possible advantage of pipe-in-pipe, and shows the small diameter pipe-in-pipe to have advantages. This research is only the beginning and it opens up more possibilities for future work.

First of all, the way to treat the trawl gear crossing response as two separate parts, impact and pull-over, needs more consideration. Obviously, the impact force also induces global deformation, and the pull-over force measured on the warp-line includes the impact response as well, as indicated in the current research. The three-point knife edge indentation problem can be solved, but how it can apply to the real situation of trawl gear crossing still needs further study. The boundary conditions in the field and the features of the trawl gear crossing problem need to be included in solving this problem. It might be that when the pipeline has a concrete coating, the impact response is more localised and more isolated from the pull-over response, but this needs to be clarified by future research.

Secondly, future work may include other types of trawl gear, such as trawl board or clump weight, since the current pull-over model test only considers beam trawls. The test set-up and instrumentations could be improved to measure more results. Hooking is not studied here, but it might be the most dangerous case. Future work could look more on this issue and study how to avoid hooking. The pull-over induced lateral buckling for pipe-in-pipe is also worthwhile to be looked into as this situation is more complicated for pipe-in-pipes, since the inner pipe is under high temperature and high pressure but the outer pipe is not.

The scaling issue should be continuously looked into until evidences are sufficient to confirm the optimal choice of scaling law. Moreover, the method to treat the distortion in the model test should be developed at the same time. The new scaling law for the model test proposed in the current research needs a corresponding full scale test to validate. Possibly, this can be studied by numerical experiments too if the numerical modelling methods can be verified. Firstly, model tests are conducted. Then FE models are built based on the model tests and verified against the model test data. After that, a full scale FE model is built based on the developed FE methodology. The FE data are scaled up and compared with the full scale FE results. The advantage of this is to avoid the statistical uncertainty. However, as this interaction is so complicated, building a correct FE model which can correctly simulate all the mechanism involving is not an easy job. Might be a quasi-static pull-over test can be informative to study the different mechanism although it is unrealistic.

More efforts can be used to include the effect of the external pressure in the impact response. The current research proved that the external pressure has an effect on the impact response, and that it helps the trawl to indent the pipe. This effect has been ignored and leads to a non-conservative estimate. Therefore, the external pressure should be included when estimate the impact response of the outer pipe of the pipe-in-pipe.

Last but not least, the design criteria for the outer pipe of the pipe-in-pipe should be established, instead of using the same criteria as for the single wall pipe. If using the same criteria for the outer pipe of the pipe-in-pipe, the advantage of the pipe-in-pipe is not so clear. Current research has only looked at the aspects of collapse and buckling that the outer pipe might suffer from when the dent depth is large. There might be other aspects which influence the operation and therefore influence the design criteria of the outer pipe. More work is needed in order to finalize the design criteria for the outer pipe.

References

ALEXANDER, C. 2007. Assessing the effects of impact forces on subsea flowlines and pipelines. *ASME Conference proceedings,* 2007**,** 417-427.

AMDAL, L. W., RØNEID, S. & ETTERDAL, B. 2011. Optimized design of pipelines exposed to trawl pull-over. *Proceedings of the twenty-first International Offshore and Polar Engineering Conference***,** 130-134.

ASKHEIM, D. O. & FYRILEIV, O. 2006. New design code for interference between trawl gear and pipelines: DNV RP-F111. *ASME Conference Proceedings,* 2006**,** 81-93.

BAI, Y. & BAI, Q. 2005. *Subsea pipelines and risers*, Elsevier.

BERGAN, P. G. & MOLLESTAD, E. 1982. Impact—response behavior of offshore pipelines. *Journal of Energy Resources Technology,* 104**,** 325-329.

BROOKER, D. C. 2005. Experimental puncture loads for external interference of pipelines by excavator equipment. *International Journal of Pressure Vessels and Piping,* 82**,** 825-832.

CALLADINE, C. 1983. An investigation of impact scaling theory. *Structural Crashworthiness.* 1st International Symposium held at University of Liverpool: Butterworth-Heinemann Ltd.

CORDER, I. & CHATAIN, P. 1995. EPRG recommendation for the assessment of the resistance of pipelines to external damage. *Paper Number 12.* The European Pipeline Research Group.

COSHAM, A. & HOPKINS, P. 2001. A new industry dcument detaling best practices in pipeline defect assessment. *Fifth International Onshore Pipeline Conference.* Amsterdam, The Netherlands.

COSHAM, A. & HOPKINS, P. 2002. The pipeline defect assessment manual. *In:* IPC2002, P. O. (ed.) *International pipeline conference.* Calgary, Alberta, Canada.

COSHAM, A. & HOPKINS, P. 2004. The effect of dents in pipelines——guidance in the pipeline defect assessment manual. *International Journal of Pressure Vessels and Piping***,** 127-139.

DE OLIVEIRA, J., WIERZBICKI, T. & ABRAMOWICZ, W. 1982. Plastic behaviour of tubular members under lateral concentrated loading.

DERUNTZ & HODGE 1963. Crushing of a tube between rigid plates. *Journal of Applied Mechanics,* 30**,** 391.

DNV, D. N. V. 2010. Interference between trawl gear and pipelines. *Recommended Practice DNV-RP-F111.*

DNV, D. N. V. 2013. Offshore standard DNV-OS-F101. *Submarine pipeline systems.*

ELLINAS, C. P. & WALKER, A. C. 1983. Damage on offshore tubular bracing members.

EMESUM, J. C. 2013. *Full scale trawl board impact testing in water.*

ENDAL, G. & WILLIAMS, K. A. 1998. The gullfaks satellites project: reel installation of 6”/10” pipe-in-pipe flowline. *OMAE98, 17th International Conference On Offshore Mechanics and Arctic Engineering.* Lisbon Portugal.

ESPINER, R., KAYE, D., GOODFELLOW, G. & HOPKINS, P. 2008. Inspection & assessment of damaged subsea pipelines: a case study. *7th International Pipeline Conference.* Semptermber, 29-October 3, 2008, Calgary, Alberta, Canada.

FYRILEIV, O., ASKHEIM, D. O., VERLEY, R. & ROLSDORPH, H. 2006. Pipeline-trawl interaction: effect of trawl clump weights. *ASME Conference Proceedings.* ASME.

FYRILEIV, O. & SPITEN, J. Trawl gear protection within platform safety Zones. 23rd International Conference on Offshore Mechanics and Arctic Engineering, 2004 Vancouver, British Columbia, Canada. 7.

FYRILEIV, O., SPITEN, J., MELLEM, T. & VERLEY, R. 1997. DNV'96, acceptance criteria for interaction between trawl gear and pipelines. *proceedings of the international conference on offshore mechanics and arctic engineering***,** 91-98.

G. HORENBERG, J. & GUIJT, J. 1987. An analytical and experimental analysis of trawl gear-pipeline interaction. *In:* CONFERENCE, O. T. (ed.) *Offshore Technology Conference.* Houston, Texas

GJØRSVIK, O., KJELDSEN, S. & LUND, S. Influence of bottom trawl gear on submarine pipelines. Offshore Technology Conference, 1975.

GUIJT, N. & HORENBERG, J. 1987a. Recent investigations concerning the effect of bottom trawl gear crossings on submarine pipeline integrity. *Offshore Technology Conference.* Houston, Texas Offshore Technology Conference.

GUIJT, N. & HORENBERG, J. Recent investigations concerning the effect of bottom trawl gear crossings on submarine pipeline integrity. 1987b.

HAGIWARA, H. & OGUCHI, N. 1999. Fatigue behavior of line pipes subjected to severe mechanical damage. *Journal of Pressure Vessel Technology,* 121**,** 6.

HERLIANTO, I. 2011. *Lateral buckling induced by trawl gears pull-over loads on high temperature/ high pressure subsea pipeline.* Master, University of Stavanger.

HERLIANTO, I., CHEN, Q. & KARUNAKARAN, D. 2012. Lateral buckling induced by trawl gears pull-over loads on high temperature/high pressure subsea pipeline. *ASME 2012 31st International Conference on Ocean, Offshore and Arctic Engineering.* Rio de Janeiro, Brazil,.

HIBBITT, KARLSSON & SORENSEN 2001. *ABAQUS/Standard: user's manual*, Hibbitt, Karlsson & Sorensen.

HIBBITT, KARLSSON & SORENSEN 2011. *Abaqus/CAE user's manual version 6.11*, Hibbitt, Karlsson & Sorensen, Inc.

HOPKINS, P. & CORBIN, P. 1988. A study of external damage of pipelines. *7th AGA/EPRG Joint Biennial Technical Meeting on Linepipe Research.* Calgary.

HOPKINS, P., CORDER.I & CORBIN, P. 1992. The resistance of gas transmission pipelines to mechanical damage. *International Conference on Pipeline Reliability.* Calgary.

HOPKINS, P., JONES, D. G. & CLYNE, A. 1983. Recent studies of the significance of mechanical damage. *The American Gas Association and European Pipeline Research Group Research Seminar V.* San Francisco, USA.

HOPKINS, P., JONES, D. G. & CLYNE, A. 1988. The significance of dents in transmission pipelines. *Pipework, Engineering&Operation.* Institution of Mechanical Engineers, London.

IGLAND, R. T. & SOREIDE, T. 2008. Advanced pipeline trawl gear impact design. *ASME Conference Proceedings,* 2008**,** 271-277.

JEE LTD 2003. Overtrawling large diameter pipelines flume tank tests - interpretive report.

JOHNSEN, I. B. 2013. *Clump-weight trawl gear interaction with submarine pipelines.* Norwegian University of Science and Technology.

JONES, D. G. & HOPKINS, P. 1983. The influence of mechanical damage on transmission pipeline integrity. *IGU 1983 International Gas Reserach Conference.* London.

JONES, N. 2012. *Structural impact seond edition,* Cambridge Univ Pr.

JONES, N. & BIRCH, R. S. 1996. Influence of Internal Pressure on the Impact Behavior of Steel Pipelines. *Journal of Pressure Vessel Technology,* 118**,** 464-471.

JONES, N., BIRCH, S. E., BIRCH, R. S., ZHU, L. & BROWN, M. 1992. An experimental study on the lateral impact of fully clamped mild steel pipes. *Proceedings of the Institution of Mechanical Engineers, Part E: Journal of Process Mechanical Engineering 1989-1996 (vols 203-210),* 206**,** 111-127.

JONES, N. & SHEN, W. Q. 1992. A theoretical study of the lateral impact of fully clamped pipelines. *Proceedings of the Institution of Mechanical*

Engineers, Part E: Journal of Process Mechanical Engineering 1989-1996 (vols 203-210), 206**,** 129-146.

KARAMANOS, S. A. & ANDREADAKIS, K. P. 2006. Denting of internally pressurized tubes under lateral loads. *International Journal of Mechanical Sciences,* 48**,** 1080-1094.

KONUK, I., FREDJ, A. & YU, S. 2005. 3-Dimensional bifurcations of pipe-in-pipe structures. *ASME Conference Proceedings*, 2005**,** 747-753.

KORMI, K. & WEBB, D. C. 1993. Use of the fem to evaluate the response of damaged pipes: part 1 - static loading. *The Pressure Vessels and Piping Conference.* Denver, CO, USA.

KRISTOFFERSEN, A. S., ASKLUND, P. O. & NYSTRØM, P. R. 2012. Pipe-in-pipe global buckling and trawl design on uneven seabed. *Twenty-second (2012) International Offshore and Polar Engineering Conference.* Rhodes, Greece.

KYRIAKIDES, S. & CORONA, E. 2007a. *Mechanics of offshore pipelines,* Elsevier.

KYRIAKIDES, S. & CORONA, E. 2007b. *Mechanics of offshore pipelines: Buckling and collapse*, Elsevier Science.

LANCASTER, E. R. & PALMER, S. C. 1992. Modal testing of mechanically damaged pipes containing dents and gouges. *Design and anlysis of pressure vessles, piping, and components,* 235**,** 143-148.

LANCASTER, E. R. & PALMER, S. C. 1993. Assessment of mechanically damaged pipes containing dents and gouges. *Service Experience and Life Management: Nuclear, Fossil, and Petrochemical Plants,* 261**,** 61-68.

LANCASTER, E. R. & PALMER, S. C. 1994. *Experimental study of strains caused by pressurisation of pipes with dents*, Cupertino, CA, ETATS-UNIS, International Society of Offshore and Polar Engineers.

LANCASTER, E. R. & PALMER, S. C. 1996a. Burst pressure of pipes containing dents and gouges. *Proc Instn Mech Engrs,* 210**,** 19-27.

LANCASTER, E. R. & PALMER, S. C. 1996b. Strain concentrations in pressurized dented pipes. *Proc Instn Mech Engrs,* 210**,** 29-38.

LIU, J. H. & FRANCIS, A. 2004. Theoretical analysis of local indentation on pressured pipes. *International Journal of Pressure Vessels and Piping,* 81**,** 931-939.

LONGVA, V. 2010. *Simulation of trawl loads on subsea pipelines.* Master, Norwegian University of Science and Technology.

LONGVA, V. & SÆVIK, S. 2012. A penalty-based body-pipeline contact element for simulation of pull-over events. *ASME 2012 31st International Conference on Ocean, Offshore and Arctic Engineering.* Rio de Janeiro, Brazil.

LONGVA, V. & SÆVIK, S. 2013. A penalty-based contact element for pipe and 3D rigid body interaction. *Engineering Structures,* 56**,** 1580-1592.

LONGVA, V., SÆVIK, S., LEVOLD, E. & ILSTAD, H. 2013. Dynamic simulation of subsea pipeline and trawl board pull-over interaction. *Marine Structures,* 34**,** 156-184.

LONGVA, V., SAEVIK, S., LEVOLD, E., ILSTAD, H. & TEIGEN, P. 2011. Dynamic simulation of free-spanning pipeline trawl board pull-over. *ASME Conference Proceedings,* 2011**,** 561-568.

MAALØ, K., ALSOS, H. S. & SÆVIK, S. 2010. Detailed analysis of clump-weight interference with subsea pipelines. *ASME 2012 31st International Conference on Ocean, Offshore and Arctic Engineering.* Rio de Janeiro, Brazil.

MALVAR, L. J. 1998. Review of static and dynamic properties of steel reinforcing bars. *ACI Materials Journal,* 95.

MELLEM, T., SPITEN, J., VERLEY, R. & MOSHAGEN, H. 1996. Trawl board impacts on pipelines *The 1996 15th International Conference on Offshore Mechanics and Arctic Engineering.* Florence, Italy.

MORRIS, A. J. 1971. Experimental investigation into the effects of indenting a cylindrical shell by a load applied through a rigid boss. *Journal of Mechanical Engineering Science,* 1959-1982 (vols 1-23)**,** 36-46.

MOSHAGEN, H. & KJELDSEN, S. 1980. Fishing gear loads and effects on submarine pipelines. *Offshore Technology Conference.* Houston, Texas Offshore Technology Conference.

NG, C. & SHEN, W. 2006. Effect of lateral impact loads on failure of pressurized pipelines supported by foundation. *Proceedings of the Institution of Mechanical Engineers, Part E: Journal of Process Mechanical Engineering,* 220**,** 193-206.

NORSOK STANDARD 2002. Subsea production systems.

ONG, L. S. 1991. Derivation of stresses associated with a long axial dent in a pressurized cylinder. *International Journal of Mechanical Sciences,* 33**,** 115-123.

ONG, L. S., SOH, A. & ONG, J. 1992. Experimental and finite element investigation of a local dent on a pressurized pipe. *The Journal of Strain Analysis for Engineering Design,* 27**,** 177-185.

ONG, L. S., WING, C. Y. & SEET, G. 1989. The elastic analysis of a dent on pressurised pipe. *International Journal of Pressure Vessels and Piping,* 38**,** 369-383.

PALMER, ZHENG, J., BRUNNING, P. & LIM, G. 2014. Fishing trawl pull-over across pipelines. *Journal of Pipeline Engineering*.

PALMER, A., TOUHEY, M., HOLDER, S., ANDERSON, M. & BOOTH, S. 2006. Full-scale impact tests on pipelines. *International Journal of Impact Engineering,* 32**,** 1267-1283.

PALMER, A. C. & KING, R. A. 2008. *Subsea pipeline engineering,* Tulsa, Okla., PennWell Corporation.

PARK, T. D. & KYRIAKIDES, S. 1996. On the collapse of dented cylinders under external pressure. *International Journal of Mechanical Sciences,* 38**,** 557-578.

REID, S. & GOUDIE, K. 1989. Denting and bending of tubular beams under local loads. *Structural failure.*

REID, S. R. & REDDY, T. Y. 1978. Effect of strain hardening on the lateral compression of tubes between rigid plates. *International Journal of Solids and Structures,* 14**,** 213-225.

RINEHART, A. & KEATING, P. 2002. Predicting the fatigue life of long dents in petroleum pipelines. *21st International Conference on Offshore Mechanics and Artic Engineering.* Oslo, Norway: ASME.

SEAFISH 2005. Basic fishing methods.

SEAFISH, IFREMER & DIFTA 1995. Otterboard performance and behaviour.

SHEN, W. Q. & JONES, N. 1991. A comment on the low speed impact of a clamped beam by a heavy striker. *Mechanics of Structures and Machines,* 19**,** 527-549.

SONG, R., KANG, Z., QIN, Y. & LI, C. 2009. Pipeline bundle: a smart solution for infield transportation---part 1: overview and engineering design. *ASME Conference Proceedings,* 2009**,** 487-500.

SOREIDE, T. & AMDAHL, J. 1982. Deformation characteristics of tubular members with reference to impact loads from collosion and dropped objects. *Norwegian Maritime Research,* No.2**,** 3-12.

SRISKANDARAJAH, T. 2001. Dynamic versus static lateral buckling of subsea pipelines. *In:* ENGINEERS, T. I. S. O. O. A. P. (ed.) *The eleventh (2001) international offshore and polar engineering conference.* Stavanger, Norway.

TEIGEN, P., ILSTAD, H., LEVOLD, E. & HANSEN, K. 2009. Hydrodynamical aspects of pipeline overtrawling. *International offshore and polar engineering conference.* Osaka, Japan.

THOMAS, S. G., REID, S. R. & JOHNSON, W. 1976. Large deformations of thin-walled circular tubes under transverse loading--I: An experimental survey of the bending of simply supported tubes under a central load. *International Journal of Mechanical Sciences,* 18.

TREVOR JEE ASSOCIATES 1999. Guidelines for trenching design of submarine pipelines. *In:* EXECUTIVE, H. A. S. (ed.) *OTH561.*

VERLEY, R. 1994. Pipeline on a flat seabed subjected to trawling or other limited duration point loads. *The Proceedings of the International Offshore and Polar Engineering Conference,* 2**,** 128-134.

VERLEY, R., MOSHAGEN, B., MOHOLDT, N. & NYGAARD, I. 1992. Trawl forces on free-spanning pipelines. *International Journal of Offshore and Polar Engineering*, 2**,** 24-31.

WALKER, A. & KWOK, M. 1986. Process of damage in thin-walled cylindrical shells. *Advances in Marine Structures Conference.* Dunfermline, Scotland

WARD, J. N. & FERRO, R. S. T. 1992. A comparison of one tenth and full-scale measurements of the drag and geometry of a pelagic trawl. SEA FISH INDUSTRY AUTHORITY Seafish Technology, SOAFE Marine laboratory.

WIERZBICKI, T. & SUH, M. S. 1988. Indentation of tubes under combined loading. *International Journal of Mechanical Sciences*, 30**,** 229-248.

A. Appendix A Specimen Details

The specimens details are shown in table A-1 to A-3.

Table A-1 Single wall pipe specimens

	D-E (mm)	*t-E (mm)*	*Length(m)*
SPS1	88.9	5.49	1
SPS2	141.3	6.55	1.5
SPS3	101.6	5.74	1
SPS4	168.3	7.11	1.5

Table A-2 Two different type of pipe-in-pipe specimens

		D-E (mm)	*t-E (mm)*
PPSA	PPSA_In	88.9	5.49
	PPSA_Out	141.3	6.55
PPSB	PPS_In	101.6	5.74
	PPS_Out	168.3	7.11

Table A-3 Pipe-in-pine specimens

PIP Specimen	*Carrier Pipe*	*Inner Pipe*	*length (m)*	*Gap (mm)*	*Spacer ID (mm)*	*Spacer OD (mm)*	*Spacing (m)*	*Spacer (m)*
PPSA1	141.3	88.9	1.5	39.3	88.9	121	1	2
PPSA2	141.3	88.9	1.5	39.3	88.9	121	1.5	2
PPSA3	141.3	88.9	1.5	39.3	88.9	121	0.5	3
PPSB1	168.3	101.6	1.5	52.48	101.6	141.6	1	2
PPSB2	168.3	101.6	1.5	52.48	101.6	141.6	1.5	2
PPSB3	168.3	101.6	1.5	52.48	101.6	141.6	0.5	3

By changing the spacing and specimen length, three different specimens for each type are developed as Table A-3 shows. For instance, there are three different types for scaled pipe-in-pipe specimen PPSA. PPSA1 and PPSA2 aim to study the different spacings, therefore, the distances between the spacers of PPSA1 and PPSA2 are different. PPSA3 aims to study the case when the indenter hits the spacer vertically from the outer pipe. In order to have one spacer in the middle, three spacers will be installed in the specimen.

B. Appendix B Indenter Design

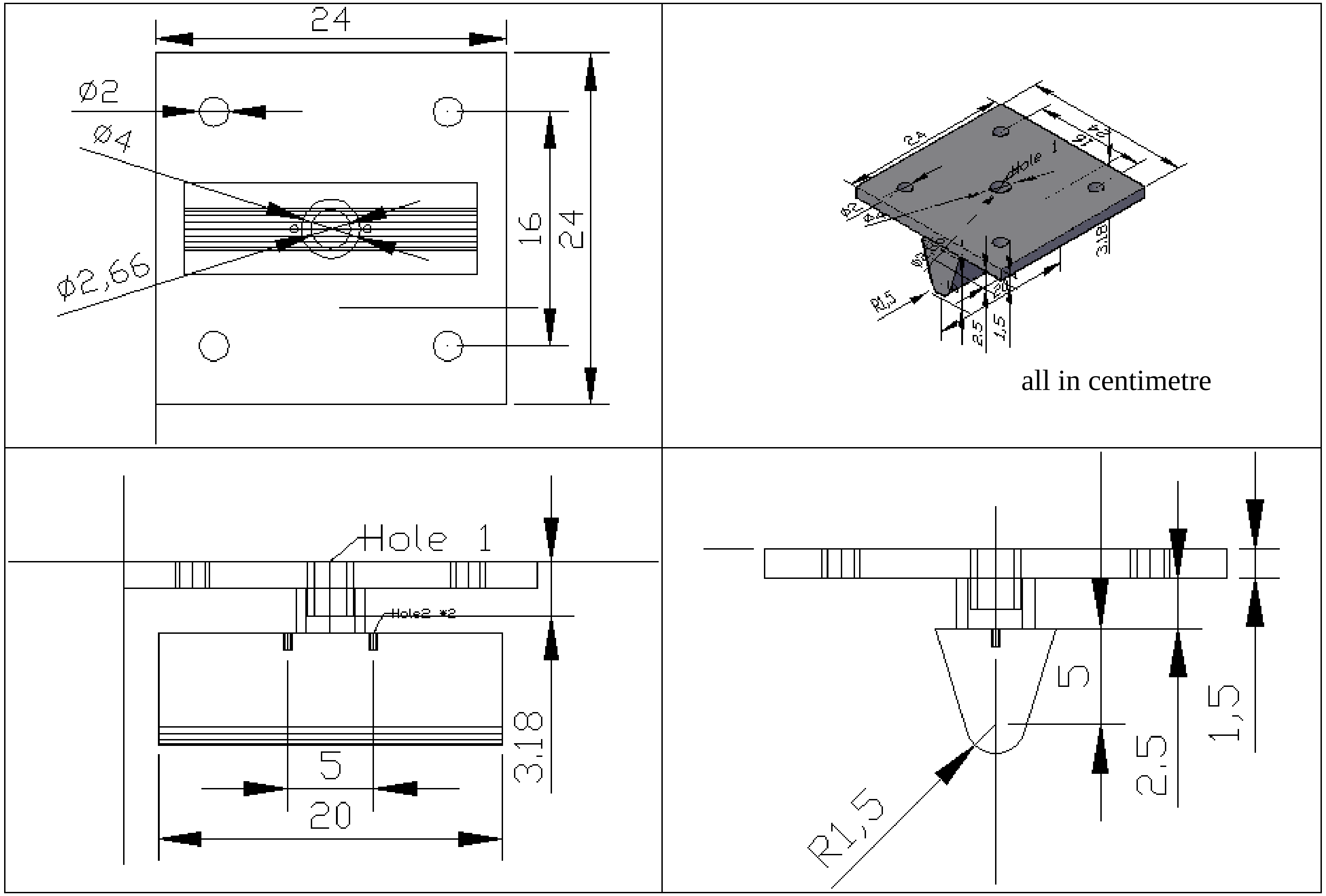
24
Ø2
Ø4
Ø2,66
16
24
Hole 1
3.18
R1,5
2,5
1,5
Hole 1
Hole2 *2
5
20
3.18
5
2,5
1,5
R1,5

all in centimetre

C. Appendix C Coupon Test Results

C.1 Coupons

The test specimens are cut longitudinally from the pipes. Based on ASEM E8/E8M, the specimen can be cut into the size shows in Figure C-1. Because the specimen has a curve, the pin-loaded type specimen is chosen.

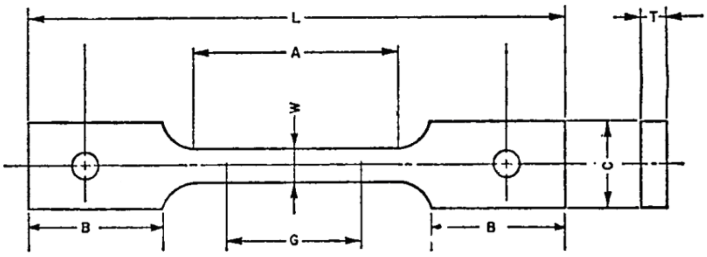

G (mm)	50	***L (mm)***	250
W (mm)	12.5	***T (mm)***	same
A (mm)	70	***B (mm)***	70

Figure C-1 Specimen Size

There are four different size pipes as Table C-1 shows. Two specimens are cut from every different type of pipe. Therefore, there are altogether eight specimens and four different sizes, the details shows in Table C-2.

Table C-1 Coupons for tensile test

Coupon	***Coupon***	***Cut from***
SPS1_A	SPS1_B	***SPS1***
SPS2_A	SPS2_B	***SPS2***
SPS3_A	SPS3_B	***SPS3***
SPS4_A	SPS4_B	***SPS4***

The loading rate is a key factor in tensile test. ASME E8/E8M requires that:

1. Unless otherwise specified, any convenient speed of testing maybe used up to one half of the specified yield strength or up to one quarter the specified tensile strength, whichever is smaller.

2. When determining yield properties, the rate of stress application shall be between 1.15 and 11.5 MPa/s.
3. When determining tensile strength, the strain rate is between 0.05 and 0.5 mm/mm/min.

Based on this requirement, after careful calculation and discussion with experienced people, in our experiment, 0.1mm/min is chosen to determine the yield properties, and 0.3 mm/min is chosen to determine the tensile strength. The transition from 0.1 to 0.3 mm/min should be slow.

During the experiment, the load cell records the tension load. Two strain gauges are attached to the specimen to measure the strain, and one extensometer is attached to the specimen to measure the strain throughout the process.

The procedure shows as follow.

1. Prepare specimen. Cut the pipe into specimen size as Figure C-1 shows, and clean the middle section, then attach the strain gauge on it.
2. Install the specimen to the universal test machine. Adjust the machine and the specimen to make sure the specimen is vertical there.
3. Attach the extensometer to the specimen.
4. Use the software to record the data.
5. Start the experiment. During the experiment, attention should be paid to the loading-deformation curve to avoid any accident.
6. After yield point, we can slightly increase the loading speed little by little until the specimen breaks.

C.2 Tensile Test Results

The stress-strain curve can be calculated by the recorded data. Based on the curve, the Young's modulus and yield stress is determined.

Test Result of SPS1

The stress-strain curve of SPS1_A and SPS1_B is shown in Figure C-2. Elastic part is used to determine the Young’s modulus. The Young’s modulus of SPS1 is 209.47 GPa.

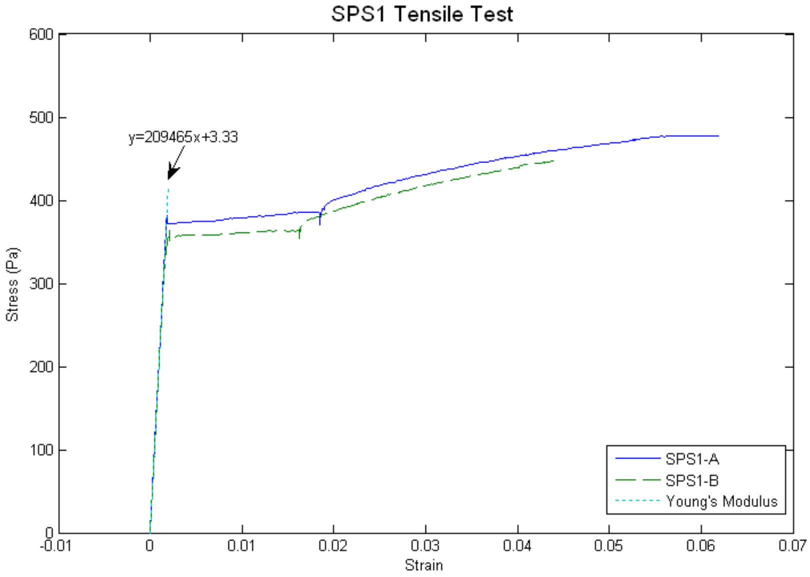

Figure C-2 SPS1 tensile test result

Test Result of SPS2

The stress-strain curve of SPS2_A and SPS2_B is shown in Figure C-3. The Young’s modulus of SPS2 is 202.64 GPa.

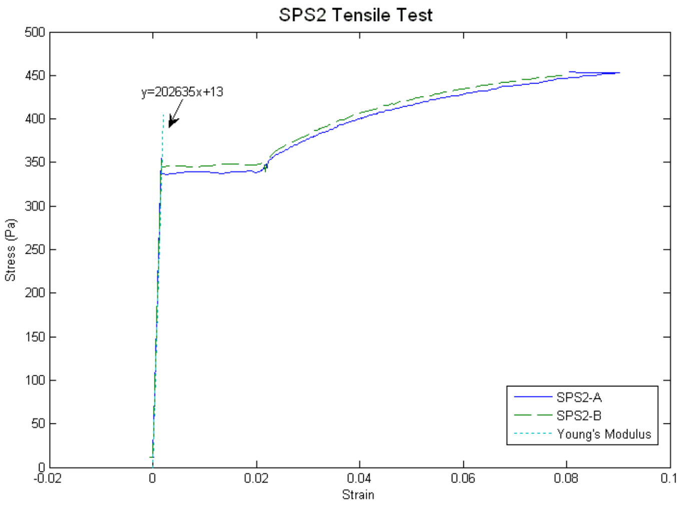

Figure C-3 SPS2 tensile test result

Test Result of SPS3

The stress-strain curve of SPS3_A and SPS3_B is shown in Figure C-4. The Young’s modulus of SPS3 is 209.39 GPa.

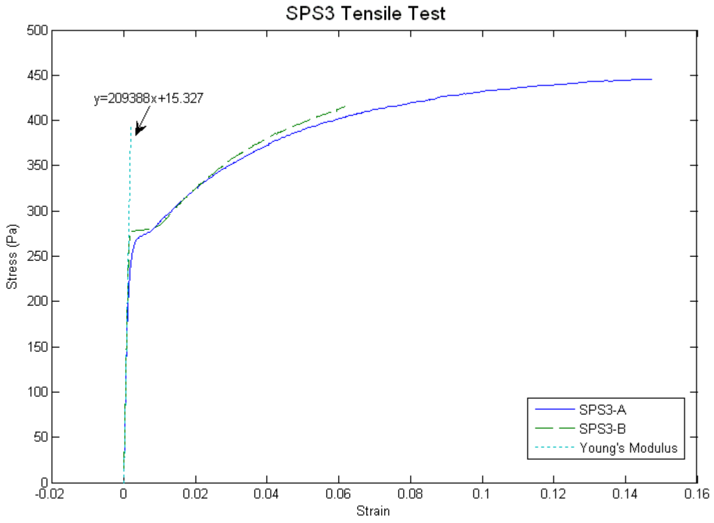

Figure C-4 SPS3 tensile test result

Test Result of SPS4

The stress-strain curve of SPS4_A and SPS4_B is shown in Figure C-5. The Young’s modulus of SPS4 is 200.98 GPa.

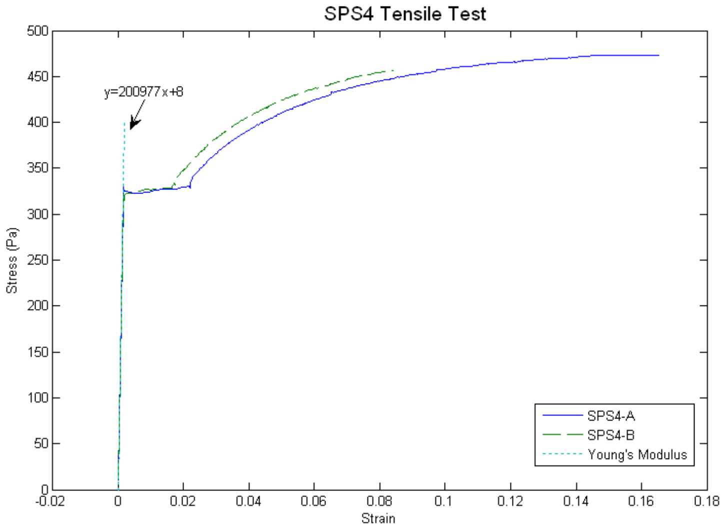

Figure C-5 SPS4 tensile test result

Yield stress is determined by the stress at 0.5% total strain. The yield stresses of four specimens are illustrated in Table C-2.

Table C-2 Tensile test results summary

Specimen	***Young's modulus (GPa)***	***Yield Stress (MPa)***
SPS1	209.47	342.38
SPS2	202.64	341.98
SPS3	209.39	275.58
SPS4	200.98	323.85

C.3 FE Modelling Material Property Input

Steel linear elastic behaviour is described by the Young’s modulus. The plastic behaviour is described by its yield point and hardening. The classical metal plasticity model in ABAQUS is adopted in the present simulation. This model uses standard von Mises yield criteria with associated plastic flow and isotropic hardening definitions. The classical metal plasticity model approximates and smoothes a stress-strain curve of the material after yield point with a series of straight lines joining the given data points. ABAQUS requires that the input stress-strain points should be true stress and true strain. Therefore, the data from the coupon tensile tests has to be calculated to true stress and true strain for ABAQUS material input.

The relationship between the true strain ϵ and the nominal strain $\varepsilon_{\mathrm{nom}}$ is:

$$\varepsilon = \ln(1 + \varepsilon_{\mathrm{nom}})$$

The relationship between the true stress σ and nominal stress σ_{nom} and nominal strain $\varepsilon_{\mathrm{nom}}$ is:

$$\sigma = \sigma_{\mathrm{nom}}(1 + \varepsilon_{\mathrm{nom}})$$

The relationship between the true plastic strain and true total strain is:

$$\varepsilon^{\mathrm{pl}} = \varepsilon^{\mathrm{t}} - \varepsilon^{\mathrm{el}} = \varepsilon^{\mathrm{t}} - \sigma/\mathrm{E}$$

(Hibbitt et al., 2011)

The nominal stress strain curves and true stress strain curves of four specimens in plastic rage are shown in Figure C-6 to Figure C-9. The stress unit is ‘Pa’ in these curves.

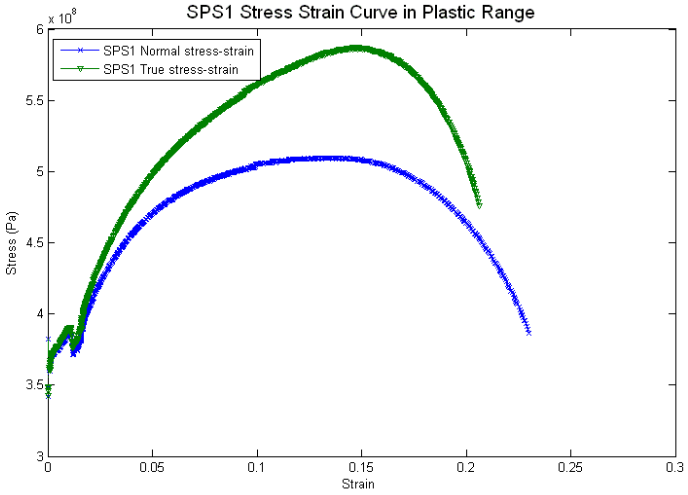

Figure C-6 SPS1 stress-strain curve in plastic range

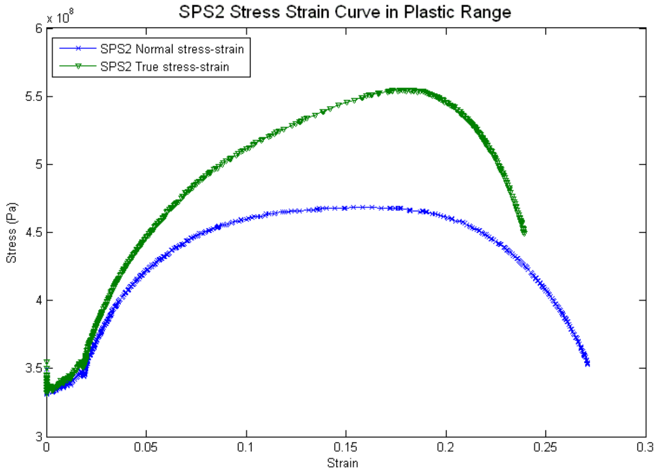

Figure C-7 SPS2 stress-strain curve in plastic range

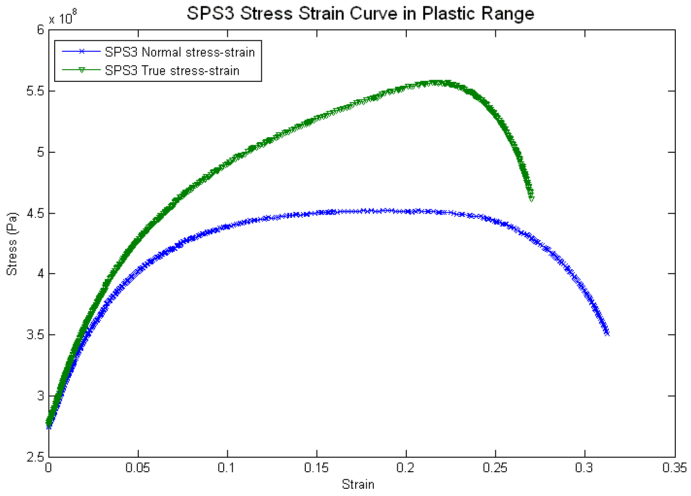

Figure C-8 SPS3 stress strain-curve in plastic range

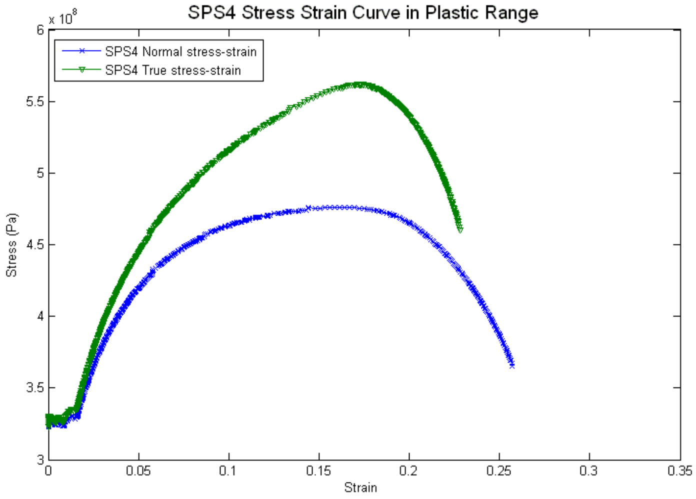

Figure C-9 SPS4 stress strain-curve in plastic range

D. Appendix D Test Specimen Details

Table D-1 Specimen details

All units are mm.

Name	Size	
SPSA	OD 26.9; t 1.6.	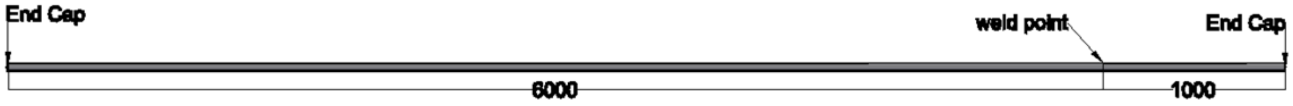 End Cap weld point End Cap 6000 1000
SPSB	OD 42.5; t 1.9.	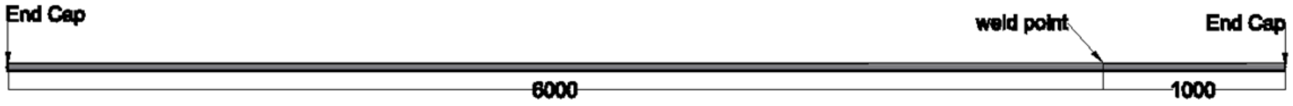 End Cap weld point End Cap 6000 1000
SPSC	OD 42.5; t 2.6.	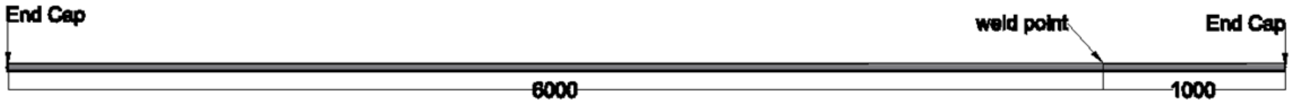 End Cap weld point End Cap 6000 1000

Name	Size	
SPSD	OD 48.4; t 2.9.	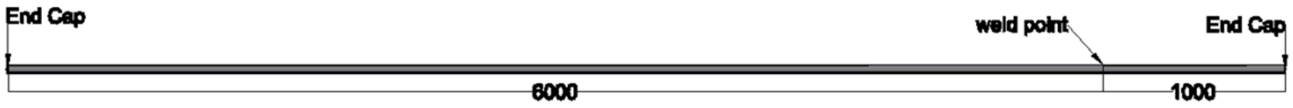 End Cap weld point End Cap 6000 1000
PIPAB	Inner pipe OD 26.9; t 1.6. Outer pipe OD 42.5; t 1.9. Spacer B ID 26.9; OD 36. Spacing 500.	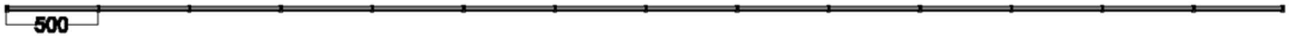 Inner pipe: with Spacer B (ID 26.9, OD 36) on, every 500. 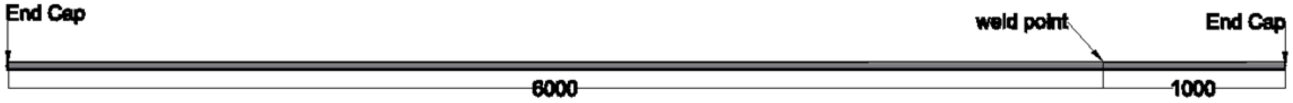 End Cap weld point End Cap 6000 1000 Outer Pipe
PIPAC	Inner pipe OD 26.9; t 1.6. Outer pipe OD 42.5; t 2.6. Spacer C ID 26.9; OD 35. Spacing 500.	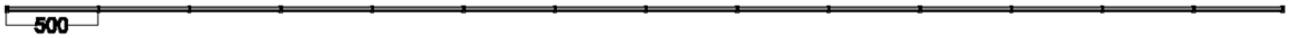 Inner pipe: with Spacer C (ID 26.9, OD 35) on, every 500. 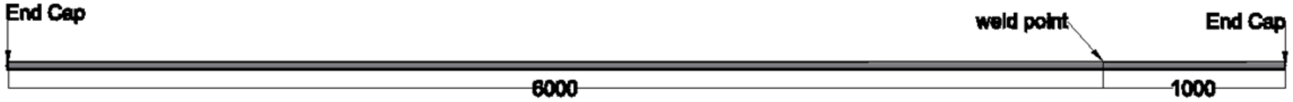 End Cap weld point End Cap 6000 1000 Outer Pipe

<table>
<tr><th>Name</th><th>Size</th><th></th></tr>
<tr><td>PIPAD</td><td>Inner pipe OD 26.9; t 1.6.
Outer pipe OD 48.4; t 2.9.
Spacer D ID 26.9; OD 40.
Spacing 500.</td><td>
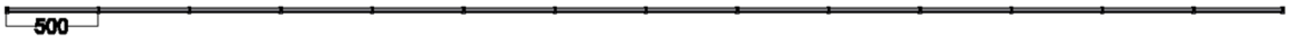

Inner pipe: with Spacer D (ID 26.9, OD 40) on, every 500.

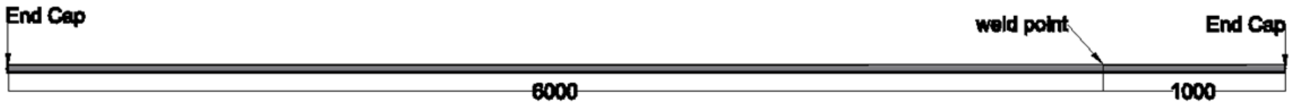
End Cap
weld point
End Cap
6000
1000

Outer Pipe
</td></tr>
<tr><td>PIPABS</td><td>Inner pipe OD 26.9; t 1.6.
Outer pipe OD 42.5; t 1.9.
Spacer B ID 26.9; OD 36.
Spacing 250.</td><td>
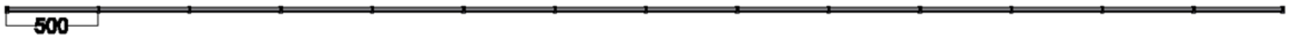

Inner pipe: with Spacer B (ID 26.9, OD 36) on, every 500.

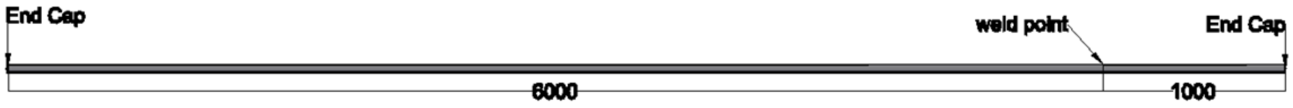
End Cap
weld point
End Cap
6000
1000

Outer Pipe
</td></tr>
</table>

E. Appendix E Dimensions of Different Trawl Gears

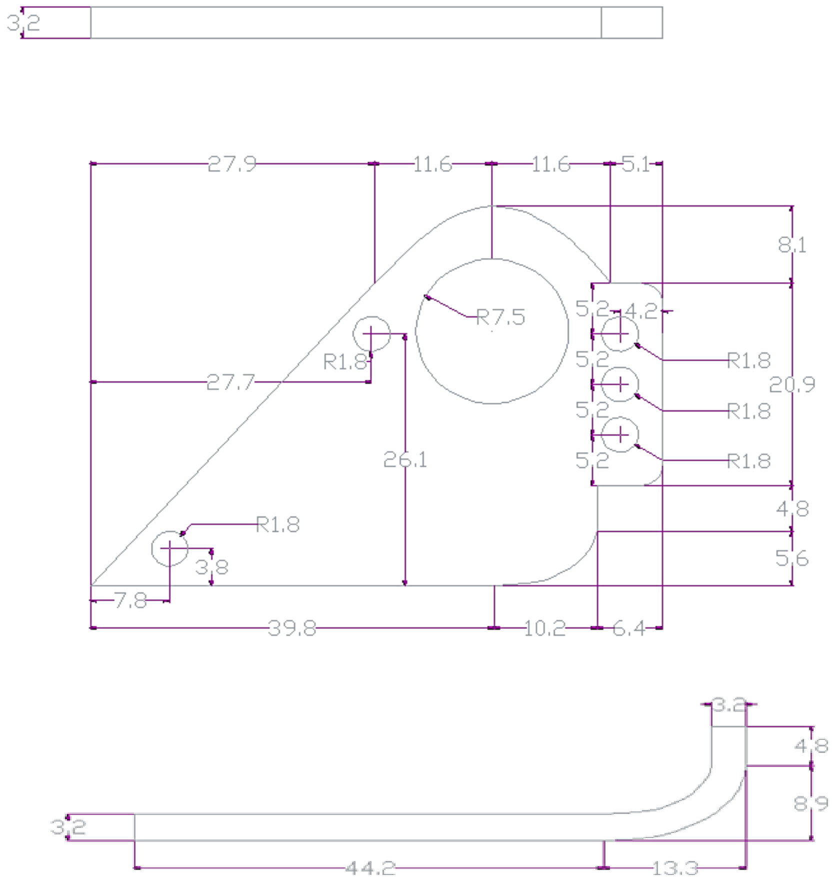
3.2
27.9
11.6
11.6
5.1
8.1
R7.5
5.2
4.2
R1.8
5.2
20.9
R1.8
5.2
R1.8
5.2
R1.8
27.7
26.1
4.8
R1.8
3.8
5.6
7.8
39.8
10.2
6.4
3.2
4.8
8.9
3.2
44.2
13.3

Figure E-1 Dimensions of SEAFISH trawl gear

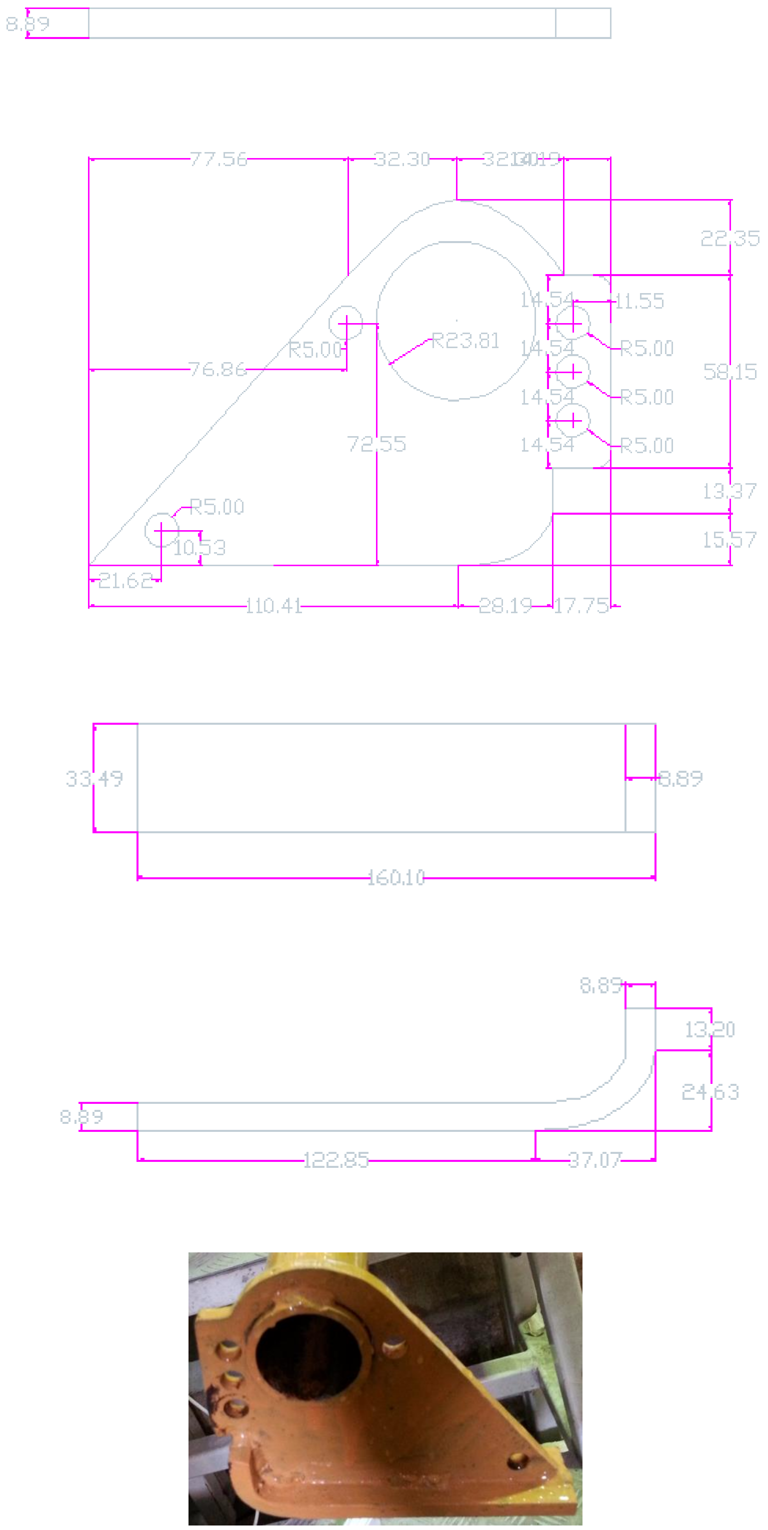
8.89
77.56
32.30
22.35
14.54
11.55
R5.00
R23.81
14.54
R5.00
76.86
58.15
14.54
R5.00
72.55
14.54
R5.00
13.37
R5.00
10.53
15.57
21.62
110.41
28.19
17.75
33.49
8.89
160.10
8.89
13.20
24.63
8.89
122.85
37.07

Figure E-2 Small scale trawl shoe design

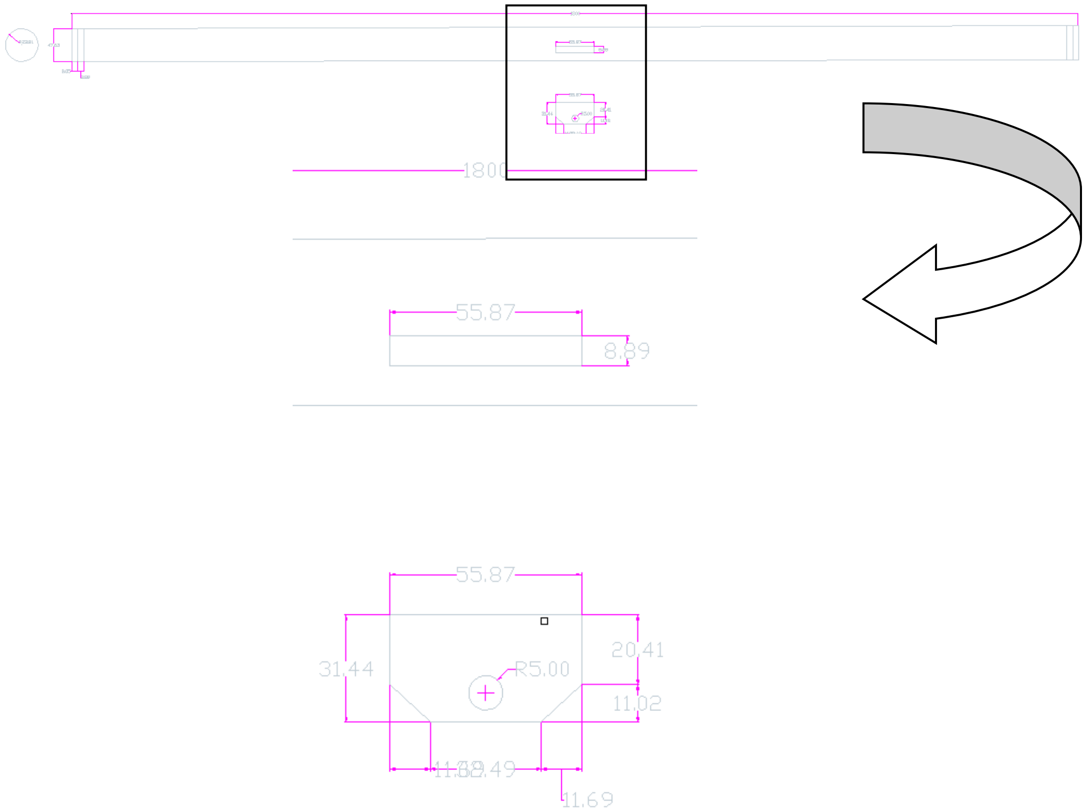
1800
55.87
8.89
55.87
31.44
R5.00
20.41
11.02
32.49
11.69

Figure E-3 Small scale beam dimension

F. Appendix F Pull-over Test Results

Table F-1 Test program

	test series	*Boundary Condition*	*Warp (N/m)*	*T G*	*weight (kg)*	*Velocity (m/s)*	*Angle*
1	SPSA-SSS2-1-90	Simple support	5.51E+04	S	27.34	2.00	90
2	SPSB- SSS2-1-90	Simple support	5.51E+04	S	27.34	2.00	90
3	SPSC- SSS2-1-90	Simple support	5.51E+04	S	27.34	2.00	90
4	SPSD- SSS2-1-90	Simple support	5.51E+04	S	27.34	2.00	90
5	PIPAB- SSS2-1-90	Simple support	5.51E+04	S	27.34	2.00	90
6	PIPAC- SSS2-1-90	Simple support	5.51E+04	S	27.34	2.00	90
7	PIPAD- SSS2-1-90	Simple support	5.51E+04	S	27.34	2.00	90
8	SPSA-FDS2-1-90	Fixed ends	1.45E+04	S	27.34	2.00	90
9	SPSB- FDS2-1-90	Fixed ends	1.45E+04	S	27.34	2.00	90
10	SPSC- FDS2-1-90	Fixed ends	1.45E+04	S	27.34	2.00	90
11	SPSD- FDS2-1-90	Fixed ends	1.45E+04	S	27.34	2.00	90
12	PIPAB- FDS2-1-90	Fixed ends	1.45E+04	S	27.34	2.00	90
13	PIPAB-FDS2-2-90	Fixed ends	1.45E+04	S	27.34	2.00	90
14	PIPAB-FDS2-3-90	Fixed ends	1.45E+04	S	27.34	2.00	90
15	PIPABS- FDS2-1-90	Fixed ends	1.45E+04	S	27.34	2.00	90
16	PIPABS-FDS2-2-90	Fixed ends	1.45E+04	S	27.34	2.00	90
17	PIPABS-FDS2-3-90	Fixed ends	1.45E+04	S	27.34	2.00	90
18	PIPAC- FDS2-1-90	Fixed ends	1.45E+04	S	27.34	2.00	90
19	PIPAD- FDS2-1-90	Fixed ends	1.45E+04	S	27.34	2.00	90
20	PIPAB-SFDS2-1-90	Fixed ends	1.45E+04	S	27.34	2.00	90
21	PIPAB-SFDS2-2-90	Fixed ends	1.45E+04	S	27.34	2.00	90
22	SPSA-FDF1-1-90	Fixed ends	1.45E+04	F	9.36	1.18	90
23	SPSB- FDF1-1-90	Fixed ends	1.45E+04	F	9.36	1.18	90
24	SPSC- FDF1-1-90	Fixed ends	1.45E+04	F	9.36	1.18	90
25	SPSD- FDF1-1-90	Fixed ends	1.45E+04	F	9.36	1.18	90
26	PIPAB- FDF1-1-90	Fixed ends	1.45E+04	F	9.36	1.18	90
27	PIPAB-FDF1-2-90	Fixed ends	1.45E+04	F	9.36	1.18	90
28	PIPAB-FDF1-3-90	Fixed ends	1.45E+04	F	9.36	1.18	90
29	PIPABS-FDF1-1-90	Fixed ends	1.45E+04	F	9.36	1.18	90
30	PIPABS-FDF1-2-90	Fixed ends	1.45E+04	F	9.36	1.18	90
31	PIPABS-FDF1-3-90	Fixed ends	1.45E+04	F	9.36	1.18	90
32	PIPAC-FDF1-1-90	Fixed ends	1.45E+04	F	9.36	1.18	90
33	PIPAD-FDF1-1-90	Fixed ends	1.45E+04	F	9.36	1.18	90
34	PIPAD-FDF1-2-90	Fixed ends	1.45E+04	F	9.36	1.18	90
35	PIPAD-FDF1-3-90	Fixed ends	1.45E+04	F	9.36	1.18	90
36	PIPAD-FDF1-4-90	Fixed ends	1.45E+04	F	9.36	1.18	90
37	SPSD-FSS2-1-90	Fixed ends	5.51E+04	S	27.34	2.00	90
38	PIPAB- FSS2-1-90	Fixed ends	5.51E+04	S	27.34	2.00	90

	test series	*Boundary Condition*	*Warp (N/m)*	*T G*	*weight (kg)*	*Velocity (m/s)*	*Angle*
39	PIPAB-FSS2-2-90	Fixed ends	5.51E+04	S	27.34	2.00	90
40	PIPAD-FSS2-1-90	Fixed ends	5.51E+04	S	27.34	2.00	90
41	SPSD-FSF1-1-90	Fixed ends	5.51E+04	F	9.36	1.18	90
42	PIPAB-FSF1-1-90	Fixed ends	5.51E+04	F	9.36	1.18	90
43	PIPAD-FSF1-1-90	Fixed ends	5.51E+04	F	9.36	1.18	90
44	SPSB-FDF2-1-90	Fixed ends	1.45E+04	F	9.36	2.00	90
45	SPSD-FDF2-1-90	Fixed ends	1.45E+04	F	9.36	2.00	90
46	PIPAB-FDF2-1-90	Fixed ends	1.45E+04	F	9.36	2.00	90
47	PIPAC-FDF2-1-90	Fixed ends	1.45E+04	F	9.36	2.00	90
48	PIPAD-FDF2-1-90	Fixed ends	1.45E+04	F	9.36	2.00	90
49	SPSB-FDS1-1-90	Fixed ends	1.45E+04	S	27.34	1.18	90
50	SPSD-FDS1-1-90	Fixed ends	1.45E+04	S	27.34	1.18	90
51	PIPAB-FDS1-1-90	Fixed ends	1.45E+04	S	27.34	1.18	90
52	PIPAC-FDS1-1-90	Fixed ends	1.45E+04	S	27.34	1.18	90
53	PIPAD-FDS1-1-90	Fixed ends	1.45E+04	S	27.34	1.18	90
54	PIPAC-FDF3-1-90	Fixed ends	1.45E+04	F	9.36	3.00	90
55	SPSB-FDS3-1-90	Fixed ends	1.45E+04	S	27.34	3.00	90
56	SPSD-FDS3-1-90	Fixed ends	1.45E+04	S	27.34	3.00	90
57	PIPAB-FDS3-1-90	Fixed ends	1.45E+04	S	27.34	3.00	90
58	PIPAC-FDS3-1-90	Fixed ends	1.45E+04	S	27.34	3.00	90
59	PIPAD-FDS3-1-90	Fixed ends	1.45E+04	S	27.34	3.00	90
60	SPS-FSF1-1-60	Fixed ends	5.51E+04	F	9.36	1.00	60
61	PIPAB-FSF1-1-60	Fixed ends	5.51E+04	F	9.36	1.00	60
62	SPSD-FSS1-1-60	Fixed ends	5.51E+04	S	27.34	1.00	60
63	PIPAB-FSS1-1-60	Fixed ends	5.51E+04	S	27.34	1.00	60
64	SPSD-FSF1-1-45	Fixed ends	5.51E+04	F	9.36	1.00	45
65	PIPAB-FSF1-1-45	Fixed ends	5.51E+04	F	9.36	1.00	45
66	SPSD-FSS1-1-45	Fixed ends	5.51E+04	S	27.34	1.00	45
67	PIPAB-FSS1-1-45	Fixed ends	5.51E+04	S	27.34	1.00	45
68	SPSD-FSF1-1-30	Fixed ends	5.51E+04	F	9.36	1.00	30
69	SPSD-FSF1-2-30	Fixed ends	5.51E+04	F	9.36	1.00	30
70	SPSD-FSF1-3-30	Fixed ends	5.51E+04	F	9.36	1.00	30
71	PIPAB-FSF1-1-30	Fixed ends	5.51E+04	F	9.36	1.00	30
72	PIPAB-FSF1-2-30	Fixed ends	5.51E+04	F	9.36	1.00	30
73	SPSD-FSS1-1-30	Fixed ends	5.51E+04	S	27.34	1.00	30
74	SPSD-FSS1-2-30	Fixed ends	5.51E+04	S	27.34	1.00	30
75	PIPAB-FSS1-1-30	Fixed ends	5.51E+04	S	27.34	1.00	30
76	PIPAB-FSS1-2-30	Fixed ends	5.51E+04	S	27.34	1.00	30
77	SPSD-FSF2-1-60	Fixed ends	5.51E+04	F	9.36	2.00	60
78	PIPAB-FSF2-1-60	Fixed ends	5.51E+04	F	9.36	2.00	60
79	SPSD-FSS2-1-60	Fixed ends	5.51E+04	S	27.34	2.00	60

	test series	*Boundary Condition*	*Warp (N/m)*	*TG*	*weight (kg)*	*Velocity (m/s)*	*Angle*
80	PIPAB-FSS2-1-60	Fixed ends	5.51E+04	S	27.34	2.00	60
81	SPSD-FSF2-1-45	Fixed ends	5.51E+04	F	9.36	2.00	45
82	PIPAB-FSF2-1-45	Fixed ends	5.51E+04	F	9.36	2.00	45
83	PIPAB-FSF2-2-45	Fixed ends	5.51E+04	F	9.36	2.00	45
84	SPSD-FSS2-1-45	Fixed ends	5.51E+04	S	27.34	2.00	45
85	PIPAB-FSS2-1-45	Fixed ends	5.51E+04	S	27.34	2.00	45
86	SPSD-FSF2-1-30	Fixed ends	5.51E+04	F	9.36	2.00	30
87	PIPAB-FSF2-1-30	Fixed ends	5.51E+04	F	9.36	2.00	30
88	SPSD-FSS2-1-30	Fixed ends	5.51E+04	S	27.34	2.00	30
89	PIPAB-FSS2-1-30	Fixed ends	5.51E+04	S	27.34	2.00	30
90	PIPAB-FSS2-2-30	Fixed ends	5.51E+04	S	27.34	2.00	30
91	SPSD-FSS3-1-60	Fixed ends	5.51E+04	S	27.34	3.00	60
92	PIPAB-FSS3-1-60	Fixed ends	5.51E+04	S	27.34	3.00	60
93	SPSD-FSS3-1-45	Fixed ends	5.51E+04	S	27.34	3.00	45
94	PIPAB-FSS3-1-45	Fixed ends	5.51E+04	S	27.34	3.00	45
95	SPSD-FSS3-1-30	Fixed ends	5.51E+04	S	27.34	3.00	30
96	SPSD-FSS3-2-30	Fixed ends	5.51E+04	S	27.34	3.00	30
97	PIPAB-FSS3-1-30	Fixed ends	5.51E+04	S	27.34	3.00	30
98	PIPAB-FSS3-2-30	Fixed ends	5.51E+04	S	27.34	3.00	30
99	SPSD-FDS3-1-30	Fixed ends	1.45E+04	S	27.34	3.00	30
100	PIPAB-FDS3-1-30	Fixed ends	1.45E+04	S	27.34	3.00	30

Table F-2 Summary of test results of 90 degree crossing

	test series	*Maximum Pull-over Force*	*Time*	*Maximum Tension*	*Maximum Displacement*
1	SPSA-SSS2-1-90	1.28	0.1442	N.A.	70
2	SPSB- SSS2-1-90	1.15	0.1319	N.A.	115
3	SPSC- SSS2-1-90	1.5	0.173	N.A.	76
4	SPSD- SSS2-1-90	1.59	0.1356	N.A.	73
5	PIPAB- SSS2-1-90	1.49	0.1191	N.A.	141
6	PIPAC- SSS2-1-90	1.38	0.1267	N.A.	123
7	PIPAD- SSS2-1-90	1.67	0.1217	N.A.	115
8	SPSA-FDS2-1-90	0.803	0.1025	8.92	122
9	SPSB- FDS2-1-90	0.961	0.1245	9.36	91
10	SPSC- FDS2-1-90	0.77	0.135	5.35	57
11	SPSD- FDS2-1-90	1.02	0.1045	2.67	33
12	PIPAB- FDS2-1-90	0.972	0.113	3.8	48
13	PIPAB-FDS2-2-90	1.43	0.1305	11.5	115
14	PIPAB-FDS2-3-90	1.34	0.1215	7.69	94
15	PIPABS- FDS2-1-90	1.14	0.125	0.61	2
16	PIPABS-FDS2-2-90	1.4	0.125	0.433	0
17	PIPABS-FDS2-3-90	1.46	0.1625	0.451	9

	test series	*Maximum Pull-over Force*	*Time*	*Maximum Tension*	*Maximum Displacement*
18	PIPAC- FDS2-1-90	0.979	0.128	4.76	53
19	PIPAD- FDS2-1-90	0.975	0.209	4.04	50
20	PIPAB-SFDS2-1-90	1.91	0.3135	0.253	17
21	PIPAB-SFDS2-2-90	1.54	0.2665	0.367	8
22	SPSA-FDF1-1-90	0.381	0.1355	0.986	21
23	SPSB- FDF1-1-90	0.458	0.102	3.08	53
24	SPSC- FDF1-1-90	0.477	0.1525	3.9	39
25	SPSD- FDF1-1-90	0.535	0.137	2.4	30
26	PIPAB- FDF1-1-90	0.491	0.131	2	32
27	PIPAB-FDF1-2-90	0.568	0.174	0.491	8
28	PIPAB-FDF1-3-90	0.539	0.245	0.227	9
29	PIPABS-FDF1-1-90	0.557	0.154	0.506	8
30	PIPABS-FDF1-2-90	0.667	0.1535	0.517	23
31	PIPABS-FDF1-3-90	0.682	0.162	0.913	8
32	PIPAC-FDF1-1-90	0.535	0.143	1.74	33
33	PIPAD-FDF1-1-90	0.579	0.1965	0.25	15
34	PIPAD-FDF1-2-90	0.561	0.139	0.451	2
35	PIPAD-FDF1-3-90	0.605	0.107	0.44	2
36	PIPAD-FDF1-4-90	0.62	0.115	0.411	2
37	SPSD-FSS2-1-90	1.91	0.116	9.13	84.4
38	PIPAB- FSS2-1-90	1.69	0.12	3.53	62
39	PIPAB-FSS2-2-90	2.01	0.14	12.2	143.2
40	PIPAD-FSS2-1-90	1.89	0.0785	1.57	16
41	SPSD-FSF1-1-90	0.66	0.1465	4.71	48
42	PIPAB-FSF1-1-90	0.587	0.1755	4.41	57
43	PIPAD-FSF1-1-90	0.653	0.143	1.75	33
44	SPSB-FDF2-1-90	0.609	0.1395	3.5	54
45	SPSD-FDF2-1-90	0.774	0.054	0.748	6
46	PIPAB-FDF2-1-90	0.583	0.0715	0.198	4
47	PIPAC-FDF2-1-90	0.687	0.076	0.1524	10
48	PIPAD-FDF2-1-90	0.737	0.0835	0.484	5
49	SPSB-FDS1-1-90	1.51	0.137	8.35	116
50	SPSD-FDS1-1-90	1.36	0.1515	7.89	101
51	PIPAB-FDS1-1-90	1.22	0.21	8.54	99
52	PIPAC-FDS1-1-90	1.31	0.2285	7.42	98
53	PIPAD-FDS1-1-90	1.32	0.2555	6.71	83
54	PIPAC-FDF3-1-90	N.A.	N.A.	N.A.	N.A.
55	SPSB-FDS3-1-90	1.29	0.109	6.06	85
56	SPSD-FDS3-1-90	1.48	0.1085	5.87	68
57	PIPAB-FDS3-1-90	1.29	0.118	4.23	67
58	PIPAC-FDS3-1-90	1.4	0.0475	3.83	31
59	PIPAD-FDS3-1-90	1.38	0.0935	2.52	34

Note 1: case 54 PIPAC-FDF3-1-90 do not have an identical pull-over phase as the velocity is too large for this trawl gear weight.

Table F-3 Summary of test results of 60, 45, 30 degree crossing

	test series	*Maximum Pull-over Force*	*Time*	*Maximum Tension*
60	SPS-FSF1-1-60	0.464	1.12E+00	2.37
61	PIPAB-FSF1-1-60	0.342	9.24E-01	0.528
62	SPSD-FSS1-1-60	0.502	5.54E-01	1.62
63	PIPAB-FSS1-1-60	0.558	1.14E+00	1.83
64	SPSD-FSF1-1-45	0.352	1.65E+00	0.601
65	PIPAB-FSF1-1-45	0.372	1.75E+00	0.517
66	SPSD-FSS1-1-45	0.537	9.25E-01	2.33
67	PIPAB-FSS1-1-45	0.456	8.97E-01	0.939
68	SPSD-FSF1-1-30	0.471	3.04E+00	0.469
69	SPSD-FSF1-2-30	0.365	3.60E+00	0.29
70	SPSD-FSF1-3-30	0.458	3.92E+00	0.396
71	PIPAB-FSF1-1-30	0.306	3.12E+00	0.462
72	PIPAB-FSF1-2-30	0.269	3.38E+00	0.403
73	SPSD-FSS1-1-30	-	-	-
74	SPSD-FSS1-2-30	-	-	-
75	PIPAB-FSS1-1-30	0.478	3.87E+00	1.61
76	PIPAB-FSS1-2-30	0.499	3.76E+00	1.72
77	SPSD-FSF2-1-60	0.605	5.74E-01	0.381
78	PIPAB-FSF2-1-60	0.473	5.10E-02	0.191
79	SPSD-FSS2-1-60	1.21	6.35E-01	0.671
80	PIPAB-FSS2-1-60	0.968	8.33E-01	3.95
81	SPSD-FSF2-1-45	0.546	9.49E-01	0.711
82	PIPAB-FSF2-1-45	0.477	9.15E-01	0.638
83	PIPAB-FSF2-2-45	0.557	9.26E-01	0.385
84	SPSD-FSS2-1-45	0.875	1.10E+00	3.1
85	PIPAB-FSS2-1-45	0.935	1.06E+00	8.74
86	SPSD-FSF2-1-30	0.418	1.62E+00	0.422
87	PIPAB-FSF2-1-30	0.48	1.60E+00	0.92
88	SPSD-FSS2-1-30	1.07	1.83E+00	2.37
89	PIPAB-FSS2-1-30	1.05	2.36E+00	2.22
90	PIPAB-FSS2-2-30	0.999	1.85E+00	2.64
91	SPSD-FSS3-1-60	1.25	4.71E-01	2.12
92	PIPAB-FSS3-1-60	1.43	4.81E-01	2.35
93	SPSD-FSS3-1-45	1.6	7.61E-01	7.77
94	PIPAB-FSS3-1-45	1.09	7.61E-01	4.88
95	SPSD-FSS3-1-30	1.22	1.50E+00	3.83

	test series	*Maximum Pull-over Force*	*Time*	*Maximum Tension*
96	SPSD-FSS3-2-30	1.52	1.50E+00	3.42
97	PIPAB-FSS3-1-30	0.818	1.90E+00	3.72
98	PIPAB-FSS3-2-30	0.953	1.76E+00	4.52
99	SPSD-FDS3-1-30	0.891	1.24E+00	3.22
100	PIPAB-FDS3-1-30	1.11	1.42E+00	7.13

Note 1: case 73 and 74, the trawl gear is blocked by the connector at the end.

Table F-4 Summary of pull-over force time history

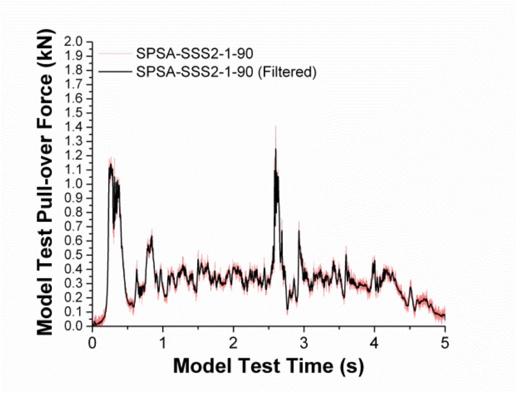

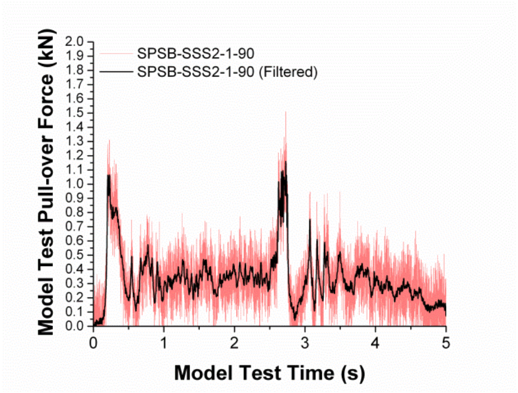

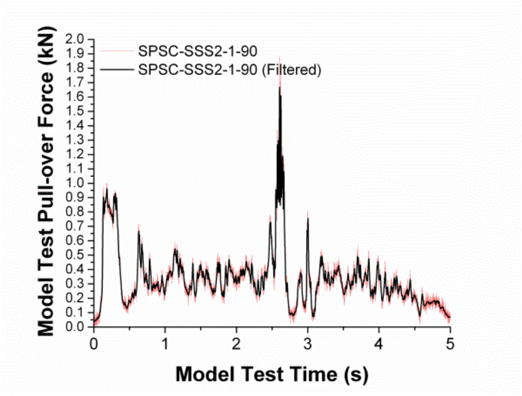

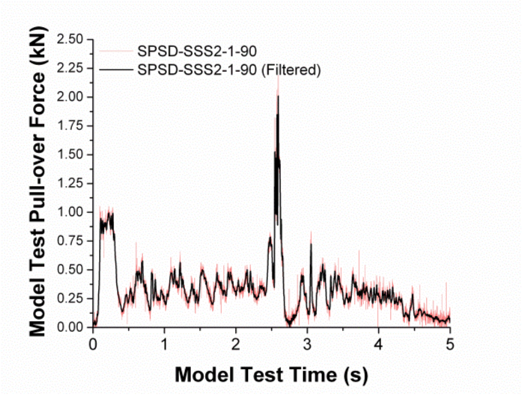

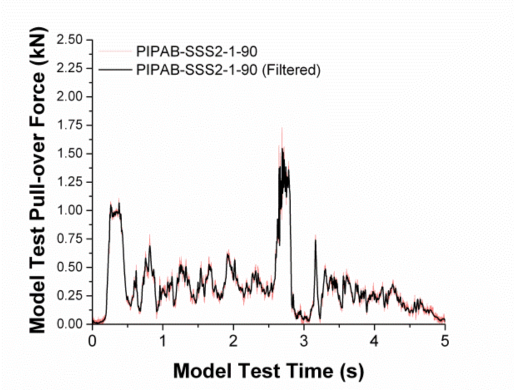
PIPAB-SSS2-1-90
PIPAB-SSS2-1-90 (Filtered)
Model Test Pull-over Force (kN)
0.00
0.25
0.50
0.75
1.00
1.25
1.50
1.75
2.00
2.25
2.50
Model Test Time (s)
0
1
2
3
4
5

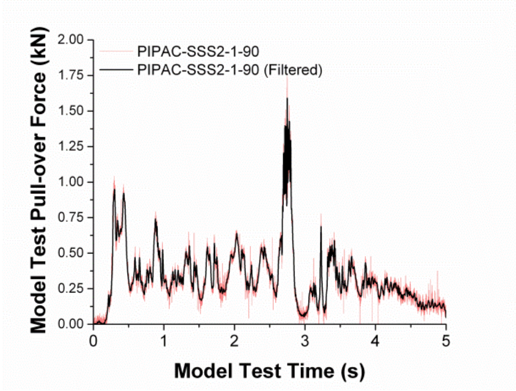
PIPAC-SSS2-1-90
PIPAC-SSS2-1-90 (Filtered)
Model Test Pull-over Force (kN)
0.00
0.25
0.50
0.75
1.00
1.25
1.50
1.75
2.00
Model Test Time (s)
0
1
2
3
4
5

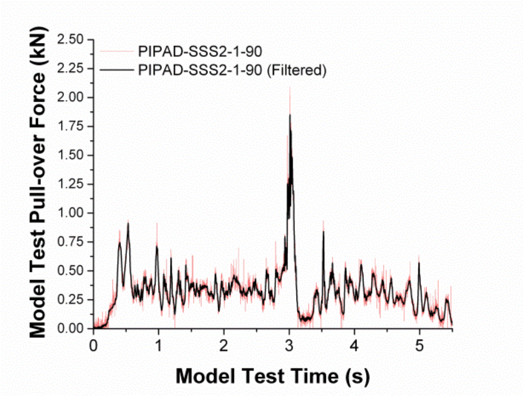
PIPAD-SSS2-1-90
PIPAD-SSS2-1-90 (Filtered)
Model Test Pull-over Force (kN)
0.00
0.25
0.50
0.75
1.00
1.25
1.50
1.75
2.00
2.25
2.50
Model Test Time (s)
0
1
2
3
4
5

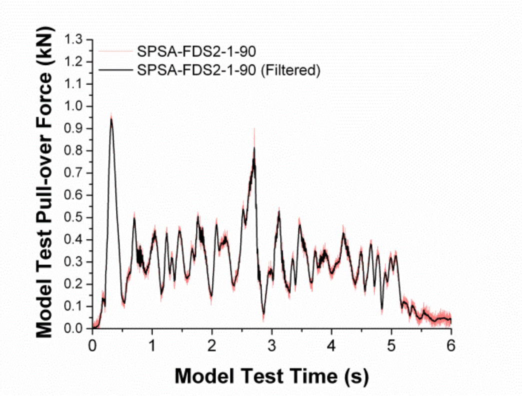
SPSA-FDS2-1-90
SPSA-FDS2-1-90 (Filtered)
Model Test Pull-over Force (kN)
0.0
0.1
0.2
0.3
0.4
0.5
0.6
0.7
0.8
0.9
1.0
1.1
1.2
1.3
Model Test Time (s)
0
1
2
3
4
5
6

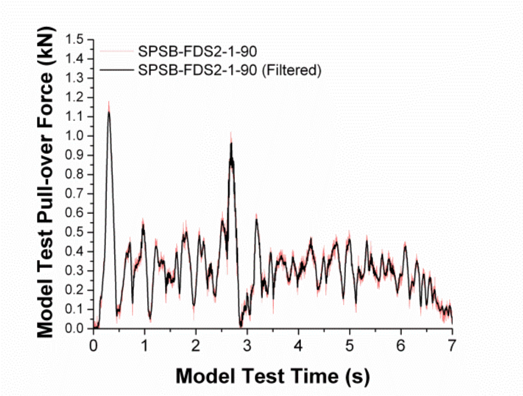
SPSB-FDS2-1-90
SPSB-FDS2-1-90 (Filtered)
Model Test Pull-over Force (kN)
0.0
0.1
0.2
0.3
0.4
0.5
0.6
0.7
0.8
0.9
1.0
1.1
1.2
1.3
1.4
1.5
Model Test Time (s)
0
1
2
3
4
5
6
7

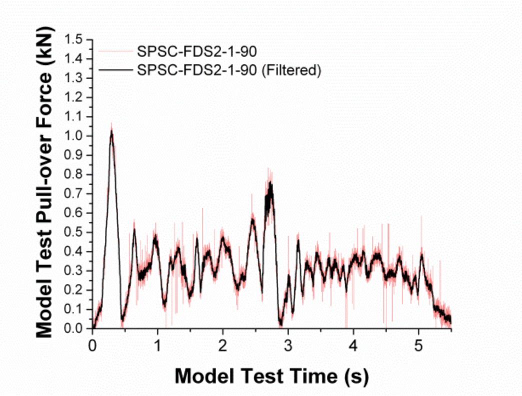
SPSC-FDS2-1-90
SPSC-FDS2-1-90 (Filtered)
Model Test Pull-over Force (kN)
0.0
0.1
0.2
0.3
0.4
0.5
0.6
0.7
0.8
0.9
1.0
1.1
1.2
1.3
1.4
1.5
Model Test Time (s)
0
1
2
3
4
5

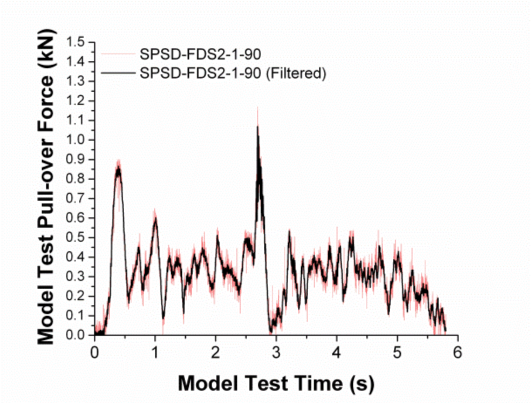
Model Test Pull-over Force (kN)
Model Test Time (s)
SPSD-FDS2-1-90
SPSD-FDS2-1-90 (Filtered)
0.0
0.1
0.2
0.3
0.4
0.5
0.6
0.7
0.8
0.9
1.0
1.1
1.2
1.3
1.4
1.5
0
1
2
3
4
5
6

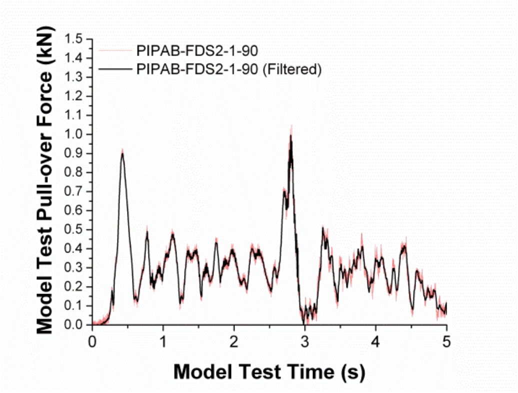
Model Test Pull-over Force (kN)
Model Test Time (s)
PIPAB-FDS2-1-90
PIPAB-FDS2-1-90 (Filtered)
0.0
0.1
0.2
0.3
0.4
0.5
0.6
0.7
0.8
0.9
1.0
1.1
1.2
1.3
1.4
1.5
0
1
2
3
4
5

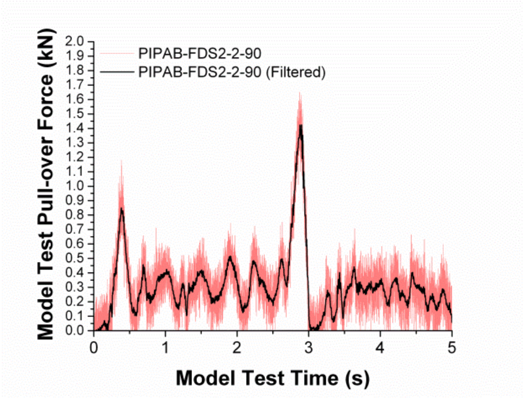
Model Test Pull-over Force (kN)
Model Test Time (s)
PIPAB-FDS2-2-90
PIPAB-FDS2-2-90 (Filtered)
0.0
0.1
0.2
0.3
0.4
0.5
0.6
0.7
0.8
0.9
1.0
1.1
1.2
1.3
1.4
1.5
1.6
1.7
1.8
1.9
2.0
0
1
2
3
4
5

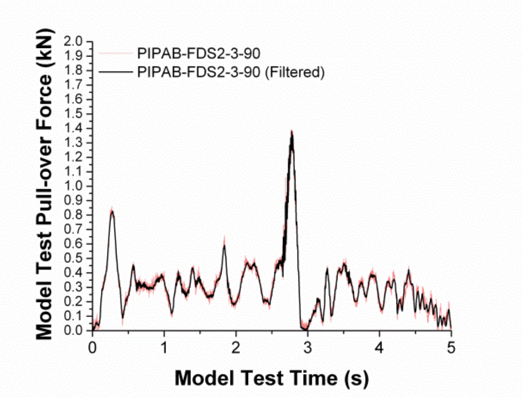
Model Test Pull-over Force (kN)
Model Test Time (s)
PIPAB-FDS2-3-90
PIPAB-FDS2-3-90 (Filtered)
0.0
0.1
0.2
0.3
0.4
0.5
0.6
0.7
0.8
0.9
1.0
1.1
1.2
1.3
1.4
1.5
1.6
1.7
1.8
1.9
2.0
0
1
2
3
4
5

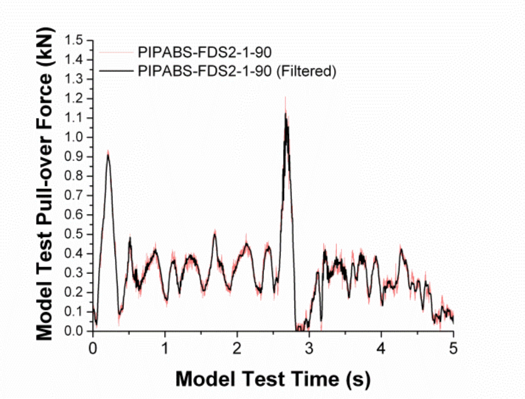
Model Test Pull-over Force (kN)
Model Test Time (s)
PIPABS-FDS2-1-90
PIPABS-FDS2-1-90 (Filtered)
0.0
0.1
0.2
0.3
0.4
0.5
0.6
0.7
0.8
0.9
1.0
1.1
1.2
1.3
1.4
1.5
0
1
2
3
4
5

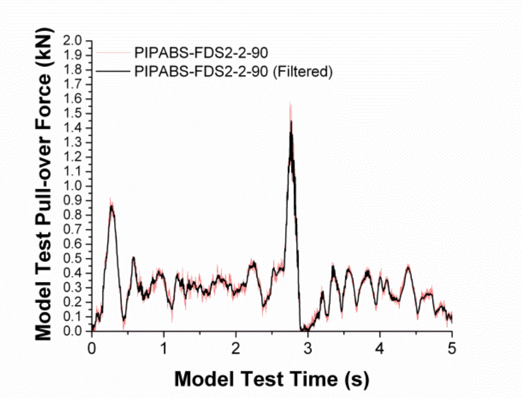
Model Test Pull-over Force (kN)
Model Test Time (s)
PIPABS-FDS2-2-90
PIPABS-FDS2-2-90 (Filtered)
0.0
0.1
0.2
0.3
0.4
0.5
0.6
0.7
0.8
0.9
1.0
1.1
1.2
1.3
1.4
1.5
1.6
1.7
1.8
1.9
2.0
0
1
2
3
4
5

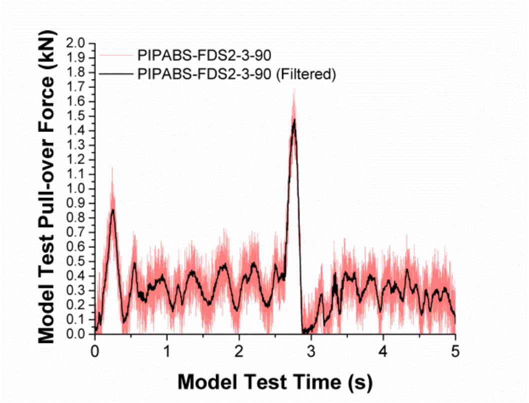
PIPABS-FDS2-3-90
PIPABS-FDS2-3-90 (Filtered)
Model Test Pull-over Force (kN)
Model Test Time (s)
0.0 0.1 0.2 0.3 0.4 0.5 0.6 0.7 0.8 0.9 1.0 1.1 1.2 1.3 1.4 1.5 1.6 1.7 1.8 1.9 2.0
0 1 2 3 4 5

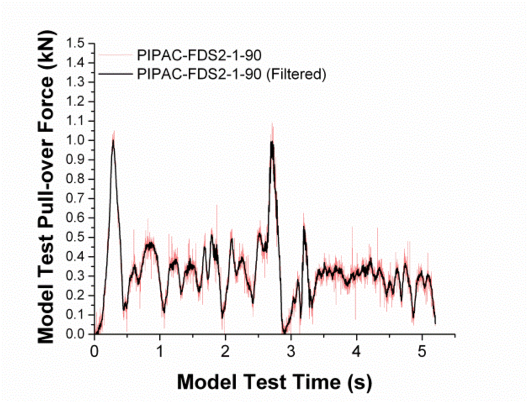
PIPAC-FDS2-1-90
PIPAC-FDS2-1-90 (Filtered)
Model Test Pull-over Force (kN)
Model Test Time (s)
0.0 0.1 0.2 0.3 0.4 0.5 0.6 0.7 0.8 0.9 1.0 1.1 1.2 1.3 1.4 1.5
0 1 2 3 4 5

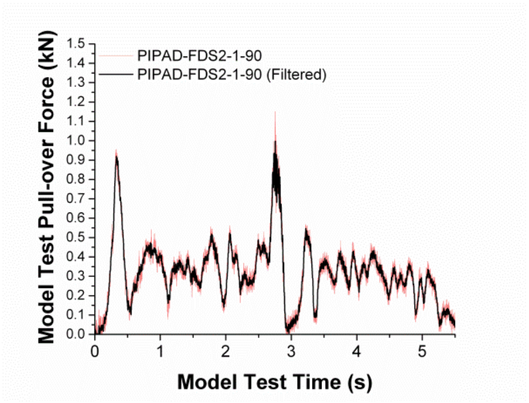
PIPAD-FDS2-1-90
PIPAD-FDS2-1-90 (Filtered)
Model Test Pull-over Force (kN)
Model Test Time (s)
0.0 0.1 0.2 0.3 0.4 0.5 0.6 0.7 0.8 0.9 1.0 1.1 1.2 1.3 1.4 1.5
0 1 2 3 4 5

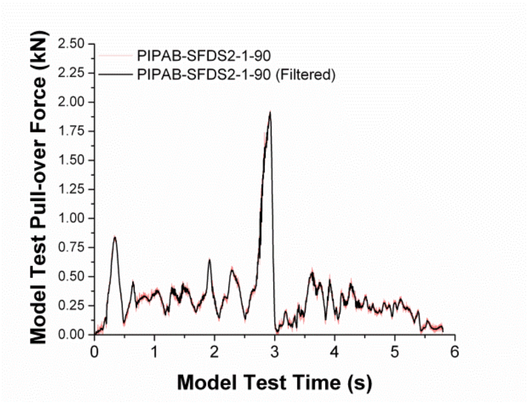
PIPAB-SFDS2-1-90
PIPAB-SFDS2-1-90 (Filtered)
Model Test Pull-over Force (kN)
Model Test Time (s)
0.00 0.25 0.50 0.75 1.00 1.25 1.50 1.75 2.00 2.25 2.50
0 1 2 3 4 5 6

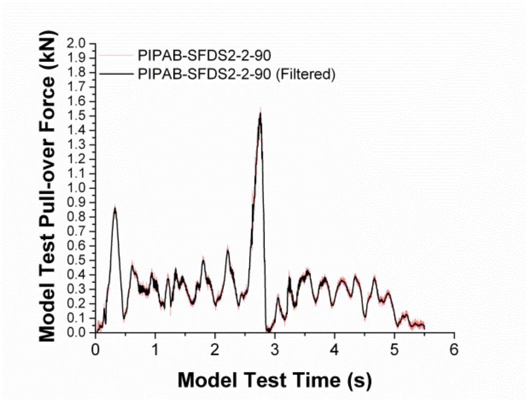
PIPAB-SFDS2-2-90
PIPAB-SFDS2-2-90 (Filtered)
Model Test Pull-over Force (kN)
Model Test Time (s)
0.0 0.1 0.2 0.3 0.4 0.5 0.6 0.7 0.8 0.9 1.0 1.1 1.2 1.3 1.4 1.5 1.6 1.7 1.8 1.9 2.0
0 1 2 3 4 5 6

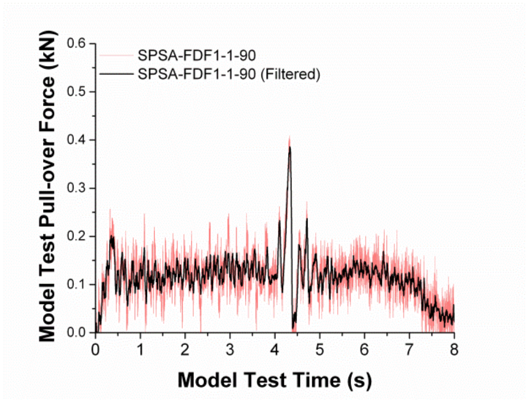
SPSA-FDF1-1-90
SPSA-FDF1-1-90 (Filtered)
Model Test Pull-over Force (kN)
Model Test Time (s)
0.0 0.1 0.2 0.3 0.4 0.5 0.6
0 1 2 3 4 5 6 7 8

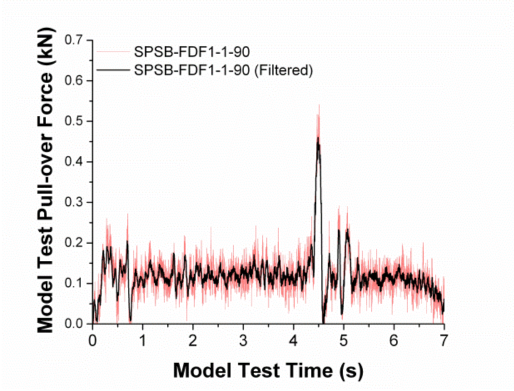
SPSB-FDF1-1-90
SPSB-FDF1-1-90 (Filtered)
Model Test Pull-over Force (kN)
0.0
0.1
0.2
0.3
0.4
0.5
0.6
0.7
0
1
2
3
4
5
6
7
Model Test Time (s)

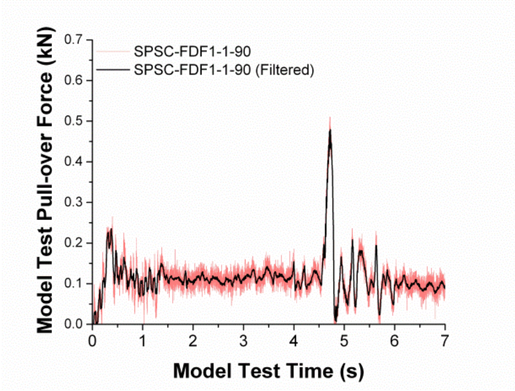
SPSC-FDF1-1-90
SPSC-FDF1-1-90 (Filtered)
Model Test Pull-over Force (kN)
0.0
0.1
0.2
0.3
0.4
0.5
0.6
0.7
0
1
2
3
4
5
6
7
Model Test Time (s)

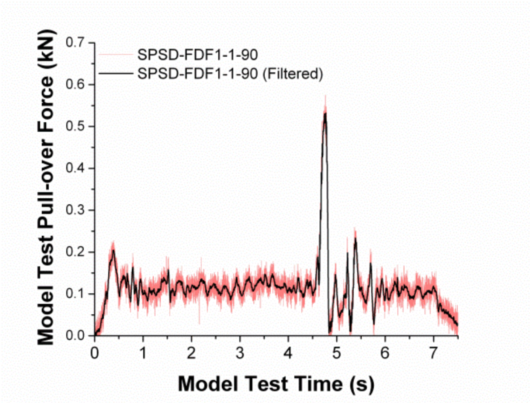
SPSD-FDF1-1-90
SPSD-FDF1-1-90 (Filtered)
Model Test Pull-over Force (kN)
0.0
0.1
0.2
0.3
0.4
0.5
0.6
0.7
0
1
2
3
4
5
6
7
Model Test Time (s)

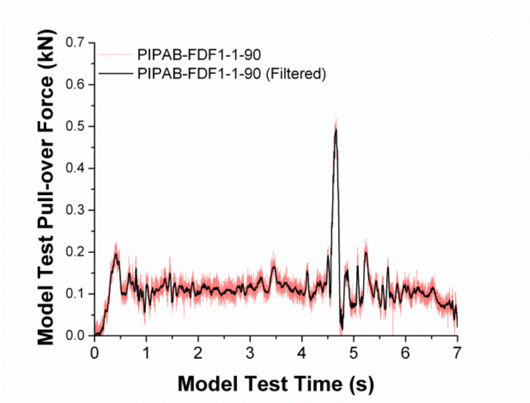
PIPAB-FDF1-1-90
PIPAB-FDF1-1-90 (Filtered)
Model Test Pull-over Force (kN)
0.0
0.1
0.2
0.3
0.4
0.5
0.6
0.7
0
1
2
3
4
5
6
7
Model Test Time (s)

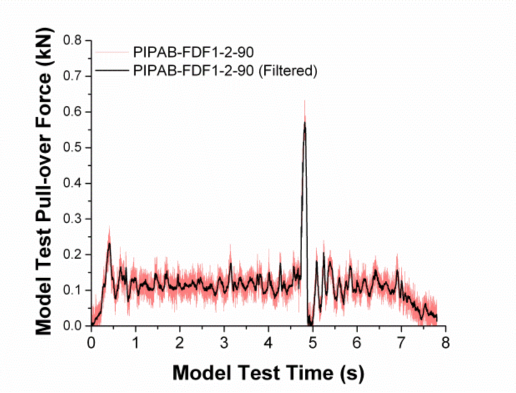
PIPAB-FDF1-2-90
PIPAB-FDF1-2-90 (Filtered)
Model Test Pull-over Force (kN)
0.0
0.1
0.2
0.3
0.4
0.5
0.6
0.7
0.8
0
1
2
3
4
5
6
7
8
Model Test Time (s)

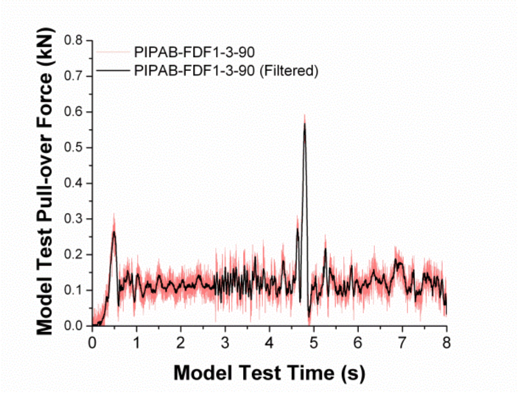
PIPAB-FDF1-3-90
PIPAB-FDF1-3-90 (Filtered)
Model Test Pull-over Force (kN)
0.0
0.1
0.2
0.3
0.4
0.5
0.6
0.7
0.8
0
1
2
3
4
5
6
7
8
Model Test Time (s)

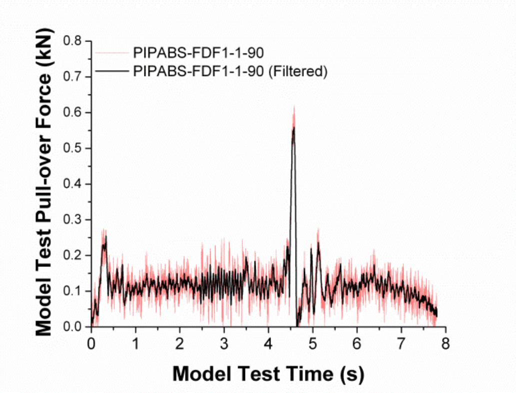
PIPABS-FDF1-1-90
PIPABS-FDF1-1-90 (Filtered)
Model Test Pull-over Force (kN)
0.0
0.1
0.2
0.3
0.4
0.5
0.6
0.7
0.8
0
1
2
3
4
5
6
7
8
Model Test Time (s)

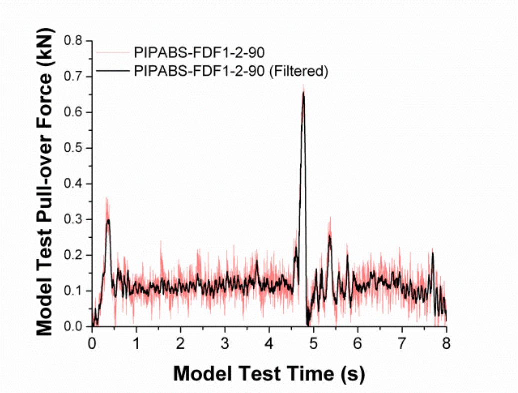
PIPABS-FDF1-2-90
PIPABS-FDF1-2-90 (Filtered)
Model Test Pull-over Force (kN)
0.0
0.1
0.2
0.3
0.4
0.5
0.6
0.7
0.8
0
1
2
3
4
5
6
7
8
Model Test Time (s)

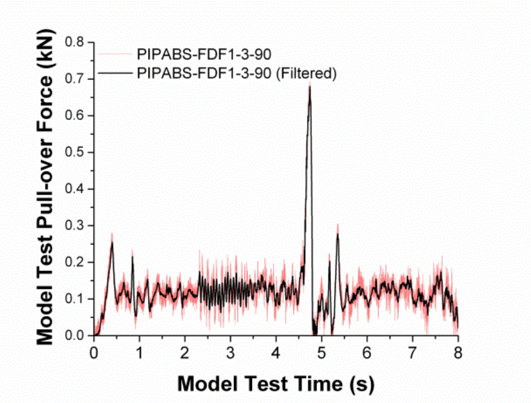
PIPABS-FDF1-3-90
PIPABS-FDF1-3-90 (Filtered)
Model Test Pull-over Force (kN)
0.0
0.1
0.2
0.3
0.4
0.5
0.6
0.7
0.8
0
1
2
3
4
5
6
7
8
Model Test Time (s)

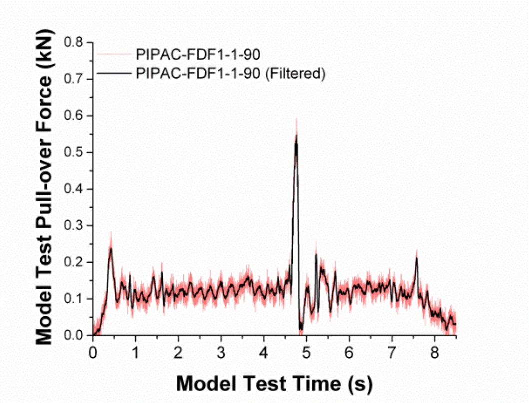
PIPAC-FDF1-1-90
PIPAC-FDF1-1-90 (Filtered)
Model Test Pull-over Force (kN)
0.0
0.1
0.2
0.3
0.4
0.5
0.6
0.7
0.8
0
1
2
3
4
5
6
7
8
Model Test Time (s)

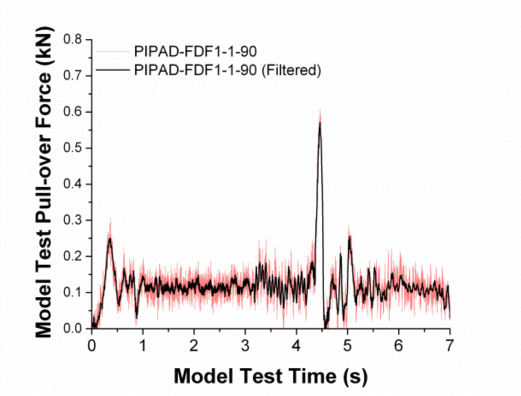
PIPAD-FDF1-1-90
PIPAD-FDF1-1-90 (Filtered)
Model Test Pull-over Force (kN)
0.0
0.1
0.2
0.3
0.4
0.5
0.6
0.7
0.8
0
1
2
3
4
5
6
7
Model Test Time (s)

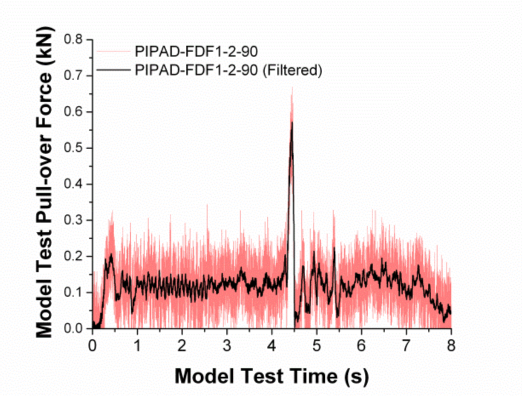
PIPAD-FDF1-2-90
PIPAD-FDF1-2-90 (Filtered)
Model Test Pull-over Force (kN)
0.0
0.1
0.2
0.3
0.4
0.5
0.6
0.7
0.8
0
1
2
3
4
5
6
7
8
Model Test Time (s)

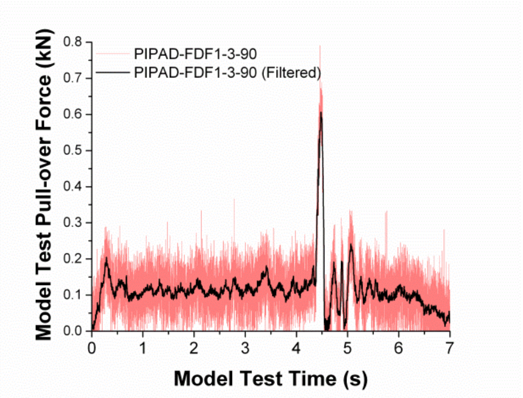
PIPAD-FDF1-3-90
PIPAD-FDF1-3-90 (Filtered)
Model Test Pull-over Force (kN)
0.0
0.1
0.2
0.3
0.4
0.5
0.6
0.7
0.8
Model Test Time (s)
0
1
2
3
4
5
6
7

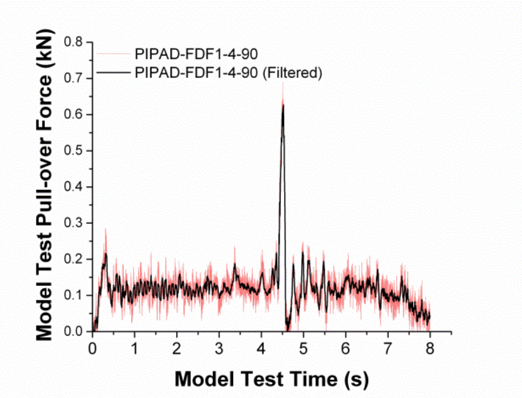
PIPAD-FDF1-4-90
PIPAD-FDF1-4-90 (Filtered)
Model Test Pull-over Force (kN)
0.0
0.1
0.2
0.3
0.4
0.5
0.6
0.7
0.8
Model Test Time (s)
0
1
2
3
4
5
6
7
8

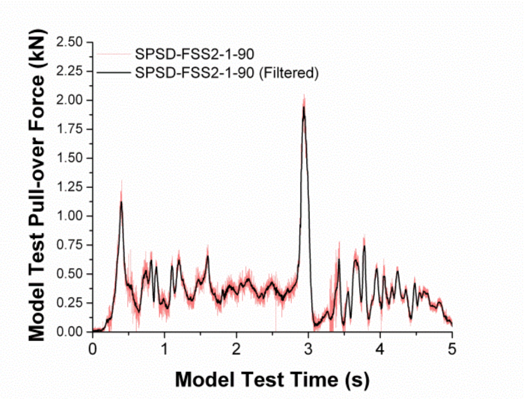
SPSD-FSS2-1-90
SPSD-FSS2-1-90 (Filtered)
Model Test Pull-over Force (kN)
0.00
0.25
0.50
0.75
1.00
1.25
1.50
1.75
2.00
2.25
2.50
Model Test Time (s)
0
1
2
3
4
5

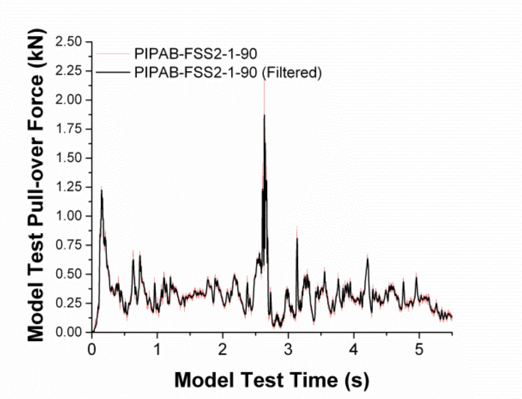
PIPAB-FSS2-1-90
PIPAB-FSS2-1-90 (Filtered)
Model Test Pull-over Force (kN)
0.00
0.25
0.50
0.75
1.00
1.25
1.50
1.75
2.00
2.25
2.50
Model Test Time (s)
0
1
2
3
4
5

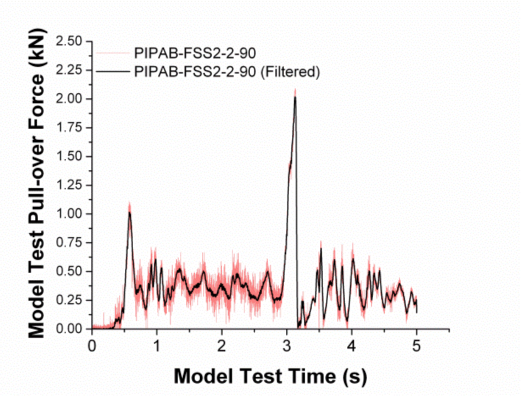
PIPAB-FSS2-2-90
PIPAB-FSS2-2-90 (Filtered)
Model Test Pull-over Force (kN)
0.00
0.25
0.50
0.75
1.00
1.25
1.50
1.75
2.00
2.25
2.50
Model Test Time (s)
0
1
2
3
4
5

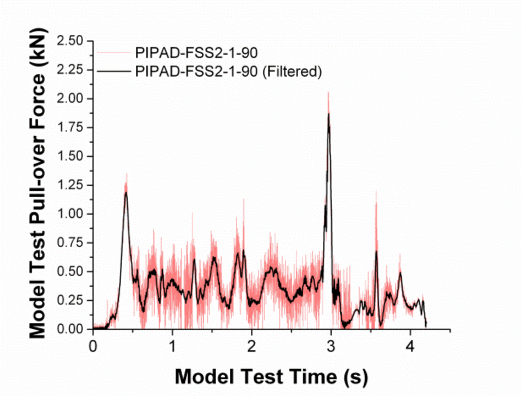
PIPAD-FSS2-1-90
PIPAD-FSS2-1-90 (Filtered)
Model Test Pull-over Force (kN)
0.00
0.25
0.50
0.75
1.00
1.25
1.50
1.75
2.00
2.25
2.50
Model Test Time (s)
0
1
2
3
4

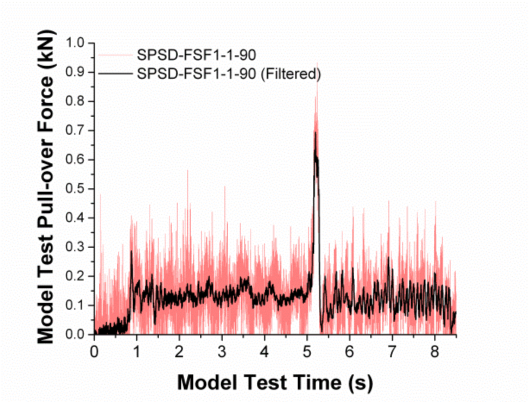
SPSD-FSF1-1-90
SPSD-FSF1-1-90 (Filtered)
Model Test Pull-over Force (kN)
1.0
0.9
0.8
0.7
0.6
0.5
0.4
0.3
0.2
0.1
0.0
0
1
2
3
4
5
6
7
8
Model Test Time (s)

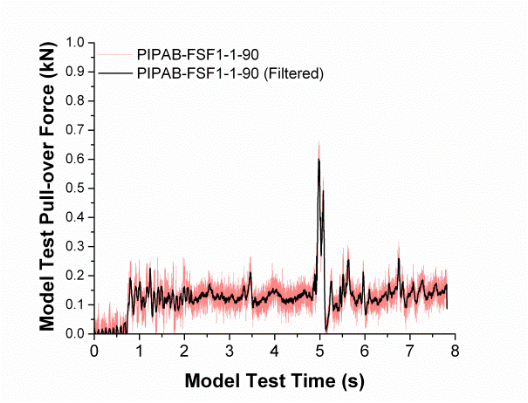
PIPAB-FSF1-1-90
PIPAB-FSF1-1-90 (Filtered)
Model Test Pull-over Force (kN)
1.0
0.9
0.8
0.7
0.6
0.5
0.4
0.3
0.2
0.1
0.0
0
1
2
3
4
5
6
7
8
Model Test Time (s)

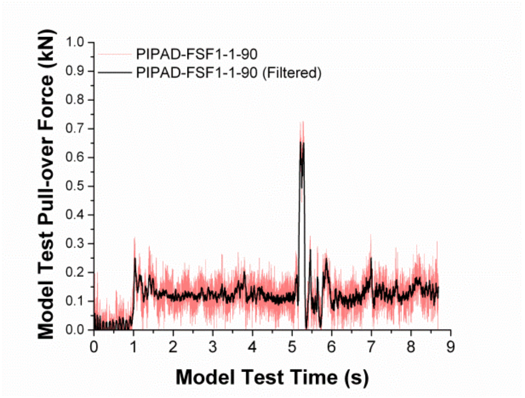
PIPAD-FSF1-1-90
PIPAD-FSF1-1-90 (Filtered)
Model Test Pull-over Force (kN)
1.0
0.9
0.8
0.7
0.6
0.5
0.4
0.3
0.2
0.1
0.0
0
1
2
3
4
5
6
7
8
9
Model Test Time (s)

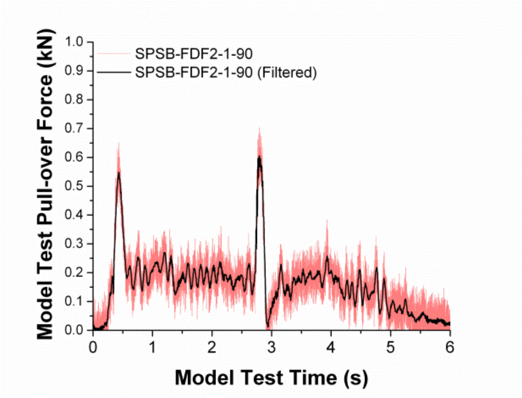
SPSB-FDF2-1-90
SPSB-FDF2-1-90 (Filtered)
Model Test Pull-over Force (kN)
1.0
0.9
0.8
0.7
0.6
0.5
0.4
0.3
0.2
0.1
0.0
0
1
2
3
4
5
6
Model Test Time (s)

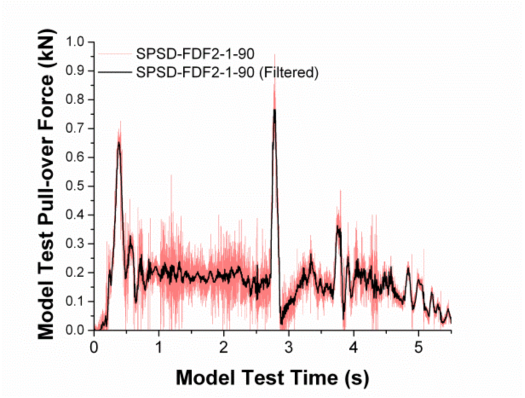
SPSD-FDF2-1-90
SPSD-FDF2-1-90 (Filtered)
Model Test Pull-over Force (kN)
1.0
0.9
0.8
0.7
0.6
0.5
0.4
0.3
0.2
0.1
0.0
0
1
2
3
4
5
Model Test Time (s)

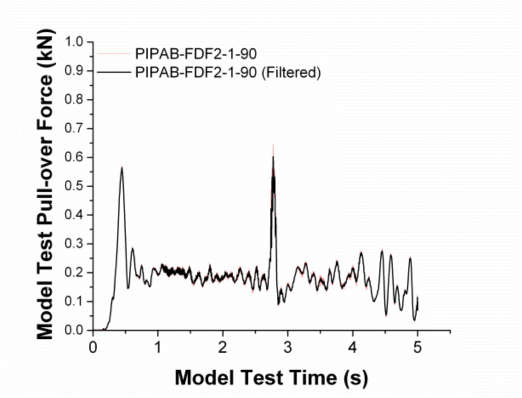
PIPAB-FDF2-1-90
PIPAB-FDF2-1-90 (Filtered)
Model Test Pull-over Force (kN)
1.0
0.9
0.8
0.7
0.6
0.5
0.4
0.3
0.2
0.1
0.0
0
1
2
3
4
5
Model Test Time (s)

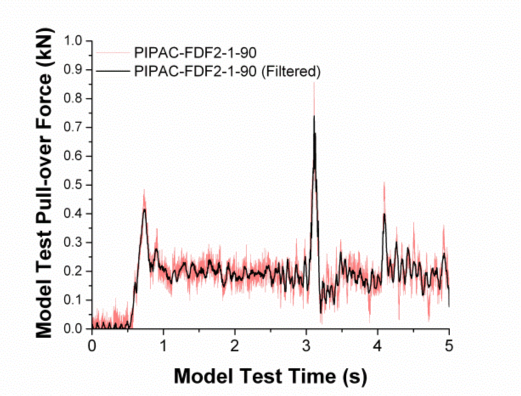
PIPAC-FDF2-1-90
PIPAC-FDF2-1-90 (Filtered)
Model Test Pull-over Force (kN)
1.0
0.9
0.8
0.7
0.6
0.5
0.4
0.3
0.2
0.1
0.0
0
1
2
3
4
5
Model Test Time (s)

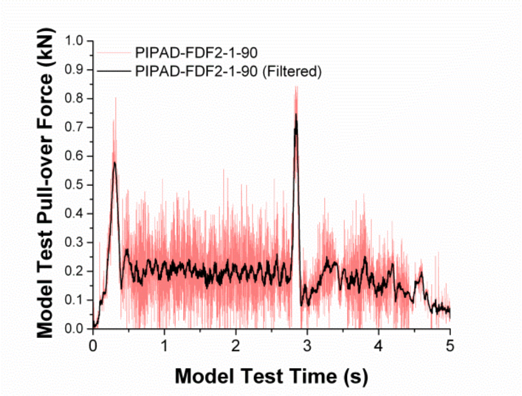
PIPAD-FDF2-1-90
PIPAD-FDF2-1-90 (Filtered)
Model Test Pull-over Force (kN)
1.0
0.9
0.8
0.7
0.6
0.5
0.4
0.3
0.2
0.1
0.0
0
1
2
3
4
5
Model Test Time (s)

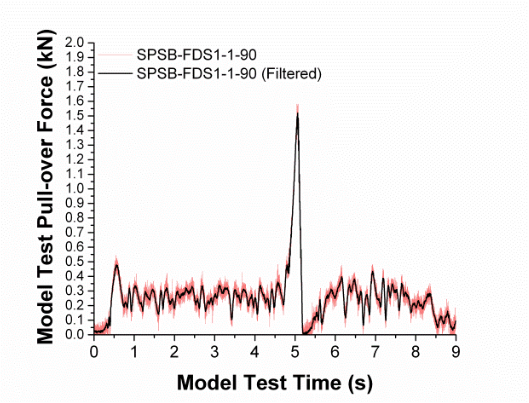
SPSB-FDS1-1-90
SPSB-FDS1-1-90 (Filtered)
Model Test Pull-over Force (kN)
2.0
1.9
1.8
1.7
1.6
1.5
1.4
1.3
1.2
1.1
1.0
0.9
0.8
0.7
0.6
0.5
0.4
0.3
0.2
0.1
0.0
0
1
2
3
4
5
6
7
8
9
Model Test Time (s)

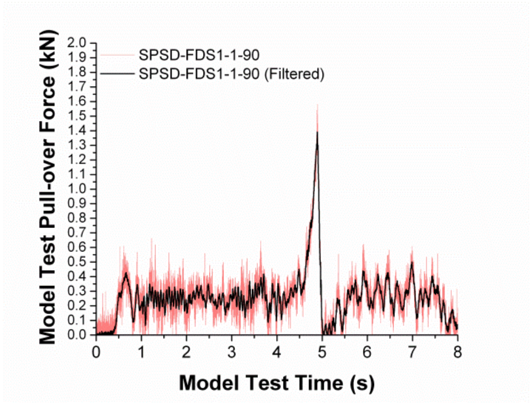
SPSD-FDS1-1-90
SPSD-FDS1-1-90 (Filtered)
Model Test Pull-over Force (kN)
2.0
1.9
1.8
1.7
1.6
1.5
1.4
1.3
1.2
1.1
1.0
0.9
0.8
0.7
0.6
0.5
0.4
0.3
0.2
0.1
0.0
0
1
2
3
4
5
6
7
8
Model Test Time (s)

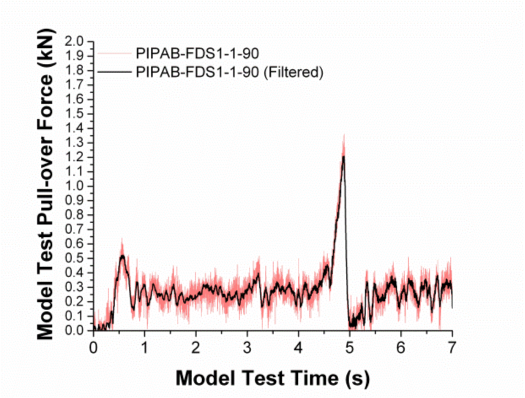
PIPAB-FDS1-1-90
PIPAB-FDS1-1-90 (Filtered)
Model Test Pull-over Force (kN)
2.0
1.9
1.8
1.7
1.6
1.5
1.4
1.3
1.2
1.1
1.0
0.9
0.8
0.7
0.6
0.5
0.4
0.3
0.2
0.1
0.0
0
1
2
3
4
5
6
7
Model Test Time (s)

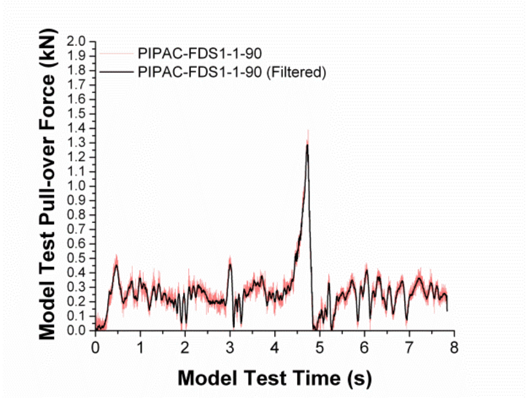
PIPAC-FDS1-1-90
PIPAC-FDS1-1-90 (Filtered)
Model Test Pull-over Force (kN)
2.0
1.9
1.8
1.7
1.6
1.5
1.4
1.3
1.2
1.1
1.0
0.9
0.8
0.7
0.6
0.5
0.4
0.3
0.2
0.1
0.0
0
1
2
3
4
5
6
7
8
Model Test Time (s)

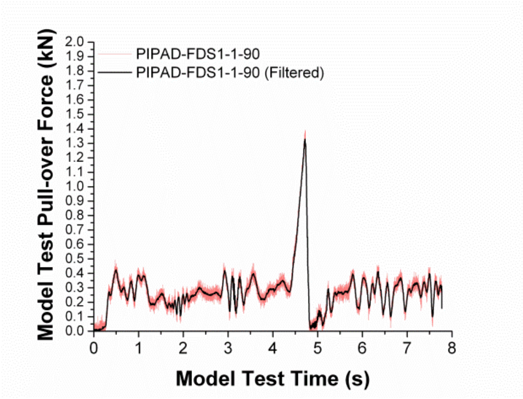
PIPAD-FDS1-1-90
PIPAD-FDS1-1-90 (Filtered)
Model Test Pull-over Force (kN)
2.0
1.9
1.8
1.7
1.6
1.5
1.4
1.3
1.2
1.1
1.0
0.9
0.8
0.7
0.6
0.5
0.4
0.3
0.2
0.1
0.0
0
1
2
3
4
5
6
7
8
Model Test Time (s)

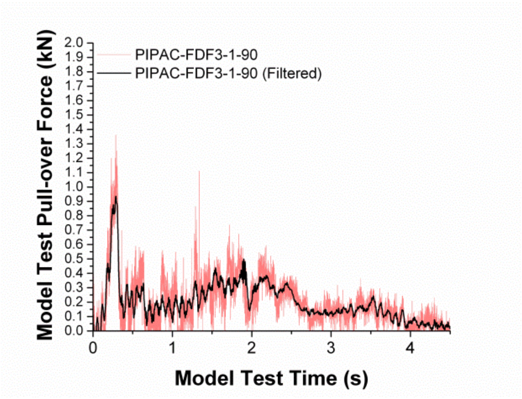
PIPAC-FDF3-1-90
PIPAC-FDF3-1-90 (Filtered)
Model Test Pull-over Force (kN)
2.0
1.9
1.8
1.7
1.6
1.5
1.4
1.3
1.2
1.1
1.0
0.9
0.8
0.7
0.6
0.5
0.4
0.3
0.2
0.1
0.0
0
1
2
3
4
Model Test Time (s)

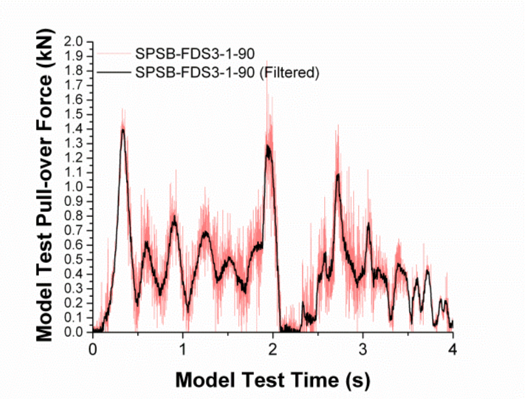
SPSB-FDS3-1-90
SPSB-FDS3-1-90 (Filtered)
Model Test Pull-over Force (kN)
2.0
1.9
1.8
1.7
1.6
1.5
1.4
1.3
1.2
1.1
1.0
0.9
0.8
0.7
0.6
0.5
0.4
0.3
0.2
0.1
0.0
0
1
2
3
4
Model Test Time (s)

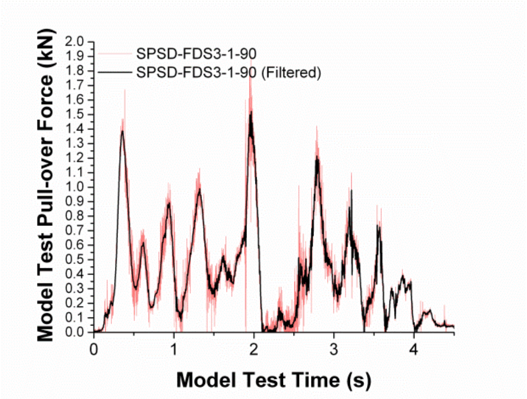
SPSD-FDS3-1-90
SPSD-FDS3-1-90 (Filtered)
Model Test Pull-over Force (kN)
2.0
1.9
1.8
1.7
1.6
1.5
1.4
1.3
1.2
1.1
1.0
0.9
0.8
0.7
0.6
0.5
0.4
0.3
0.2
0.1
0.0
0
1
2
3
4
Model Test Time (s)

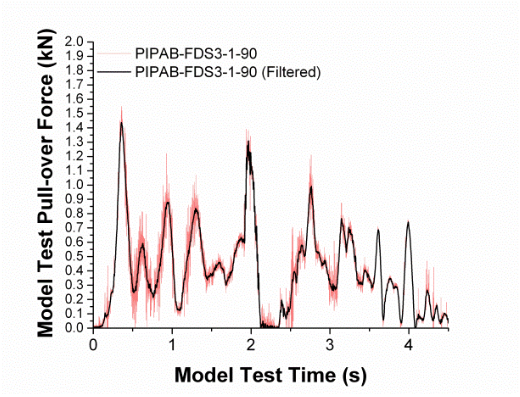
PIPAB-FDS3-1-90
PIPAB-FDS3-1-90 (Filtered)
Model Test Pull-over Force (kN)
2.0
1.9
1.8
1.7
1.6
1.5
1.4
1.3
1.2
1.1
1.0
0.9
0.8
0.7
0.6
0.5
0.4
0.3
0.2
0.1
0.0
0
1
2
3
4
Model Test Time (s)

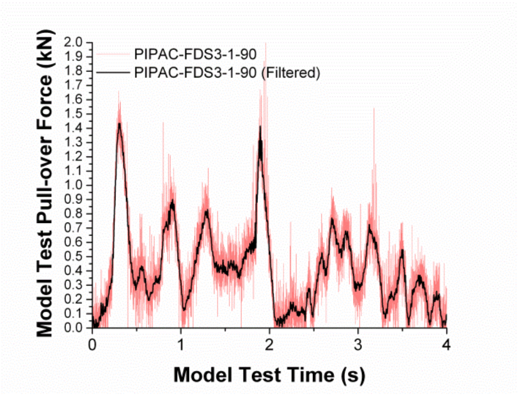
PIPAC-FDS3-1-90
PIPAC-FDS3-1-90 (Filtered)
Model Test Pull-over Force (kN)
2.0
1.9
1.8
1.7
1.6
1.5
1.4
1.3
1.2
1.1
1.0
0.9
0.8
0.7
0.6
0.5
0.4
0.3
0.2
0.1
0.0
0
1
2
3
4
Model Test Time (s)

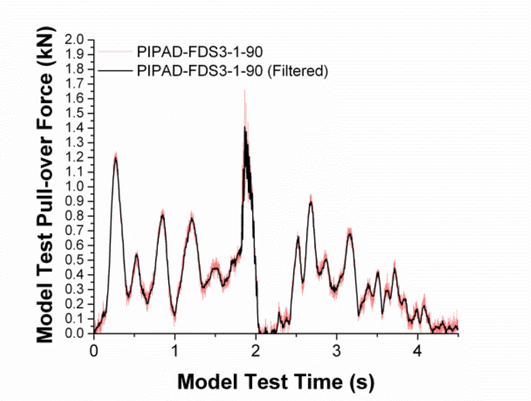
PIPAD-FDS3-1-90
PIPAD-FDS3-1-90 (Filtered)
Model Test Pull-over Force (kN)
0.0
0.1
0.2
0.3
0.4
0.5
0.6
0.7
0.8
0.9
1.0
1.1
1.2
1.3
1.4
1.5
1.6
1.7
1.8
1.9
2.0
0
1
2
3
4
Model Test Time (s)

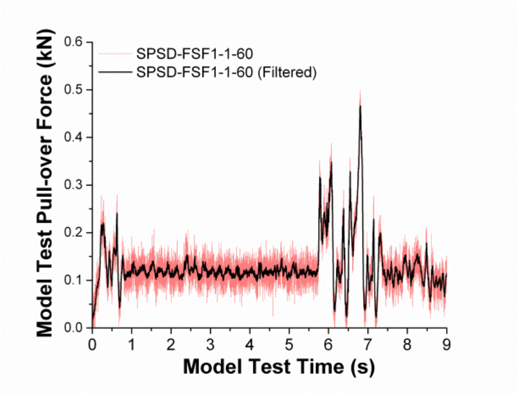
SPSD-FSF1-1-60
SPSD-FSF1-1-60 (Filtered)
Model Test Pull-over Force (kN)
0.0
0.1
0.2
0.3
0.4
0.5
0.6
0
1
2
3
4
5
6
7
8
9
Model Test Time (s)

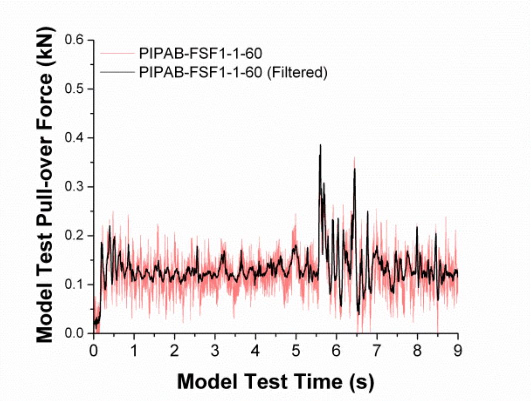
PIPAB-FSF1-1-60
PIPAB-FSF1-1-60 (Filtered)
Model Test Pull-over Force (kN)
0.0
0.1
0.2
0.3
0.4
0.5
0.6
0
1
2
3
4
5
6
7
8
9
Model Test Time (s)

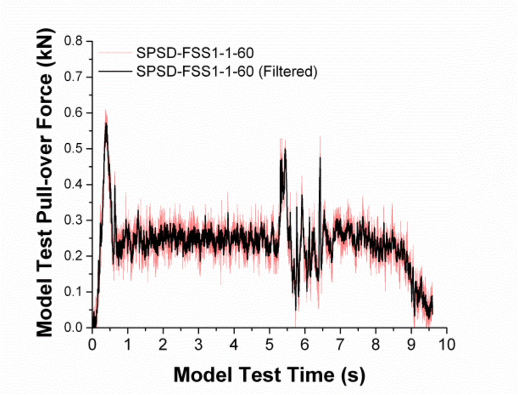
SPSD-FSS1-1-60
SPSD-FSS1-1-60 (Filtered)
Model Test Pull-over Force (kN)
0.0
0.1
0.2
0.3
0.4
0.5
0.6
0.7
0.8
0
1
2
3
4
5
6
7
8
9
10
Model Test Time (s)

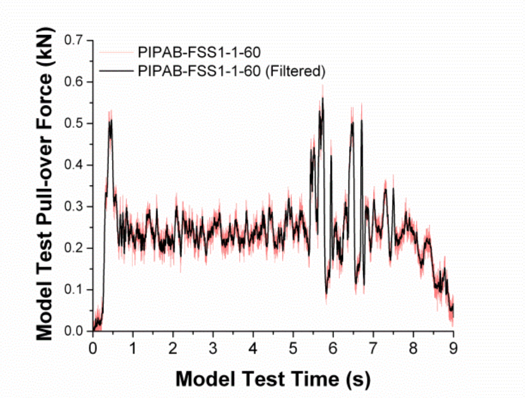
PIPAB-FSS1-1-60
PIPAB-FSS1-1-60 (Filtered)
Model Test Pull-over Force (kN)
0.0
0.1
0.2
0.3
0.4
0.5
0.6
0.7
0
1
2
3
4
5
6
7
8
9
Model Test Time (s)

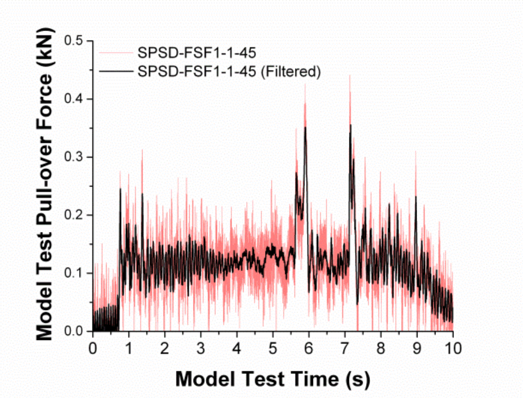
SPSD-FSF1-1-45
SPSD-FSF1-1-45 (Filtered)
Model Test Pull-over Force (kN)
0.0
0.1
0.2
0.3
0.4
0.5
0
1
2
3
4
5
6
7
8
9
10
Model Test Time (s)

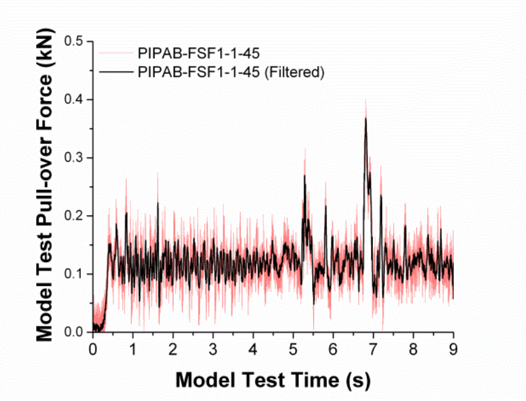
Model Test Pull-over Force (kN)
0.0
0.1
0.2
0.3
0.4
0.5
0
1
2
3
4
5
6
7
8
9
Model Test Time (s)
PIPAB-FSF1-1-45
PIPAB-FSF1-1-45 (Filtered)

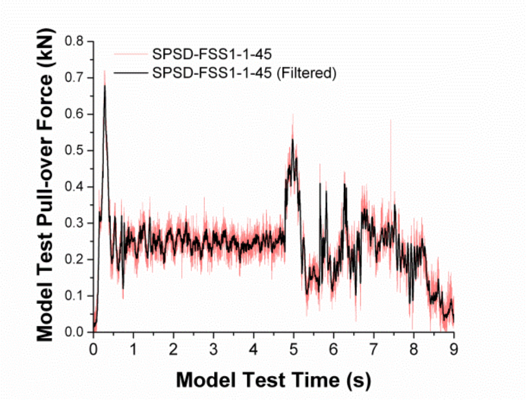
Model Test Pull-over Force (kN)
0.0
0.1
0.2
0.3
0.4
0.5
0.6
0.7
0.8
0
1
2
3
4
5
6
7
8
9
Model Test Time (s)
SPSD-FSS1-1-45
SPSD-FSS1-1-45 (Filtered)

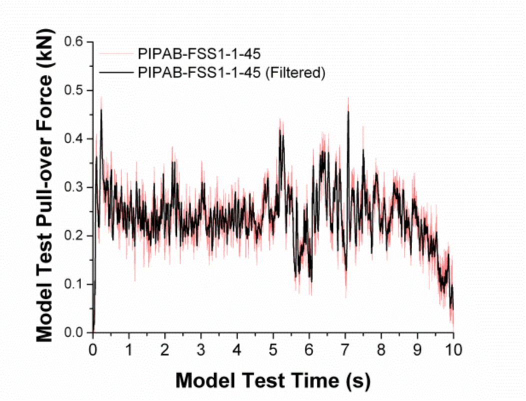
Model Test Pull-over Force (kN)
0.0
0.1
0.2
0.3
0.4
0.5
0.6
0
1
2
3
4
5
6
7
8
9
10
Model Test Time (s)
PIPAB-FSS1-1-45
PIPAB-FSS1-1-45 (Filtered)

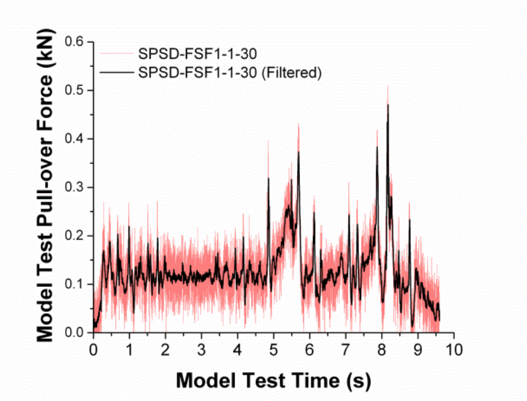
Model Test Pull-over Force (kN)
0.0
0.1
0.2
0.3
0.4
0.5
0.6
0
1
2
3
4
5
6
7
8
9
10
Model Test Time (s)
SPSD-FSF1-1-30
SPSD-FSF1-1-30 (Filtered)

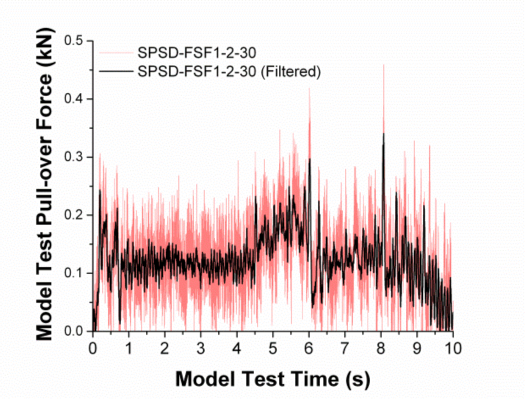
Model Test Pull-over Force (kN)
0.0
0.1
0.2
0.3
0.4
0.5
0
1
2
3
4
5
6
7
8
9
10
Model Test Time (s)
SPSD-FSF1-2-30
SPSD-FSF1-2-30 (Filtered)

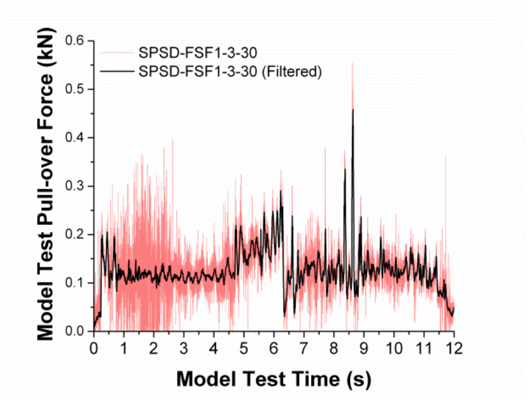
Model Test Pull-over Force (kN)
0.0
0.1
0.2
0.3
0.4
0.5
0.6
0
1
2
3
4
5
6
7
8
9
10
11
12
Model Test Time (s)
SPSD-FSF1-3-30
SPSD-FSF1-3-30 (Filtered)

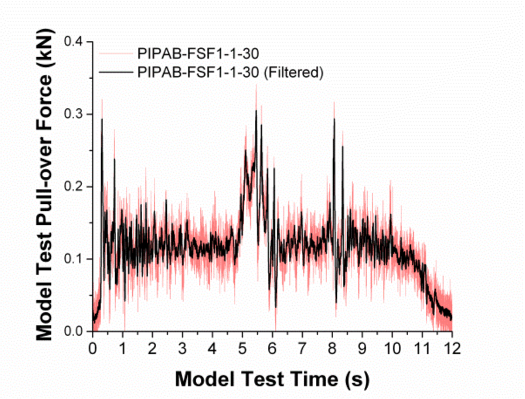
PIPAB-FSF1-1-30
PIPAB-FSF1-1-30 (Filtered)
Model Test Pull-over Force (kN)
0.0
0.1
0.2
0.3
0.4
Model Test Time (s)
0 1 2 3 4 5 6 7 8 9 10 11 12

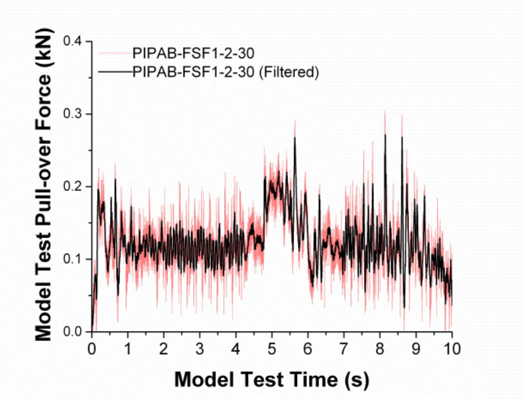
PIPAB-FSF1-2-30
PIPAB-FSF1-2-30 (Filtered)
Model Test Pull-over Force (kN)
0.0
0.1
0.2
0.3
0.4
Model Test Time (s)
0 1 2 3 4 5 6 7 8 9 10

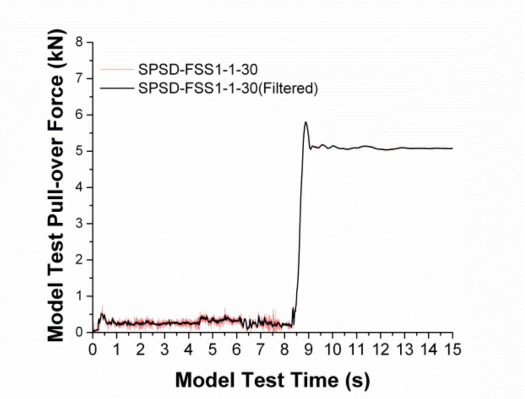
SPSD-FSS1-1-30
SPSD-FSS1-1-30(Filtered)
Model Test Pull-over Force (kN)
0
1
2
3
4
5
6
7
8
Model Test Time (s)
0 1 2 3 4 5 6 7 8 9 10 11 12 13 14 15

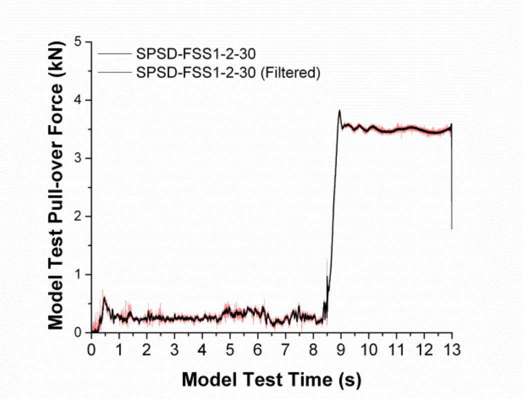
SPSD-FSS1-2-30
SPSD-FSS1-2-30 (Filtered)
Model Test Pull-over Force (kN)
0
1
2
3
4
5
Model Test Time (s)
0 1 2 3 4 5 6 7 8 9 10 11 12 13

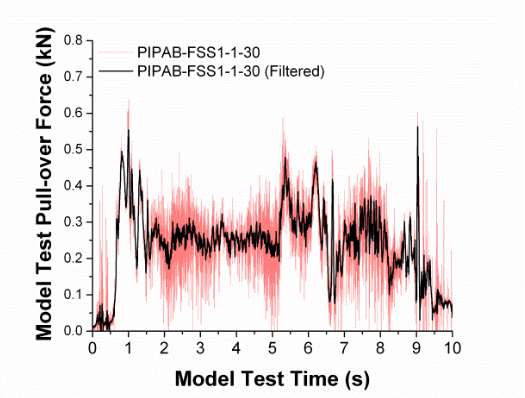
PIPAB-FSS1-1-30
PIPAB-FSS1-1-30 (Filtered)
Model Test Pull-over Force (kN)
0.0
0.1
0.2
0.3
0.4
0.5
0.6
0.7
0.8
Model Test Time (s)
0 1 2 3 4 5 6 7 8 9 10

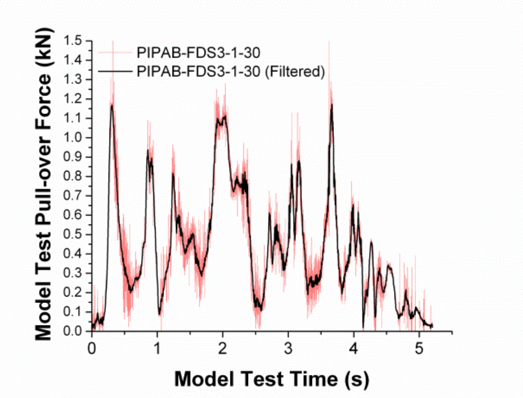
PIPAB-FDS3-1-30
PIPAB-FDS3-1-30 (Filtered)
Model Test Pull-over Force (kN)
0.0
0.1
0.2
0.3
0.4
0.5
0.6
0.7
0.8
0.9
1.0
1.1
1.2
1.3
1.4
1.5
Model Test Time (s)
0 1 2 3 4 5

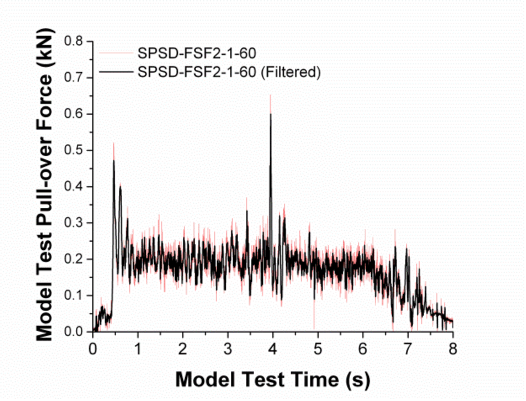
SPSD-FSF2-1-60
SPSD-FSF2-1-60 (Filtered)
Model Test Pull-over Force (kN)
0.0
0.1
0.2
0.3
0.4
0.5
0.6
0.7
0.8
Model Test Time (s)
0
1
2
3
4
5
6
7
8

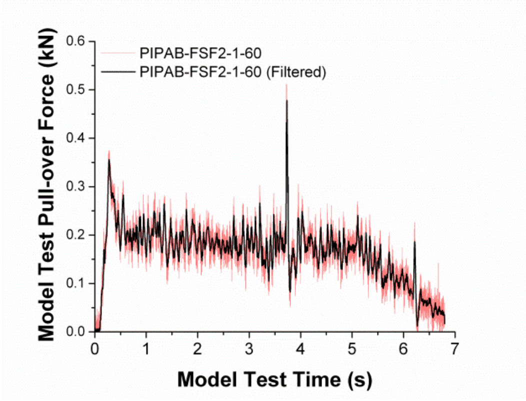
PIPAB-FSF2-1-60
PIPAB-FSF2-1-60 (Filtered)
Model Test Pull-over Force (kN)
0.0
0.1
0.2
0.3
0.4
0.5
0.6
Model Test Time (s)
0
1
2
3
4
5
6
7

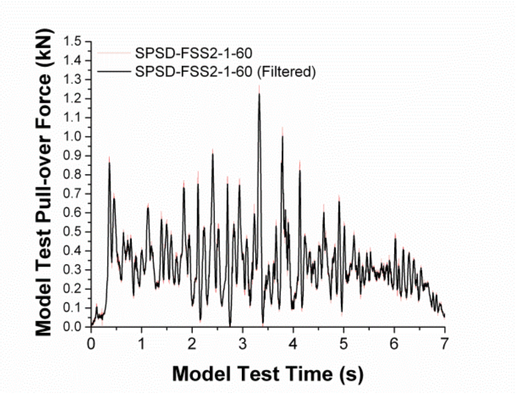
SPSD-FSS2-1-60
SPSD-FSS2-1-60 (Filtered)
Model Test Pull-over Force (kN)
0.0
0.1
0.2
0.3
0.4
0.5
0.6
0.7
0.8
0.9
1.0
1.1
1.2
1.3
1.4
1.5
Model Test Time (s)
0
1
2
3
4
5
6
7

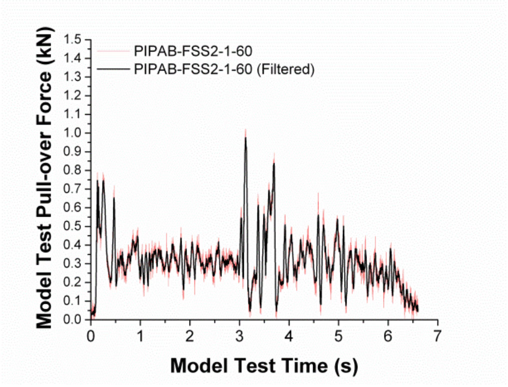
PIPAB-FSS2-1-60
PIPAB-FSS2-1-60 (Filtered)
Model Test Pull-over Force (kN)
0.0
0.1
0.2
0.3
0.4
0.5
0.6
0.7
0.8
0.9
1.0
1.1
1.2
1.3
1.4
1.5
Model Test Time (s)
0
1
2
3
4
5
6
7

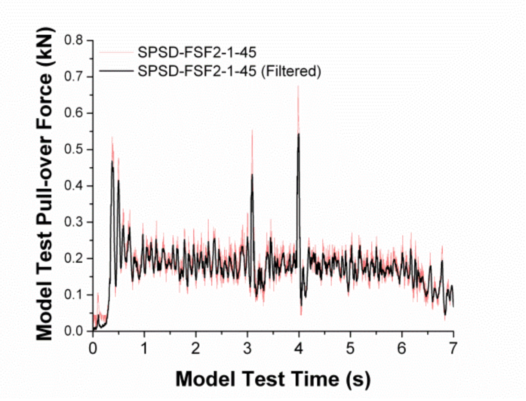
SPSD-FSF2-1-45
SPSD-FSF2-1-45 (Filtered)
Model Test Pull-over Force (kN)
0.0
0.1
0.2
0.3
0.4
0.5
0.6
0.7
0.8
Model Test Time (s)
0
1
2
3
4
5
6
7

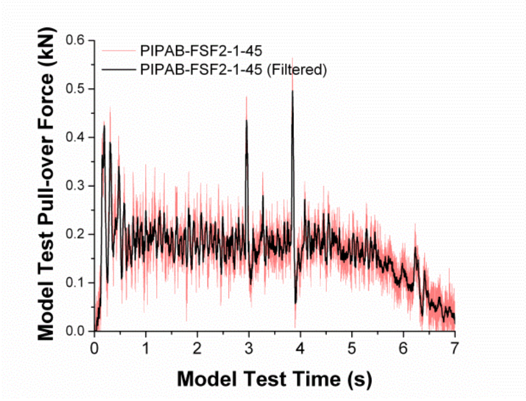
PIPAB-FSF2-1-45
PIPAB-FSF2-1-45 (Filtered)
Model Test Pull-over Force (kN)
0.0
0.1
0.2
0.3
0.4
0.5
0.6
Model Test Time (s)
0
1
2
3
4
5
6
7

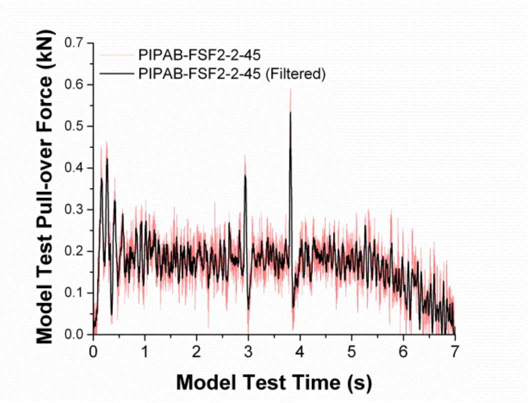
PIPAB-FSF2-2-45
PIPAB-FSF2-2-45 (Filtered)
Model Test Pull-over Force (kN)
0.0
0.1
0.2
0.3
0.4
0.5
0.6
0.7
Model Test Time (s)
0
1
2
3
4
5
6
7

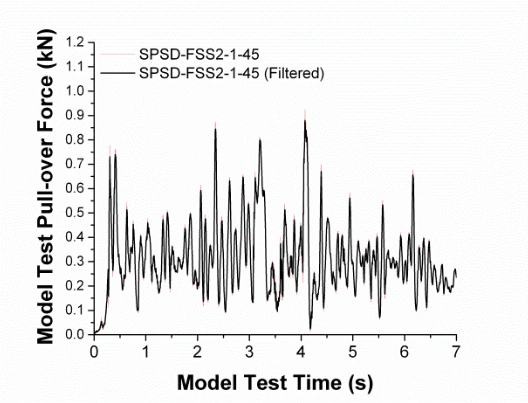
SPSD-FSS2-1-45
SPSD-FSS2-1-45 (Filtered)
Model Test Pull-over Force (kN)
0.0
0.1
0.2
0.3
0.4
0.5
0.6
0.7
0.8
0.9
1.0
1.1
1.2
Model Test Time (s)
0
1
2
3
4
5
6
7

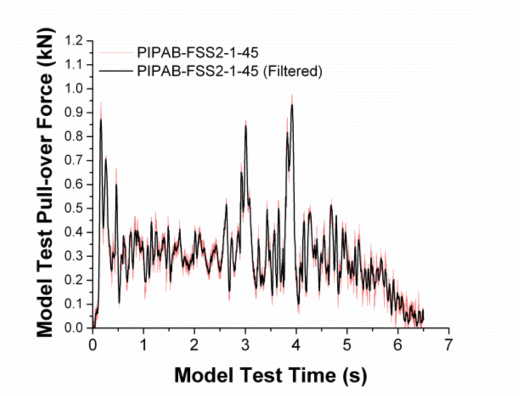
PIPAB-FSS2-1-45
PIPAB-FSS2-1-45 (Filtered)
Model Test Pull-over Force (kN)
0.0
0.1
0.2
0.3
0.4
0.5
0.6
0.7
0.8
0.9
1.0
1.1
1.2
Model Test Time (s)
0
1
2
3
4
5
6
7

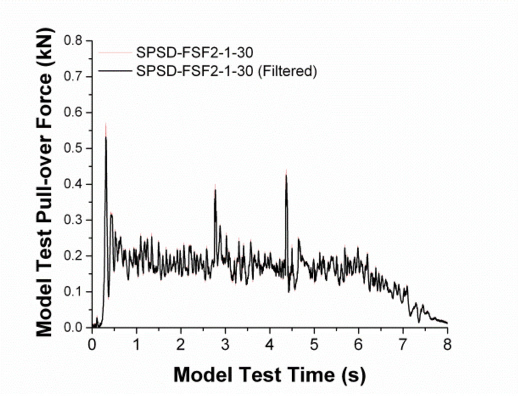
SPSD-FSF2-1-30
SPSD-FSF2-1-30 (Filtered)
Model Test Pull-over Force (kN)
0.0
0.1
0.2
0.3
0.4
0.5
0.6
0.7
0.8
Model Test Time (s)
0
1
2
3
4
5
6
7
8

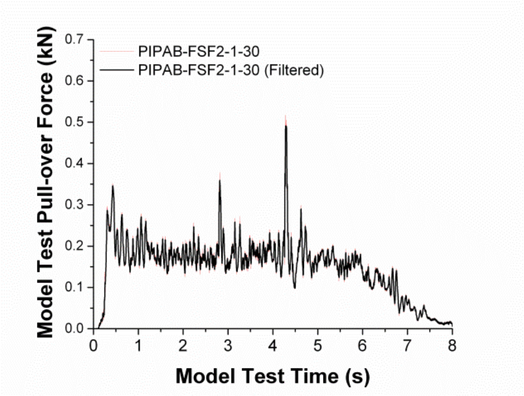
PIPAB-FSF2-1-30
PIPAB-FSF2-1-30 (Filtered)
Model Test Pull-over Force (kN)
0.0
0.1
0.2
0.3
0.4
0.5
0.6
0.7
Model Test Time (s)
0
1
2
3
4
5
6
7
8

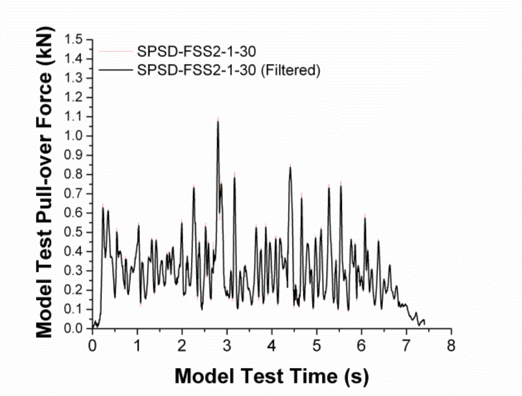
SPSD-FSS2-1-30
SPSD-FSS2-1-30 (Filtered)
Model Test Pull-over Force (kN)
0.0
0.1
0.2
0.3
0.4
0.5
0.6
0.7
0.8
0.9
1.0
1.1
1.2
1.3
1.4
1.5
Model Test Time (s)
0
1
2
3
4
5
6
7
8

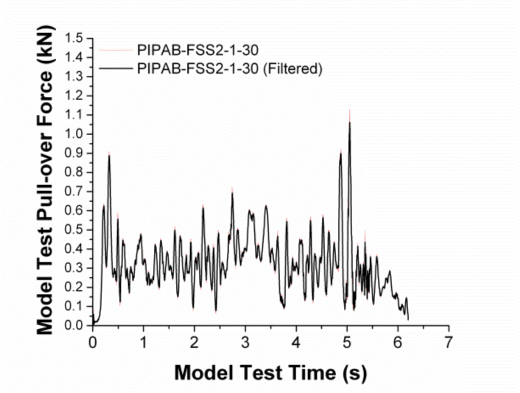
PIPAB-FSS2-1-30
PIPAB-FSS2-1-30 (Filtered)
Model Test Pull-over Force (kN)
0.0 0.1 0.2 0.3 0.4 0.5 0.6 0.7 0.8 0.9 1.0 1.1 1.2 1.3 1.4 1.5
0 1 2 3 4 5 6 7
Model Test Time (s)

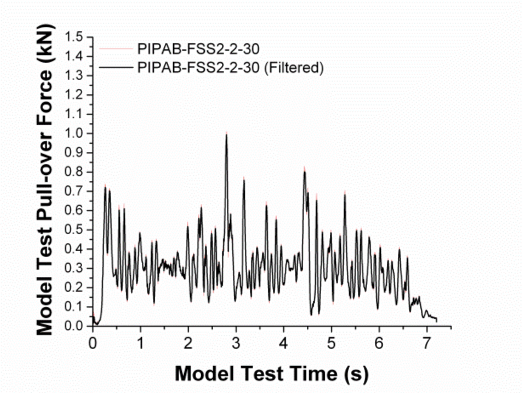
PIPAB-FSS2-2-30
PIPAB-FSS2-2-30 (Filtered)
Model Test Pull-over Force (kN)
0.0 0.1 0.2 0.3 0.4 0.5 0.6 0.7 0.8 0.9 1.0 1.1 1.2 1.3 1.4 1.5
0 1 2 3 4 5 6 7
Model Test Time (s)

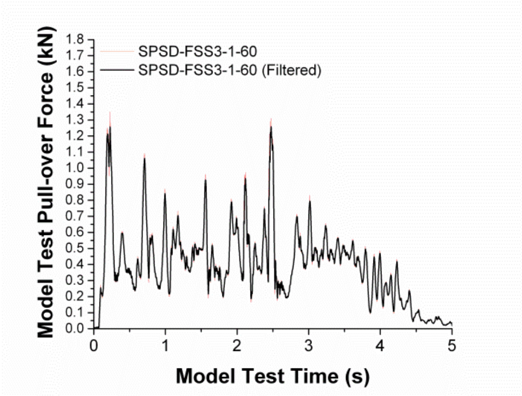
SPSD-FSS3-1-60
SPSD-FSS3-1-60 (Filtered)
Model Test Pull-over Force (kN)
0.0 0.1 0.2 0.3 0.4 0.5 0.6 0.7 0.8 0.9 1.0 1.1 1.2 1.3 1.4 1.5 1.6 1.7 1.8
0 1 2 3 4 5
Model Test Time (s)

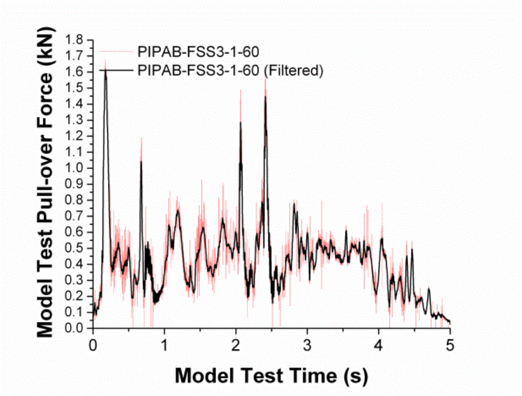
PIPAB-FSS3-1-60
PIPAB-FSS3-1-60 (Filtered)
Model Test Pull-over Force (kN)
0.0 0.1 0.2 0.3 0.4 0.5 0.6 0.7 0.8 0.9 1.0 1.1 1.2 1.3 1.4 1.5 1.6 1.7 1.8
0 1 2 3 4 5
Model Test Time (s)

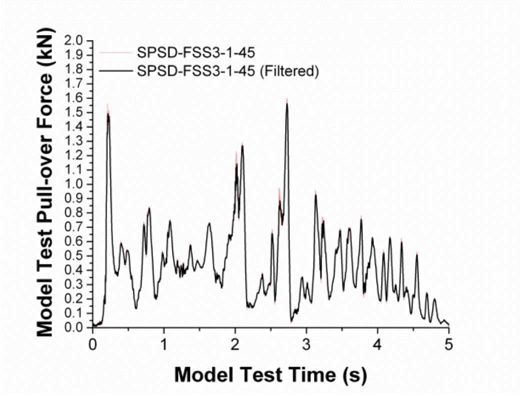
SPSD-FSS3-1-45
SPSD-FSS3-1-45 (Filtered)
Model Test Pull-over Force (kN)
0.0 0.1 0.2 0.3 0.4 0.5 0.6 0.7 0.8 0.9 1.0 1.1 1.2 1.3 1.4 1.5 1.6 1.7 1.8 1.9 2.0
0 1 2 3 4 5
Model Test Time (s)

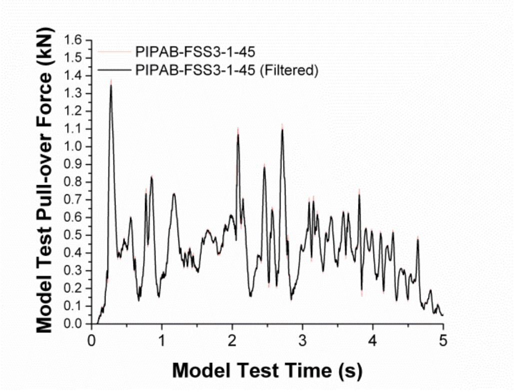
PIPAB-FSS3-1-45
PIPAB-FSS3-1-45 (Filtered)
Model Test Pull-over Force (kN)
0.0 0.1 0.2 0.3 0.4 0.5 0.6 0.7 0.8 0.9 1.0 1.1 1.2 1.3 1.4 1.5 1.6
0 1 2 3 4 5
Model Test Time (s)

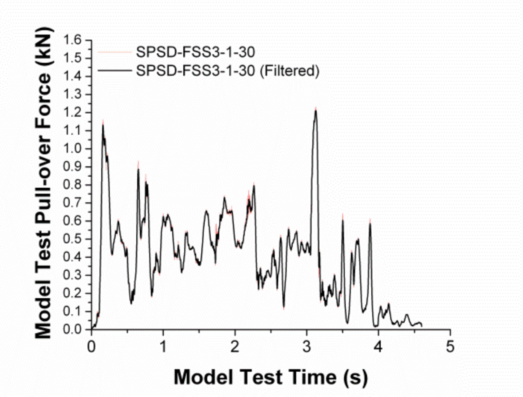
Model Test Pull-over Force (kN)
0.0
0.1
0.2
0.3
0.4
0.5
0.6
0.7
0.8
0.9
1.0
1.1
1.2
1.3
1.4
1.5
1.6
SPSD-FSS3-1-30
SPSD-FSS3-1-30 (Filtered)
0
1
2
3
4
5
Model Test Time (s)

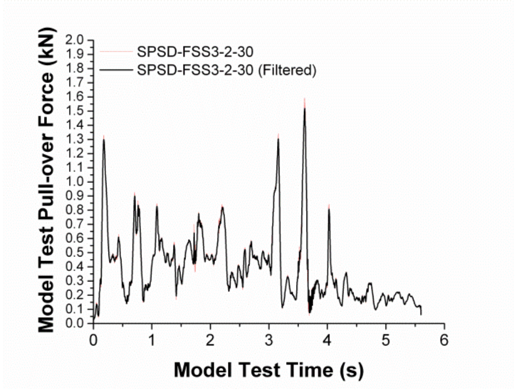
Model Test Pull-over Force (kN)
0.0
0.1
0.2
0.3
0.4
0.5
0.6
0.7
0.8
0.9
1.0
1.1
1.2
1.3
1.4
1.5
1.6
1.7
1.8
1.9
2.0
SPSD-FSS3-2-30
SPSD-FSS3-2-30 (Filtered)
0
1
2
3
4
5
6
Model Test Time (s)

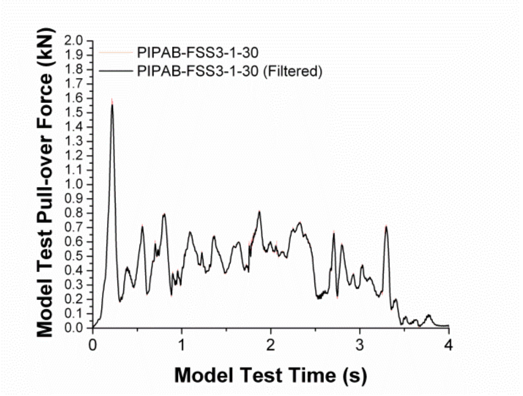
Model Test Pull-over Force (kN)
0.0
0.1
0.2
0.3
0.4
0.5
0.6
0.7
0.8
0.9
1.0
1.1
1.2
1.3
1.4
1.5
1.6
1.7
1.8
1.9
2.0
PIPAB-FSS3-1-30
PIPAB-FSS3-1-30 (Filtered)
0
1
2
3
4
Model Test Time (s)

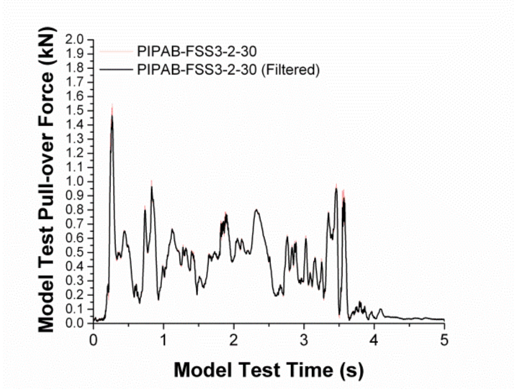
Model Test Pull-over Force (kN)
0.0
0.1
0.2
0.3
0.4
0.5
0.6
0.7
0.8
0.9
1.0
1.1
1.2
1.3
1.4
1.5
1.6
1.7
1.8
1.9
2.0
PIPAB-FSS3-2-30
PIPAB-FSS3-2-30 (Filtered)
0
1
2
3
4
5
Model Test Time (s)

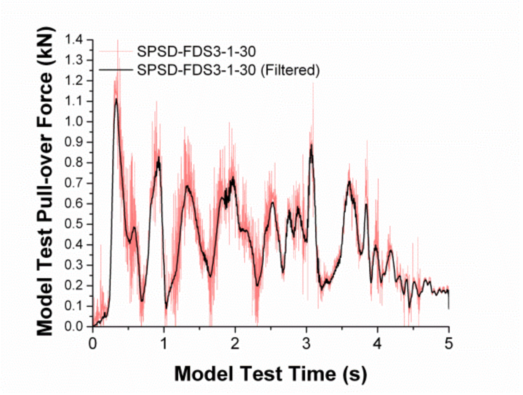
Model Test Pull-over Force (kN)
0.0
0.1
0.2
0.3
0.4
0.5
0.6
0.7
0.8
0.9
1.0
1.1
1.2
1.3
1.4
SPSD-FDS3-1-30
SPSD-FDS3-1-30 (Filtered)
0
1
2
3
4
5
Model Test Time (s)

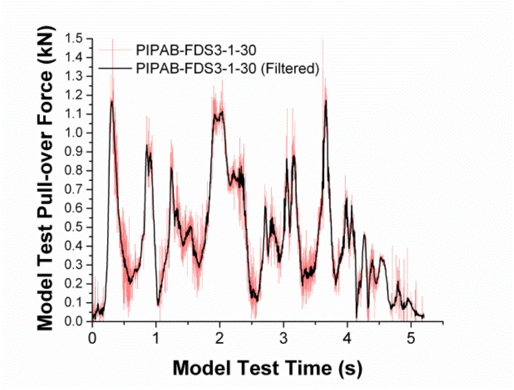
Model Test Pull-over Force (kN)
0.0
0.1
0.2
0.3
0.4
0.5
0.6
0.7
0.8
0.9
1.0
1.1
1.2
1.3
1.4
1.5
PIPAB-FDS3-1-30
PIPAB-FDS3-1-30 (Filtered)
0
1
2
3
4
5
Model Test Time (s)

G. Appendix G Papers

The published papers are listed here:

1. ZHENG, J., PALMER, A. C., LIPSKI, W. & BRUNNING, P. Impact damage on pipe-in-pipe systems. Twenty-second International Offshore and Polar Engineering Conference, 2012 Rhodes, Greece.
2. ZHENG, J., PALMER, A. & BRUNNING, P. 2013. Overtrawlability and Mechanical Damage of Pipe-in-Pipe. Journal of Applied Mechanics, 81, 031006-1-031006-11.
3. Zheng, J., Palmer, A.C., Brunning, P., Gan, C. T. (2014). "Indentation and external pressure on subsea single wall pipe and pipe-in-pipe." Ocean Engineering 83(0): 125-132.
4. Zheng, J., Palmer, A.C., et al. (2014). Method to Assess the Overtrawlability of Pipe-in-Pipe. Offshore Technology Conference Asia. 2014 Kuala Lumpur.
5. Palmer, A.C., Zheng, J., et al. (2014). "Fishing trawl pull-over across pipelines." Journal of Pipeline Engineering 13(1).